

**DEVELOPMENT OF NOVEL PHOTOCATALYTIC
REACTOR FOR DYE WASTEWATER TREATMENT**

THESIS

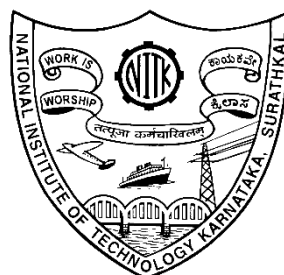
Submitted in partial fulfillment of the requirements for the degree of

DOCTOR OF PHILOSOPHY

by

SUMAN DAS

Register No. 158039CH15F13



**DEPARTMENT OF CHEMICAL ENGINEERING
NATIONAL INSTITUTE OF TECHNOLOGY KARNATAKA
SURATHKAL, MANGALORE - 575 025
FEBRUARY, 2020**

DECLARATION

I hereby *declare* that the Thesis entitled “**DEVELOPMENT OF NOVEL PHOTOCATALYTIC REACTOR FOR DYE WASTEWATER TREATMENT**” which is being submitted to the **National Institute of Technology Karnataka, Surathkal** in partial fulfillment of the requirements for the award of the Degree of **Doctor of Philosophy** in Chemical Engineering is a *bonafide report of the research work carried out by me*. The material contained in this Thesis has not been submitted to any University or Institution for the award of any degree.

Name: Suman Das

Register number: 158039CH15F13

Department of Chemical Engineering

Place: Surathkal

Date: 27-02-2020

C E R T I F I C A T E

This is to *certify* that the Thesis entitled “**DEVELOPMENT OF NOVEL PHOTOCATALYTIC REACTOR FOR DYE WASTEWATER TREATMENT**” submitted by **SUMAN DAS (Register Number: 158039CH15F13)** as the record of the research work carried out by him, *is accepted as the Thesis submission* in partial fulfillment of the requirements for the award of degree of **Doctor of Philosophy**.

Research Guide

Dr. Hari Mahalingam
Associate Professor
Department of Chemical Engineering
NITK Surathkal

Chairman- DRPC

ACKNOWLEDGMENTS

This thesis is developed in years of research that has been undertaken since I came to this prestigious institute, NITK. By that time, I had an opportunity to work with a number of people whose contribution in different ways to the research and the making of the thesis deserves a special mention. It is a pleasure to convey my gratitude to all of them in my humble acknowledgment.

First and foremost, I wish to express my sincere gratitude to my Research Guide, **Dr. Hari Mahalingam**, Associate professor, Department of Chemical Engineering, NITK Surathkal. Without his valuable guidance, support, enthusiasm and encouragement, I could never finish my Doctoral work. His vast knowledge of chemical engineering and logical way of thinking has been great value for me. I thank him for graciously taking the time to read and offer the required improvements to the manuscripts and thesis. It is not sufficient to express my gratitude with only a few words.

I am extremely thankful to the RPAC committee members, **Dr. Arun, M.**, Department of Mechanical Engineering and **Dr. Jagannathan, T. K.**, Department of Chemical Engineering, for their valuable advice and suggestions which enabled me to notice the flaws in my research work and make necessary improvements according to their reviews and comments.

I humbly express my sincere gratitude to **The Director**, NITK Surathkal. I wish to thank our former H.O.D.s **Dr. Rajmohan B**, Professor, and present H. O. D., **Dr. Prasanna B.D.**, Associate Professor, **Department of Chemical Engineering, NITK Surathkal** for providing me necessary facilities, funding, and support during the phase of this research work. I would also like to thank all the faculty members of the **Department of Chemical Engineering, NITK Surathkal** for their valuable support and encouragement. I would as well like to express my sincere thanks to **Mrs. Shashikala Mohan, Mr. Sadashiva, Mrs. Thrithila, Mrs. Bhavyashree, and Ms. Vijetha** and all other non-teaching staffs for their helpful suggestions and timely maintenance of the laboratory equipment.

I gratefully acknowledge to my friends **Dr. Sushma Havanur, Mr. Rohit Kalnake, Mr. Akash Anand, Ms. Manasa M, Dr. Sunil S.W., Mr. Lister Herington Fallero, Dr. Kezia Buruga, Ms. Shwetha Karanth, Dr. Sivananth Murugesan, Dr. Vishnu M, Mrs. Vrushali Kadam, Mrs. Amruta S Shet, Mr. Tabish Wahidi, Dr. Anjana, M., and Dr. Rasheeda Ansari** for their care, support and encouragement.

SUMAN DAS

**DEDICATED
TO A MAN WHO
DOESN'T NEED TO
READ IT: MY
MENTOR Dr. HARI
MAHALINGAM**

A B S T R A C T

Over the years, industrial development has increased, causing a rapid increase in all form of pollution. A large amount of organic waste released into the freshwater bodies have increased water pollution several folds. In this regard, an effective environmentally friendly process for wastewater treatment is urgently needed, because sometimes it is difficult to degrade different toxic pollutants efficiently by conventional methods. Photocatalytic nanoparticles are an excellent choice for the mineralization of organic pollutants present in wastewater. The use of the photocatalyst nanoparticle into a reactor is also challenging since a light source is compulsory to activate the catalysts.

In this work, TiO_2 , rGO, g- C_3N_4 and $\text{TiO}_2/\text{rGO}/\text{g-}\text{C}_3\text{N}_4$ mixture in two forms: an admixture and chemically synthesized composite photocatalysts were immobilized in polystyrene films and employed as a photocatalytic film. The characterizations were done using SEM-EDX, FTIR, XPS, XRD, ICP-OES, BET-Surface area analyzer, particle size analyzer, band-gap analyzer, etc. Initially, the photocatalytic performance of the prepared TiO_2 polystyrene film was checked followed by (TiO_2 , rGO, and g- C_3N_4)-admixture and then $\text{TiO}_2/\text{rGO}/\text{g-}\text{C}_3\text{N}_4$ -chemical composite. The photocatalytic oxidation of synthetic dye wastewater (Remazol Turquoise Blue) under ultra-violet and sunlight irradiation was carried out in different types of photocatalytic reactors (batch, scaled-up a batch with recirculation, and multiphase reactors). The reactor volume was varied from 200 to 2900 mL, and the degradation of Remazol Turquoise Blue was confirmed by TOC and HPLC analysis. The optimization of photocatalytic reaction parameters (effect of catalyst loadings, pH, initial dye concentration, light source, polystyrene photocatalytic film thickness, recyclability the film, oxidizing agents, etc), as well as the reactor parameters (recirculation rate, air flow rate, diameter ratio, etc), were investigated in detail systematically. The synergistic effect of the photocatalysts was also analyzed by using the admixture of the photocatalysts, which showed a great significance in this work.

The photocatalytic treatment of RTB dye under optimized conditions shows that there was more than 90% decolorization in most of the reactors after 90 min of irradiation. Among

various reactors used in this study, the multiphase photocatalytic reactor has unique way to utilize the photocatalyst, which makes it novel and efficient. Also, the multiphase reactor showed the best performance since the observed decolourization and degradation were almost same. To make this study cost-efficient and suitable for large scale application, waste polystyrene was used as a substrate material instead of pristine polystyrene.

This work presents a simple, easy, economical, and eco-friendly way to deal with the toxic organic pollutants. The photocatalytic reactors used in this work are highly efficient and can be easily scaled up for the industrial-scale application and employed for any other organic pollutant present in the water.

Key words: Photocatalyst, Immobilization, Polystyrene, Remazol Turquoise Blue, Multiphase photocatalytic reactor, Degradation.

TABLE OF CONTENTS

CHAPTER NO.	TITLE	PAGE NO.
	ABSTRACT	i
	TABLE OF CONTENT	iii
	LIST OF FIGURES	xi
	LIST OF TABLES	xvii
	ABBREVIATIONS	xix
	NOMENCLATURE	xx
1	INTRODUCTION	1-12
	1.1. Background and rationale	1
	1.2. Sources of potable water and wastewater	2
	1.3. The necessity of treating wastewater	4
	1.4. Treatment processes for industrial wastewater	5
	1.5. Photocatalysis	7
2	LITERATURE REVIEW	13-56
	2.1. Invention and evolution of photocatalysis	13
	2.2. Different forms of heterogeneous photocatalysts	14
	2.2.1. Pure form	14
	2.2.2. Doped form	15
	2.2.3. Co-doped form	15
	2.2.4. Composites	18
	2.2.5. Other forms	18
	2.3. Mineralization of different types of contaminants from wastewater by photocatalysis	18
	2.4. Remazol turquoise blue (RTB)	25
	2.5. Selection of photocatalysts - TiO ₂ , g-C ₃ N ₄ , and rGO	26

CHAPTER NO.	TITLE	PAGE NO.
	2.6. Disadvantages in slurry form and strategy to overcome these disadvantages	26
	2.7. Various parameter effecting the photocatalytic process	35
	2.8. Substrate materials	41
	2.9. Immobilization techniques	41
	2.10. Polymer as a substrate	42
	2.11. Photocatalytic reactors - different types, major challenges	43
	2.12. Various aspects of multiphase photocatalytic reactor design for wastewater treatment	54
	2.13. Scope and objectives	54
3	MATERIALS AND METHODS	57-72
	3.1. Materials used	57
	3.2. Methodology	57
	3.2.1. Synthesis of photocatalysts	57
	3.2.2. rGO synthesis	57
	3.2.3. Preparation of graphitic carbon nitride (g-C ₃ N ₄)	58
	3.2.4. Photocatalyst composite preparation	59
	3.2.5. Preparation of waste polystyrene for reuse	59
	3.2.6. Immobilisation of photocatalyst	60
	3.2.6.1. Preparation of immobilized TiO ₂ film	60
	3.2.6.2. Preparation of immobilized TiO ₂ , g-C ₃ N ₄ , and rGO admixture film	61
	3.2.6.3. Preparation of immobilised TiO ₂ /rGO/g-C ₃ N ₄ –composite film	61

CHAPTER NO.	TITLE	PAGE NO.
3.2.7.	Photocatalytic activity analysis	61
3.2.7.1.	Batch study	61
3.2.7.2.	Recirculation study	62
3.2.7.3.	Photocatalytic activity analysis in a multiphase airlift reactor under UV light	64
3.2.7.4.	Photocatalytic activity analysis in a multiphase airlift reactor under solar light	65
3.3.	Characterizations of the photocatalysts and polymer nanocomposite films	66
3.3.1.	X-ray powder diffraction (XRD)	66
3.3.2.	Scanning Electron Microscope– Energy Dispersive X-ray (SEM–EDX)	66
3.3.3.	Fourier Transform Infrared Spectroscopy (FTIR)	67
3.3.4.	X-ray Photoelectron Spectroscopy (XPS)	67
3.3.5.	Particle size analysis	67
3.3.6.	Contact angle analysis	68
3.3.7.	Profilometer	68
3.3.8.	Diffuse reflectance spectra (DRS)	68
3.3.9.	Brunauer Emmett Teller (BET) surface area analysis	68
3.3.10.	Inductively coupled plasma–optical emission spectrometry (ICP–EOS)	68
3.3.11.	Density measurement	69

CHAPTER NO.	TITLE	PAGE NO.
3.4.	Characterization of the decolourized/ degraded RTB solution	69
3.4.1.	UV–Vis Spectrophotometer	69
3.4.2.	Total Organic Carbon (TOC)	69
3.4.3.	High Performance Liquid Chromatography (HPLC)	70
3.4.4.	Mass Spectrometer (LC–MS)	70
3.5.	The equipment used for the characterization of various samples	70
4	POLYSTYRENE – TiO₂ PHOTOCATALYTIC FILMS: BATCH REACTOR STUDIES, SCALEUP AND RECIRCULATION ASPECTS	73-96
4.1.	Introduction	73
4.2.	Results and discussions	73
4.2.1.	Characterization of immobilised TiO ₂ film	73
4.2.1.1.	XRD analysis	73
4.2.1.2.	SEM and Profilometry analysis	74
4.2.1.3.	FTIR and ICP–OES analysis	75
4.2.1.4.	XPS analysis	77
4.2.2.	Photocatalytic activity analysis and optimization study	78
4.2.2.1.	Effect of catalyst loading	78
4.2.2.2.	Effect of pH	79
4.2.2.3.	Effect of initial dye concentration and reaction kinetics	79
4.2.2.4.	Effect of film thickness	82
4.2.2.5.	Effect of different light source	82

CHAPTER NO.	TITLE	PAGE NO.
	4.2.2.6. Comparison with other dyes	82
	4.2.2.7. Comparison with slurry catalyst	83
	4.2.2.8. Effect of light intensity (distance between the light source and the photocatalytic film)	83
	4.2.2.9. Effect of temperature	85
	4.2.2.10. Effect of salts and alcohols	87
	4.2.2.11. Effect of UV light on the film	88
	4.2.2.12. Recyclability	89
	4.2.2.13. Batch scale-up study of RTB solution	90
	4.2.2.14. Recirculation study	91
	4.2.3. Photocatalytic degradation analysis of RTB	92
	4.2.3.1. Total organic carbon analysis in RTB solution	92
	4.2.3.2. LC-MS analysis of RTB dye solution after degradation	93
	4.3. Conclusions	94
5	POLYSTYRENE – TiO₂, g-C₃N₄ AND rGO ADMIXTURE PHOTOCATALYTIC FILM: BATCH REACTOR STUDIES	97-114
	5.1. Introduction	97
	5.2. Results and discussions	97
	5.2.1. Characterization of photocatalyst	97
	5.2.1.1. SEM-EDX analysis	97
	5.2.1.2. FTIR analysis	99
	5.2.1.3. XRD analysis	101
	5.2.1.4. XPS analysis	102

CHAPTER NO.	TITLE	PAGE NO.
	5.2.1.5. Contact angle analysis and Particle size measurement	102
	5.2.1.6. ICP–OES analysis	104
5.2.2.	Optimization of photocatalytic parameters	104
5.2.2.1.	Effect of catalyst loading	104
5.2.2.2.	Effect of pH	105
5.2.2.3.	Effect of initial dye concentration on reaction kinetics	106
5.2.2.4.	Effect of light source	107
5.2.2.5.	Effect of H ₂ O ₂	108
5.2.2.6.	Slurry and immobilized form comparison	109
5.2.2.7.	Recyclability of PST film	110
5.2.3.	Photocatalytic degradation analysis of RTB	111
5.2.3.1.	Total organic carbon content (TOC) analysis	111
5.2.3.2.	HPLC–MS analysis	112
5.3.	Conclusions	114
6	POLYSTYRENE TiO₂, g–C₃N₄ AND rGO ADMIXTURE PHOTOCATALYTIC FILMS: MULTIPHASE AIRLIFT PHOTOCATALYTIC REACTOR STUDIES	115-128
6.1.	Introduction	115
6.2.	Results and discussions	115
6.2.1.	Characterization of photocatalyst	115
6.2.2.	Optimization of photocatalytic parameters	115
6.2.2.1.	Effect of catalyst loading	115
6.2.2.2.	Effect of D _i /D _o ratio	117
6.2.2.3.	Effect of airflow rate	118

CHAPTER NO.	TITLE	PAGE NO.
	6.2.2.4. Effect of initial dye concentration and reaction kinetics	119
	6.2.2.5. Effect of Different dyes	120
	6.2.2.6. Reusability of the catalyst film	121
	6.2.2.7. Comparison of slurry and immobilized catalyst performance	122
	6.2.2.8. Effect of different oxidizing agents in the presence of immobilized photocatalytic film (IP)	123
	6.2.3. Photocatalytic degradation analysis of RTB	124
	6.2.3.1. TOC analysis	124
	6.2.3.2. HPLC/LC – MS analysis	125
	6.3. Conclusions	127
7	POLYSTYRENE – TiO₂/g-C₃N₄/rGO COMPOSITE PHOTOCATALYTIC FILM: MULTIPHASE AIRLIFT PHOTOCATALYTIC REACTOR	129-144
	7.1. Introduction	129
	7.2. Results and discussions	130
	7.2.1. Characterization of photocatalyst and the PPCF	130
	7.2.1.1. SEM–EDX, BET surface area and Particle size analysis	130
	7.2.1.2. XRD analysis	131
	7.2.1.3. XPS analysis	132
	7.2.1.4. FTIR and Bandgap energy analysis	134
	7.2.1.5. ICP–OES analysis	135
	7.2.2. Optimization of photocatalytic parameters	137
	7.2.2.1. Effect of g-C ₃ N ₄ concentration	137

CHAPTER NO.	TITLE	PAGE NO.
	7.2.2.2. Effect of catalyst loading	137
	7.2.2.3. Effect of initial RTB concentration and reaction kinetics	138
	7.2.2.4. Effect of slurry and immobilized photocatalyst	139
	7.2.2.5. Effect of catalyst reuse	140
	7.2.2.6. Effect of waste polystyrene as a substrate material	141
	7.2.3. Photocatalytic degradation analysis of RTB	141
	7.2.3.1. TOC analysis	141
	7.2.3.2. HPLC–MS analysis	142
	7.3. Conclusions	144
8	SUMMARY AND CONCLUSIONS	145-148
	8.1. Summary	145
	8.2. Conclusions	146
	8.3. Scope for future work	147
	REFERENCES	149-196
	APPENDICES	197-202
	RESEARCH PUBLICATIONS	203
	BIO DATA	204

LIST OF FIGURES

FIGURE NO.	TITLE	PAGE NO.
1.1	Major pollutants present in wastewater	3
1.2	Wastewater treatment methods containing dye	6
1.3	Different types of AOPs	6
1.4	Mechanism of photocatalytic degradation of organic pollutant	7
1.5	Application of photocatalysts in several area of science	10
2.1	Conventional reactor selection criteria	44
3.1	rGO synthesis procedure	58
3.2	Synthesis of waste polystyrene	59
3.3	Catalyst immobilization procedure	60
3.4	Batch process for RTB dye degradation, a) polystyrene TiO ₂ film, and b) 10 ppm dye solution before and after use	62
3.5	Batch process for RTB dye degradation	63
3.6	Methodology of photocatalytic reactor scale-up studies	63
3.7	Schematic diagram of the fabricated internal loop airlift photocatalytic reactor	64
3.8	Schematic of the multiphase photocatalytic reactor under solar light	66
4.1	XRD spectra of a) Degussa P25–TiO ₂ powder, b) PST film with 12 wt.% catalyst	74

FIGURE NO.	TITLE	PAGE NO.
4.2	SEM images of a) Cross-sectional view, b) TiO ₂ powder, c) Unused polystyrene film, d) After using once under optimised condition, e) After using 10 times under optimised condition	75
4.3	FTIR data of a) plain polystyrene film, b) PST film with 12 wt.% catalyst, c) 12 wt% PST film after using once, d) 12 wt.% PST film after using 10 times	76
4.4	a) Low-resolution XPS survey spectra of the PST film b) Ti2p XPS spectra, c) C 1s spectra, d) O 1s spectra	77
4.5	Effect of catalyst loading and pH. Conditions: 200 mL of 10 ppm RTB solution, catalyst loading: 12 wt.%	79
4.6	Effect of initial dye concentration. Conditions: 200 mL of 10 ppm RTB solution, catalyst loading: 12 wt.%	80
4.7	RTB concentration vs time for different initial concentrations of RTB dye at optimized conditions a) for 30 ppm RTB solution, b) for 10, 15 and 20 ppm RTB solution	81
4.8	Decolourisation of 10 ppm 200 mL RTB solution, with catalyst loading of 12 wt.% in immobilized form using different film thickness	82
4.9	Decolourisation of 10 ppm 200 mL RTB solution, with 12 wt.% catalyst loading under UV-C, UV-A and sunlight at ambient temperatures	83
4.10	Decolourisation of different dyes. Conditions: 200 mL of 10 ppm RTB solution, catalyst loading: 12 wt.%	84
4.11	Decolourisation of 10 ppm 200 mL RTB solution, with catalyst loading of 12 wt.% in immobilized form and 0.18 g/L in slurry	84
4.12	Decolourisation of 10 ppm 200 mL RTB solution, with catalyst loading of 12 wt.% in immobilized form under different light intensity	86

FIGURE NO.	TITLE	PAGE NO.
4.13	Decolourisation of 10 ppm 200 mL RTB solution, with catalyst loading of 12 wt.% in immobilized form at different temperature	86
4.14	Decolourisation of 10 ppm 200 mL RTB solution, with catalyst loading of 12 wt.% in immobilized form under the influence of salts and alcohols	87
4.15	Decolourisation of 10 ppm 200 mL RTB solution, with catalyst loading of 12 wt.% in immobilized form prepared by different drying process	88
4.16	Recyclability test of the PST film. Conditions: 200 mL of 10 ppm RTB solution, catalyst loading: 12 wt.%	89
4.17	The physical appearance of PST films a) 12 wt.% PST film before use, b) 12 wt.% PST film after using once for RTB decolourisation, c) 12 wt.% PST film after using 10 times for RTB decolourisation	90
4.18	Effect of scale up in batch process under the optimized condition, b) Effect of recirculation for decolourisation of RTB dye at different flowrates, reactor volume 550 mL and reservoir volume 2350 mL	90
4.19	% change in TOC during the photocatalytic process. Conditions: 200 mL of 10 ppm RTB solution, catalyst loading: 12 wt.%	92
4.20	LC-MS analysis, a) HPLC data confirming degradation of RTB, before degradation (black line), after degradation (pink line). b) MS spectra after degradation at 3.2 min. Conditions: 200 mL of 10 ppm RTB solution, catalyst loading: 12 wt.% of polymer	93
4.21	Proposed degraded by-products formed after the photocatalytic degradation of RTB	94
5.1	SEM images of a) TiO ₂ , b) rGO, c) g-C ₃ N ₄ , d) cross-sectional SEM of PPF, e) PPF surface f) EDX analysis of PPF	98

FIGURE NO.	TITLE	PAGE NO.
5.2	FTIR Analysis of catalysts, a) TiO ₂ , b) rGO, c) g-C ₃ N ₄ , d) plain polystyrene film, e) PPF	99
5.3	XRD analysis of catalysts, a) TiO ₂ , b) rGO, and c) g-C ₃ N ₄	102
5.4	XPS analysis of a) photocatalyst loaded polymer film and High resolution scanning of b) C1s, c) O1s, d) Ti2p, and e) N1s	103
5.5	Investigation of unary, binary and ternary ad-mixtures in polystyrene film	105
5.6	pH Optimization (a), comparison of degradation efficiency after 60 min of UV irradiation (b)	106
5.7	Effect of dye concentration (a) on reaction kinetics (b)	107
5.8	Effect of the light source under UV-C, UV-A, and photolysis	108
5.9	Effect of H ₂ O ₂ on decolourization of RTB dye (a) and optimum H ₂ O ₂ loading (b)	109
5.10	Comparison of slurry and immobilized photocatalysts	110
5.11	Reuse of PPF under optimised conditions (each cycle 2 h).	111
5.12	TOC Analysis of the degraded dye solution	112
5.13	HPLC-MS analysis of the dye solution, a) HPLC analysis and b) MS spectra	113
5.14	The possible degraded compounds after photocatalytic treatment	113
6.1	Effect of catalyst loading (Draft tube diameter = 6 cm)	116

FIGURE NO.	TITLE	PAGE NO.
6.2	Schematic diagram of photocatalytic activity of an admixture	117
6.3	Effect of inner draft column diameter	118
6.4	Effect of aeration flowrate	119
6.5	(a) Effect of initial dye concentration and (b) reaction kinetics	120
6.6	Decolourization of RTB and two other dyes	121
6.7	Recyclability test of the photocatalytic film	122
6.8	Comparison of immobilized and slurry photocatalytic activity	123
6.9	Effect of different oxidising agents on photocatalytic activity	124
6.10	TOC analysis of the degraded RTB dye	125
6.11	HPLC–MS analysis of RTB dye	126
6.12	Degraded hypothetical by–products	126
7.1	SEM image of the a) composite photocatalyst powder, b) EDX analysis of composite powder, c) elemental mapping of composite powder, d) surface morphology of PPCF (10 wt% catalyst loading), e) EDX analysis of PPCF (10 wt% catalyst loading) and f) cross–sectional image of PPCF (10 wt% catalyst loading)	130
7.2	XRD spectra of the photocatalyst powders a) g–C ₃ N ₄ , b) rGO c) TiO ₂ , d) TiO ₂ /rGO/g–C ₃ N ₄ composite and e) PPCF film (10 wt% catalyst loading)	131
7.3	XPS spectra of the a) PPCF (10 wt% catalyst loading), b) C 1s, c) O 1s, d) Ti 2p, e) N 1s	133

FIGURE NO.	TITLE	PAGE NO.
7.4	FTIR spectra of plain polystyrene film and PPCF (10 wt% catalyst loading)	134
7.5	a) Absorbance spectra of TiO ₂ , rGO and TiO ₂ /rGO/g-C ₃ N ₄ composite and b) calculated bandgap of the composite material	136
7.6	Schematic mechanism of self-sensitized composite photocatalyst (LUMO: lowest unoccupied molecular orbital, HOMO: highest occupied molecular orbital)	136
7.7	Effect of a) g-C ₃ N ₄ loading (10 wt% catalyst loading, 10 ppm RTB) and b) catalyst loading on photocatalytic activity (10 ppm RTB).	137
7.8	(a) Effect of initial concentration of the dye and (b) the kinetics of the reaction	138
7.9	Comparison of immobilized and slurry photocatalytic activity (10 wt% catalyst loading, 10 ppm RTB)	139
7.10	Reuse of the PPCF under optimized conditions (10 wt.% catalyst loading, 10 ppm RTB).	140
7.11	a) Comparison of the photocatalytic activity of the film made with waste and pristine polystyrene, b) TOC analysis of the treated solution; (10 wt.% catalyst loading, 10 ppm RTB)	141
7.12	HPLC analysis of the solution before and after treatment (a) and MS spectra of degraded solution (b).	142
7.13	Degraded by-products from the parent dye (RTB) molecule, (HP- Hypothetical Product)	143

LIST OF TABLES

TABLE NO.	TITLE	PAGE NO.
2.1	Summary of literature regarding pure photocatalysts	16
2.2	Summary of literature regarding doped photocatalysts	19
2.3	Summary of literature regarding co-doped photocatalysts	20
2.4	Summary of literature regarding composite photocatalysts	22
2.5	Summary of literature regarding photocatalysts along with different materials (metal or non-metallic substance) or self-sensitized behaviour	23
2.6	Summary of literature regarding different types of pollutant removal by photocatalysis	27
2.7	Summary of literature regarding removal of RTB	36
2.8	Advantages of slurry and immobilized photocatalytic system	38
2.9	Disadvantages of slurry and immobilized photocatalytic system	38
2.10	Few recent studies done using polymers	45
2.11	Studies done using different types of photocatalytic reactors	47
3.1	The characterization of various sample carried out in this work	72
4.1	Kinetic study of Remazol Turquoise Blue (RTB) decolourization for different initial concentrations	81

TABLE NO.	TITLE	PAGE NO.
5.1	Details of FTIR spectra of catalysts and PPF	99
5.2	Decolourization reaction kinetics of the RTB dye	107
6.1	Kinetic study of RTB decolourization for different initial concentrations	120
7.1	Details of FTIR spectra for the PPCF film (10 wt% catalyst loading)	135
7.2	Kinetic study of RTB decolourization for different initial concentrations	139
8.1	Performance of the photocatalytic films based on decolourization, degradation, reaction rate and reuse	145

ABBREVIATIONS

BOD	Biological oxygen demand
CD	Catalyst dosage
COD	Chemical oxygen demand
D_0	inner diameter of outer tube
D_i	Outer diameter of inner draft tube
$g-C_3N_4$	Graphitic carbon nitride
IP	Immobilized photocatalytic film
MB	Methylene Blue
PC	Pollution concentration
PPF	Polystyrene photocatalytic film
PS	Polystyrene
rGO	Reduced graphene oxide
RhB	Rhodamine B
RTB	Remazol Turquoise Blue
SnO_2	Tin oxide
TiO_2	Titanium dioxide
TOC	Total organic carbon
UV	Ultra violet
WO_3	Tungsten trioxide
ZnO	Zinc oxide

N O M E N C L A T U R E

°C	Degree Celsius
λ_{\max}	Maximum Absorbance Wavelength
C	Concentration of Dye at time t
C_0	Initial Concentration of Dye
CFU	Colony forming unit
cm	Centimeter
eV	Electron Volt
g	Gram
h	Hour
k	Rate constant
Klx	Kilolux
L	Liter
\ln	Natural Logarithm
mg	Milligram
min	Minutes
mL	Milliliter
mM	Millimole
mmol	Millimole
mol	Mole
mW	Milli Watt
N	Normality
nm	Nano Meter

ppm	Parts Per Million
R ²	Regression coefficient
s	Second
U/mL	Units Per Milliliter
V	Volume
v/v	Volume/Volume
W	Watt
wt. %	Weight percentage
μm	Micrometer
μ	Microns
at.%	Atomic%
μmol	Micromole
MW	Molecular Weight

CHAPTER 1

INTRODUCTION

CHAPTER 1

INTRODUCTION

Water is one of the essential components of life on earth and access to clean drinking water is a basic human right (Angel and Loftus 2019). Due to the rapid growth of industries, climate change and demographic expansion, depletion in potable water sources is increasingly a global issue (Zhao et al. 2019). Also, different types of harmful chemical contaminants are added to the waterbodies every year thus causing a depletion in drinking water levels (Chen et al. 2019). Consequently, almost one-third of the world's population suffers from water scarcity and over one billion people lack access to clean drinking water (Zheng et al. 2017). The presence of contaminants in drinking water resources leads to water-borne diseases and a large amount of the population is affected (Ocwelwang and Tichagwa 2014). According to the World Health Organization (WHO), 3.2 million people (including children) die every year worldwide due to contaminated water consumption (Saravanan et al. 2017). The detailed analysis of wastewater sources, the impact on human life, modern treatment processes, and various other aspects are discussed in the next section.

1.1. Background and rationale

In this age, water contamination is one of the major issues to be concerned about since the rapid depletion of fresh groundwater level and the lack of managing wastewater guarantees an unsustainable life (Saravanan et al. 2017). The accumulation of toxins present in the environment occurs because of the excessive human needs and overpopulation (Ong et al. 2016). Usually, small amounts of water contaminants have a large impact on human and other living animals life directly or indirectly as it is very toxic and harmful (Luan et al. 2017). In spite of abundant sources of freshwater, the necessity of maintaining water quality is important and equally necessary for a healthy life (Renu et al. 2017). An extensive variety of complex contaminants streaming openly from various industrial and farming activities have turned into a vital issue that is influencing the environmental security. Thus, various important wastewater decontamination techniques were developed by the scientists to mineralize the differ-

ent types of pollutants present in the water (Ong et al. 2011; Deng and Zhao 2015; Hong et al. 2016).

The principal wastewater sources are from the industrial release of synthetic substances, farming developments, and other natural changes (stormwater runoff, animal feces or carcass) and can be very difficult to treat by conventional methods. The chemical water pollutants from industrial activities may exist in various forms like pharmaceutical wastes, pesticides, herbicides, dyes, and phenolic components (Carbonaro et al. 2013; Gogate and Pandit 2004). Consequently, this type of wastewater release from different sources requires appropriate wastewater treatment process plants. The innovation of different inexpensive and effective techniques for wastewater treatment are necessary to get safe drinking water. The conventional wastewater treatment methods such as sedimentation, aerobic process, chlorination (Leshuk et al. 2018; Pirilä et al. 2015; Nidheesh et al. 2018) are unfit or inefficient or expensive or time-consuming or unable to breakdown the pollutant completely into an end product that is harmless. When compared with different techniques, photocatalysis is one of the best methods for environmental remediation because of its inherent advantages (Hennig and Billing 1993; Hashimoto et al. 2006). This chapter mainly discusses about the photocatalytic process, its essential principles, mechanism, benefits, and the difficulties of photocatalysis in detail.

1.2. Sources of potable water and wastewater

The natural sources of water can retain the contamination stack up to a specific limit without any impact on its quality (Nan et al. 2010; Kant 2012). In fact, there could be no issue of water contamination if the impurity load remains constant and below the safe discharge limit. In the recent decades, water contamination has moved to the highest point of the global political plan because of its undesirable health and environmental impacts (Angel and Loftus 2019). The contaminants discharged from human activities are the principal source, which affects the majority of the potable or fresh water bodies in the environment (Zolgharnein et al. 2011; Renu et al. 2017). Among several sources of potable water (streams, river, rainwater, ground water etc.), most of the sources are getting contaminated or easily inaccessible to human.

The major pollutant sources are (Herrmann and Guillard 2000; Carbonaro et al. 2013 ; Eng et al. 2014 ; Ulson de Souza et al. 2007) domestic (kitchen, restaurants, bathroom,

toilet, hospitals etc.), agriculture (Dairy farming, fertilizer, pesticide, slaughtering house etc.), industrial (pulp and paper, dye and paint, food, petrochemical, textile etc.) and natural (death of marine animals, volcano eruption near water sources etc.).

It has been reported that the organic dye colours are one of the main components of toxic compounds discharged into wastewater from industries such as textile, dye and pigment, pulp and paper, and tannery industries etc (Han et al. 2009; Sridewi et al. 2011; Rodríguez Couto et al. 2002; Sivakumar et al. 2013). Out of these industries, the textile industries release a huge number of contaminants, often untreated, into the water bodies thus posing a serious threat to the environment. About 10–15% of the dyes used during the manufacturing processes in the world are lost as waste and discharged as effluents into the environment (Kuen and Tayade 2014). On a worldwide scale, over 0.7 million tons of organic dyes are produced each year mainly to be used in the textile, leather goods, printing, food, and cosmetics. There are millions of products produced by dye utilizing industries every year leaving coloured wastewater behind (Saravanan et al. 2017). The main contaminants in dye wastewaters are suspended solids, COD, colour, acidity, and other dissolvable substances (**Figure 1.1**) (Sadi et al. 2015).

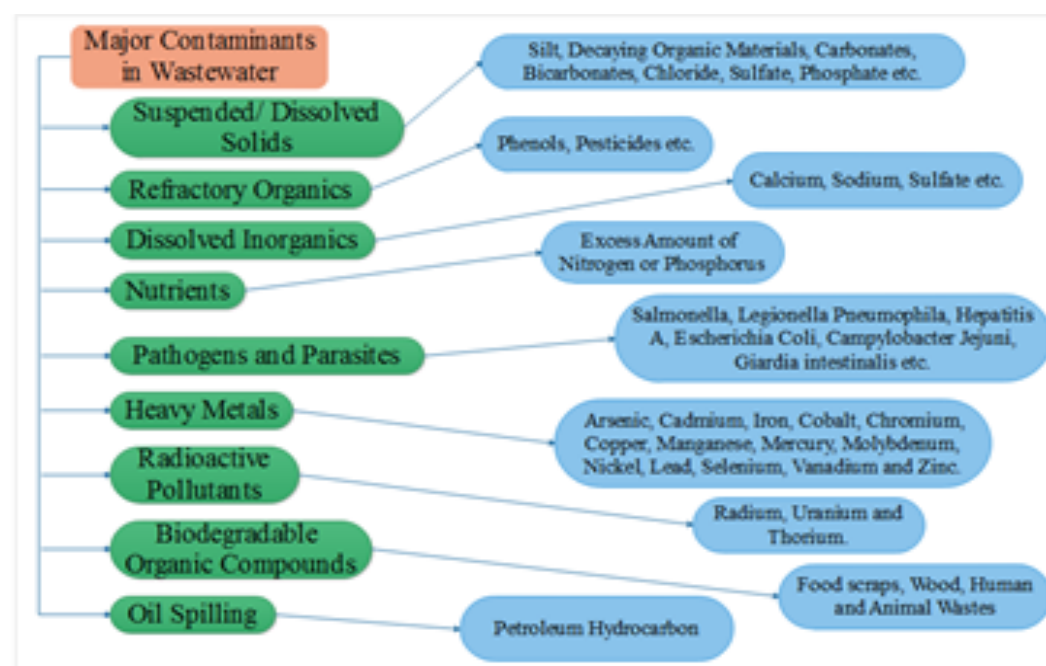


Figure 1.1: Major pollutants present in wastewater.

The textile industry utilizes around 21–377 m³ of water for each ton of textile produced and subsequently produces substantial amounts of toxic wastewater from the various steps of dyeing and finishing in every batch (Saravanan et al. 2017). The wastewater created by the textile industry is evaluated as the dirtiest among every single industry. The textile industry uses around 10,000 distinct dyes and pigments, over half of which are azo dyes (~50-70%) (Kuen and Tayade 2014).

The textile wastewater treatment is an intense issue because of a few reasons which are described as follows:

- ❖ Presence of toxic metals (reason for strong colours in synthetic dyes, the presence of metals like Cr, As, Cu etc.) (Marchis et al. 2011)
- ❖ The presence of large amounts of dissolved solids in the effluent (Gupta et al. 2015)
- ❖ Dyes are recalcitrant molecules. Recalcitrant means that the molecules are complex in structure and therefore very difficult or resistant to break down easily (Pardiwala et al. 2017; Vaiano et al. 2014)
- ❖ The presence of dissolved silica and free chlorine (Frontistis et al. 2012)

Most dyes utilized in the textile industries are not affected by light and not naturally degradable since dyes usually have a synthetic origin and complex aromatic molecular structures which make them highly stable and more difficult to biodegrade. Pagga and Brown (1986) reported that out of 87 dyes tested, only 62% are biodegradable. The same authors estimated that about 12–15% of these dyes are discharged as effluents during the manufacturing process.

1.3. The necessity of treating wastewater

Water is a key component of life and has to be consumed in fresh form else it can cause critical health problems. Since wastewater contains toxic components, it is necessary to treat it before discharging it to any waterbody. A few important reasons to treat wastewater before discharging it into the environment (Salgot and Folch 2018) such as, a) to meet the need of freshwater, b) to protect the aquatic animals from exposure to harmful chemicals, c) to protect the environment, d) to overcome the water scarcity, e) to reuse it for different purposes, and f) to restore the balance of nature.

1.4. Treatment processes for industrial wastewater

Wastewater treatment and reuse is a crucial part; several conventional economical processes such as physical, chemical, and biological treatments (Pang and Abdullah 2013) are in use for a long time. The major ecological problem is the mineralization of colour containing wastewater from textile and dyestuff effluent. Several number of traditional treatment processes such as coagulation, anaerobic process, membrane separation have been utilized in different industrial wastewaters, such as chemical, food, pharmaceutical, and textile effluents (Goode et al. 2013; Lin et al. 2017; Ghaly et al. 2013). Traditional organic wastewater treatment processes are not effective as the dyes are recalcitrant in nature and the dye wastewaters carry a high salt content. Chlorination and ozonation are very effective processes in this regard, but their high operating cost makes them unpopular (Kato et al. 2005; Zhang and Gamage 2010). The traditional physical techniques, for example, adsorption on activated carbon, reverse osmosis, ultrafiltration, coagulation with chemical agents, ion exchange, and so on (**Figure 1.2**), have been in use for the removal of dyes from wastewater (Vijayageetha et al. 2014; Munari et al. 1990; Sivamani and Leena 2009). These methods are effective to transfer the organic pollutants from the liquid phase to the solid phase, thereby creating secondary contamination which requires additional treatment of solid wastes and recovery or regeneration of the solid phase which makes the process costlier.

The following fundamental factors must be considered in the dye wastewater treatment processes such as, a) Treatment capability, b) Complete mineralization of parent and intermediate contaminants, c) The total productivity of the wastewater treatment process, d) Recycling capacity and potential utilization of treated water, e) Cost-adequacy and environmental safety.

For these reasons, the total oxidation of the pollutants into CO₂ and H₂O has been taken into consideration by the advanced oxidation processes (AOPs), which seems to be one of the most effective processes in this regard (Deng and Zhao 2015). As of date, AOPs are the most appropriate, modern and popular method to mineralize the organic pollutants present in wastewater. Based on the catalyst and pollutant phase, AOPs can be classified as shown in **Figure 1.3** (Chan et al. 2011).

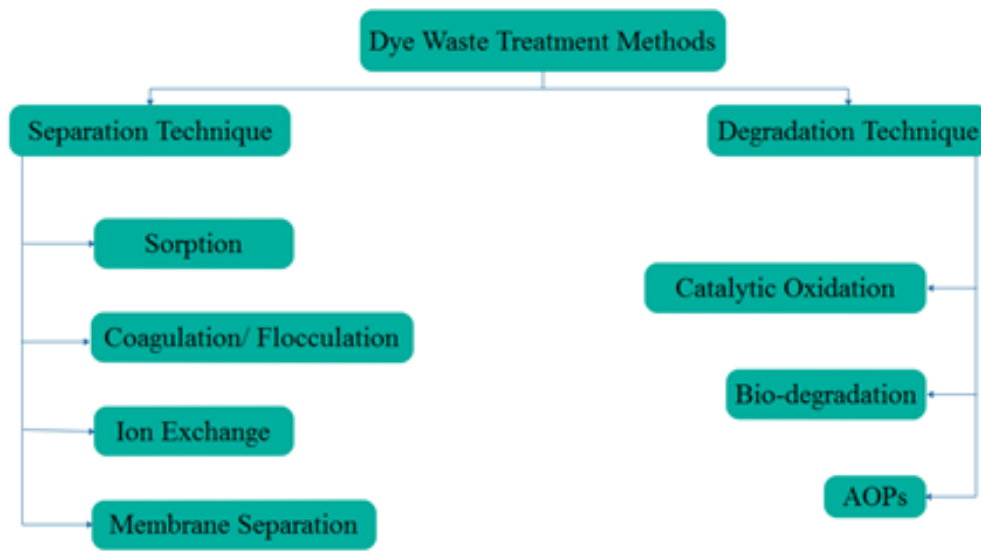


Figure 1.2: Wastewater treatment methods containing dye.

AOPs are capable of destroying various pollutant present in wastewater such as pesticides, dyes, herbicides, organic halogens, and petroleum constituents. The above mentioned AOPs basically use three different oxidizing reagents (oxygen, ozone and hydrogen peroxide) in a different combination or applied with UV irradiation and/or with various types of homogeneous or heterogeneous catalyst mixture (Hisaindee et al. 2013; Stasinakis 2008; Kuen and Tayade 2014; Verfahrenstechnik 1996; Miguel et al. 2012; Rajeshwar 2011; Osugi et al. 2006). The generation of high $\dot{O}H$ radicals or super oxidant radicals (\dot{O}_2^-) leads to higher oxidation rates. Among the several AOPs, photocatalysis is one of the widely used wastewater treatment processes for its various beneficial aspects.

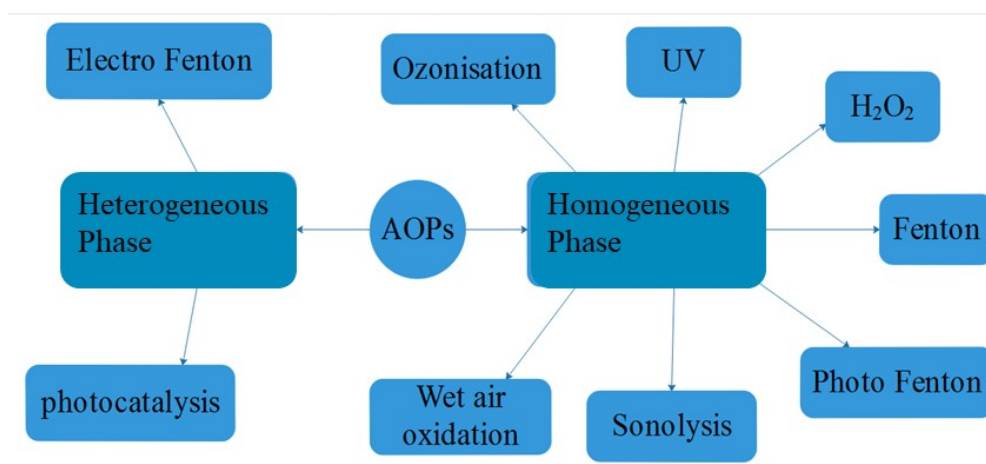


Figure 1.3: Different types of AOPs.

1.5. Photocatalysis

The photoexcitation of semiconductor with UV light is one of the best-advanced oxidation technologies among all (Lai and Lee 2009). Photoactivated semiconductor produces electron-hole pairs, electrons (e^-) jumps to the conductivity band, and holes (h^+) are assembled in the valence band (**Figure 1.4**) (Jarandehi et al. 2008; Turchi 1990; Regmi et al. 2018; Tang et al. 2018).

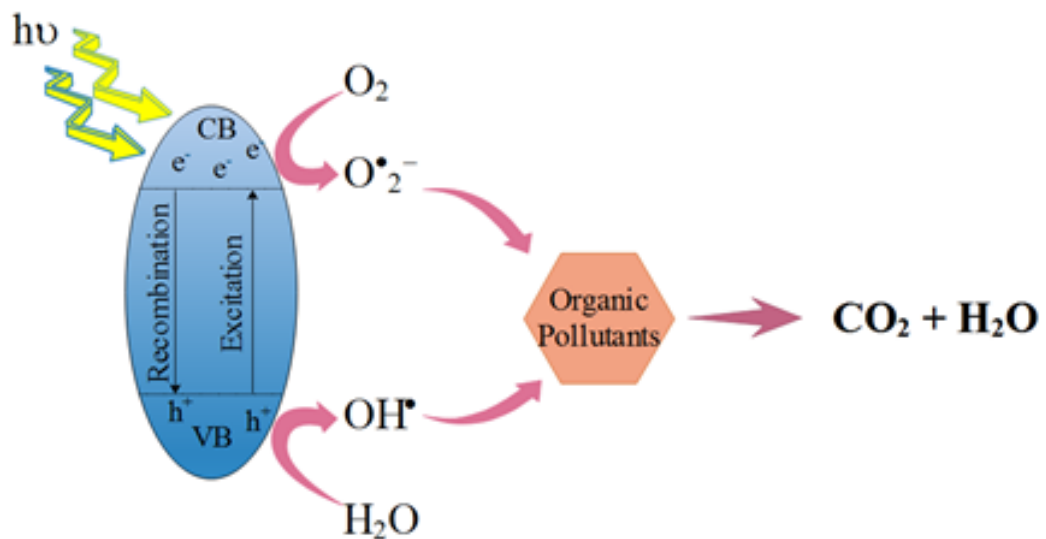
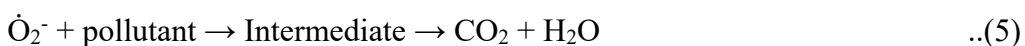
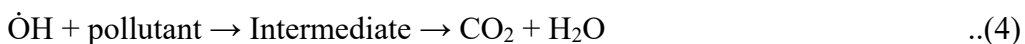
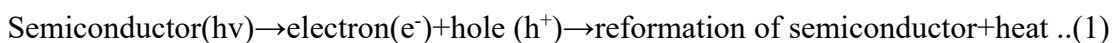


Figure 1.4: Mechanism of photocatalytic degradation of organic pollutant.

The photogenerated electrons and holes are expected to diffuse to the surface and react with the electrophilic oxygen molecule and a nucleophilic water molecule to produce super oxidant radical and hydroxyl radical respectively. The generated \dot{O}_2^- and $\dot{O}H$ radicals reacts with the organic pollutants present in the wastewater leaving CO_2 and H_2O behind (Fujishima et al. 2000). The photocatalysis process can be described by four simple steps namely, a) absorption of light to generate electron-hole pairs, b) separation of excited charges, c) transfer of electrons and holes to the surface of photocatalysts, d) the utilization of charges on the surface for oxidation reactions (Singh et al. 2013; Zhu and Wang 2017).



There are two types of photocatalysis i.e., homogeneous and heterogeneous photocatalysis. In homogeneous photocatalysis (Ollis 1984; Chen et al. 2000), the catalyst, as well as the reactant, are in the same phase. Most commonly used homogeneous photocatalysts include photo-fenton and ozone system. The main parameters affecting this process are the concentration of oxidizing agent, pH of the solution and intensity of UV. In homogeneous photocatalysis, at least three important challenges need to be addressed before it can be more widely used.

- ❖ The solubility of the photocatalysts makes it difficult and almost impossible to separate them from the solution after operation either for reuse or for the purification of products or both.
- ❖ Homogeneous molecules absorb very small amount of solar irradiation
- ❖ The photocatalytic activity and stability of homogeneous photocatalysts depend on their molecular structure.

In the case of heterogeneous photocatalysis (López-Muñoz et al. 2011; Chen et al. 2000), the catalyst and reactant exist in different phases. Catalyst usually exists in a solid phase while reactant is in a liquid phase. Heterogeneous photocatalysis possesses some advantages over homogeneous photocatalysis, such as separation and regeneration of the catalyst, eco-friendliness and complete mineralization of pollutant without producing any harmful end-products. The semiconductor metals are generally used as a heterogeneous photocatalyst such as ZnO, TiO₂, WO₃ etc.

There are several advantages of the heterogeneous photocatalytic process (Stasinakis 2008)

- ❖ **Green technology:** does not produce any sludge or harmful product after the waste treatment.
- ❖ **Versatility:** can be used for multiple applications in one operation; H₂ production as well as pollutant degradation, water splitting as well as electricity production etc. Organic or inorganic contaminants can be removed simultaneously from wastewater by oxidation or reduction reaction.
- ❖ **Energy efficiency:** since multiple applications are possible in the same operation, saves time as well as energy. In a typical photocatalytic wastewater treatment pro-

cess very less amount of energy is required compared to RO, UV, and membrane separation etc.

- ❖ **Cost-effectiveness:** since this process needs only light energy to activate the catalyst for carrying out the degradation process, it is expected to be cost effective.
- ❖ **Higher resistance to toxic pollutants:** the semiconductor photocatalysts are capable of mineralizing the toxic pollutants without affecting itself.
- ❖ **The mineralization of low concentrations of contaminants:** According to recent research, photocatalysis can be used to treat very small or trace amounts (in ppm or even ppb levels) of pollutants present in wastewater.
- ❖ **Simple, light apparatus:** the photocatalytic process is very simple, and reactors consist of only a few simple parts. It can be easily fabricated at low cost.

An ideal photocatalyst should have the following properties (Singh et al. 2013), (a) highly stable, (b) economical, (c) non-toxic (to environment or humans), (d) high turnover, (e) can be supported on various substrates easily, (f) complete destruction of organic pollutants into harmless compound, (g) high catalytic activity, (h) strong oxidizing power, (i) stable against photo-corrosion, (j) chemically and biologically inert.

TiO₂ is one of the most widely used photocatalysts as it has almost all the characteristics of an ideal photocatalyst. There are other photocatalysts that work as good as TiO₂, namely graphene oxide, g-C₃N₄, ZnO, SnO₂, ZrO₂, WO₃, Si, CdS, ZnS, SrTiO₃, WSe₂, Fe₂O₃ etc (Bhatkhande et al. 2002).

The application of photocatalysts is not limited only in water treatment or disinfection process; it is widely recognized as a feasible solution to environmental related problems. The photocatalysts are being used in a variety of applications across a broad range of research areas, including especially in the pharmaceutical and energy-related fields. The photocatalyst can also be used to maintain the indoor air quality by removing volatile organic compounds, air borne bacteria, virus, fungi, microorganisms from residences, office buildings, factories, spacecraft and aircraft (Yu et al. 2016; Shang et al. 2003; Kato et al. 2005; McCullagh et al. 2011). The biological, hospital and the medical applications include disinfection, bioimplants, and tumor treatment (Zhang and Gamage 2010). In cosmetics (as a sunblock), medicines, tablets, toothpastes and

food (as a colouring agent), low concentrations of TiO_2 is used frequently (Taoda 2009). There are other applications of photocatalysts as shown in **Figure 1.5**.

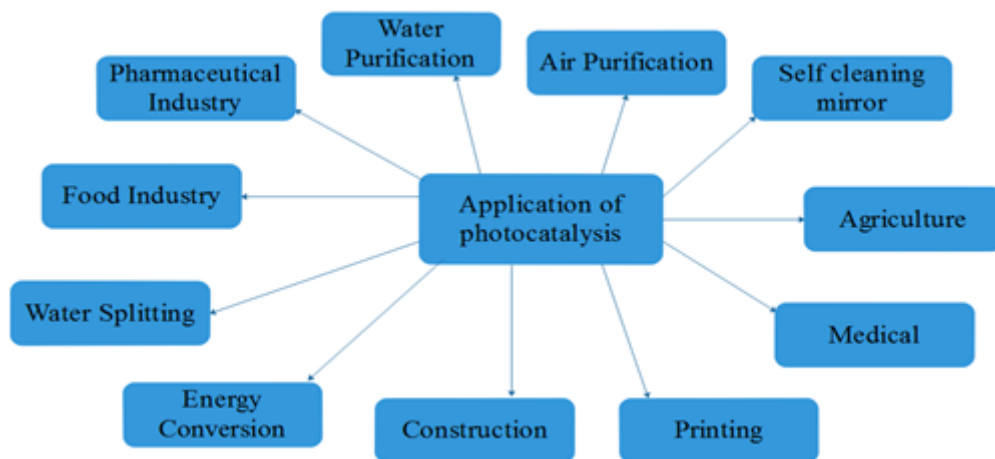


Figure 1.5: Application of photocatalysts in several area of science.

Even though the photocatalytic process has several advantages, it has a few drawbacks, which are listed below with strategies to overcome these difficulties such as

- ❖ **Separation:** The separation of powdered photocatalysts after the operation in the slurry reactor is a big challenge as of now. It is also time-consuming, expensive and difficult. To overcome this disadvantage, photocatalysts can be immobilized into different substrate materials (Devipriya and Yesodharan 2005; Abdel-Maksoud et al. 2018).
- ❖ **Reusability:** The adsorption and photocatalytic activity both are taking place on the catalyst surface; there is a great possibility of reduction in catalyst activity. To overcome this problem, photocatalyst can be reactivated by catalyst surface cleaning (Zhu et al. 2012; Sharma and Singhal 2014; Xue et al. 2016).
- ❖ **Activation energy:** Most of the photocatalysts work under UV light, which means high operating cost. To defeat this problem photocatalysts can be doped with some other metal or non-metallic substance (Dillip et al. 2017; Haarstrick et al. 1996; Yu et al. 2016; McIntock 1965; Perkowski et al. 2006).
- ❖ **Low photon quantum yield:** The quantum yield is the ratio of photons emitted to photon absorbed. In case of high bandgap photocatalysts, the quantum yield is very low since high activation energy is required. To solve this problem, photocatalysts with low bandgap or composite or doped or co-doped ma-

terials can be used instead (Dillip et al. 2017; Rajeshwar 2011; Brooms et al. 2014).

In this thesis, the commercially available TiO_2 and synthesized rGO, g- C_3N_4 , and $\text{TiO}_2/\text{rGO}/\text{g-C}_3\text{N}_4$ -composite nanostructured powders were immobilized in polystyrene films and employed for the photocatalytic degradation of RTB dye. The characterizations were done using SEM-EDX, FTIR, XPS, XRD, ICP-OES, BET-Surface area analyzer, particle size analyzer, DRS, etc. Initially, the photocatalytic performance of the prepared TiO_2 polystyrene film was checked in a batch reactor, scaled up batch reactor, and recirculation reactor under UV light. To enhance the photocatalytic activity, a polystyrene (TiO_2 , rGO, and g- C_3N_4)-admixture film was used in a batch reactor as well as in a novel multiphase airlift photocatalytic reactor under UV light. The detailed analysis of the synergistic effect of the catalyst admixture was analyzed in this work. To make this process economical and suitable for large scale application, a polystyrene $\text{TiO}_2/\text{rGO}/\text{g-C}_3\text{N}_4$ -chemical composite film was used in an airlift reactor under sunlight. The volume of the reactors was varied from 200 – 2900 mL, and the degradation of Remazol Turquoise Blue was confirmed by TOC and HPLC analysis. The optimization of photocatalytic reaction parameters (effect of catalyst loadings, pH, initial dye concentration, light source, polystyrene photocatalytic film thickness, recyclability the film, oxidizing agents, waste polystyrene, etc) as well as the novel reactor parameters (recirculation rate, air flow rate, diameter ratio, etc) were investigated in details systematically. The possible effect of several parameters on photodegradation is studied and analyzed with proper justifications. Another approach has been used to make this process appropriate for industrial scale application namely the use of waste polystyrene as a substrate material which showed significant promise in this regard.

CHAPTER 2

**LITERATURE
REVIEW**

CHAPTER 2

LITERATURE REVIEW

2.1. Invention and evolution of photocatalysis

Photocatalysis dates back to the 1930s when Plotnikov mentioned photocatalysis in his book “Allgemeine Photochemie” (Dhar 1937). Later in the early 1950s, a kinetic study of photo-oxidation in aqueous suspension is published in a book named “Chemical Kinetics” by Keith J. Laidler (Laidler 1950). Since then, a new study was reported in 1965, by Markham and Upreti on the photolysis effect of zinc oxide electrode (Markham and Upreti 1965). Later at the beginning of the 1970s photocatalysis gained much attention and various reports were brought out describing the chemical reaction taking place on the surface of the TiO_2 and ZnO metal oxides (Bickley and Munuera 1973; Childs and Ollis 1980; Frank and Bard 1977; Fujishima and Honda 1972; Hashimoto et al. 2006; Hsiao et al. 1983; Kraeutler and Bard 1978; Matsunaga et al. 1985a; Takizawa et al. 1978).

In 1972, Fujishima and Honda noticed the water splitting phenomenon by TiO_2 electrode under the influence of UV light (Fujishima and Honda 1972). Though this was a groundbreaking invention, it was not accepted by other electrochemists as it was difficult to believe that the light can be used for energy source and production of oxygen is possible in such a low voltage (1.23 V). That point forward, for basic understanding and improvement of this process, substantial research work was performed by physicists, chemists, and chemical engineers (Bickley and Munuera 1973; Frank and Bard 1977). At the end of the 1970s and the early 1980s, with the increasing interest and urgent need of eco-friendly waste treatment and energy generation concerning environmental safety, researchers started paying attention to photocatalysis processes (Frank and Bard 1977; Kraeutler and Bard 1978; Takizawa et al. 1978). Such studies are frequently related to air pollution, wastewater treatment, energy renewal and energy storage. Most of the research was carried out using TiO_2 since it is considered as an almost ideal photocatalyst. In this work, the main focus has been given in wastewater treatment by photocatalysis (Boonen and Beeldens 2014; Jitta et al. 2015).

2.2. Different forms of heterogeneous photocatalysts

Since small particle size is directly proportional to the high surface area, nanoparticles of the photocatalyst are preferable for most of the photocatalytic process (Bolis et al. 2012). Since the 1970's, photocatalysts have evolved a lot; modified or decorated or altered or transformed photocatalysts are getting popular among scientists and researchers. Several kinds of modified photocatalysts (pure, doped, co-doped, surface sensitised, composite etc) (Shen et al. 2017a) used for wastewater decontamination discussed below:

2.2.1. Pure form

In the beginning, photocatalytic nanoparticles have been used in pure form, which works only under UV light in most of the cases since the bandgap is high (Pujara et al. 2007). Among several pure photocatalyst, TiO_2 is the most popular kind because of its various benefits as mentioned earlier (Singh et al. 2013). TiO_2 can be synthesised from the mined ore containing titanium by the chloride process and the sulphate process for industrial scale, but in lab scale hydrothermal and sol-gel is the most popular method to consider for the synthesis (Wahyuningsih et al. 2018). The chemical and physical properties of the photocatalyst exhibits different characteristic based on the synthesis procedure; co-precipitation, flame hydrolysis, impregnation and chemical vapor deposition are few more photocatalyst synthesis process used now and then based on the requirement (Bin Mukhlis et al. 2013). The pure photocatalyst means that there is no modification in the photocatalyst interior. Few examples of pure photocatalyst for wastewater treatment application are given below in **Table 2.1**.

From the table, it can be seen that the TiO_2 photocatalyst was used most of the time, since it is the most popular catalyst for wastewater treatment. All the above-mentioned operations are carried out under UV light because of the large bandgap possess by the pure photocatalysts. The degradation rate of the wastewater was different as the pollutants were non-identical in each case with distinct concentrations and volume.

2.2.2. Doped form

Doping is a mixture of different material but single phase where alteration of the element takes place in atomic level to change their properties and in this case to make it work under visible light or sunlight. The doped material can be developed by several methods such as, sol-gel (Ren et al. 2016), thermal hydrolysis (Stengl et al. 2016), solvothermal method (Huang et al. 2016; Sun et al. 2013), ionothermal method (Lai et al. 1996), solution-based reduction method, combustion method (Ahmad et al. 2015; Dhiman et al. 2012), vapor-fed aerosol flame synthesis, evaporation-induced self-assembly method, solution-based oxidative method, metallic reduction method (Huang et al. 2018). In most of the cases, doped material works under visible light which makes it more efficient and cost-effective as mentioned in **Table 2.2**.

From **Table 2.2** it can be easily concluded that the doped photocatalyst works better than the pure catalyst under visible light. Also, doping of the photocatalyst enhances the photocatalytic activity.

2.2.3. Co-doped form

For further reduction in band gap energy, sometimes more than one material is introduced into the pure photocatalyst. The co-doping of the photocatalyst can take place by several methods such as, sol-gel method (Xue et al. 2016a), microemulsion method (Lavand and Malghe 2016), ionic liquid assisted method (Yu et al. 2013) etc. The photocatalytic efficiency increases and reuse of the catalyst also possible for several times without notable reduction in performance. From **Table 2.3** it can be concluded that the incorporation of the doping metal or non-metal ions into the photocatalyst leads to reduction in the electron-hole pair recombination that enhanced the photocatalytic activity upon light irradiation.

2.2.4. Composites

Creating photocatalyst composites containing multicomponent heterojunctions in a semiconductor material is an effective approach to design an effective photocatalyst system (Tan et al. 2013). The popular methods used for the synthesis of photocatalyst

Table 2.1: Summary of literature regarding pure photocatalysts.

Photocatalyst	Pollutant	Parameters/ optimized conditions	Light source	Findings	Reference
TiO ₂	Nitrobenzene sulfonic acids	CD in Slurry: 2 g/L. Immobilized materials: red brick, fibres, and glass.	UV	Almost complete mineralization occurred in less than 1 h in slurry form, whereas in immobilized condition into fibre and glass substrate, it took 15 and 30 h respectively for 100% degradation.	(Rachel et al. 2002)
TiO ₂ in fluidised bed reactor	RhB	CD: 25 g/L, PC: 5-29 mM	UV	Best degradation efficiency (>90%) noticed with 4 lamps within 180 min.	(Na et al. 2004)
TiO ₂ in a bubble column reactor	4-Nitrophenol	Gas flow: 5 L/min, PC: 0.25 mM, V: 4 L	UV	Almost complete destruction of the pollutant, as well as TOC removal, noticed within 400 min.	(Christensen et al. 2005)
TiO ₂	phenol-4-sulfonic acid	CD: 0.02% (w/v), pH: 4.5, presence of anions: reduces the efficiency, PC: 80 ppm, and photon flux: 0.594 mol photons/(m ² hr)	UV	90% degradation occurred in 4 h.	(Pujara et al. 2007)
TiO ₂	Flumequine (18 ppm)	CD: 8.97 g, pH: 1.5, light wavelength 254 nm.	UV	80% degradation in 20 min	(Mansilla et al. 2007)

Photocatalyst	Pollutant	Parameters/ optimized conditions	Light source	Findings	Reference
ZnO	MB	-	UV	More than 95% of degradation occurred in 60 minutes	(Nirmala et al. 2010)
TiO ₂	Soda pulp bleaching effluents (100 mL) from chlorination (C) and alkaline extraction (E).	Effluent C: CD: 3 g/L, pH: 6, NaOCl conc.: 0.01 mol/L; Effluent E: CD: 2.5 g/L, pH: 4, NaOCl conc.: 0.03 mol/L.	UV	Effluent C and E showed 30% and 57% COD removal, and 47% and 37% degradation in 6 h respectively.	(Dhir et al. 2011)
TiO ₂ /Perlite	Ammonia (80 to 850 ppm, 1.5 L)	CD: 11.7 g, PC: 170 ppm, pH: 11, V: 1 L, UV light power 250 W	UV	68% degradation occurred in 180 minutes; nitrogen gas production rate is higher at 60 min (12×10^6 mol/min).	(Shavisi et al. 2014)
TiO ₂	Triton X-100 (20 ppm)	CD: 1g/L, pH: 6, PC: 20 ppm, addition of hydrogen peroxide, potassium persulfate, and Tert-butyl alcohol.	UV	Within 120 min, 200 ppm of Triton X-100 can be degraded up to 67% by the addition of both 1 g/L titania and 1 g/L H ₂ O ₂ .	(Zhang 2014)
TiO ₂ -perlite	Phenol (10 ppm, 30 mL), and MB	CD: 100 mg/ 30 mL	UV	85% degradation of MB	(Długosz et al. 2014)

composite material are hydrothermal (Tan et al. 2013), chemical etching (Iatsunskyi et al. 2015), ultrasonic dispersion (Xu et al. 2016b), sol-gel (Shang et al. 2003), ion-implantation (Devipriya and Yesodharan 2005) etc. the composite materials used in several studies for the wastewater treatment have shown promising outcome as shown in **Table 2.4**. The table explains the destruction of various pollutant present in wastewater by using composite material. From the table, it can also be observed that the composite material shows improved photocatalytic activity under visible light or solar light in most of the cases.

2.2.5. Other forms

There are few other form of photocatalyst, which can be used for wastewater treatment process as discussed in **Table 2.5**. The photocatalyst in any form, described in the tables can be used for the wastewater treatment, but the outcome can differ based on the catalyst use.

2.3. Mineralization of different types of contaminants from wastewater by photocatalysis

Though wastewater coming from distinct sources contains different types of pollutants, the photocatalytic treatment process is identical. The major studies reported on photocatalytic wastewater treatment includes removal of several toxic constituents from contaminated water such as, carcinogenic heavy metals, sewage, petroleum oil, food oil, Pesticides and fertilizer, Organic compounds, Insecticides and herbicides, Surfactants, Pharmaceuticals, Microorganisms, dyes etc (Lenzi et al. 2011; Shivaraju 2011; Soroush et al. 2017; Mukherjee et al. 2014; Abdennouri et al. 2015; Pardiwala et al. 2017). The toxic heavy metals discharged from (Barakat 2011) various sources into freshwater can be a lethal source of poison. The major sources of the toxic heavy metals (arsenic, cadmium, copper, chromium, nickel, mercury, lead etc.) into the water are from mining and industrial wastes, lead-acid batteries, fertilizers, treated woods, paints, and aging water supply bodies (Dou and Chen 2011; Idris et al. 2011; Fatehizadeh et al. 2014). Heavy metal intoxication is rare but it is dangerous, whereas water pollution by sewage is very frequent. The term 'sewage' is used for wastewater that usually contains urine, faeces, and laundry waste.

Table 2.2: Summary of literature regarding doped photocatalysts.

Photocatalyst	Pollutant	Parameters/ optimised conditions	Light source	Findings	Reference
B-TiO ₂ , and N-TiO ₂	MO	Doped catalyst: TiO ₂ -B ₉ -N ₅ , PC: 18 ppm, V: 350 mL	Visible light	Addition of Boron and Nitrogen enhances the photocatalytic activity.	(Gombac et al. 2007)
Ag doped TiO ₂	Direct Red 23	CD: 3 g/L of 1.5%Ag-TiO ₂ , pH: 6.	UV	More than 54% degradation noticed after 20 minutes	(Sobana et al. 2008)
Nitrogen-doped TiO ₂	RhB	CD: 50 g, PC: 3 mM	Visible light	Almost complete decolourization occurred within 60 minutes.	(Mekprasart and Pecharapa 2011)
N-doped TiO ₂ /g-C ₃ N ₄ composites	RhB	CD: 0.2 g, PC: 2.5 ppm, V: 100 mL	Fluorescent lamp	C ₃ N ₄ -TiO ₂ of 8 wt.% shows the highest photocatalytic activity.	(Yang et al. 2011)
Silver doped TiO ₂ nanoparticles	MO	CD: 0.2 g of 1.5 mol% of Ag-doped-TiO ₂ , PC: 10 ⁻⁴ M, V: 500 mL	UV-visible light	Doped TiO ₂ works better compared to plain TiO ₂ .	(Nainani et al. 2012)
TiO ₂ -AgCl	MB	The different calcination temperature is used to prepare doped TiO ₂ -AgCl	UV	Calcined TiO ₂ -AgCl at 400 degrees is more efficient than the P25 TiO ₂	(Sangchay et al. 2012)
N-doped TiO ₂ /s-PS aerogels	MB	CD: 0.13 g/L, PC: 7.5 ppm, V: 75 mL	Visible light	N-doped TiO ₂ /s-PS aerogels converts 30% dye in 180 minutes	(Vaiano et al. 2014)
NiO/N-doped TiO ₂ nanotubes	RhB	Ni ²⁺ concentration: 1 mol/L, PC: 5 ppm, V: 15 mL	Visible light	The photocurrent density of doped material is about 9.6 times that of TiO ₂	(Li et al. 2015a)

Photocatalyst	Pollutant	Parameters/ optimised conditions	Light source	Findings	Reference
				nanotube.	
Yttrium-doped CeO ₂	Acetaldehyde	CD: 10 mg (1:0.1 mole ratio)	UV	Doped catalysts showed better performance.	(Xu et al. 2016a)

Table 2.3: Summary of literature regarding co-doped photocatalysts.

Photocatalyst	Pollutant	Parameters/ optimised conditions	Light source	Findings	Reference
Boron – iron Co-doped and boron-doped TiO ₂	Toluene	B-TiO ₂ , V: 7 µL	UV or visible light	Complete degradation achieved in 3 h.	(Khan et al. 2008)
Fluorinated B/C-codoped TiO ₂	RhB	CD: 40 mg, PC: 10 ⁻⁵ M, V: 20 mL	Visible light	Doped catalyst enhances the photocatalytic activity.	(Yu et al. 2013)
B , Ce Co- doped TiO ₂	Phenol	CD: 1 g/L of B _{0.02} Ce _{0.008} –TiO ₂ fibers, PC: 20 ppm	UV	90% degradation within 4 h.	(Qiu et al. 2014)
B-N-codoped TiO ₂ in parlite	RhB	CD: 0.018 g/ cm ² , B _{0.57} –N-TiO ₂ /EP, PC: 2.5 ppm	Visible light	94% degradation in 3 h.	(Wang et al. 2015)

Photocatalyst	Pollutant	Parameters/ optimised conditions	Light source	Findings	Reference
Silver/copper-nitrogen co-doped sodium hexatitanate nanostructure	MO (10-5 mol/L) and 4-chlorophenol (5×10^{-5} mol/L)	CD: 1 g, V: 80 mL	Visible light	70% degradation noticed after 3 h.	(Veldurthi et al. 2015)
B-N-TiO ₂ /expanded perlite	RhB	CD: 6 mg/g (24 wt.% TiO ₂), V: 60 mL, PC: 10 ppm	UV and visible light	99.1% degradation under visible light (5 h), 99.8% degradation under UV light (1 h).	(Xue et al. 2016a)
Carbon- and iron-modified TiO ₂	Ethidium bromide	CD: 1 g/L, Temperature: 300 degree C, PC: 10 ppm, Irradiation time: 90 min	Visible light	Almost complete degradation observed in 90 minutes.	(Lavand and Malghe 2016)
Co-B-codoped TiO ₂	p-nitrophenol and RhB	CD: (Co (0.1 at.%) & B (2 at.%) 20 mg, PC: 10 ppm, V: 50 mL.	Visible light	For more than 90% degradation p-nitrophenol took 4 h, whereas RhB took only 2 h with co-doped photocatalyst.	(Jaiswal et al. 2016)

Table 2.4: Summary of literature regarding composite photocatalysts.

Photocatalyst	Pollutant	Parameters/ optimised conditions	Light source	Findings	Reference
Carbon nanotube-TiO ₂	Four different Phenolic compounds	CD: 1.2 g/L, pH: natural (5.6), hydrogen peroxide concentration, substrate amount, V: 250 mL	UV and visible	Degradation rate: 4-nitrophenol < 4-hydroxy-benzoic acid < 4-chlorophenol < 4-aminophenol.	(Silva and Faria 2010)
TiO ₂ /ZnO/chitosan nano-composite	MO	CD: 0.5 g/L, pH: 5.6, PC: 15 ppm, V: 100 mL	Simulated solar irradiation	More than 97% degradation in 4 h.	(Zhu et al. 2012a)
MnTiO ₃ /TiO ₂ Heterojunction Composites	Reactive Blue 4	PC: 50 to 250 ppm, V: 100 mL	UV	After 5 th recycle the degradation efficiency decreases from 92% to 81%.	(Sivakumar et al. 2013)
Polyaniline /TiO ₂ /ZnO Composite	Phenol (101 ppm) and p-cresol (106 ppm)	CD: 0.5/TiO ₂ / ZnO, pH: 7.2, V: 1 L	UV	99.2% and 97% degradation of phenol and p-cresol in 10 h. High reduction in BOD and COD have been observed.	(Brooms et al. 2014)
BiO ₁ /Bi ₂ WO ₆ hierarchical heterostructure	2,4-DCP	CD: 0.05 g of 10% BiO ₁ /Bi ₂ WO ₆ , effluent flow rate: 0.8 mL/min, pH: 8, PC: 30 ppm, V: 50 mL	Visible light	More than 95% degradation was observed.	(Chen et al. 2014)

Photocatalyst	Pollutant	Parameters/ optimised conditions	Light source	Findings	Reference
g-C ₃ N ₄ /GO/rGO nano-composites	Phenol	CD: 0.5 g/L, V: 160 mL, PC: 10 ppm	Visible light	Best performing photocatalyst among different combination: rGONPs-g-C ₃ N ₄	(Aleksandrak et al. 2017)
Black TiO ₂ nanobelts/g-C ₃ N ₄ nanosheets laminated hetero junctions	MO	CD: 30 mg, V: 30 mL, PC: 10 ppm	Visible light	95% degradation and 555 μmol/h/g hydrogen evolution	(Shen et al. 2017a)
Polyaniline-TiO ₂ nano-composite	Reactive Blue-19	CD: 1 g/L, pH: 3, PC: 50 ppm, V: 100 mL, light source: solar	Visible light and solar light	Almost complete degradation with 86% COD removal within 120 min.	(Kalikeri et al. 2017)

Table 2.5: Summary of literature regarding photocatalysts along with different materials (metal or non-metallic substance) or self-sensitized behaviour.

Photocatalyst	Pollutant	Parameters/optimised conditions	Light source	Findings	Reference
Mixture of TiO ₂ and Pt (10:1)	Lactobacillus acidophilus, Saccharomyces cerevisiae and Escherichia coli.	Light intensity: Metal halide lamp: 4600 micro Einstein/m ² /s, Xenon lamp: 4600 micro Einstein/m ² /s, PC: 10 ³ cell/mL	400 W Metal halide lamp, a 300-W xenon lamp, and 500-W white fluorescent lamp.	100% degradation of microbial cells under Metal halide lamp and xenon lamp in 120 min.	(Matsunaga et al. 1985b)
Dye sensitized TiO ₂	Indigo carmine	CD: 4 g/L, PC: 20 ppm	Visible light	Complete mineralization was observed in 140 min	(Ding et al. 2005)

Surface modified TiO ₂ -toluene 2,4-diisocyanate	Dichlorophenol	CD: 0.1 g, V: 100 mL, PC: 100 ppm	Visible light	More than 80% degradation observed in 240 min.	(Chen et al. 2009a)
TiO ₂ /Ozonation in an air-lift reactor	1-amino-4-bromoanthraquinone-2-sulfonic acid (ABAS)	Ozone dosage: 27.6 mg/min, V: 4.5 L, PC: 100-1000 ppm	UV	90% decolorization with 50% COD removal observed in 12 h.	(Wang et al. 2012)
Pd modified WO ₃	Geosmin	CD: 150 mg/L, light intensity: 0.8 mW/cm ² , pH: 7, V: 80 mL.	Simulated solar light	More than 98% of degradation occurred in 20 min. High dissolved oxygen concentration is not suitable for the degradation of geosmin.	(Xue et al. 2016b)
Self-sensitized TiO ₂	Orange II and RhB	CD: 20 mg, PC: 5 ppm, light intensity: 5.3 mW/cm ² , V: 30 mL.	Visible light	Almost complete mineralization of the Orange II and RhB dye after 6 and 4 h of irradiation respectively.	Molla et al. 2017a
Self-dye-sensitized TiO ₂ and ZnO	Orange II and MO	CD: 20 mg, PC: 5 ppm, V: 30 mL.	Fluorescent and LED light	90% and 40% of degradation of the Orange II and RhB dye after 5.5 h of irradiation respectively.	Molla et al. 2017b

There are more than 7.5 billion people on the earth, so sewage treatment is a big priority. Even though the sewage waste is mostly biodegradable and most of it broken down environmentally, a little amount of sewage waste in potable water can cause diseases such as diarrhea. Sometimes the sewage water contains chemicals and pharmaceuticals flushed by human, harmful bacteria and virus from the sick people (Shivaraju 2011; Yuan et al. 2014; Wang 2016). Other common water pollution causes by the humans is regular exercise of oil based petroleum products. Oil has countless application in various fields, starting from petroleum oil to food oil, all are an essential part of our daily life. This used or unused oil can pollute the water several way and effect the aquatic life as well as the human health. The oil can come into water from petroleum industries, oil spilling, food industries, car industrial waste, domestic use etc (Yang et al. 2017; Shivaraju et al. 2016; Mustafa et al. 2014). On the other hand pharmaceutical industries, dye and textile industries are not lagging behind in this race (Bin Mukhlis et al. 2013; Na et al. 2004; Marandi et al. 2013). Every day millions of tons of organic matter is being discharged by those industries into the water. All those pollutants can seriously damage the eco-system. For this reason, a serious need of effective, efficient, economical and eco-friendly process is in need for wastewater treatment. There are numerous studies that have been done on the photocatalytic decomposition of wastewater as shown below in **Table 2.6**.

2.4. Remazol turquoise blue (RTB)

Reactive or remazol dyes are most commonly used in various textile industries, because of its good fastness properties, which makes the dye bonding during the dyeing process. Reactive dyes are available in wide range of colours and it is specifically used for the silk, fibre, wool and flax. Remazol dyes are having a masking group which prevents it to react with water thereby makes it long lasting in water. Moreover, most of the reactive dyes are having metal in its structure, makes it very difficult to breakdown. Remazol turquoise blue is one of the most complex dye with copper pthelocynine bond in the core, which makes it difficult to break down with low energy (Ghaly et al. 2014). Very few studies are reported (**Table 2.7**) on the degradation of RTB, additionally only three work is published on photocatalytic degradation of RTB and all of them are in small scale and slurry form.

2.5. Selection of photocatalysts - TiO₂, g-C₃N₄, and rGO

As mentioned above, there are numerous photocatalysts have been studied till date, but TiO₂ is one of the most extensively used photocatalyst because of its several inevitable properties such as, a) Chemically inert, b) Highly oxidizing agent, c) Non-toxic, d) Environmental friendly, e) Economical, f) Highly stable, g) High catalytic activity, h) complete mineralization of the pollutant, and i) self-cleaning property. Moreover, TiO₂ exists in three different phases anatase, brookite and rutile, among which mixture of anatase and rutile (3:1) (Bott 2011; Ohno et al. 2001) are used widely as P25TiO₂ because of its superior photocatalytic performance. Considering all these aspects TiO₂ is choose for this study.

Two more catalysts are used in this study namely reduced graphene oxide (rGO) and graphitic carbon nitride (g-C₃N₄). The literature survey shows that the reduced graphene oxide is having high adsorption capability, which is also a photocatalyst. Moreover, it is inexpensive and environmental friendly, which makes it more suitable for this application (Monteserín et al. 2017; Velasco-Soto et al. 2015). At the same time, g-C₃N₄ exhibits a unique high stability, including the heat withstand capacity and chemical resistance (Dong et al. 2014). The other basic properties of g-C₃N₄, which makes it appropriate for this work includes low band gap, low cost, easy to synthesis, and eco-friendly.

2.6. Disadvantages in slurry form and strategy to overcome these disadvantages

The photocatalytic degradation of the pollutant in slurry form possess a substantial practical application problem that include, post separation of the catalyst after the photocatalytic operation (Silva 2012; Srikanth et al. 2017). The surface area or the particle size of the photocatalyst plays an important role in degradation efficiency, the smaller the particle size greater the surface area, which leads to high photocatalytic performance (Rachel et al. 2002). In most of the cases the photocatalysts are in nano size, which makes it more difficult to separate from the water matrix. However, there are few approaches have been made to separate the powder photocatalysts but all are in small scale operation.

Table 2.6: Summary of literature regarding different types of pollutant removal by photocatalysis.

Pollutant type	Photocatalyst	Pollutant	Parameters/ optimized conditions	Light source	Findings	Reference
Surfactants	TiO ₂	Sodium dodecyl benzene sulfonate and Benzyl dodecyl dimethylammonium chloride	CD: 0.1 g/50 mL, PC: 0.1 mM/50 mL	UV	Mineralization of both the pollutants are almost same (~25%) after 10 h of UV irradiation.	(Zhao et al. 1993)
	TiO ₂	Polyoxyethylene sorbitan monooleate	CD: 200 g/m ³ , pH: 7, light intensity/m: 31.4 W/m	UV	Within 2 h of UV irradiation complete mineralization occurred.	(Yoshikawa et al. 2003)
	TiO ₂ immobilized in glass	4,4-Dichloro-Diphenyl-1,1,1-Trichloroethane	PC: 0.01 ppm, airflow: 200 mL/L,	UV	87% degradation observed at optimized condition in 40 min of irradiation	(Sinha et al. 2009)
	TiO ₂	Bentazone	PC: 40 ppm, CD: 0.5-1.5 g/L	Simulated sunlight	Complete mineralization of the pollutant occurred in 4 h	(Davezza et al. 2012)
	ZnO	Linear alkylbenzene sulfonates	V: 50 mL, pH: 7, CD: 0.2 g/L,	UV	More than 94% degradation was achieved in 120 min	(Giahi et al. 2013)
Oil from food industry	TiO ₂ and ZnO	Protocatechuic acid	CD: 1 g/L, V: 250 mL, PC: 50 ppm	Sunlight and artificial light	Approximately 95% of degradation happened within 150 min	(Poulios et al. 1999)
	TiO ₂ /PrSO ₃ H	Used cooking oil	Reaction time, catalyst loading, the mole ratio of methanol to used cooking	-	More than 98% of fatty acid methyl esters can be	(Gardy et al. 2017)

Pollutant type	Photocatalyst	Pollutant	Parameters/ optimized conditions	Light source	Findings	Reference
			oil ratio and the reaction temperature		produced within 9 h of reaction time	
Insecticides and herbicides	TiO ₂	Herbicides: atrazine, propazine, cyanazine, prometryne, and irgarol; Insecticides: ethyl parathion, methyl parathion, ethyl bromophos, methyl bromophos, and dichlofenthion	CD: 100 mg/L, PC: herbicides(10 ppm) and insecticides(1 ppm)	Solar light	Proposed degradation pathway makes this study easy to analyze the final breakdown products	(Konstantinou et al. 2001)
	TiO ₂	Chlorpyrifos	V: 35 mL, PC: 5 ppm, CD: 0.2 g/L	UV, visible and sunlight	Complete degradation of the pollutant was observed after 300 min under UV light	(Muhamad 2010)
	Tourmaline-Coated-TiO ₂	2,4-Dichlorophenoxyacetic Acid	PC: 20 ppm, air flow rate: 3 mL/s, V: 3 L	UV	Complete degradation of pollutant observed in 40 min	(Bian et al. 2013)
	TiO ₂	Isoproturon	CD: 0.5 g/L, pH: 5, PC: 25 ppm,	UV	96% COD and 90% TOC removal observed at optimized parameters in 3 h	(Verma et al. 2014)
	Pt/TiO ₂	2,4-dichlorophenoxyacetic acid and 2-(2,4-dichlorophenoxy)	V: 800 mL, PC: 20 ppm, CD: 0.5-3% pt/TiO ₂	UV	More than 88% degradation of pollutant occurred in 90 min	(Abdennouri et al. 2015)

Pollutant type	Photocatalyst	Pollutant	Parameters/ optimized conditions	Light source	Findings	Reference
Synthetic dye	TiO ₂	Rhodamine B	Catalyst dosage: 25 g/L,	UV light	More than 90% decolorization occurred in 180 min	(Na et al. 2004)
	ZnO	Methylene blue	ZnO dosage is 0.1g/L	UV light	97% Methylene Blue removal after 30 min	(Xu et al. 2012)
	TiO ₂	Methylene blue and Congo red	0.5 g TiO ₂ , 50 mL dye solution, 5 ppm	Solar light	Almost 90% decolorization in 600 min for both the dyes	(Bin Mukhlis et al. 2013)
Micro-organism	TiO ₂ ~PVA polymer composite	Thiram	PC: 0.0001 mol/L, CD: 100 mg	UV and Visible light	Complete degradation of pollutant occurred in 150 min	(Thakare and Bhawe 2005)
	TiO ₂	Tetracycline	CD: 0.5 g/L, PC: 40 ppm, V: 750 mL,	UV-A	The TOC depletion observed under UV and solar light, reaching 90 and 75% after 2 h	(Reyes et al. 2006)
	Ag ₁ /TiO ₂	Pathogenic Bacteria	Catalyst concentration: 0.2 g/L, bacteria cell concentration: ~8*10 ⁷ cfu/mL, volume of contaminants: 30 mL	Visible Light	Acidic pH boosts the antibacterial activity	(Hu et al. 2007)
	Pt doped TiO ₂ /SiO ₂	E. coli bacteria	Catalyst concentration: 0.05 g/L, bacteria cell concentration: <1 cfu/mL	UV	Complete destruction of the pollutant occurred in 5 min	(Ahmadi et al. 2008)
Oil from petroleum industry	TiO ₂	Hydrocarbons	CD: 200-250 mg/ 50 mL, H ₂ O ₂ concentration: 0.5% (v/v), PC: 100-200 ppm	UV	Drum type reactor works better than the flat plate	(Robertson et al. 2008)

Pollutant type	Photocatalyst	Pollutant	Parameters/ optimized conditions	Light source	Findings	Reference
					reactor, but both the reactors reduced 90% hydrocarbons in 10 min	
	TiO ₂	Polycyclic Aromatic Hydrocarbons	CD: 5 mg, H ₂ O ₂ loading: 0.8 mL/L	Solar light	Complete degradation of pollutants in 96 h	(Rocha et al. 2014)
	TiO ₂	Oily wastewater	CD: 75 mg/L, temperature: 30 °C, pH: 5, PC: 1000 ppm, H ₂ O ₂ : 400 ppm, Fe ²⁺ : 40 ppm	UV	77% removal of waste occurred in 150 minutes.	(Mustafa et al. 2014)
	N-doped TiO ₂	Oil and grease	PC: 25 ppm, CD: 5 g/L, V: 200 mL, irradiation time: 6-24 h	Sunlight	96-100% pollutant removal under sunlight in 24 h	(Shivaraju et al. 2016)
	TiO ₂ immobilized in concrete	Petroleum hydrocarbons	V: 5 L, storage tank: 60 L, aerated rate: 270 L/h, pH: 5, CD: 60 /gm ² , PC: 100 ppm, H ₂ O ₂ dosage: 2000 ppm	Solar light	The highest COD removal was 65% in 320 min	(Soroush et al. 2017)
	TiO ₂	Heavy hydrocarbons	CD: 1–5%, water holding capacity: 0–300%	UV-A, UV-C	20% total hydrocarbon removal occurred in 24 h	(Yang et al. 2017)
Toxic heavy metal	Silica-titania composites	Hg	PC: 100 ppm, surface area: 200 m ² /g, pH: 7, TiO ₂ particle diameter: 10 nm (sp.surface area: 200 m ² /g).	UV-C	90% removal of mercury within 1 h	(Byrne and Mazzyck 2009)
	TiO ₂	Hg(II)		UV	More than 65% Hg removal achieved within 30 min	(Dou and Chen 2011)
	Magnetic	Cr(VI)	CD: 25% (v/v), PC: 25	Sunlight	Complete removal of Cr	(Idris et al.

Pollutant type	Photocatalyst	Pollutant	Parameters/ optimized conditions	Light source	Findings	Reference
	ferro-photo gel		ppm, pH: 1.		is achieved within 1 h for low pollutant concentration	(2011)
	TiO ₂ and Ag/TiO ₂	Hg(II)	V: 0.5 and 1 L, CD: 2 g/L, pH: 4, oxygen flow rate: 0.5 cm ³ /min	UV	Almost complete removal of Hg occurred within 2 and 3 h for TiO ₂ and Ag/TiO ₂ respectively	(Lenzi et al. 2011)
	TiO ₂	Cd ²⁺ and Pb ²⁺	CD: 0.9 g/L, PC: 25 ppm, pH: 11.	UV	Almost complete removal of the pollutants occurred within 120 min	(Fatehizadeh et al. 2014)
Organic compounds	Activated Carbon-Supported TiO ₂	Terephthalic acid	CD: 11% TiO ₂ in activated carbon with 7 g/L loading, irradiation time: 7 h, V: 100 mL, initial COD: 4823 ppm	UV	64% COD removal achieved under optimized conditions in 7 h	(Chen et al. 2009b)
	Fe(III) doped TiO ₂ immobilized on sintered glass frits	Dissolved organic carbon	Catalyst area: 12.57 cm ² , PC: 0.623 mg of material/min, flow rate: 5 mL/min, V: 100 mL, pH: 6.8,	Visible light	Almost complete degradation observed in 340 min	(Mwangi et al. 2013)
	TiO ₂	Methylene blue dye and E. coli and P. aeruginosa bacteria	CD: 0.5 g/L, PC: 8 ppm dye and 108 cfu mL bacteria, V: 250 mL	UV-A	Within 2 h maximum inactivation rate was observed at optimal conditions	(Wang et al. 2013a)
	TiO ₂ - polymeric membrane	Aspirin	V: 250 mL, UV lamp intensity: 22 mW/cm ² , solar simulator light intensity	UV and solar light	After 450 min the degradation of the pollutant was approximately 90%	(Mukherjee et al. 2014)

Pollutant type	Photocatalyst	Pollutant	Parameters/ optimized conditions	Light source	Findings	Reference
	P25-TiO ₂	Diuron, P-coumaric acid, Bisphenol A, Phthalic anhydride	27 mW/cm ² , pH: 4.5 PC: 15 ppm, CD: 100-200 mg/L, pH: 3-9.6	UV-A	under UV light as well as sunlight. Over 70% of pollutant was removed from the wastewater matrix in 180 min	(Pirilä et al. 2015)
Azo dye	TiO ₂	Reactive Black 5	pH: 3, CD: 1.5 g/L, PC: 20 ppm	UV	12 h of photocatalyst treatment reduces only 70% TOC	(Sharma et al. 2012)
	NiFe ₂ O ₄ immobilized in clinoptilolite in a Circulating Fluidized Bed Reactor	Acid Yellow 23	pH: 5, CD: 40 (mg/L), PC: 45 ppm, H ₂ O ₂ concentration: 30 ppm and temperature: 20 °C	UV	Almost complete mineralization of dye was observed in around 50 min	(Marandi et al. 2013)
	Immobilized Zn(II), Cu(II), Ni(II), Co(II), Fe(III) and Pd(II) in meso-tetraphenylporphyrin (TTP)	Reactive orange, reactive red, reactive black, reactive blue and reactive yellow	PC: 15 mL, V: 50 ppm, metal -TTP content: 3.6 × 10 ⁻⁵ mmol, CD: 10 mg, H ₂ O ₂ loading: 1 mL (30 vol.%),	Visible light	Most of the dyes get mineralized within 120 min	(Shao et al. 2013)
	g-C ₃ N ₄ -P25/photosynthetic bacteria composite	Reactive brilliant red X-3b	V: 100 mL, CD: 0.1 g, PC: 20-50 ppm,	Visible light	94% and 85% color removal and COD removal was observed respectively in 5 h.	(Zhang et al. 2017)

Pollutant type	Photocatalyst	Pollutant	Parameters/ optimized conditions	Light source	Findings	Reference
	TiO ₂ and ZnO	Reactive blue 21	PC: 50 mg/L, CD: 0.8 g, pH: 7, irradiation time: 4 h	Sunlight	99% color removal and 80% COD removal with TiO ₂ ; 99% color removal and 75% COD removal with ZnO in 210 min of irradiation.	(Pardiwala et al. 2017)
Pesticide and fertilizer	TiO ₂	Chlorpyrifos, cypermethrin and chlorothalonil	CD: 1.5 g/L, H ₂ O ₂ : 100 ppm, pH: 6, irradiation time: 5 h	UV-A	COD and TOC reductions was 26% and 9% after photocatalytic activity under optimized condition after 300 min	(Affam and Chaudhuri 2013)
	ruthenium [Ru(bipy) ₃] ²⁺ doped TiO ₂ - SiO ₂	bentazone, carbofuran, clomazone, diuron, tebuconazole and pyraclostrobin	Catalyst loading: 20 mg/ 250 mL wastewater, pesticide concentration: 10 ppm, pH: 7, reaction time: 110 min, and adsorption equilibrium time: 15 min.	High-pressure mercury UV lamp.	Pesticide removal efficiency between 71.00 and 99.98% was observed in 110 min.	(Guimarães et al. 2016)
	TiO ₂ and titanium pillared purified clays	2,4-dichloro phenoxyacetic acid (2,4-D) and 2,4-dichloro- phenoxypropionic acid (2,4-DP)	CD: 1.15-10.5 mmol Ti/ g clay, PC: 20 ppm, V: 800 mL	UV	More than 80% of contaminants were removed within 90 min	(Abdennouri et al. 2016)
	ZnO	Methyl parathion and parathion	CD: 85 mg/L, O ₂ : 40% (v/v), pH: 6.7	UV	80% of the pesticide was removed within 100 min	(Sharma et al. 2016)

Pollutant type	Photocatalyst	Pollutant	Parameters/ optimized conditions	Light source	Findings	Reference
	TiO ₂ immobilized in the glass plate	Imidacloprid pesticide	PC: 20 ppm, pH: 5, light intensity: 17 W/m ²	UV-C	More than 90% pollutant removal in 3 h	(Akbari Shor-goli and Shokri 2017)
Pharmaceuticals	TiO ₂	Sodium alkylbenzene sulfonate (5 ppm) and fulvic acids (10 ppm)	V: 0.44-0.625 L, ozone dosage: 0.8-2 mg/(L min),	UV	35-80% TOC removal was observed for fulvic acid removal in 30 min	(Shvadchina et al. 2013)
	TiO ₂ immobilized in sand	Propranolol, diclofenac, and carbamazepine	PC: 5 ppm, irradiation intensity: 159 Lux, V: 500 mL, CD: 25 g, sand particle size: 200-500 μ	Simulated solar light	Complete mineralization of first two pollutants was achieved, whereas carbamazepine showed only 76% removal efficiency in 96 h	(He et al. 2016)
	TiO ₂ in photo-reactor	Ethenzamide	PC: 15 ppb -2 ppm, CD: 10 g/L, V: 150 mL,	UV, visible-UV	More than 62% removal achieved in 24 min by TiO ₂	(Xu et al. 2016c)
	TiO ₂	Diclofenac, ibuprofen, and carbamazepine	CD: 50 mg/L, pH: 7,	UV-A and Visible light	The highest removal rate of Diclofenac, ibuprofen was exceeded 96%, whereas for carbamazepine, it reached 79% in 60 min	(Kudlek et al. 2016)

Separation of the particles by centrifugation (Giwa et al. 2012; Zhang et al. 2016), magnetizing the photocatalysts (Shi-Hong et al. 2013; Linley et al. 2013), membrane separation (Molinari et al. 2017; Zheng et al. 2017) and few other techniques (Shivaraju 2011) have been tried but all the processes are either expensive or not feasible for practical large scale operations. Due to this inevitable disadvantage of slurry photocatalyst, the large scale operation becomes almost impossible.

To overcome the problem, photocatalyst can be integrate/attach in a support or carrier (Mohd Adnan et al. 2018). The attached photocatalyst in a substrate material surely decreases the surface area of the catalyst but separation process becomes very easy, which makes the catalyst reusable and economically feasible. Comparison of slurry and immobilized system are tabulated below in **Table 2.8 and Table 2.9** (Abdel-Maksoud et al. 2018; Lea and Adesina 1999; Srikanth et al. 2017; Silva 2012).

The photocatalytic efficiency of the slurry or immobilized photocatalyst is same if the active surface area of the catalyst is considered. As the small part of the catalyst is attached with the support material in immobilized form, the surface area of the catalyst reduces so as the active surface area. According to the requirement, the catalysts are attached into the substrate material.

2.7. Various parameter effecting the photocatalytic process

The decomposition of an organic pollutant present in wastewater at the surface of the photocatalyst is a complex phenomenon because it depends on many factors, such as, **Catalyst dosage:** For effective degradation of contaminant, good interaction between the pollutant molecule and the catalyst surface is required. For that reason, the amount of catalyst plays a significant role. In heterogeneous photocatalysis, the reaction rate is known to rise relatively to the concentration of the photocatalyst. The ideal dosage is commonly determined to avoid overuse of catalyst and to ensure the efficient and total adsorption of photons (Satuf et al. 2007; Govindan et al. 2017; Singh et al. 2011).

Effect of pH: At more alkaline pH values, the photocatalyst surface is negatively charged whereas, in acidic medium, the surface is positively charged (TiO_2) (Zhu et al. 2012). At alkaline pH, the pollutant, as well as the catalyst surface, is negatively

Table 2.7: Summary of literature regarding removal of RTB.

Photocatalyst/ oxidative reagent	Optimum conditions/ Reaction condition	Light source	Reactor volume	Performance	References
Fenton process, ferric coagulation and H ₂ O ₂ /pyridine/Cu(II) system	pH- 7, ferric coagulation (FeCl ₃ .6H ₂ O, initial concentration: 100 mg/L), at [Fe(II)]:[H ₂ O ₂] molar ratio of 1.21:1	-	The mixture of 50 mg/L RTB and 100 mg/L Polyvinyl alcohol	100% decolourization efficiency in 45 min	(Bali and Karagözoğlu 2006)
Ti/TiO ₂ thin-film electrodes	0.5 mol/L Na ₂ SO ₄ pH 8	UV light	-	100% and 79.6% absorbance and TOC removal in 180 min	(Osugi et al. 2006)
Enzyme horseradish peroxidase	pH- 4-5, dye concentration 100 mg/L, enzyme concentration 29.85(Um/L), H ₂ O ₂ concentration 2×10 ⁻³ mmol/L	-	100 mL RTB	59% decolourization in 45 min	(Ulson de Souza et al. 2007)
Soybean peroxidase	pH – 3, 240 min of treatment at 25 °C of the solution of RTB (200 ppm) with Soybean peroxide 2.06×10 ⁻⁷ M and H ₂ O ₂ 9.98×10 ⁻⁵ M	-	3 mL RTB	96% degradation after 240 min	(Marchis et al. 2011)
H ₂ O ₂	pH – 9, presence of Na ₃ PO ₄ (1 mM, sol pH 10.6) – 55% decolourization, NaNO ₃ (1 mM, sol pH 5.9)- 47% decolourization,	365 nm and 254 nm UV light	25 ppm RTB and 3 mM H ₂ O ₂ , 50 mL	50% decolourization in 10 min	(Kalsoom et al. 2012)
Turnip peroxidase	Dye concentration 30 ppm, containing: H ₂ O ₂ 100 µmol/L (0.4 mL), contact time 50 min, enzyme concentration (20.3 U/mL), sodium	-	50 ppm 1.5 mL RTB	57.7% decolourization in 50 min	(Silva et al. 2012)

Photocatalyst/ oxidative reagent	Optimum conditions/ Reaction condition	Light source	Reactor volume	Performance	References
AC/TiO ₂ Immobilized in glass plates using Polyethylene glycol (MW = 10,000 g/mol) as binder.	phosphate buffer, 0.05 mol/L, pH 7.0 (1.2 mL)				
	Catalyst loading (3.00 g catalyst/L solution) Initial dye solution pH-3.00, UV intensity (2.50 mW/cm ²), Re-circulating flow rate (100 mL/s)	254-nm UV lamp	15 ppm, 1000 mL RTB	86.40% and 38.5% colour removal in 6 h under UV and visible light irradiation respectively.	(Gallo et al. 2015)
TiO ₂ and ZnO	dye concentration 50 mg/L, catalyst dosage 0.8 g, pH-7	Microwave and UV light irradiation	50 ppm	TiO ₂ : 80% COD and 99% color removal, ZnO: 75% COD and 99% color removal in 240 min	(Pardiwala et al. 2017)

Table 2.8: Advantages of slurry and immobilized photocatalytic system.

Advantages of slurry system	Advantages of immobilized system
High surface area of catalyst	Easy separation process
High mass transfer rate between catalyst and pollutant	Reuse of catalyst is also possible
High photocatalytic activity	Extended photocatalyst lifetime
High rate of electron-hole pair generation	Economically viable
High throughput	Proper utilization of the irradiated light
Better mixing	

Table 2.9: Disadvantages of slurry and immobilized photocatalytic system.

Disadvantages of slurry system	Disadvantages of immobilized system
Catalyst recovery is tedious and expensive	Low surface area
Catalyst agglomeration takes place	Mass transfer rate is relatively low
Opacity of the wastewater solution increases, can block the light irradiation on the catalyst surface	Low photocatalytic yield (can compensate by increasing the irradiation time)
Continuous agitation at a particular rate is necessary	Low photon accessibility
Large scale application is quite difficult	Waste of small portion of the catalyst

charged, due to which the repellent effect of the two species is a common phenomenon. However, with acidic pH, the negatively charged pollutant molecules were easily gets adsorbed on the positively charged photocatalyst surface. This phenomenon benefited the degradation of contaminants present in wastewater (Singh et al. 2011; Kumar et al. 2017).

Effect of temperature: the high temperatures increase the collision frequency of molecules. Hence, the mobility of the reactant molecules continued to escalate and gradually reached a plateau. However, generally, photocatalysis is affected by the electron-hole pair generation and at high temperature it is easy as the bandgap energy reduces. Therefore, the increase in pollutant degradation was most likely due to the enhanced collision frequency with the rise in reaction temperature (Soares et al. 2007; Zhu et al. 2012).

Effect of size and surface area: the smaller the photocatalytic particle, the higher the surface area; which means more contact between photocatalyst and pollutant. This more contact rate promotes the high photocatalytic activity and mineralisation of pollutants (Raj and Viswanathan 2009; Kumar et al. 2017).

Effect of pollutant concentration: The increased initial concentration decreased the degradation ratio. Generally, the formation of activated radicals (e.g., OH and O_2^-) on the photocatalyst surface remains constant for particular light intensity, catalyst amount, and irradiation time. A higher pollutant concentration corresponds to a higher requirement for activated radicals, resulting in prolonged reaction time for the complete decomposition (Pirilä et al. 2015; Silva and Faria 2010).

Effect of bandgap energy: The energy required for an electron to jump from valence band to conduction band in an insulator or semiconductor is generally known as band gap energy. The bandgap energy or activation energy of a particular semiconductor photocatalyst is constant and need a specific amount of energy to activate, which can be delivered only by a specific amount of energy source. The lower the bandgap the energy required for the activation is also low (Koč et al. 2010; Serra et al. 2016; Dillip et al. 2017; Lazar et al. 2012).

Effect of light intensity and irradiation time: Under different light source the same photocatalyst will show non-identical results since the energy emitting from each source is different. Even though the activation energy is the same in all the cases for a particular photocatalyst, the more energy from the light source leads to high productivity. The energy released from the different light source (UV-C<UV-B<UV-A<Sunlight<Visible light) is directly proportional to the production of electron-hole pairs. At low light intensity and accordingly low carrier concentrations, the rate of oxidation of

a particular pollutant is directly proportional to light intensity, while at higher light intensity the rate is dominated by charge carrier recombination and has a square-root dependence on the intensity of light. (Zhu et al. 2012).

Moreover, the percentage of photocatalytic oxidation of pollutant increases with increase in irradiation time (Govindan et al. 2017). The reaction rate reduces with irradiation time since it follows first-order kinetics most of the time and furthermore along with the parent pollutant the intermediate compounds also degrade by photocatalyst resulting reduction in reaction time. Few other reasons for the slow reaction of pollutant mineralisation after a certain period of time is due to: the difficulty in converting the N-atoms or S-atoms of a pollutant into oxidised compounds the slow reaction of short-chain intermediate products with $\bullet\text{OH}$ radicals, and the short life-span of the photocatalyst, because of the active sites inactivation by strong by-products deposition (carbon etc.) (Konstantinou and Albanis 2004).

Effect of crystallinity: The high crystallinity of catalyst particles predominantly increases the lifetime of electron-hole pairs, which accordingly leads to an improvement in the performance of degradation (Tanaka et al. 1991).

Effect of immobilization on/in a substrate: A powder photocatalyst has a larger surface area compared to the same photocatalyst in immobilized form. The larger surface area means more photocatalytic activity, but according to few studies, the photocatalytic efficiencies are the same considering the active catalyst surface area while other parameters are constant. Different substrate materials with the same catalyst show non-identical outcome as the active surface area of the catalyst also changes (Li et al. 2010; Li et al. 2012; Kraeutler and Bard 1978).

Effect of the presence of inorganic ions: The dissolved inorganic ions are very common in dye-containing industrial wastewater. Most of the time the dye wastewater contains solvents, a mixture of organic compounds, dissolved organic matter and few other pollutants if mixed with another effluent stream. These mixed pollutants cover the active sites of the photocatalyst and hamper the photocatalytic activity. On the other hand, it also acts as a light screen which increases the opacity of the wastewater and reduces the photon receiving capability (Kudlek et al. 2016; Konstantinou and Albanis 2004).

2.8. Substrate materials

The immobilization of the catalyst can be done using different substrate materials. A good substrate material should have the following characteristics, catalyst should not leach out, provide maximum catalyst surface area possible, should not affect the photocatalytic activity, should not get effected by UV irradiation or the strong oxidizing agents during the operation, chemically and mechanically stable (Singh et al. 2013; Xing et al. 2018). There are several reported study on immobilized photocatalyst, among which most popular substrate materials are glass, ceramic, rock, brick, cement, metal, cork, and polymer (Rachel et al. 2002; Chen et al. 2001; Srikanth et al. 2017). These substrate materials used in those studies are having almost all the characteristics of a good substrate should be having. Moreover, most of the substrates are heavy and sink in water, which makes it a little difficult in some cases especially where colored wastewater is being treated, as colored water can block the photons to come in contact with the catalyst. To overcome this problem, new studies are diverted towards buoyant substrate materials such as hollow microspheres, perlite, quartz tube, vermiculite, quartz sand particles, natural porous pumice, activated carbon, clay granules, polyurethane foam, alginate beads, cork, polyethylene and polystyrene beads (Singh et al. 2015a; Wang et al. 2015; Leshuk et al. 2018; Xing et al. 2013; Li et al. 2015b; Xing et al. 2018; Jackson and Wang 1991). The immobilization techniques used for the integration of the photocatalyst into the substrate varies based on the requirement and substrate material used.

2.9. Immobilization techniques

The selection of the immobilization technique adopted must be in such a way so that it carry out the photocatalytic operation without effecting the process. A large number of techniques have been reported which includes, sol-gel process, dip coating, spin coating, spread coating, photo-etching, cold plasma discharge, spray pyrolysis, electrophoric deposition etc. Most of the above mentioned techniques are unable to comply with the requirement of the polymer immobilization process. Although, sol-gel process was considered to be one of the low temperature photocatalyst deposition on the polymeric substrates, but the generation of electron and hole pair can be generated only in well crystalline phase and this requires high temperature calcination. Hence, the polymer

with high thermal stability can only be used for this purpose which bounds the application of the sol-gel process. Other popular techniques for catalyst immobilization into the polymer substrates includes thermal treatment, hot pressing, electrophoretic deposition, solvent casting, in-situ chemical oxidative polymerisation, impregnation, spin and dip coating, mixing in solution, and hydrothermal process. In few recent work, solvent casting method is used extensively for different polymer substrate and promising results have been shown. Solvent casting method is not only simple, economical and easy, it can be employed to almost all polymer.

2.10. Polymer as a substrate

Among all the buoyant substrate materials, polymers are one of the most popular choice (Mohd Adnan et al. 2018). There are numerous polymer available that can be used as a potent substrate materials to improve the reusability property of the photocatalysts such as, polyethylene (Reza et al. 2016), polypropylene (Han and Bai 2009; Kamrannejad et al. 2014), polyvinyl chloride (Peerakiathajorn and Chawengkijwanich 2012), polycarbonate (Latthe et al. 2014), poly (methyl methacrylate) (Yousif et al. 2016; Mirhoseini and Salabat 2015), polyaniline (Yang and Luan 2012; Luan et al. 2017), polyvinyl acetate (Singh et al. 2013), polyvinyl alcohol (Lei et al. 2012), cellulose (Li 2010), fluoropolymer (Kanmani et al. 2003), polyethylene terephthalate (De Barros et al. 2014), polypropylene (Kamrannejad et al. 2014), polystyrene (Singh et al. 2015a), parylene (Zhiyong et al. 2008), rubber latex (Stropa et al. 2015) etc. There are few inevitable properties of polymer (Singh et al. 2013; Singh et al. 2015a), makes it better choice than other substrate material such as,

- 1) *Stability*: Polymers are highly stable since it is chemically inert, even after exposing it into chemicals there is no change in chemical properties. Moreover, upon UV irradiation in presence of photocatalyst, the degradation rate is very slow which makes it mechanically stable.
- 2) *Hydrophobicity*: The water repelling property of most of the polymers are in favor of adsorption of pollutant on the surface as well as it boosts the photocatalytic oxidation.

- 3) Thermoplastic: Thermoplastic property of a polymers make it better substrate material than others. By simple heat treatment of polymer at lower temperature (< 150 degree C in most of the cases) the shape can be change easily and use it according to the need.
- 4) Buoyant: The low density polymers are very useful in case of special type of photocatalytic reactor, where catalyst should be on the upper surface of the wastewater to absorb the maximum amount of photon irradiation.
- 5) Availability: Most of the polymers are inexpensive, reusable and readily available.

From **Table 2.10** it can be easily concluded that the different polymers were used for immobilization of the photocatalyst. Moreover, most of the reactors are having less than 500 mL volume and work under UV light. Another noticeable part is that the polystyrene is the only substrate material used more often than other polymers and showed effective results.

2.11. Photocatalytic reactors - different types, major challenges

Photocatalytic reactors are generally multiphase reactors used for wastewater treatment. Application of multiphase reactors are not limited to the manufacture of petroleum based products, pharmaceuticals, pesticides, refining of ores, production of polymers etc. Multiphase reactor usually involves liquid-gas, liquid-solid, solid-gas, gas-liquid-solid materials. Nowadays, the conventional multiphase reactors are trying to employ for the wastewater treatment processes. The multiphase reactors are usually having few significant properties such as, high mass transfer rate, processing of solid is simple, highly efficient, low maintenance, simple design etc., which makes it valuable and worthy choice. Moreover, multiphase reactors are usually vessels, provides an environment conducive for reactions, especially by providing proper mixing and contact among various components with temperature and pressure control. There are several multiphase conventional reactors, which can be used as a photocatalytic reactor for wastewater treatment, but it might need slight modification since light irradiation is needed to carry out the photocatalytic process. Those conventional reactors includes

bubble column reactor, fluidised bed reactor, trickle bed reactor, slurry photocatalytic reactor, thin film reactor and airlift reactor. The photocatalytic wastewater treatment process is not only limited to those few conventional reactors, various innovative photocatalytic reactors have been developed according to the need and purpose such as, annular falling film reactor, optical fibre reactor, photo capillary reactor, submerged membrane reactor, recirculating batch reactor, compound parabolic reactor etc. In above mentioned multiphase photocatalytic reactor contains at least one free interface. Based on the reaction phases and requirement of reactors can be chosen as shown in **Figure 2.1** (Dudukovic et al. 1999; Pangarkar 2015).

But in case of wastewater treatment, the reactor can be chosen based on pollutant type, photocatalyst variety, photocatalyst attachment, light source etc. various conventional and non-conventional reactors used for the photocatalytic wastewater treatment are described below in **Table 2.11**.

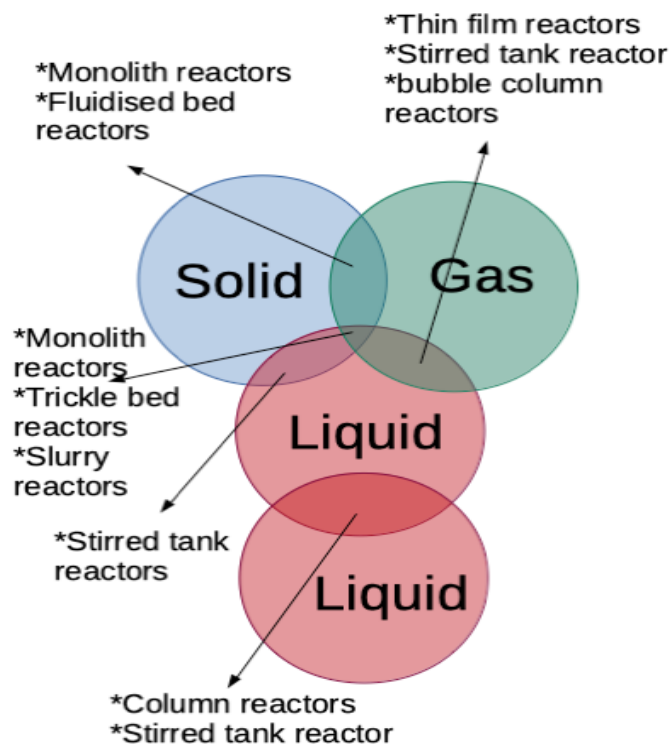


Figure 2.1. Conventional reactor selection criteria.

Table 2.10: Few recent studies done using polymers.

Photo-catalyst	Polymer	Details	Model pollutant	Light source	Reactor volume	Performance	References
TiO ₂	Polystyrene	Beads, 18 wt.% cat. loading	50 ppm methylene blue, indigo carmine, and drimaren red.	UV light	200 mL	8, 17 and 20% decolourisation of the methylene blue, indigo carmine, and drimaren red, respectively after 300 min of reaction.	Magalhães and Lago 2009
TiO ₂	Polycaprolactone	Film, 5 wt.% catalyst loading	20 ppm Chlorophenol	UV-C and UV-A	50 mL	85% and 89% degradation under UV-A and UV-C irradiation respectively in 150 min.	Sivlim et al. 2012
TiO ₂	Polystyrene	Film, 10 wt% cat. loading	5 ppm Methylene Blue	UV-C	50 mL	93% decolourization in 450 min.	Singh et al. 2013
ZnO	Polycarbonate optical disk substrate	Polycarbonate optical disk substrate	2×10^{-5} M Methyl orange	UV-C	500 mL	95% in 160 min.	Chen et al. 2013
TiO ₂	Polystyrene	Film, 10 wt.% catalyst loading	5 ppm MB	UV-C	50 mL	96% decolourization in 390 min.	Singh et al. 2015b
ZnO	Polystyrene	Polystyrene pellets with 1.1 wt.% loading	25 ppm caffeine and paracetamol	UV-LEDs	50 mL	caffeine and paracetamol degradation were about 90 and 77%, respectively, after 240 min.	Saran et al. 2016
TiO ₂	Polyaniline-carbon nanotubes	Immersion area of the immobilized	1 ppm Diethyl phthalate	LED light	100 mL	Highest degradation achieved was 50.8% in 120 min	Yuan et al. 2017

Photo-catalyst	Polymer	Details	Model pollutant	Light source	Reactor volume	Performance	References
		photocatalysts was 80.2 cm ²					
TiO ₂	TiO ₂ -PANI/Cork floating photocatalyst	TiO ₂ -PANI (50 wt. %)/Cork floating photocatalyst	15 ppm MO	Natural sunlight	100 mL	degradation rates after 210 min are 93%, 60.6%, 85.3%, 73.4%, 65.5%, 68.2% and 65.0% were attained for MO, phenol, 581 4-nitrophenol, 2,4-dinitrophenol, toluidine, salicylic acid and benzoic acid, respectively.	Sboui et al. 2017
TiO ₂	Poly(vinylidene fluoride-trifluoroethylene)	8 wt.% TiO ₂ Poly(vinylidene fluoride-trifluoroethylene) membrane	Tartrazine	Sunlight	1000 mL	78% degradation in 300 min	Aoudjit et al. 2018

Table 2.11: Studies done using different types of photocatalytic reactors.

Photocatalytic reactor type	Photocatalyst	Pollutant	Light source	Findings	Reference
Shallow Pond	TiO ₂	4-chlorophenol (12.8 and 51 ppm)	Solar light	Maximum 90% degradation observed in 2 h.	Klausner et al. 1994
Airlift reactor	TiO ₂ thin film (6.5 g/ m ² , >99% anatase) supported on a glass surface	1-amino-4-bromoanthraquinone-2-sulfonic acid (100-1000 ppm, 5 L)	UV	90% colour removal, 50% COD removal and more than 90% TOC. removal observed in 12 h	Verfahrenstechnik 1996
	TiO ₂ Immobilized on diatomaceous earth particles	Polyoxy ethylene alkyl ether (surfactant of 1-3 g/ m ³ , 5 L; substrate bulk density of 0.45 g/cm ³ and surface area of 70 m ² /g)	UV	Approximately 90% degradation in 3 h.	Chan et al. 2003
	TiO ₂ in porous Nickel (0.25 m ² /g)-Coated TiO ₂ film (8.5 m ² /g)	Quinoline (10 - 120 ppm, 3.5 L)	UV	Almost complete degradation of quinoline was observed within 60 min of irradiation.	Zhu et al. 2012b
	Slurry ZnO (6.6 nm)	MB (6 ppm, 15 L)	UV	97% colour removal occurred in 30 min.	Xu et al. 2012

Photocatalytic reactor type	Photocatalyst	Pollutant	Light source	Findings	Reference
	Slurry TiO ₂ (10-15 nm)	MB (4.08-6.73 ppm, 15 L)	UV	98% dye was removed within 40 min of irradiation.	Xu et al. 2013
	Fe-doped TiO ₂	Alizarin Green (15 ppm, 1.5 L)	UV	86% degradation was achieved in 100 min.	Si et al. 2015
Fountain reactor	TiO ₂	Salicylic acid (20 ppm, flow rate: 0.2 L/min)	UV	21% degradation attained	Puma and Yue 2001; Abdel-Maksoud et al. 2016
Compound parabolic reactor	TiO ₂	Cyanide (50 ppm, 2000 L)	Sunlight	975 L cyanide was mineralised in 3 days.	Malato et al. 2002
	TiO ₂	Municipal wastewater (200 ppm DOC,; 35 L)	Solar light	Only 18% DOC reduction observed in 6 h.	Kositzi et al. 2004
	TiO ₂ immobilized in glass spheres	15 different emerging contaminants (0.1 ppm, 10 L)	Sunlight	85% of the pollutants were degraded within 2 h.	Miranda-García et al. 2011
	TiO ₂ immobilized in pumice stone	Triclosan (12.12 ppm, 21 L)	Sunlight	50.5% degradation was observed in 2 h.	Martínez et al. 2014

Photocatalytic reactor type	Photocatalyst	Pollutant	Light source	Findings	Reference
	TiO ₂ coated in stainless steel	Benzoic acid (100 ppm, 7 L)	Solar light	30% TOC removal in 3 h.	Vaiano et al. 2018
Optical fibre reactor	TiO ₂ -immobilized optical-fiber	Giardia lamblia (cell/cm ³ 3-5×10 ⁵ , 1.3 L)	UV	83% Disinfection observed in h at 40 °C	Yu and Q 2004
Submerged membrane reactor	TiO ₂	Fulvic acid	UV	73% TOC reduction achieved within 2 h.	Fu et al. 2005
Tubular reactor	Platinized TiO ₂ supported on silica gel	Benzene, toluene, ethylbenzene, and xylene mixture (2.25 ppm)	Solar light	Complete distraction occurred within 6.35 min	Farrell 2006
Pebble bed reactor	TiO ₂ coated silica rich white pebbles	Mixture of six different reactive dyes (83 ppm TOC, 10 L)	Sunlight	15% TOC reduction was achieved in 5 h.	Neti et al. 2012
Flat plate reactor	TiO ₂	Pyrimethanil (15 ppm, 15 L)	Solar light	86% degradation by photocatalysis is observed in 52 h.	Plantard et al. 2012
	N-doped TiO ₂ immobilized on glass spheres	MB (10 ppm, 0.375 L)	UV	90% degradation achieved in 6.5 h.	Vaiano et al. 2015
	TiO ₂	Chlorophenol	Solar light	60% chlorophenol degraded within 2.5 h.	Abdel-Maksoud et al. 2016

Photocatalytic reactor type	Photocatalyst	Pollutant	Light source	Findings	Reference
Photo capillary reactor	TiO ₂ slurry and immobilized in capillary tube	Salicylic acid (100 ppm, 45 mL)	UV	Only 10% reduction in efficiency was observed after 3 consecutive use of immobilized catalyst.	Hurtado et al. 2016
Solar photoreactor	TiO ₂ coated in plastic granuals	MB (25 ppm, 10 L)	Solar light	Almost complete decolourization occurred within 20 h.	Sutisna et al. 2017
Tray reactor	Sand supported TiO ₂	Phenol (25 ppm, 3 L)	UV	44% degradation was observed in 4 h.	Abdel-Maksoud et al. 2018
Packed bed reactor	N-doped TiO ₂	MB (7 ppm, liquid flow rate: 50 mL/min)	Visible light	Almost total decolourisztion of the dye within 2 h.	Sacco et al. 2019

The above-mentioned photocatalytic reactors (**Table 2.11**) are mostly employed for lab scale or pilot scale, still waiting to cross the barrier to industrial scale. An efficient design and scale-up of the photocatalytic reactor is still a difficult task. To design a photocatalytic reactor it is very essential to consider important parameters, such as the kind of light source needed (Stropa et al. 2015), maximum utilization of light (Cheriyannan et al. 2013), type of photocatalyst (immobilized or suspended) (Pujara et al. 2007; Rodríguez Couto et al. 2002), and minimum volume of reactor to catalyst surface area required to achieve maximum efficiency etc. Even though there are several number of photocatalytic reactors are suggested, the industrial scale up implementation is still need some attention regarding the following common difficulties (Ray 1997):

- 1) Surface area to volume ratio: To produce the high ratio of irradiated surface area to total volume is difficult especially in case of immobilized catalyst (AL-Mashhadani et al. 2015; Amano et al. 2013; Motegh et al. 2014). For slurry operation, the nano size particles can be a good choice for high surface area to volume ratio, whereas for immobilized operation, substrate material with high surface area can be a good alternative such as pumice stone, perlite etc (Chan et al. 2011; Sadi et al. 2015).
- 2) External light source and transparent material: Photocatalytic reactor needs to be specifically designed according to the light source used. Transparent outer shell of reactor is needed if external light source is used, which is very difficult in scale up of a reactor. Mainly glass is used as a transparent material in reactor construction, which imposes size limitation, sealing problem and breakage risk. The choice of the light source very often decides that what kind of photocatalytic reactor could be used or vice-versa (Gómez et al. 2016; Thakare and Bhave 2005). Instead of using glass, any other transparent material (perspex) can be used which is not fragile and easily implementable for photocatalytic reactor (Wang et al. 2012). The use of transparent reactor vessel can be eliminated from the scenario by placing the light source inside the reactor (Na et al. 2005; Pongyeela et al. 2013).

- 3) **Distribution of light:** It is very difficult, distribution of light uniformly on the surface of catalyst into the photocatalytic reactor. Nanoparticles have large surface area, in a vertical column photocatalytic reactor only a portion of suspended nanoparticles gets to absorb the light from external light source. In case of immobilized nanoparticles, a very thin film of catalyst is coated in a carrier surface; so, the active part of the catalyst is very less which comes in contact with light, even though surface area of catalyst is high (Mukherjee and Ray 1999a; Vishnu Pareek, Siewhui Chong 2008; Ray and Beenackers 1998; Yoshikawa et al. 2003). The light source can be maintained as close as possible to the catalyst surface and in case the light source is outside the reactor vessel, the transparent vessel should not absorb the light which is irradiated for the catalyst activation. Use of reflector can also help in this regard.
- 4) **Catalyst surface area:** Large catalyst surface area is needed for photocatalytic reactor driven by solar light. As it has already been discussed that nanoparticles have large surface area but only a small portion of it will be active; so, nanoparticle with larger surface area will be more preferable (Mukherjee and Ray 1999b; Kete et al. 2018).
- 5) **Efficient catalyst:** Solar light focused photocatalytic reactor need efficient catalyst that shows appreciable photocatalytic activity under solar light. photocatalyst with large surface area and reusable for several times, having same efficiency property will be an innovative idea (Bai et al. 2012; Lin et al. 2016; Mukherjee et al. 2014).
- 6) **Pollutant concentration:** Based on pollutant concentration, the catalyst amount should be present into the reactor medium. This problem may restrict the capacity of the reactor and the necessary time required to achieve high conversion (Nan and Jin 2012; Shen et al. 2017b; Sivakumar et al. 2013; Soares et al. 2007).
- 7) **Residence time:** Longer residence time for the catalyst is beneficial for the pollutant degradation, but the use of baffles or any such strategy can reduce the

light irradiation on catalyst surface hence bring down the photocatalytic efficiency (Abid 2015; Lea and Adesina 1999; Rodríguez Couto et al. 2002; Xu et al. 2016c). Highly efficient photocatalyst, which shows better productivity with less residence time can be a good addition in this regard.

- 8) Weather dependency: Solar light driven photocatalytic reactor face another problem i.e. dependence on weather. Hence the reactor should be designed in such a way that the simulated solar light can also be used for the same purpose (Chan et al. 2003; Farrell 2006).
- 9) Reuse: The Reuse of photocatalyst for beyond four times is usually not worthwhile. In case the photocatalyst is coated on the reactor inner surface, the catalyst has to be replenished after three or four recycles (Magalhães et al. 2011; Gilmour et al. 2013; Vaiano and Iervolino 2018; Wang et al. 2016).
- 10) Temperature: Maintaining the equilibrium temperature in industrial scale reactor is difficult, especially in case of transparent reactor outer surface, because the cooling jacket cannot be provided which can block the light irradiation. Cool air can be circulated into the reactor, but that can again increase the operating cost (Bhatkhande et al. 2002; Saien and Shahrezaei 2012; Zhu et al. 2012b).
- 11) Catalyst immobilization: The immobilization of the catalyst can be done using various substrate materials (brick, rock, polymer, glass, metal, ceramic, perlite, cork etc.). The shape, size and physical properties of the substrate material also plays an important role in this regard. Also, the way of using the substrate material can also be a vital factor for the efficient outcome. Based on the material packing (irregular shape, regular shape, film, floatability etc.) the reactor performance can change.

2.12. Various aspects of multiphase photocatalytic reactor design for wastewater treatment:

Most of the photocatalytic reactors are capable of complete degradation or removal of contaminants but still there are some parameters that need to be improved for an ideal photocatalytic reactor. Those parameters are, a) reduction of residence time, b) reuse of photocatalyst for several times without reducing efficiency, c) high performance catalyst, d) effective design of photocatalytic reactor, f) effective use of solar light, g) reduce the fabrication cost of a photocatalytic reactor, h) reduce the reactor surface area, i) high mass transfer between gas and liquid, j) selection of suitable substrate material for the immobilization of the catalyst, k) reduce the fabrication and operating cost of the reactor.

2.13. Scope and objectives

From the literature, it has been identified that there is no reported industrial scale photocatalytic reactor. The scope of this work is to find out a highly efficient photocatalyst that works under visible light. Also, the issues associated with catalyst immobilization and reuse, scale-up in photocatalytic reactors, and development of a novel solar light photocatalytic reactor are sought to be explored in this work. The objectives of this work include:

I. Synthesis and characterization of

- a) rGO and g-C₃N₄ Catalyst powder
- b) TiO₂ – PS film
- c) (TiO₂/rGO/g-C₃N₄) – PS film (admixture)
- d) (TiO₂/rGO/g-C₃N₄) – PS film (chemical composite)

II. Evaluation of the photocatalytic activity of (I(b)) for the degradation of RTB dye wastewater under UV irradiation

- a) Batch reactor studies
- b) Optimization of conditions
- c) Scale-up and recirculation aspects

III. Development of a novel multiphase reactor utilizing the catalysts in (I(b) and (c)) for RTB degradation under UV irradiation.

IV. Evaluation of the catalyst developed as mentioned in (I(d)) in the same reactor under sunlight.

V. Extension of the above work to utilize waste polystyrene for the synthesis of the photocatalyst and evaluation of its performance.

CHAPTER 3

MATERIALS AND METHODOLOGY

CHAPTER 3

MATERIALS AND METHODOLOGY

3.1. Materials used

Melamine, graphite powder (20 μ) and polystyrene (MW \sim 350,000) were acquired from Sigma Aldrich. Titanium dioxide (Degussa P25, 3.2 eV bandgap, 20–30 nm) was procured from Evonik. Nitric acid and sulphuric acid were purchased from Loba Chemie Pvt. Ltd. Mumbai. Potassium permanganate was purchased from Molychem, Mumbai. Ethanol was obtained from Changshu Hongsheng Fine Chemical Co. Ltd, Changshu City. Chloroform was purchased from Merck Life Science Private Limited, Mumbai. Hydrogen peroxide was procured from Medilise chemicals, Kannur. Remazol Turquoise Blue (G– 133, $\text{CuC}_{40}\text{H}_{24}\text{N}_9\text{O}_{17}\text{S}_6\text{Na}_4$) (**Figure A1**) was supplied by Sisco Research Laboratories Pvt. Ltd., Mumbai. The waste polystyrene, which is basically thermocol, was procured from various packing materials available locally. The procured chemicals were used without further purification, and distilled water was used to prepare all the solutions. Remazol orange 16 ($\text{C}_{20}\text{H}_{17}\text{N}_3\text{Na}_2\text{O}_{11}\text{S}_3$) (**Figure A2**) and Remazol black 5 ($\text{C}_{26}\text{H}_{21}\text{N}_5\text{Na}_4\text{O}_{19}\text{S}_6$) (**Figure A3**) are purchased from SRL Pvt. Ltd. Rhodamine B (**Figure A4**), Methylene Blue (**Figure A5**) and Congo Red (**Figure A6**) was procured from Nice Chemicals Pvt. Ltd, Merck Life Science Pvt. Ltd, and Loba Chemie Pvt. Ltd, respectively. The properties of the dyes are given in **Table A1**.

3.2. Methodology

3.2.1. Synthesis of photocatalysts

In this work, four different photocatalysts (TiO_2 , rGO, g- C_3N_4 , and $\text{TiO}_2/\text{rGO}/\text{g}-\text{C}_3\text{N}_4$ -composite) were used. Among them, only TiO_2 was purchased and rest of the photocatalysts were synthesized. rGO was prepared by modified staudenmaier method (Moo et al. 2014; Zhu et al. 2010), whereas g- C_3N_4 , and $\text{TiO}_2/\text{rGO}/\text{g}-\text{C}_3\text{N}_4$ -composite were synthesized by calcination method (Zhai et al. 2013; Shen et al. 2017).

3.2.2. rGO synthesis

rGO was synthesized from graphite powder by the modified Staudenmaier's method is shown in **Figure 3.1** (Moo et al. 2014). Known quantities of sulfuric acid and nitric

acid was added to a reaction flask and the mixture was cooled in an ice bath at 8 °C for 15 min. Graphite powder is then slowly added to the mixture under vigorous stirring to avoid agglomeration and to obtain a homogeneous dispersion. Potassium permanganate was slowly added to the mixture to avoid a sudden increase in temperature. After the complete dissolution of potassium permanganate, the reaction flask was kept in a fume hood under vigorous stirring to allow the evolution of gas at room temperature. The resulting mixture was then poured into distilled water (1 L) and filtered, to remove excess acid from the GO (**Figure A7**). The GO was then re-dispersed and repeatedly washed until a neutral pH of the filtrate was obtained. The GO slurry was then dried in a hot air oven at 100 °C for two days before use. The oxidation of the activated carbon takes place during the preparation of GO and for further oxidation, H₂O₂ (10 mL) is added to the GO powder dropwise (Monteserín et al. 2017). After addition of the H₂O₂, the solution was stirred for the next 24 h. The final solution was centrifuged and separated solid (rGO) was washed several times till it shows constant pH value. Before using the prepared rGO, it was dried and ground properly.

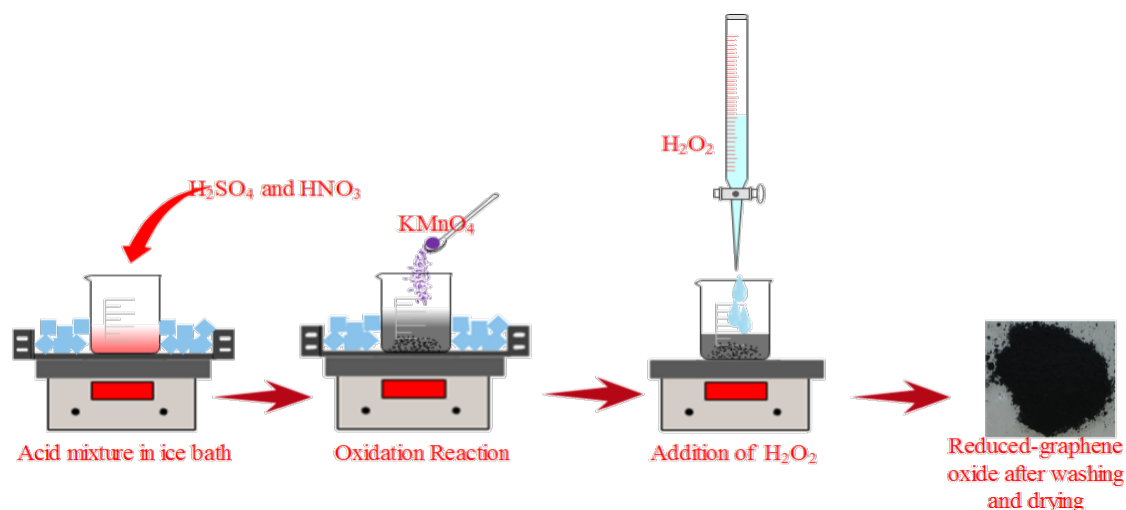


Figure 3.1. rGO synthesis procedure.

3.2.3. Preparation of graphitic carbon nitride (g-C₃N₄)

Melamine (1.0 g) was heated in a muffle furnace at 520 °C for 4 h. After cooling down to room temperature, the obtained pale yellow g-C₃N₄ powder (**Figure A8**) is ground into a powder (Zhai et al. 2013; Liu et al. 2016).

3.2.4. Photocatalyst composite preparation

A modified method was used for the synthesis of the composite material. The $\text{TiO}_2/\text{rGO}/\text{g-C}_3\text{N}_4$ composite was prepared by a facile calcination method as described in (Shen et al. 2017). Instead of using only melamine, a mixture of TiO_2 , rGO, and powder melamine was kept in a furnace for 4 h at 520°C to prepare the composite material. Since $\text{g-C}_3\text{N}_4$ was synthesized by calcination of its raw material (melamine), by varying the amount of melamine (7–42 g) while keeping the amounts of TiO_2 and rGO (2 g and 5 g) constant, different photocatalyst composites were prepared and the resulting composites analyzed for their photocatalytic activity.

3.2.5. Preparation of waste polystyrene for reuse

Thermocol is an expanded polystyrene that can be produced easily by applying air and steam in controlled conditions and is large in size however very light weight which makes it popular as a packing material (Sudeep and Sunil 2018). The collected thermocol was dissolved using acetone and dried at ambient temperatures as shown in **Figure 3.2**. This dried polystyrene was reused as a substrate material instead of fresh or pristine polystyrene to immobilize the photocatalyst for the comparison study.



Figure 3.2. Synthesis of waste polystyrene.

3.2.6. Immobilisation of photocatalyst

The photocatalyst immobilization is done using solvent casting method in polystyrene substrate (Sivlim et al. 2012). The thickness of the prepared polystyrene–photocatalyst film was kept constant. All the photocatalysts are immobilized by the same method but the application is different based on the reactor design.

The immobilization of the photocatalyst in polystyrene (both pristine and waste polystyrene) was done using a solvent casting method (**Figure 3.3.**) (Vaiano et al. 2018). A mixture of polystyrene (42.5 g) and catalyst (known amount of TiO_2 or admixture of (TiO_2 , rGO, and $\text{g-C}_3\text{N}_4$) or $\text{TiO}_2/\text{rGO}/\text{g-C}_3\text{N}_4$ –composite)) was added to a solvent (a mixture of chloroform (400 mL) and ethanol (50 mL)) and sonicated for 1 h followed by heating and mixing for 4 h in a hot magnetic stirrer at $110\text{ }^\circ\text{C}$. The thickened solution was cast in a glass tray of dimensions $28\text{ cm}\times 32\text{ cm}$ and cooled in a fume hood at ambient temperature. After the complete evaporation of the solvent, the dried film was taken out from the tray and cut to the desired shape for the photocatalytic study.

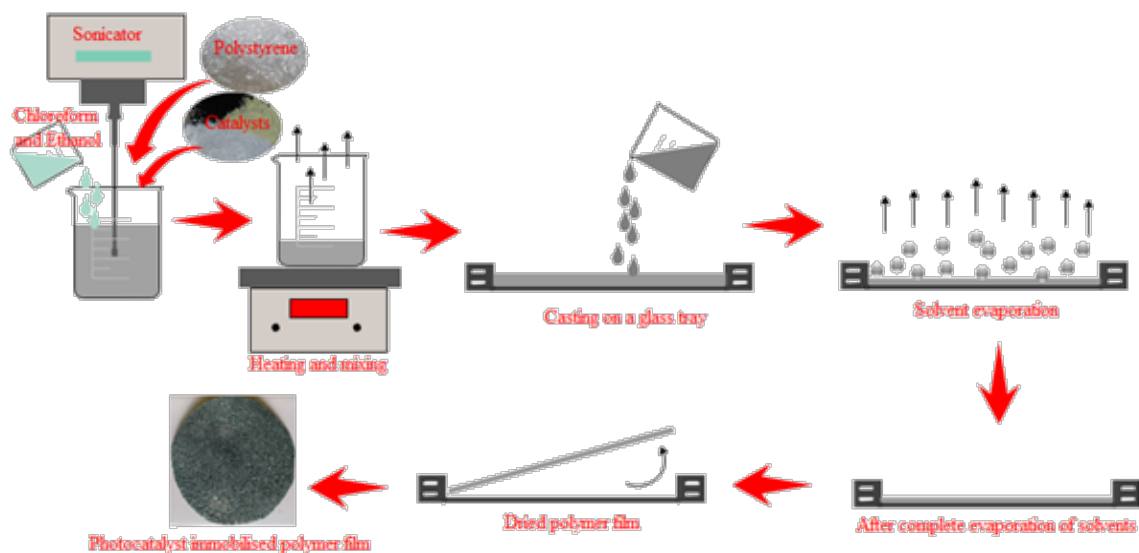


Figure 3.3. Catalyst immobilization procedure.

3.2.6.1. Preparation of immobilized TiO_2 film

The polymer–supported photocatalytic film was prepared by addition of a 42.5 g of the polystyrene granules and titanium dioxide (a known weight percentage with respect to the amount of polymer used e.g., 2 wt.% and so on).

3.2.6.2. Preparation of immobilized TiO₂, g-C₃N₄, and rGO admixture film

A different amount and combination of catalysts (unary, binary and ternary mixture with different ratio) were used for the immobilization of TiO₂, g-C₃N₄, and rGO admixture (10 wt.% of polystyrene).

3.2.6.3. Preparation of immobilised TiO₂/rGO/g-C₃N₄ –composite film

The same procedure was used for the immobilization of the catalyst (8, 10, 12 and 14 wt.% with respect to the amount of polystyrene (42.5 g)).

3.2.7. Photocatalytic activity analysis

The immobilized photocatalyst into polystyrene is used in different reactors for photocatalytic analysis. The photocatalytic decolourization and degradation of the RTB dye are done in various photocatalytic reactors. The degradation analysis is done considering several operating parameters. Moreover, the adsorption study is also carried out each time prior the photocatalytic study (Singh et al. 2013). The calibration curve for RTB is shown in **Figure A9** and all the photocatalytic experiments were repeated at least twice.

3.2.7.1. Batch study

Before illumination, a 9 cm diameter PST film (**Figure 3.4a**) was dipped in 200 mL of 10 ppm dye solution in a crystallizing dish (**Figure 3.4b**) of 10 cm diameter and kept in the dark for 30 min under stirring for attaining adsorption–desorption equilibrium (denoted as –30 to 0 min in the graphs). After the adsorption study, the photocatalytic decolourization study was carried out under UV–C irradiation for the next 2 h (Singh et al. 2015). The surface UV illumination was provided by five tube lights of 20 W (Philips T18 UV–C tube light, 1.07 Klux). Samples were collected from the solution every 10 min. The absorbance of each sample was measured using a UV–Visible Spectrophotometer (Hitachi Model GBC PM&E101) at a λ_{max} of 666 nm.

A similar batch study using 550 mL of 10 ppm dye solution and a 15 cm diameter PST film was performed in an 1100 mL crystallising dish. The scale–up criteria was based

on constant pollutant volume to catalyst surface area ratio. The same procedure was used for evaluating the photocatalytic activity under UV-A (Philips 18W).

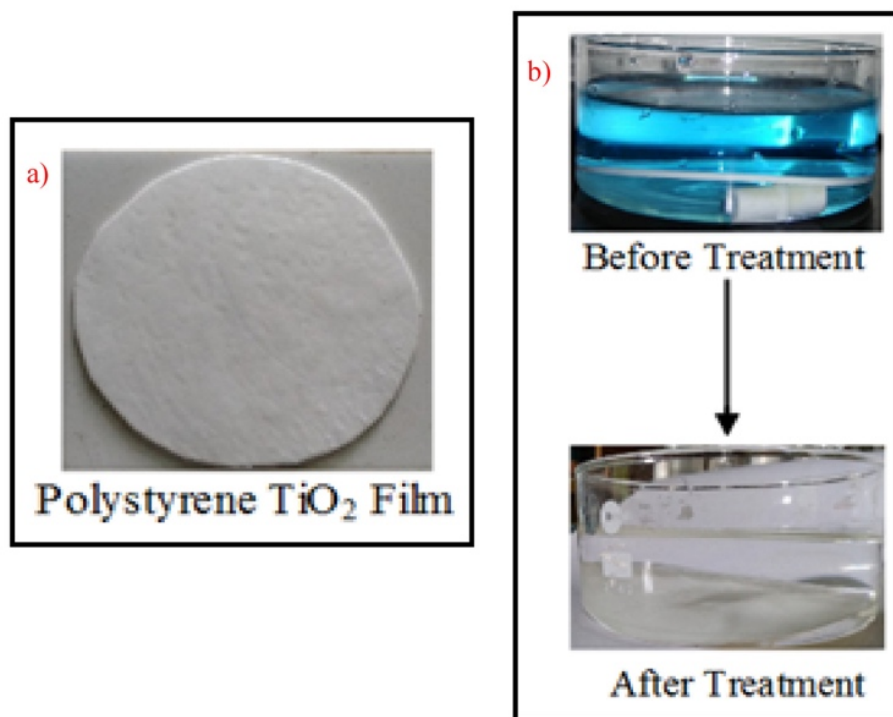


Figure 3.4. Batch process for RTB dye degradation, a) polystyrene TiO₂ film, and b) 10 ppm dye solution before and after use.

3.2.7.2. Recirculation study

A recirculation study (schematic shown in **Figure 3.5.**) with 550 mL reactor volume of 10 ppm dye solution (using the same crystallizing dish with a 15 cm diameter PST film) and 2350 mL solution (~ 4 times the reactor volume) in the reservoir is conducted for 6 h. A peristaltic pump (Acuflo-D150AX) was used to recirculate the liquid and samples were collected in every 30 min. The methodology for the efficiency comparison of batch, batch scale-up and scale-up recirculation process is summarized in **Figure 3.6.**

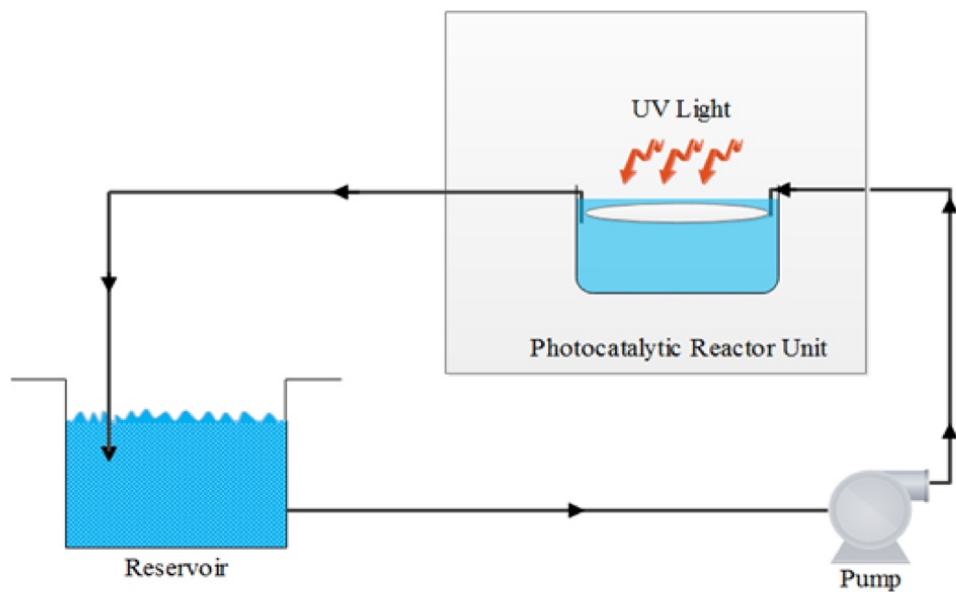


Figure 3.5. Batch process for RTB dye degradation.

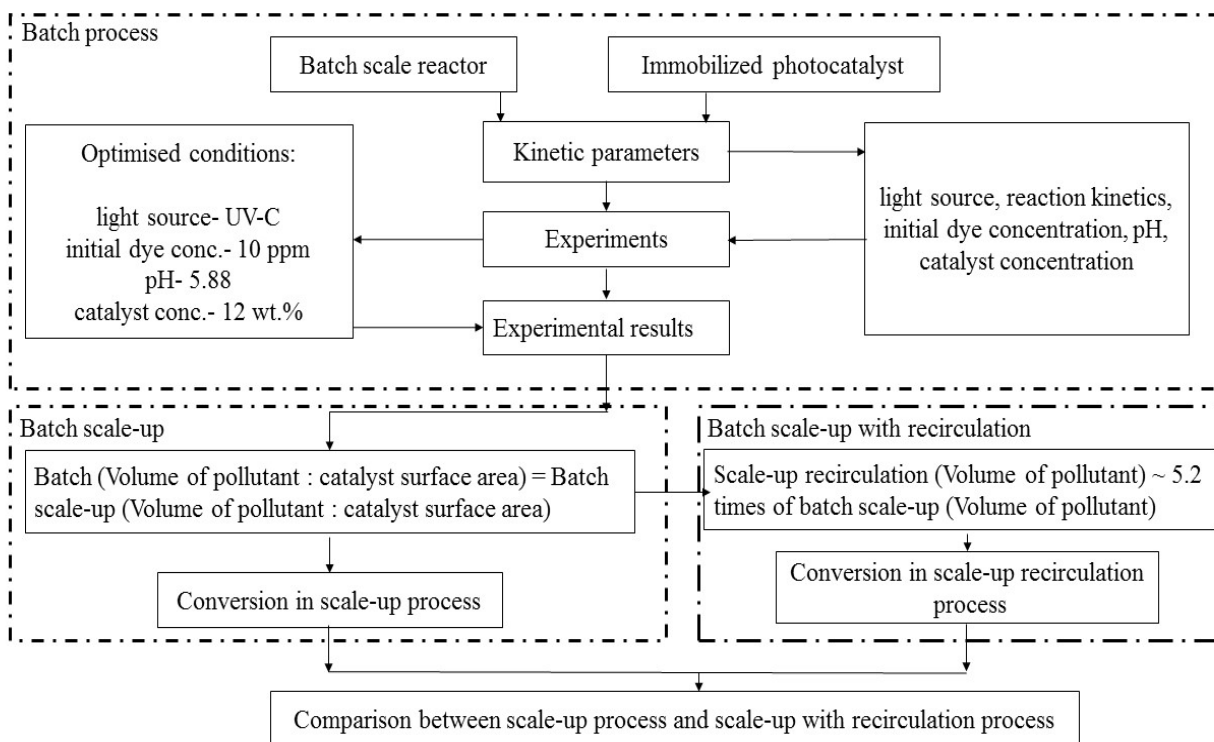


Figure 3.6. Methodology of photocatalytic reactor scale-up studies.

3.2.7.3. Photocatalytic activity analysis in a multiphase airlift reactor under UV light

The photocatalytic system with immobilized photocatalyst mixture is as shown in **Figure 3.7**. An internal loop ALTR was fabricated from a quartz glass column 8 cm ID (D_o) and 30 cm long (volume 1500 mL, quartz glass) and an inner draft tube of 2/4/6 cm OD (D_i) and 22 cm long. The reactor was installed in a rectangular wooden box chamber (60 cm \times 50 cm \times 50 cm) with vertically fixed UV lights (Philips 20-watt UV-C lamp, light intensity 1.97 Klux) on the walls (one side of the wall is adjustable). Just like in conventional airlift reactors, in this reactor also, mixing or liquid circulation is induced by bubbling the air (from the air compressor, SC150-PM & E-2A, Elgi Equipments Limited, India) using a sintered porous sparger from the bottom of the reactor through the inner draft tube. The airflow was monitored using a rotameter. The outer surface of the inner draft tube was wrapped with the prepared polystyrene photocatalytic film (IP), and the UV lights were placed approximately 10 cm from the reactor vessel. To avoid the effect of the increasing temperature inside the reactor unit due to the use of UV light, an exhaust fan is used.

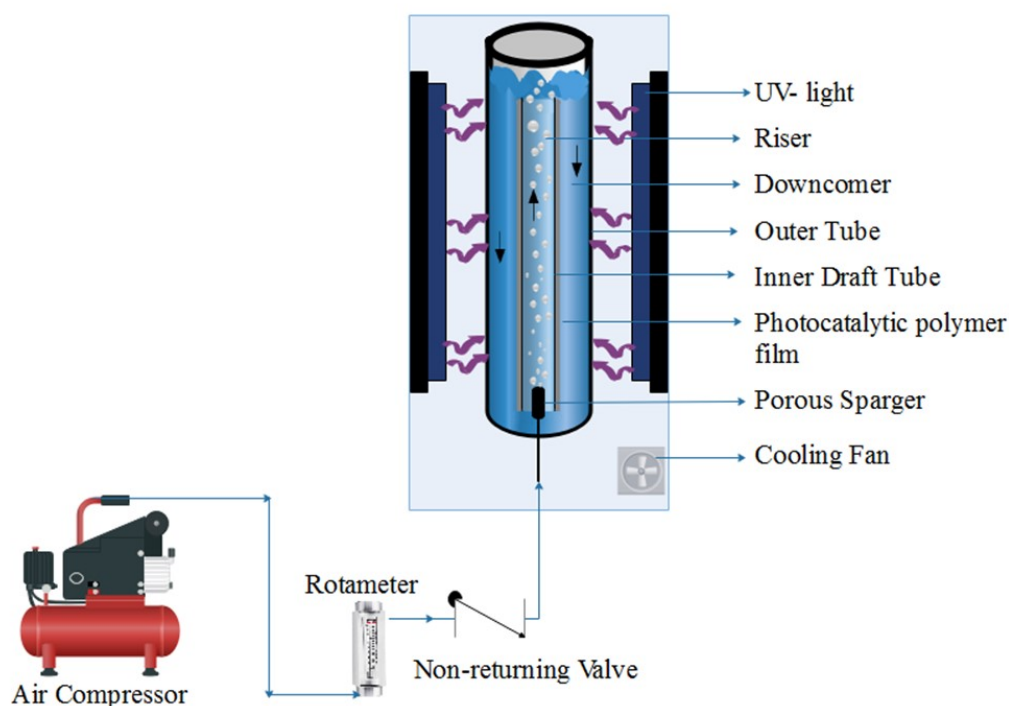


Figure 3.7. Schematic diagram of the fabricated internal loop airlift photocatalytic reactor.

For the photocatalytic study, 1200 mL (working volume of the reactor) of 10 ppm Remazol Turquoise Blue (RTB) dye water has been used as synthetic wastewater. The immobilized photocatalytic film (415 cm² surface area) was attached to the outer surface of the inner draft tube. Adsorption study was carried out for 30 min in the dark, followed by photocatalytic study for another 180 min.

3.2.7.4. Photocatalytic activity analysis in a multiphase airlift reactor under solar light

The same airlift reactor was used for the degradation of the RTB dye under solar light (**Figure 3.8.**). The working volume of the reactor was 1200 mL and the air flowrate 2 LPM. 1200 mL of 10 ppm RTB dye (natural pH 5.88) solution was used for the photocatalytic decolourization and degradation study. Before proceeding for the photocatalytic operation, the adsorption study was performed each time for 30 min under dark conditions. To analyse the decolourization and degradation of the dye, samples were collected from the reactor during the experiment (90 min per run) at specific intervals of time. The mineralization or degradation study of the dye is also carried out by the same procedure used for decolourization, and measured by TOC analysis. All the experiments were carried out twice during the time of September to November 2018 from 12 p.m. to 2:30 p.m. The location, temperature and light intensity of the conducted experiments (latitude 13.011186 and longitude 74.795736, elevation 23 m; environment temperature 30–32 °C, sunlight intensity 69–72 Klux) were noted down. The reduction of RTB concentration during the photocatalytic experiment was measured using a UV–spectrophotometer (Spectro Photometer Labomad NCR III 40) at maximum absorbance (λ_{max}) of 666 nm.

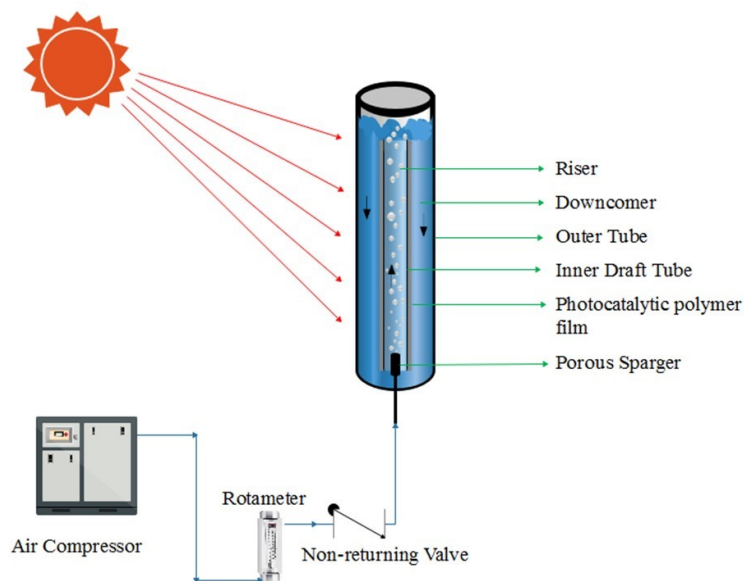


Figure 3.8. Schematic of the multiphase photocatalytic reactor under solar light.

3.3. Characterization of the photocatalysts and polymer nanocomposite films

3.3.1. X-ray powder diffraction (XRD)

X-ray powder diffraction (XRD) is a common analytical technique primarily used for crystalline nature and phase identification of a solid powder material and its unit cell dimensions. XRD works on constructive interfaces of X-rays from a crystalline sample. The monochromatic X-rays produced from cathode ray tube are collimated and redirected towards the sample, which produces constructive interference according to Bragg's law ($n\lambda = 2d \sin\theta$). This law illustrates the relation among the electromagnetic radiation wavelength, diffraction angle and lattice spacing of a crystalline sample. The diffracted x-rays are perceived/identified, processed and calculated by scanning the sample at a range of 2θ . The characteristic diffraction pattern produced in a typical XRD analysis provides a unique identification of the crystal sample (Namatame and Sato 2013; Akhavan et al. 2016). In this work, XRD analysis is used for the product identification as well as phase identification.

3.3.2. Scanning Electron Microscope– Energy Dispersive X-ray (SEM–EDX)

Scanning Electron Microscope– Energy Dispersive X-ray (SEM–EDX) Analysis is used to acquire a high-resolution image using a focused beam of electrons. It is useful for evaluating surface morphology, flaws or contaminants of materials. Particularly,

EDX analysis provides quantitative elemental analysis (chemical composition) of a sample (Williamson et al. 2004; Laskin and Cowin 2001; Srivastava et al. 2009; Pachauri et al. 2013). SEM and EDX analysis provides a detailed inspection of material properties and give valuable insights of the sample.

3.3.3. Fourier Transform Infrared Spectroscopy (FTIR)

Fourier Transform Infrared Spectroscopy (FTIR) Analysis is an analytical technique used to identify organic, inorganic, and polymeric materials. In FTIR analysis method, infrared light is used to scan the samples and observe the chemical properties. The Infrared radiation (usually 100–10,000 cm^{-1} in wave number) transmitted through the sample gets absorbed partially while the remainder passes through. The absorbed radiation gets converted into rotational or vibrational energy and the resulting signal detector presents a unique spectrum (typically between 4000 – 400 cm^{-1}) for a particular sample. FTIR analysis is used to identify and analyze unknown materials (solids, films, powders, or liquids), contaminants present in a material (particles, powders, fibers or liquids), oxidation, decomposition etc (Mudunkotuwa et al. 2014; Ashokkumar and Ramaswamy 2014; Kosa et al. 2017).

3.3.4. X-ray Photoelectron Spectroscopy (XPS)

X-ray Photoelectron Spectroscopy (XPS) is the most widely used surface analysis technique for broad range of materials for quantitative elemental analysis. XPS is usually done by exciting a sample surface with mono-energetic x-rays causing photoelectrons to be emitted from the sample surface. The energy of the emitted photoelectrons is measured by using an electron energy analyzer. From the binding energy and photoelectron peak intensity, the elemental identity, chemical state of the sample, and quantity of a detected element can be determined (Wang et al. 2001; Shallenberger 2014; Ba et al. 2016; Addepalli 2019).

3.3.5. Particle size analysis

In nanotechnology the size of the particle is considered as a crucial parameter to attain the best outcome from it and particle size analyzer is an easy way to find it out (Barth et al. 1987).

3.3.6. Contact angle analysis

The wettability of a solid surface can be calculated by a unique contact angle between solid–liquid interface at a particular temperature and pressure. The contact angle decides the hydrophilic and hydrophobic nature of the material (Kwok et al. 1997).

3.3.7. Profilometer

Profilometer is a technique used to identify the topographical data of a surface. A profilometer is usually used to analyze the surface morphology, step height or surface roughness of a sample. A physically moving probe is used on various points of the sample to identify the different characteristics of the sample (Bullman 2003; Cuesta et al. 2013). In this case, it was used for the surface roughness calculation.

3.3.8. Diffuse reflectance spectra (DRS)

Diffuse reflectance spectra (DRS) is a well–accepted technique for the physico–chemical technique of an opaque solid sample. It works on the principle that the attenuation of the beam of light when it passes through the sample surface or reflects from the sample surface (Zagórski 2003). To quantify the band gap of the photocatalysts DRS is used in here.

3.3.9. Brunauer Emmett Teller (BET) surface area analysis

Brunauer Emmett Teller (BET) is an important analytical tool for the specific surface area analysis of a solid sample. The specific surface area of a powder material is determined by physical adsorption of a gas on the material surface of the solid and by calculating the amount of adsorbed gas corresponding to the single molecular layer on the surface (Choma and Jaroniec 2001).

3.3.10. Inductively coupled plasma–optical emission spectrometry (ICP–EOS)

Inductively coupled plasma–optical emission spectrometry (ICP–OES) is a technique used to find out the elemental composition of a sample (mostly in water) by using plasma and spectrometer. A trace amount of material can be easily identified present in a liquid solution by the ICP–OES (Olesik 2012). In this work, ICP–OES was used to

quantify the amount of leached catalyst from the immobilized polystyrene photocatalytic film.

3.3.11. Density measurement

Density of the waste polystyrene is measured by a simple technique to analyze the effect on the dye decolourization. The following equation is used to calculate the specific density of the waste polystyrene.

$$\text{Specific density of solid} = (X/(X+Y-Z)) \quad (6)$$

Where, X = Weight of sample, Y = Weight of (water + specific gravity bottle), and Z = Weight of (sample + water + specific gravity bottle).

3.4. Characterization of the decolourized/ degraded RTB solution

3.4.1. UV–Vis Spectrophotometer

The UV–Vis Spectrophotometer generally used for the quantitative determination of various analytes, such as transition metal ions, organic compounds, and biological macromolecules. In UV–Vis Spectrophotometer, a beam of 200 to 900 nm wavelength is passes through the sample and the quantity of the sample can be find out based on the absorption of the beam (Hameed et al. 2018).

The photocatalytic performance of the catalyst was calculated by the following equation:

$$\text{Decolourization (\%)} = (1 - (C_t/C_0)) \times 100 \quad (7)$$

Where, C_t = Concentration of dye after time t, C_0 = Initial concentration of the dye at t = 0.

3.4.2. Total Organic Carbon (TOC)

The Total Organic Carbon (TOC) is an important parameter in the assessment of the total organic containment present in water. The absolute quantity of carbon can exactly be defined by TOC. In this study TOC was used to quantify the organic carbon present in the sample (Foss 2002).

The photocatalytic performance of the catalyst was calculated by the following equation:

$$\text{Degradation/Mineralization/TOC percentage (\%)} = (1 - (\text{TOC}_t/\text{TOC}_0)) * 100 \quad (8)$$

Where, TOC_t = Total Organic Carbon after time t , TOC_0 = Initial Total Organic Carbon at $t = 0$.

3.4.3. High Performance Liquid Chromatography (HPLC)

High Performance Liquid Chromatography (HPLC) is a modern analytical technique used to separate, identify, and quantify components present in a mixture. HPLC works on a principle of separation of the materials according to their molecular weight and polarity. The materials that are passing through the chromatography column takes different time based on the affinity of the molecule with the stationary phase (solid or liquid) and the mobile phase (liquid or gas). The ones that have more affinity with the stationary phase takes longer to pass through and vice versa (Ali et al. 2011; Ang et al. 2014; Aniszewski 2015). HPLC helped to quantify the decolourization of the dye.

3.4.4. Mass Spectrometer (LC-MS)

Mass Spectrometer (MS) ionizes the atoms or molecules to facilitate the separation and detection process in accordance with their molecular mass and charge (mass to charge ratio). MS can be used in various applications, such as atomic physics and biochemical (Ardrey 2003; Pitt 2009). In this work it was used to identify the by-products, which has formed during the photocatalytic degradation of the RTB dye.

3.5. The equipment used for the characterization of various samples:

The characterization of the catalyst powder as well as the photocatalytic film were analyzed using various techniques as mentioned in **Table 3.1**. The X-ray diffraction (Rigaku Ultima-IV diffractometer) study of the photocatalysts was carried out in the range (2θ) of $20 - 65^\circ$ with an increment of 0.02° . The morphology of the photocatalytic films (Kamrannejad et al. 2014) were analyzed using SEM (JEOL JSM-6300 LV analytical scanning electron microscope). To quantify the surface roughness, an optical profilometer is used (Bruker Dektak XT). To determine the polarity of the film, a contact angle analyzer (FTA 200 Firsten angstroms) was used. The stability of the

prepared catalyst film analyzed by FTIR (Bruker Spectrometer). Particle size analysis (Horiba SZ-100) was done to know the size of the prepared photocatalyst particles. To analyze the stability of the prepared catalyst film, FTIR (Bruker Spectrometer) measurements were performed. ATR mode of operation was used and 0.1 mg of sample was analyzed over the range of 4000–500 cm^{-1} . A PHI 5000 Versa Probe-II and Omicron ESCA+ photoelectron spectrometer equipped with a wide scan of 0 – 1100 eV was used for the XPS study. The surface area of the prepared composite catalyst was measured by BET (Brunauer–Emmett–Teller) Surface Area Analyzer (Tristar II). The total organic carbon (TOC) present in the dye solution is measured by a TOC analyser (Shimadzu TOC-V-CSN) before and after degradation. High-performance liquid chromatography–mass spectrometry (Shimadzu LCMS-2020) was used to confirm the degradation and find out the final products after the degradation studies. The leachability of the catalyst in the PST film is measured using ICP–OES (Agilent Technologies, 5100 ICP–OES).

High-performance liquid chromatography–mass spectrometry (Shimadzu LC-MS-2020) was used to confirm the degradation and find out the final products after the degradation studies. A volume of 10 μL of sample was injected, and the separation was performed in a 5 μm C18 column (Shim-pack GIST, Japan; 4.6 \times 250 mm; column temperature 35 $^{\circ}\text{C}$). Water and acetonitrile were used as mobile phase and mobile phase b (1:1 ratio) respectively, at a flow rate of 0.1 mL/min. The RTB sample was analyzed at a maximum wavelength of 666 nm, and it took about 20 min to complete the analysis.

Table 3.1. The characterization of various samples carried out in this work.

Sample	Characterization Techniques									
	SEM-EDX	XRD	FTIR	XPS	DRS	ICP-OES	Particle size analyzer	BET Surface area analysis	Profilmometry	Contact angle analysis
TiO ₂ , g-C ₃ N ₄ , and rGO Powders	YES	YES			YES		YES	YES		
TiO ₂ /C ₃ N ₄ /rGO – Composite powder	YES	YES			YES		YES	YES		
Polystyrene – TiO ₂ film	YES		YES	YES		YES			YES	YES
Polystyrene – TiO ₂ , g-C ₃ N ₄ and rGO admixture film	YES		YES	YES		YES				YES
Polystyrene – TiO ₂ /g-C ₃ N ₄ /rGO – Composite film	YES		YES	YES		YES				

CHAPTER 4 RESULTS AND DISCUSSION

**(POLYSTYRENE – TiO₂
PHOTOCATALYTIC FILMS: BATCH
REACTOR STUDIES, SCALEUP AND
RECIRCULATION ASPECTS)**

CHAPTER 4

POLYSTYRENE – TiO₂ PHOTOCATALYTIC FILMS: BATCH REACTOR STUDIES, SCALEUP AND RECIRCULATION ASPECTS

4.1. Introduction

In this section, polystyrene immobilised TiO₂ film is used for the photocatalytic decomposition of RTB dye. The reasons for choosing TiO₂ as the photocatalyst and polystyrene as the substrate material are already stated in Chapter 2. The characterization of the immobilised film is done by SEM, XRD, FTIR, XPS, ICP–OES and Profilometry. First, a small scale batch reactor study was done, followed by scale–up and recirculation studies for the degradation of RTB dye. The main parameters affecting the degradation are studied along with a brief discussion of their effects. The parameters considered for the photocatalytic degradation are pH, catalyst loading, initial pollutant concentration, light source, light intensity, polystyrene film thickness, reusability and a comparison of slurry versus immobilised catalyst efficiencies. The optimised parameters obtained from the small scale study is employed in scale–up study as well as scale–up with recirculation study.

The immobilization procedure of the photocatalyst in the polystyrene was described in section 3.2.6.1 and the photocatalytic activity analytical procedure was described in section 3.2.7.1 and 3.2.7.2.

4.2. Results and discussions

4.2.1. Characterization of immobilised TiO₂ film

4.2.1.1. XRD analysis

In **Figure 4.1a**, the pattern of crystalline TiO₂ has two main characteristic peaks at $2\theta = 25.12^\circ$ (crystal plane (101), according to JCPDS Card no. 21–1272) and $2\theta = 27.27^\circ$ (crystal plane (110), according to JCPDS Card no. 21–1276), indicating the anatase and rutile phases respectively. The x–ray diffraction pattern of the PS– TiO₂ nanocomposite film is also shown in **Figure 4.1b**. This type of pattern confirms that the amorphous

phase is present in the compound because of polystyrene. The two characteristic peaks at 25.12° and 27.27° confirm the presence of crystalline TiO_2 in the film. In addition, the broad peak noticed at 20° corresponds to amorphous polystyrene. The rest of the peaks (except $2\theta = 25.12^\circ$ and 27.27°) observed in **Figure 4.1a** and **b** correspond to anatase TiO_2 . No significant differences in the XRD pattern were observed when this PST film was used for once (**Figure 4.1c**) and 10 times (**Figure 4.1d**). It indicates that the degree of crystallinity remains mostly invariant even after exposing the film under the UV–C light.

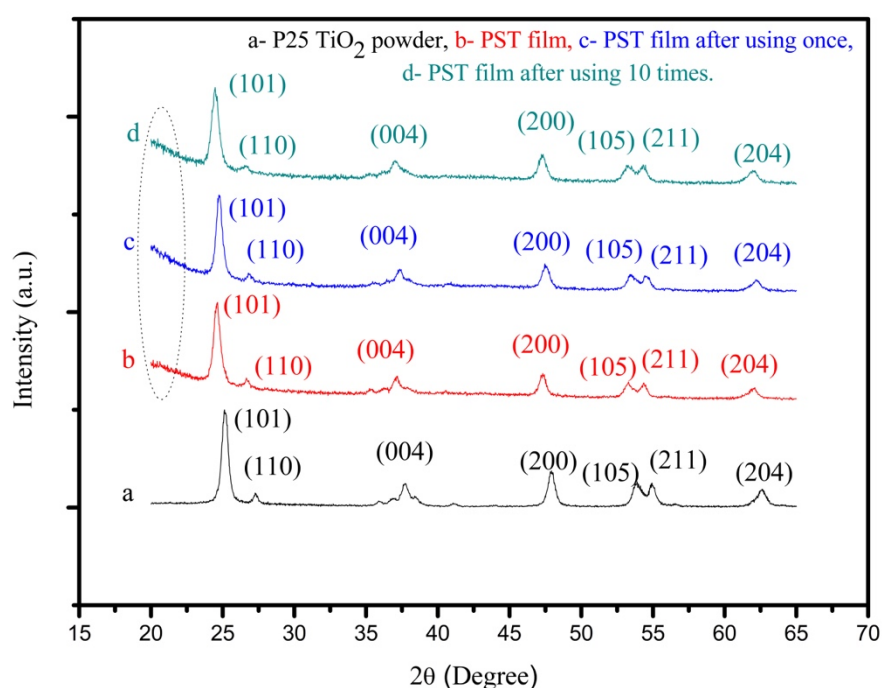


Figure 4.1. XRD spectra of a) Degussa P25– TiO_2 powder, b) PST film with 12 wt.% catalyst, c) PST film after using once, d) PST film after using 10 times.

4.2.1.2. SEM and Profilometry analysis

To find out the thickness of the polymer film, a cross-sectional view of the film using SEM is shown in **Figure 4.2a**. From this and the measurements using a profilometer, the thickness of the PST film is determined as $555 \mu\text{m}$ with an average roughness of $0.33235 \mu\text{m}$ ($\pm 5.6\%$). The SEM image (**Figure 4.2b** and **c**) shows the morphology of the TiO_2 powder and unused PST film along with the TiO_2 particles distributed on the surface of the film. After using the PST film once in the photocatalytic study, the

corresponding SEM image is shown in **Figure 4.2d**. It is evident that there are not many changes in the morphology of the film. From the FTIR spectra (**Figure 4.2c**) it can be observed that some mild changes have occurred in the film. The surface morphology of PST film after ten times use was checked as shown in **Figure 4.2e**. The polystyrene film itself is getting degraded in the presence of TiO₂ under UV light, but the degradation rate is very, very slow (for instance, calculated as 4.1% weight loss for 250 h of continuous UV exposure according to Shang et al. (2003)). It is noted that the total time of exposure under UV–C light in the experiments was 20 h (each experiment = 2 h).

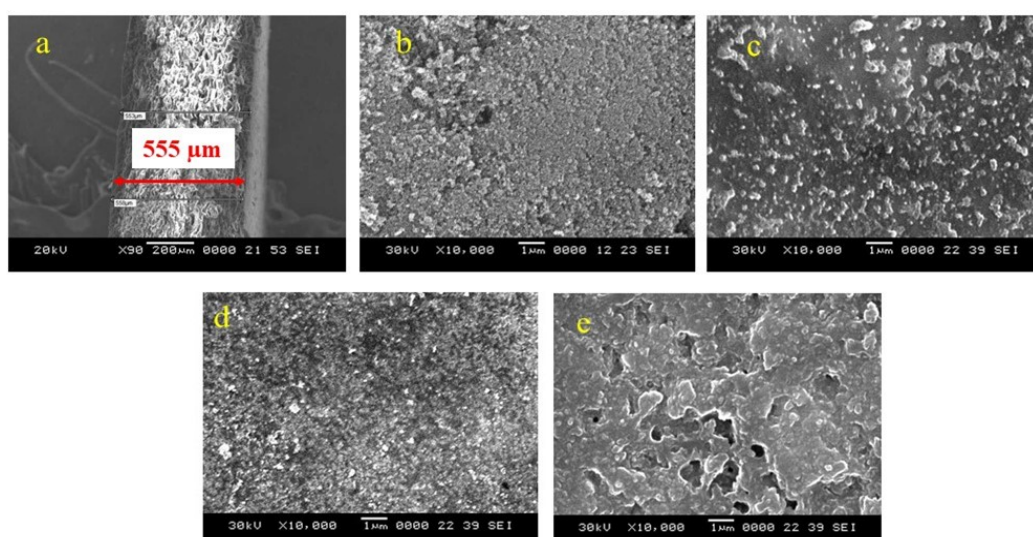


Figure 4.2. SEM images of a) Cross-sectional view, b) TiO₂ powder, c) Unused polystyrene film, d) After using once under optimised condition, e) After using 10 times under optimised condition.

4.2.1.3. FTIR and ICP–OES analysis

Figure 4.6. shows a sequence of FTIR spectra beginning with that for blank polystyrene film, unused wt% PST film, 12 wt% PST film after using once, and finally, the spectrum for 12 wt% PST film after using ten times. In **Figure 4.3a**, the FTIR spectrum of polystyrene film, the first peak is observed at 3026 cm⁻¹, corresponding to the stretching vibration of the C–H bond of the benzene ring present in polystyrene while the second peak is for C–H stretching at 2921.61 cm⁻¹ occurring possibly due to the presence of

some impurities on the sample (Jang et al. 2005). The next peak is observed around 1500 cm^{-1} , corresponding to the bending modes of the C–C bond of benzene ring present in polystyrene. The next three peaks are located at 1600 , 1496 and 1455 cm^{-1} respectively indicating the aromatic C–H bond stretching vibration. The peaks at 1080 , 1031 , 725 and 693 cm^{-1} correspond to the aromatic C–H deformation vibration. In **Figure 4.3b**, the spectra of PST film with 12 wt% catalyst showed some distinct peaks at 2348 and 613 cm^{-1} which proves the presence of the catalyst in polystyrene (Luo et al. 2008). The same peaks are also present in **Figures. 4.3c** and **4.3d** which represents the 12 wt% PST film after using once and ten times for 10 ppm 200 mL RTB dye decolourisation respectively. An inclined lower pitch at the beginning and end of the **Figure 4.3d** is noticed which exemplify the changes on the surface of the PST film (also confirms the SEM image in **Figure 4.2e**). These changes may be due to the slight degradation of the PST film or adsorption of RTB dye on the PST film surface.

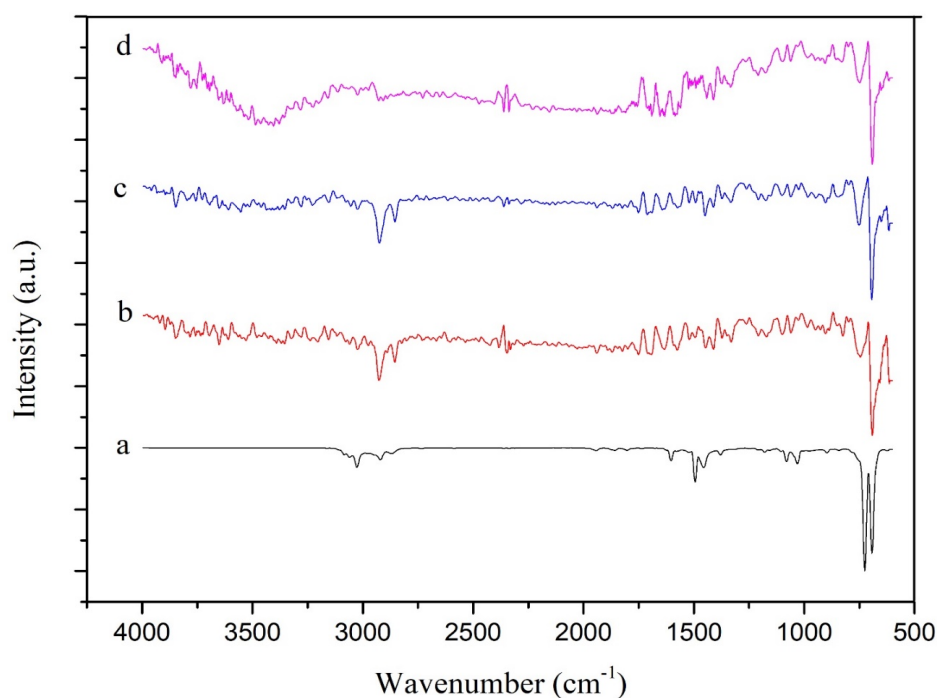


Figure 4.3. FTIR data of a) plain polystyrene film, b) PST film with 12 wt.% catalyst, c) 12 wt% PST film after using once, d) 12 wt.% PST film after using 10 times.

The 24 h of vigorous stirring of PST film in distilled water confirms the leaching of the catalyst from the PST film. The ICP–OES analysis is used to quantify the exact amount

of leached catalyst which is 0.04 ppm (0.0022% of original amount added). This minute quantity of leached catalyst confirms that the polystyrene is a good choice for substrate material for the immobilisation of the photocatalyst.

4.2.1.4. XPS analysis

To investigate the surface composition and chemical states of TiO₂, XPS analysis was done as shown in **Figure 4.4**. The full survey spectrum of the **Figure 4.4a** indicates the presence of titanium (Ti2p), carbon (C1s), and oxygen (O1s) in the PST film (Moo et al. 2014; Suárez et al. 2016). The Ti2p XPS peak at 457.0 is characteristic of Ti³⁺ and 462.8 eV both represents Ti⁴⁺ species in **Figure 4.4b**.

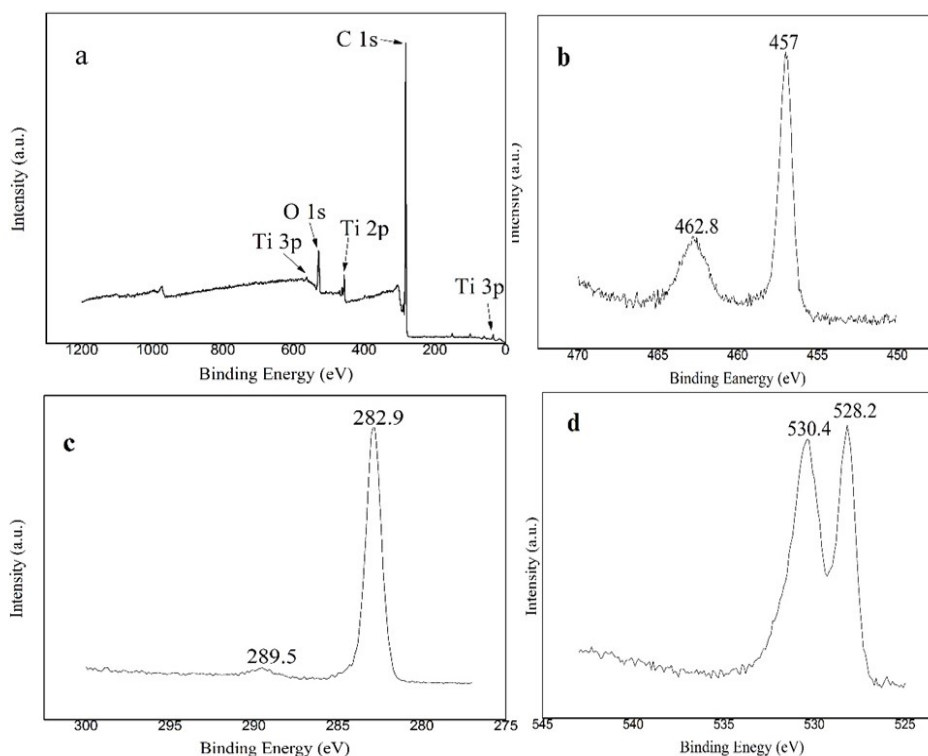


Figure 4.4. a) Low-resolution XPS survey spectra of the PST film b) Ti2p XPS spectra, c) C 1s spectra, d) O 1s spectra.

The peaks at 282.9 and 289.5 eV for C1s spectrum is ascribed to the C–C bond with sp² orbital and C=O bonds, respectively in **Figure 4.4c**. The main peak of the O 1s spectrum at 528.2 and 530.4 eV is attributed to Ti=O and C–OH, respectively in **Figure 4.4d** (Wegewitz et al. 2014). From the above graphs, we can confirm the presence of TiO₂ in

the PST film. The quantitative analysis from XPS study showed that the actual amount of TiO₂ was 0.111167 g, whereas the calculated value was 0.12 g in 1 g of polystyrene (Erdem et al. 2001). This equates to 11.1 wt% of the photocatalyst present in the film showing reasonable agreement with the intended catalyst loading during the preparation of the film.

4.2.2. Photocatalytic activity analysis and optimization study

4.2.2.1. Effect of catalyst loading

To analyse the effect of catalyst loading on the decolourisation of RTB dye, the photocatalytic experiment was performed on the model pollutant with different catalyst loadings ranging from 2 to 20 wt.%. The effect of the catalyst loading on the photocatalytic decolourisation of RTB is shown in **Figure 4.5**. The photocatalytic activity is almost the same for catalyst loadings of 2 to 10 wt.%, and at 12 wt.%, the best photocatalytic activity is observed. For catalyst loadings more than 12 wt.%, it is observed that the photocatalytic activity has decreased. The increased loading of the catalyst causes a rise in the generation rate of electron/hole pairs and thus, the formation of •OH radicals, leading to the improvement in photodegradation. When the catalyst loading is low, the surface area due to the pores created on the PST surface during the solvent casting method is relatively unaffected, thus favouring adsorption of the dye molecules on the film and consequently, photodegradation. On the other hand, an excess of catalyst on the PST film may reduce the pore size as well as the number of pores due to the agglomeration of the catalyst particles on the film surface thus causing a slight decline in the photocatalytic activity. This may explain why the photocatalytic activity of the PST film increased with increasing catalyst loading up to 12 wt.% and then decreases.

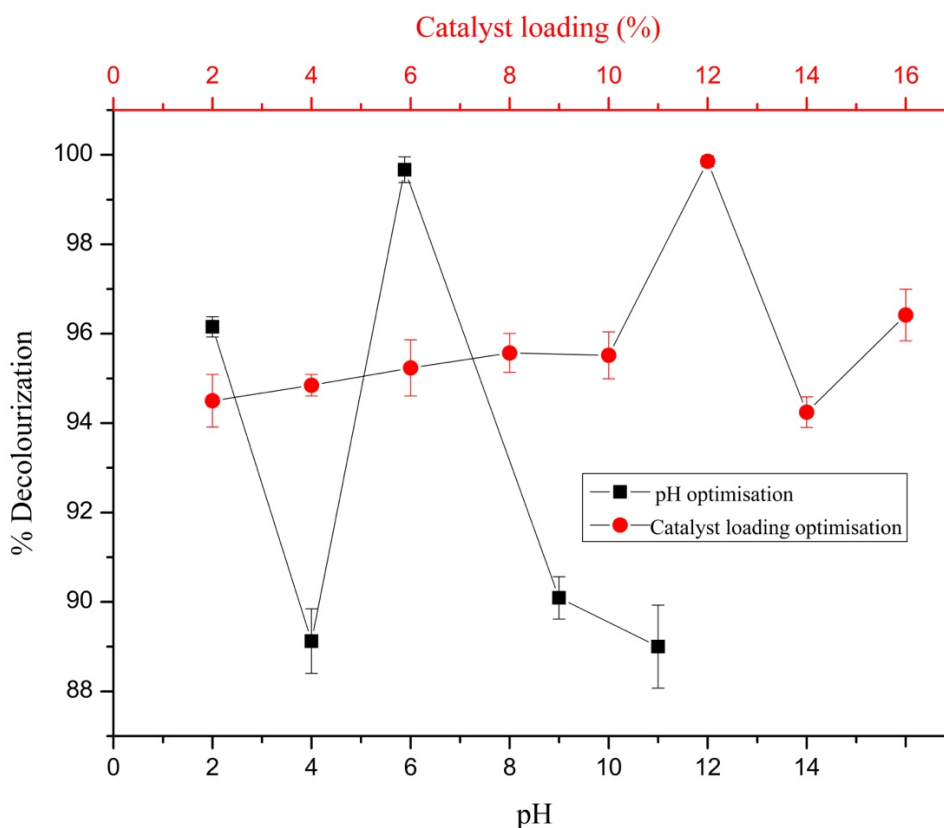


Figure 4.5. Effect of catalyst loading (Conditions: 200 mL of 10 ppm RTB solution, pH: 5.88) and pH (Conditions: 200 mL of 10 ppm RTB solution, catalyst loading: 12 wt.%).

4.2.2.2. Effect of pH

The dependence of the RTB decolourisation on the pH is presented in **Figure 4.5**. The decolourisation of RTB dye is good in both acidic as well as an alkaline medium but the best (complete) decolourisation of RTB within 1.5 h is observed at the natural pH, i.e. 5.88. At high alkaline (pH 11) values, the PST film surface is negatively charged, which slightly hinders the adsorption/photodegradation process. At high acidic values (pH 2), the PST film surface is positively charged, which attracts the negatively charged RTB dye molecules to be adsorbed on the catalyst surface easily thus giving a better photodegradation than in an alkaline medium.

4.2.2.3. Effect of initial dye concentration and reaction kinetics

The effect of the initial RTB concentration on the decolourisation efficiency was investigated in the range of 10 – 30 mg/L, as shown in **Figure 4.6**. It is observed that

the complete decolourisation of 10, 15, 20 and 30 ppm RTB dye solution takes place within 90, 120, 140 and 200 min respectively showing that the decolourisation efficiency decreases with increasing initial dye concentration. Usually, the amount of active radicals present on the surface of the film remains constant for a given light intensity, catalyst loading, irradiation time and pH. A higher RTB concentration requires higher amounts of active radicals to complete the decolourisation process. Since the amount of catalyst is constant and the RTB concentration increased, the adsorption of the dye on film surface will also increase which affects the catalytic activity of the photocatalyst thus reducing the efficiency. The increase in RTB concentration also causes attenuation in the light reaching the surface of the catalyst thus decreasing the number of photons entering into the dye solution leading to a decrease in productivity.

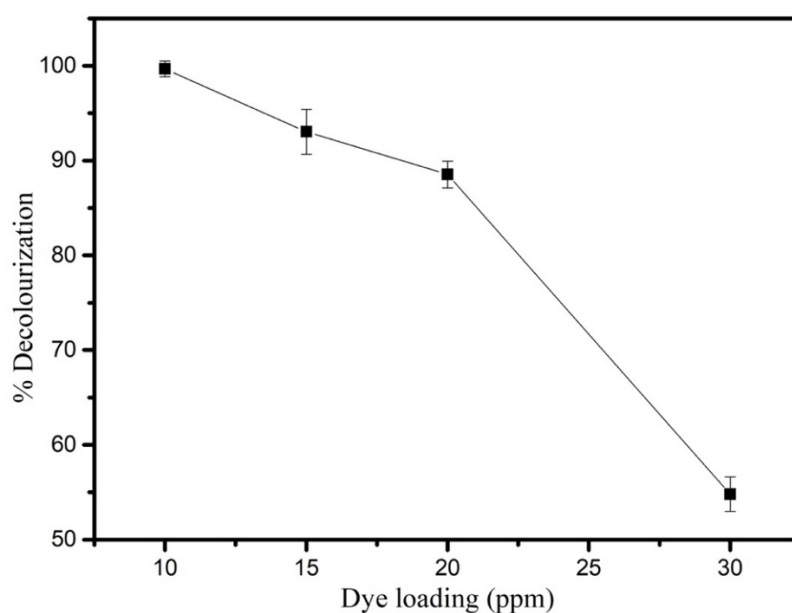


Figure 4.6. Effect of initial dye concentration. Conditions: 200 mL of 10 ppm RTB solution, catalyst loading: 12 wt.%.

The reaction kinetics of the RTB decolourisation study for different initial concentrations (10, 15, 20 and 30 ppm) of RTB is shown in **Figure 4.6**. The equations representing the zeroth order and first order reaction kinetics (Islam et al. 2013; Bickley et al. 2005) are given below:

$$C = C_0 - kt \quad (\text{zero order}) \quad (9)$$

$$\ln C = \ln C_0 - kt \quad (\text{first order}) \quad (10)$$

Where, C_0 and C are as defined in eqn.1, k = reaction rate constant. **Figure 4.7a** shows that the 30 ppm RTB solution decolourisation follows the zeroth order kinetics. **Figure 4.7b** shows the kinetic study for 10, 15 and 20 ppm dye solutions which fits the first order kinetics. The R^2 and k values are given in **Table 4.1**. It can be observed that at lower concentrations of dye, first-order reaction kinetics is followed and for very high values of the initial dye concentration, zeroth order kinetics is followed implying that the reaction is now independent of the dye concentration.

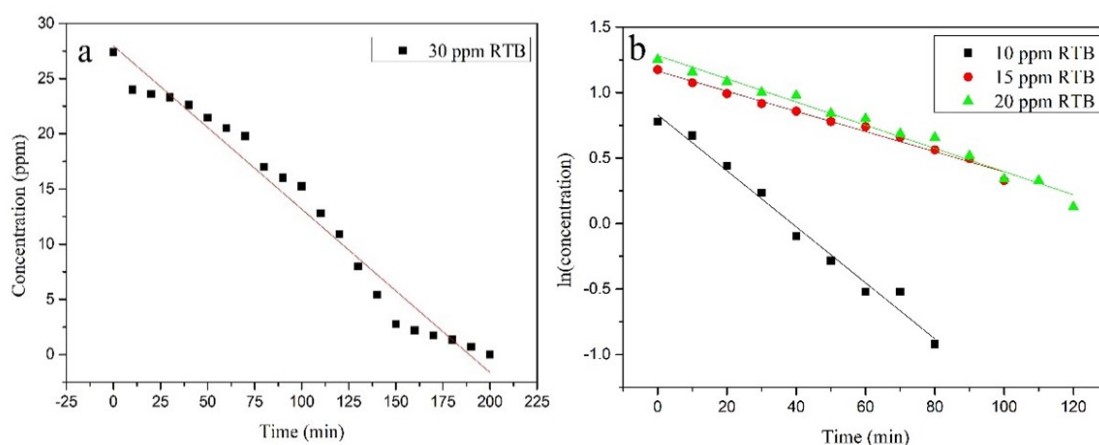


Figure 4.7. RTB concentration vs time for different initial concentrations of RTB dye at optimized conditions a) for 30 ppm RTB solution, b) for 10, 15 and 20 ppm RTB solution.

Table 4.1. Kinetic study of Remazol Turquoise Blue (RTB) decolourisation for different initial concentrations.

Concentration (ppm)	Rate constant (k)	R^2 value	Order of reactions
10	0.0214 min^{-1}	0.9842	First
15	0.0177 min^{-1}	0.9869	First
20	0.0204 min^{-1}	0.9804	First
30	$0.0148 \text{ mole L}^{-1}\text{min}^{-1}$	0.9729	zero

4.2.2.4. Effect of film thickness

The influence of the polymer film thickness was investigated as shown in **Figure 4.8**. Films with three different thicknesses were prepared and the results indicate that the decolourisation efficiency increases with increasing thickness becoming constant after 0.5 mm thickness because the film with low thickness (0.25 mm) getting rolled up and minimizes the active catalyst surface area. Hence, in the remainder of this study, 0.5 mm was taken as the optimal thickness.

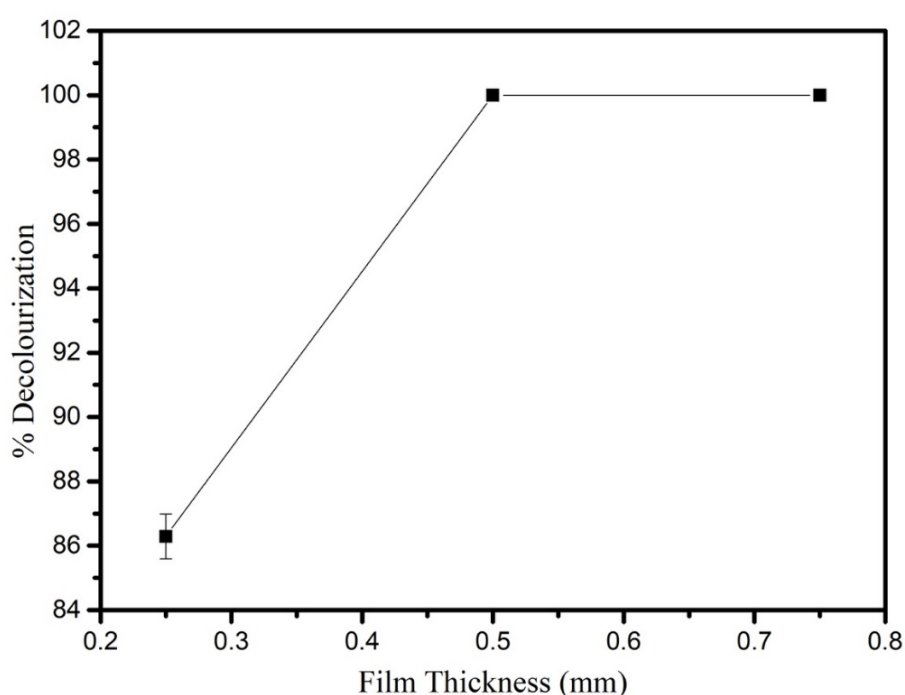


Figure 4.8. Decolourisation of 10 ppm 200 mL RTB solution, with catalyst loading of 12 wt.% in immobilized form using different film thickness.

4.2.2.5. Effect of different light source

The effect of different light sources on the photocatalytic activity is shown in **Figure 4.9**. It is clear that the best decolourisation is achieved under UV–C irradiation giving complete decolourisation of RTB within 1.5 h corresponding to 23.1% for UV–A and 15.6% for sunlight. The bandgap energy of the photocatalyst used in this work is 3.2 eV which suggests that the catalyst will work efficiently under UV–C irradiation only.

The photolysis study was also carried out under each light source, but there was not much decolorization observed (~1% after 24 h) of the dye.

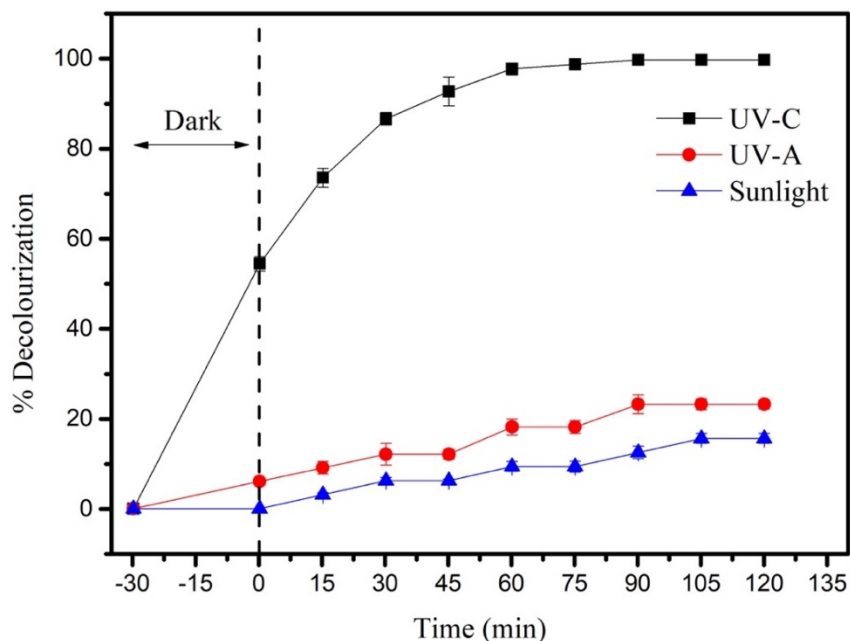


Figure 4.9. Decolourisation of 10 ppm 200 mL RTB solution, with 12 wt.% catalyst loading under UV-C, UV-A and sunlight at ambient temperatures.

4.2.2.6. Comparison with other dyes

From **Figure 4.10**, it can be concluded that among four different dyes (RTB, Congo Red, Methylene Blue, Rhodamine B) used in this study, the best decolourizing efficiency in a 2 h period is shown by RTB followed by Methylene Blue, Rhodamine B, and Congo Red in that order. This may be due to the increasing complexity of the dye molecule and indicates that this catalyst is quite suitable for RTB decolourisation.

4.2.2.7. Comparison with slurry catalyst

Figure 4.11. presents the comparison of the photocatalytic activity for both slurry and immobilised forms of the photocatalyst. While complete decolourisation after about 1.5 h is noticed in the immobilised form, the slurry form of the photocatalyst gives 91% decolourisation in 30 min. However, even after 2 h of irradiation, the decolourisation efficiency is observed to be constant at 91%.

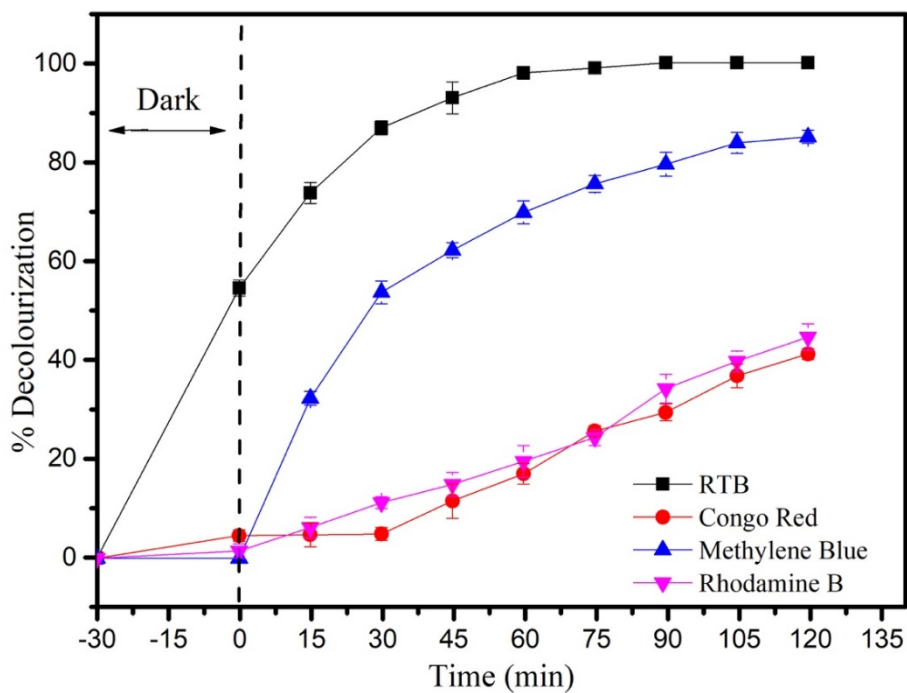


Figure 4.10. Decolourization of different dyes. Conditions: 200 mL of 10 ppm RTB solution, catalyst loading: 12 wt.%.

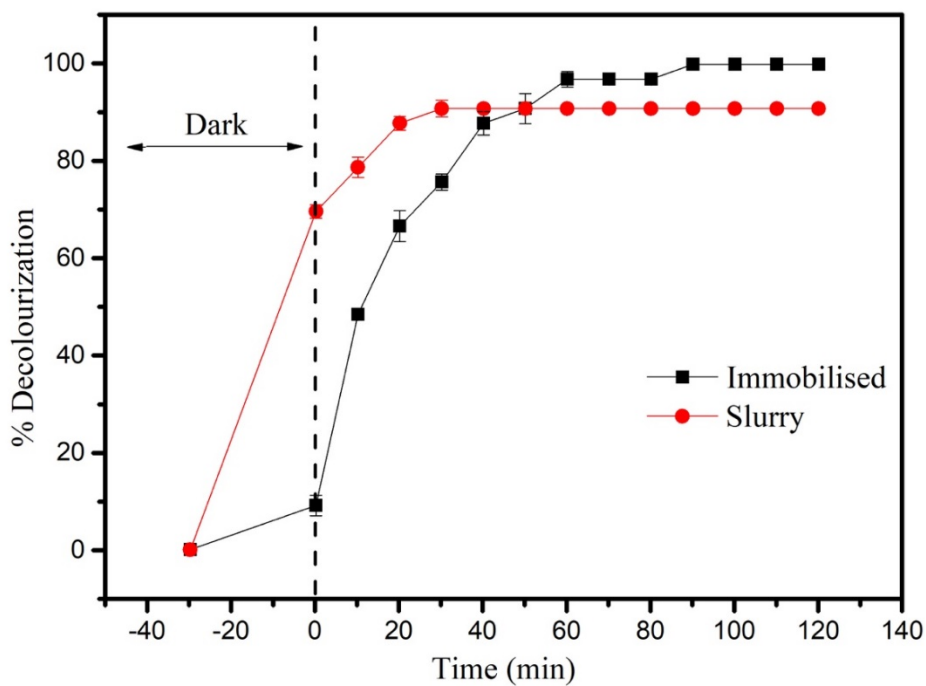


Figure 4.11. Decolourization of 10 ppm 200 mL RTB solution, with catalyst loading of 12 wt.% in immobilized form and 0.18 g/L in slurry.

In slurry form, as expected, the adsorption of the dye on the photocatalyst surface is high compared to immobilised form due to the larger surface area available. However, **Figure 4.11** hints that in the longer timeframes, the immobilised photocatalysts may be better and thus more suitable for large-scale use.

4.2.2.8. Effect of light intensity (distance between the light source and the photocatalytic film)

At the different intensity of the UV-C bulb, the degradation efficiency of RTB has been observed and plotted in **Figure 4.12**. The distance between the polymer film and light source has been varied while other parameters were constant. It is clear from the graph that the closer the distance, the better decolourization of RTB dye takes place. The intensity of the light source was higher when the distance is less and was measured by using a lux meter. When the distance was 7 cm, 17 cm and 27 cm between the light source and polymer film, the intensity of the light was 2.97 Klux, 1.26 Klux, and 0.62 Klux respectively. From the closest distance, the complete degradation /decolourization of RTB takes place within 90 min, while from 17 cm and 27 cm distance it was slightly higher than 85% and 75% respectively, for the same time frame. The main reason for the higher decolourization efficiency at smallest distance (7 cm) was due to the generation of more number of electron and hole pair compared to higher distances (17 and 27 cm). Rest of the studies were carried out at 7 cm distance between the catalyst surface and light source.

4.2.2.9. Effect of temperature

The temperature was found to effect the RTB decolourization (**Figure 4.13**). With increasing the temperature, the decolourization of the dye also increased. According to **Figure 4.13**, almost complete decolourization occurred after 30 min of irradiation at 55 and 40 °C, whereas at the room temperature (30 °C) it was around 85%. A possible reason could be the reduction in the bandgap energy of the TiO₂ since it is indirectly proportional to the temperature and photocatalyst with lower bandgap energy can easily be activated by the low-intensity light source (depending on the catalyst). Another

possible reason may be the breaking down of the dye molecules is easier at high temperature.

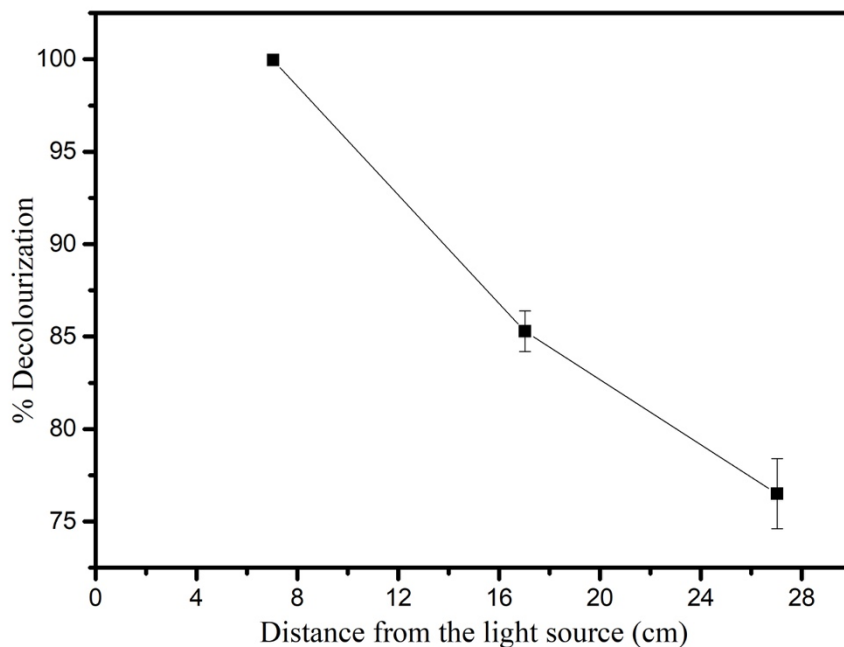


Figure 4.12. Decolourization of 10 ppm 200 mL RTB solution, with catalyst loading of 12 wt.% in immobilized form under different light intensity.

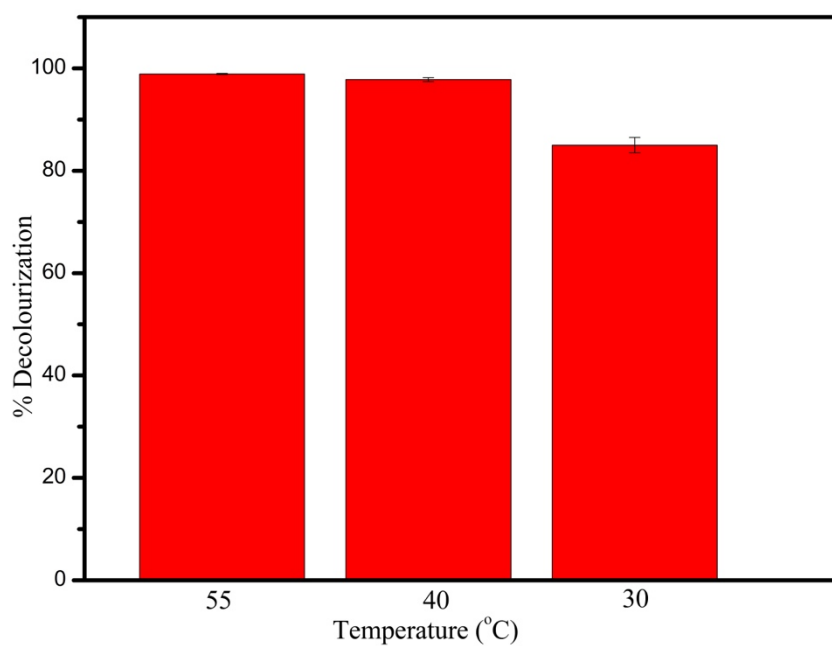


Figure 4.13. Decolourization of 10 ppm 200 mL RTB solution, with catalyst loading of 12 wt.% in immobilized form at different temperature.

4.2.2.10. Effect of salts and alcohols

The presence of salts (Na_2CO_3 and CuSO_4) and alcohols (iso-propanol and ethanol) can also influence the decolourization efficiency as can be seen in **Figure 4.14**. The presence of salts and alcohols surely reduces the decolourization efficiency as compared to the absence of any of those materials. As observed in **Figure 4.12**, the complete decolourization of the dye can take place within 90 min of UV irradiation, but the presence of salt or alcohol ions undoubtedly hampers the photocatalytic oxidation of the dye molecule even after same irradiation time. The deposition of CO_3^{2-} or SO_4^{2-} ions may have taken place on the catalyst surface, due to which the decolourization efficiency has reduced. On the other hand, the carbon molecules present in the alcohols may have deposited on the catalyst surface, blocking the irradiation on the catalyst surface due to which the RTB decolourization efficiency has reduced.

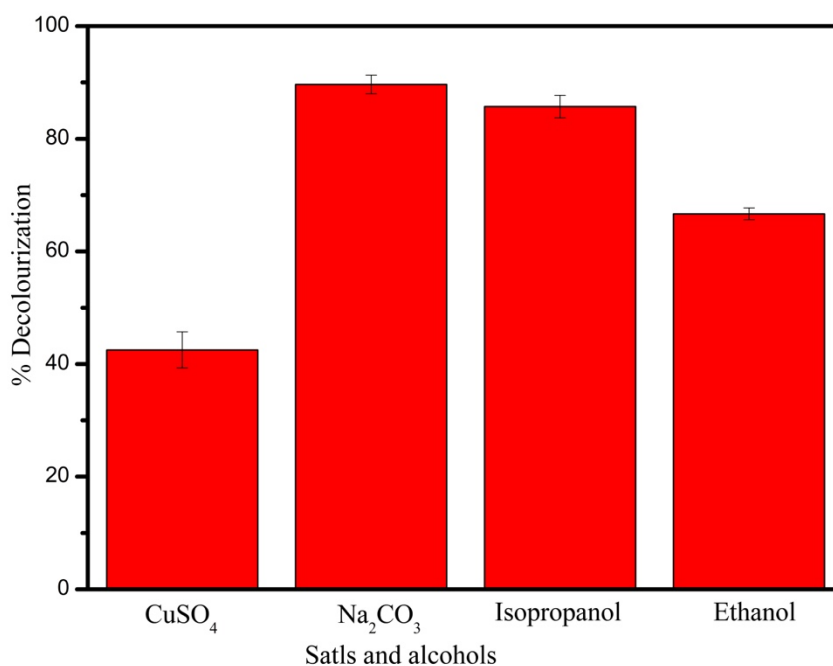


Figure 4.14. Decolourisation of 10 ppm 200 mL RTB solution, with catalyst loading of 12 wt.% in immobilized form under the influence of salts and alcohols.

4.2.2.11. Effect of UV light on the film

The drying of the prepared photocatalytic film during the immobilization also plays an important role in the decolourization of RTB, as can be seen in **Figure 4.15**. The photocatalytic efficiency increases when the film was dried under UV light and exposed for 1 h before employing it for the RTB degradation (shown in **Figure 4.15a**). The complete decolourization occurred after 50 min of irradiation. When the film was dried without UV exposure, but the dried film was exposed under UV irradiation for 1 h prior (**Figure 4.15b**) to use for RTB decolourization it showed ~94% efficiency for the same irradiation time. On the other hand, the decolourization efficiency was 66% when the film was dried under UV irradiation but was not exposed under UV light (**Figure 4.15c**) before using for the photocatalytic study. The conclusion can be withdrawn from this analysis is that the exposure of the photocatalytic film under UV light, prior using for the photocatalytic study enhances the photocatalytic efficiency. This kind of behaviour was noticed maybe because the catalyst is activated and generates several numbers of electron-hole pair, which contributes to the photocatalytic process later on.

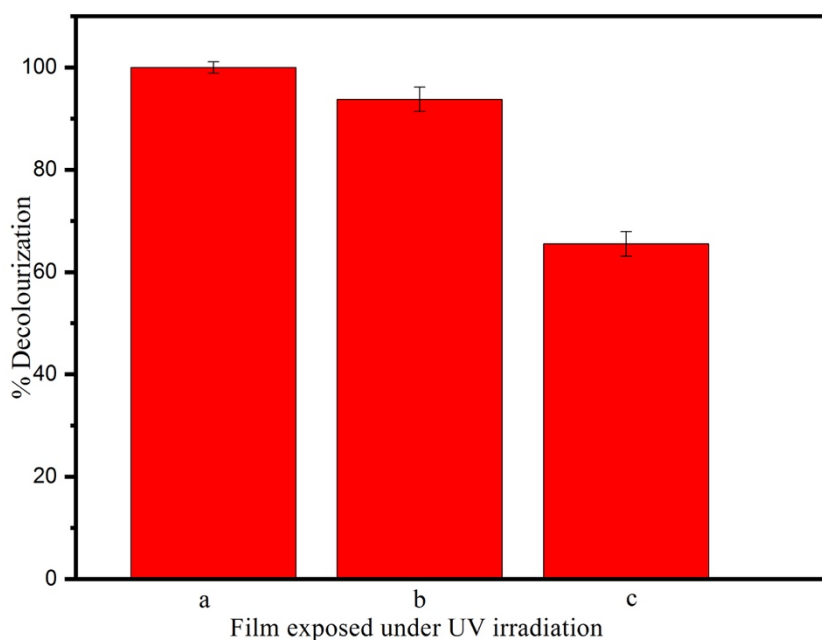


Figure 4.15. Decolourization of 10 ppm 200 mL RTB solution, with catalyst loading of 12 wt.% in immobilized form prepared by different drying process.

4.2.2.12. Recyclability

The recyclability or reuse of the PST film without any intermediate washing was examined and from **Figure 4.16**, it can be observed that there is a mild decline in the efficiency over the first four runs. However, the efficiency is seen to rapidly decline over the next four runs before stabilising at around 70% over the next three runs. In **Figure 4.17**, the physical appearance of the film is shown before use, after using once and after using it ten times. The surface of the film after ten times of reuse becomes completely blue due to the adsorption of dye which may be the reason for the decline in the productivity of the photocatalyst (Sobana et al. 2008).

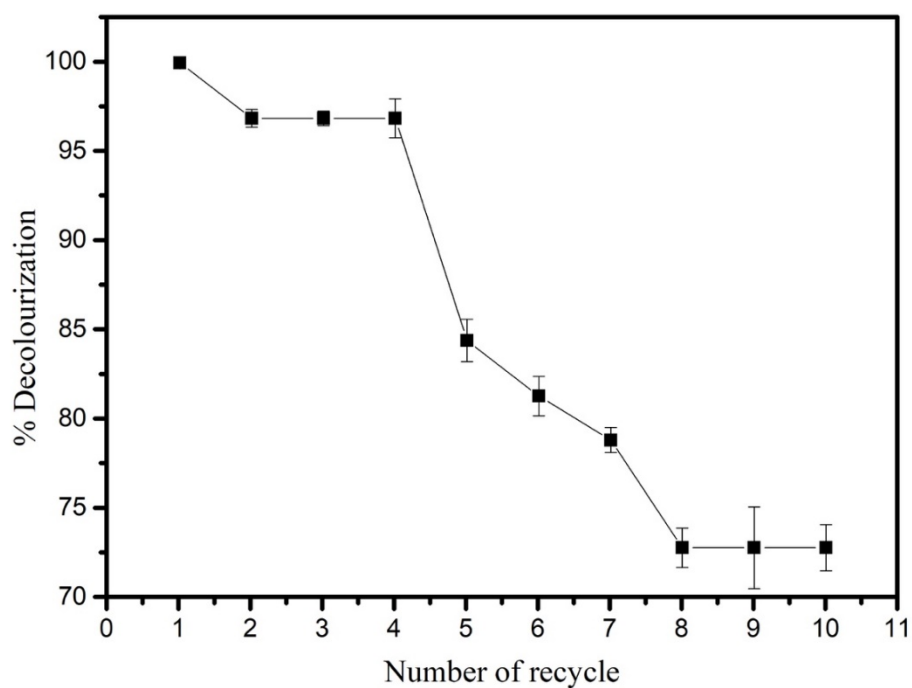


Figure 4.16. Recyclability test of the PST film. Conditions: 200 mL of 10 ppm RTB solution, catalyst loading: 12 wt.%.

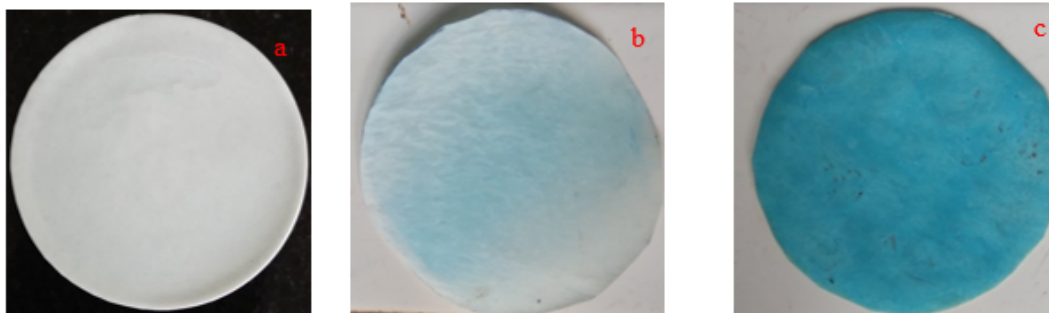


Figure 4.17. The physical appearance of PST films a) 12 wt.% PST film before use, b) 12 wt.% PST film after using once for RTB decolourisation, c) 12 wt.% PST film after using 10 times for RTB decolourisation.

4.2.2.13. Batch scale-up study of RTB solution

A similar batch study is done by using a larger volume (550 mL) instead of 200 mL, and the results are as shown in **Figure 4.18a**. The scale-up criteria used is the ratio of the polymer film surface area to reactor volume, and the same value is used in the larger reactor volume.

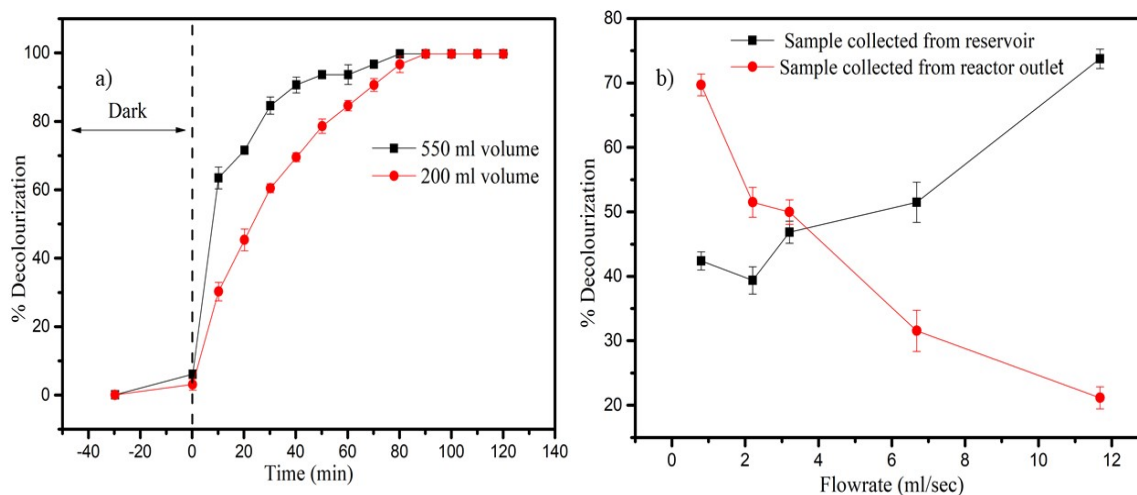


Figure 4.18. Effect of scale up in batch process under the optimized condition, b) Effect of recirculation for decolourization of RTB dye at different flowrates, reactor volume 550 mL and reservoir volume 2350 mL.

It can be observed from **Figure 4.18a** that the photocatalytic activity in both reactor volumes is very similar thus confirming the scale-up criteria adopted in this study. However, a mild improvement in the efficiency (100% decolourisation at 80 min compared to 90 min for the smaller volume) is observed.

4.2.2.14. Recirculation study

As shown in **Figure 4.18b**, for different flowrates (0.4 – 12 mL/s), a recirculation study is conducted with sampling done at the reactor outlet as well as from the reservoir. The decolourisation of the solution in the reactor decreases with increasing flow rate which agrees well with the observation that a higher flow rate leads to lower residence time in the reactor thus reducing the photocatalytic efficiency of the process. On the other hand, the decolourisation of the solution in the reservoir is observed to increase with increasing flow rate. This clearly shows the accumulative effect of recirculation on the decolourisation as more volume of the dye solution can be circulated through the reactor (approximately 29 times at the highest flow rate when compared to that at the lowest flow rate). However, the effect of any dead zone or incomplete mixing in the reactor is not considered in this study. Comparison of these results with the corresponding results from the 550 mL batch study shows that the recirculation study does not fare better in terms of the time required for decolorization of the solution (100% decolorization in 90 min for the batch study compared to ~75% decolourisation in 6 hrs for the recirculation study; the latter percentage is in accordance with the results of the previous section). However, the volume of the dye solution handled in the recirculation process is much larger (more than five times) than that in the batch study and therefore viewed in this context, the results of this study seem to be encouraging compared to few other scaled-up photocatalytic processes with slurry photocatalysts (Satuf et al. 2007; Priya and Kanmani 2013; Valadés-Pelayo et al. 2015; Li et al. 2010; Kim et al. 2017; Pardiwala et al. 2017). Further work in this regard is needed.

4.2.3. Photocatalytic degradation analysis of RTB

4.2.3.1. Total organic carbon analysis in RTB solution

To confirm the degradation of the dye by the prepared photocatalyst, the TOC values of the treated wastewater in the 200 mL batch study for a one-time use of the PST film were measured and the results are shown in **Figure 4.19**. Initially, it is observed that the % change in TOC values are negative, implying that the TOC values have increased. This may be due to the breakdown of the complex dye molecule into some intermediate compounds (see the next section for further details). After some time (around 90 min), the % change in TOC values become positive indicating that the TOC values are now reducing indicating that the intermediate products are also getting degraded. The overall TOC reduction only is 24% (compared to 100% decolourisation in the same time frame) indicating that some colourless intermediate compounds may still be present in the treated solution. This points to the need for further studies focusing on the TOC reduction aspect of this problem.

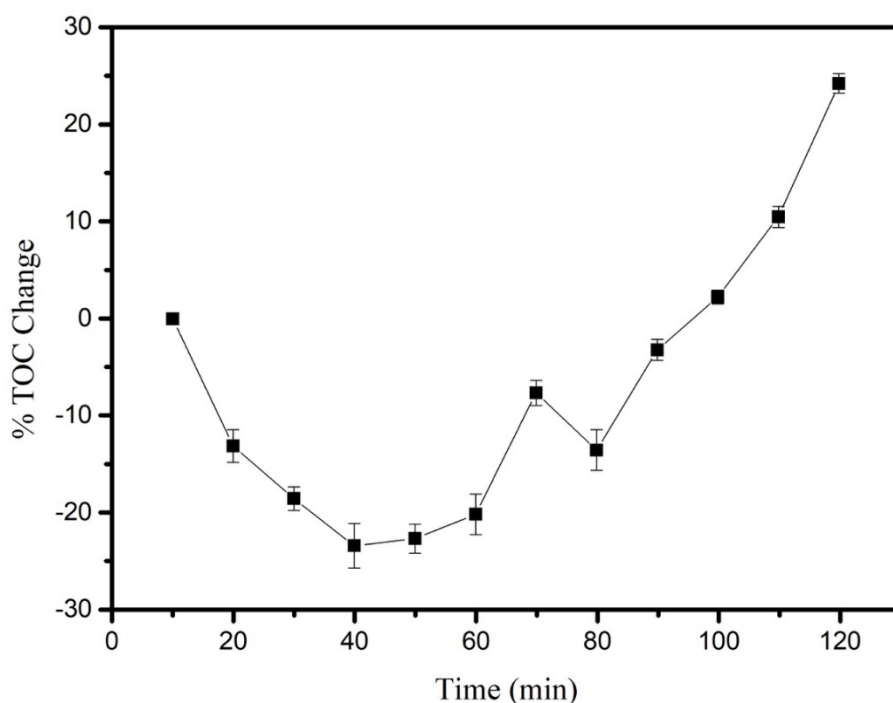


Figure 4.19. % change in TOC during the photocatalytic process. Conditions: 200 mL of 10 ppm RTB solution, catalyst loading: 12 wt.%.

4.2.3.2. LC–MS analysis of RTB dye solution after degradation

The dye solution at the end of the irradiation under optimised conditions was subjected to LC–MS analysis. As shown in **Figure 4.20a**, the black line shows the freshly prepared 10 ppm dye solution whereas the pink line (peak at 3.2 min) shows the after degradation of 10 ppm dye solution in optimised condition after 2 hrs. It can be concluded that the breakdown of RTB dye does take place. **Figure 4.20b** shows the MS spectra of the treated solution. After 2 hrs of degradation, it is observed that there are four significant peaks at $m/z = 279, 293, 391, 478$ respectively. It is noted that RTB has a copper phthalocyanine ring as shown by its chemical structure in **Figure 4.21**. The degradation of dye is thus confirmed by the LC–MS spectra (Marchis et al. 2011; Xing et al. 2018) from the literature, one of these intermediate compounds namely the one at $m/z = 279$ is 2-(4-Aminophenylsulfonyl hydrogen sulphate) (Pardiwala et al. 2017). The other hypothetical product at $m/z = 478$ is 2,7,12,17-Tetraethyl-3,8,13,18-tetramethyl-21H,23H-porphin. The proposed degradation mechanism is shown in **Figure 4.21**.

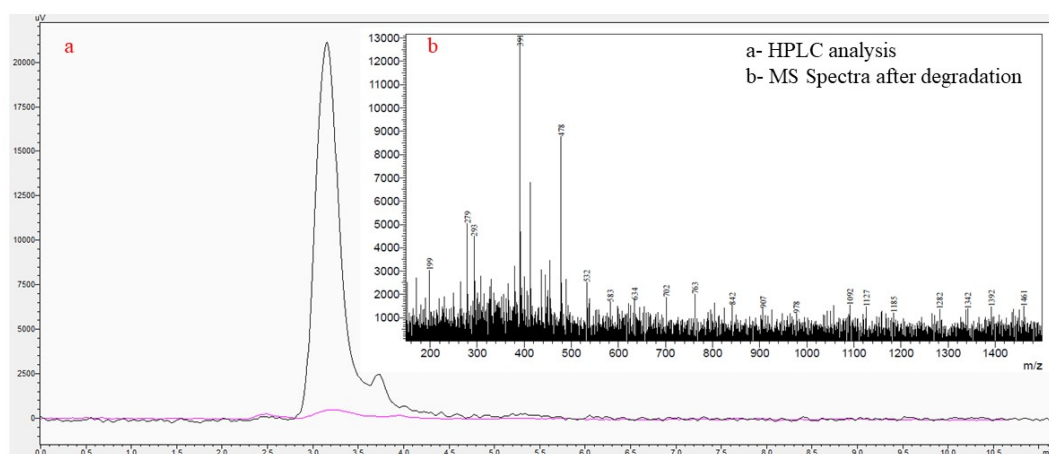


Figure 4.20. LC–MS analysis, a) HPLC data confirming degradation of RTB, before degradation (black line), after degradation (pink line). b) MS spectra after degradation at 3.2 min. Conditions: 200 mL of 10 ppm RTB solution, catalyst loading: 12 wt.% of polymer.

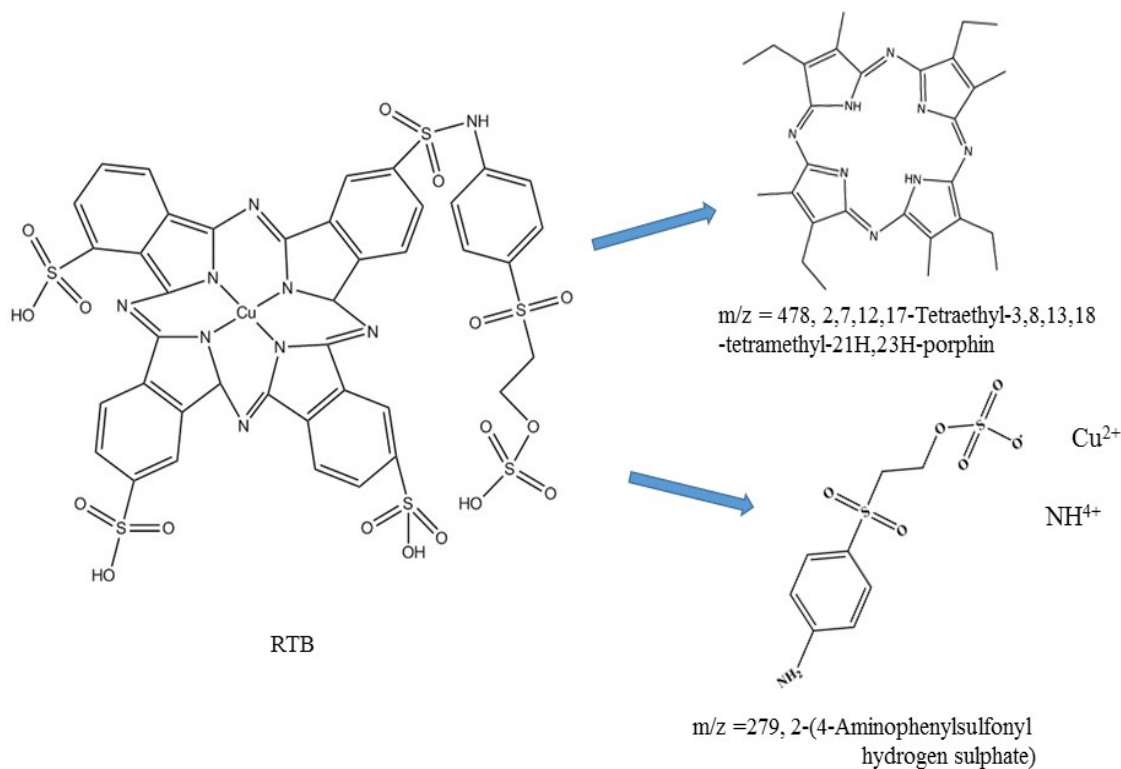


Figure 4.21. Proposed degraded by-products formed after the photocatalytic degradation of RTB.

4.3. Conclusions

Based on the current development of photocatalytic technology and photocatalysis principle, the immobilized TiO_2 photocatalyst film performance was evaluated through the degradation experiment of RTB dye. Conclusions can be summed up as follows:

- This work systematically examines the efficient degradation of RTB dye using TiO_2 photocatalyst immobilized in a polystyrene film.
- The synthesized polymer films before and after use have been characterized. A 10 ppm (200 – 2900 mL) RTB dye solution took 1.5 h for complete degradation using a film with a catalyst loading of 12 wt.% under UV-C light irradiation at a natural pH of 5.88.
- The effect of scale-up as well as recirculation was investigated to test the further applicability of the prepared photocatalytic film.

- The recyclability of polymer films is tested promising a decolourization efficiency of at least 70%.
- The degraded dye solution was characterized by TOC measurements as well by LC–MS analysis and the likely intermediate by–products of the photocatalytic reaction identified.
- Overall, the immobilized photocatalyst developed in this work seems to be a promising candidate for the large–scale treatment of dye wastewater treatment.
- Preliminary TOC data shows that the carbon content in water has increased till 50 min, after that, it has started decreasing and at the end of 2 h the TOC reduction was 24%.

CHAPTER 5

RESULTS AND DISCUSSION

**(POLYSTYRENE – TiO₂, g-C₃N₄ AND
rGO ADMIXTURE
PHOTOCATALYTIC FILM: BATCH
REACTOR STUDIES)**

CHAPTER 5

POLYSTYRENE – TiO₂, g–C₃N₄ AND rGO ADMIXTURE PHOTOCATALYTIC FILM: BATCH REACTOR STUDIES

5.1. Introduction

In the previous chapter, TiO₂ immobilized in a polystyrene film was used for photocatalytic degradation of RTB in a batch reactor. To further enhance the photocatalytic degradation of the RTB dye, it was proposed to investigate the effect of two more photocatalysts in addition to TiO₂. The unary, binary and ternary admixtures of three popular photocatalysts immobilized in a polystyrene film are studied in this section. A systematic study of the synergistic effect of the photocatalysts is detailed here. The reasons for choosing these catalysts are already clarified in Chapter 2. The prepared films were evaluated for its photocatalytic activity using RTB dye as a model organic pollutant in a small-scale reactor. The parameters effecting the photocatalytic activity are analysed here namely catalyst loading, pH, initial dye concentration, light source, presence of oxidising agents such as H₂O₂ etc. A comparison of slurry vs immobilized performance and its reusability were examined.

The catalyst immobilization technique and the photocatalytic activity analytical method is described in section 3.2.6.2. and 3.2.7.1. (200 mL batch study) respectively.

5.2. Results and discussions

5.2.1. Characterization of photocatalyst

5.2.1.1. SEM–EDX analysis

The resulting catalyst powder and PPF were characterised by scanning electron microscopy (SEM). The SEM images of pure TiO₂, rGO, and g–C₃N₄ powder with the same magnification are shown in **Figure 5.1(a–c)**. As can be seen, the surface morphology of each catalyst is different. The crystalline TiO₂ shows a wrinkled sheet surface, whereas crystalline g–C₃N₄ and rGO show a small sheet aggregate structure and nanosheet-like surface respectively, which can be confirmed from Zan et al. (2004);

Mhamane et al. (2011); Liu et al. (2016); Dillip et al. (2017); and Shen et al. (2017). The cross-sectional SEM image of the PPF shows that the average thickness of the film is 425 μm (Figure 5.1d). Figure 5.1e shows the SEM image of the PPF with the optimised catalyst ratio (section 5.3.2.1); the surface of the film appears to be very smooth and homogeneous without any pores showing the equal and uniform distribution of catalysts on the polystyrene surface. From the SEM results, it is clear that the catalyst admixture was embedded on the PPF successfully, but it shows a different morphology than the individual catalyst powders. The grafted catalyst particles are dispersed so well on the polystyrene that it is tough to recognise the individual particles from the SEM image. This result justifies that the solvent casting method for the immobilization of the photocatalysts with uniform distribution in polystyrene is an effective method. Also, the EDX spectrum of PPF (Figure 5.1f) sample reveals the presence of significant elements Ti, C, O, and N present in the film.

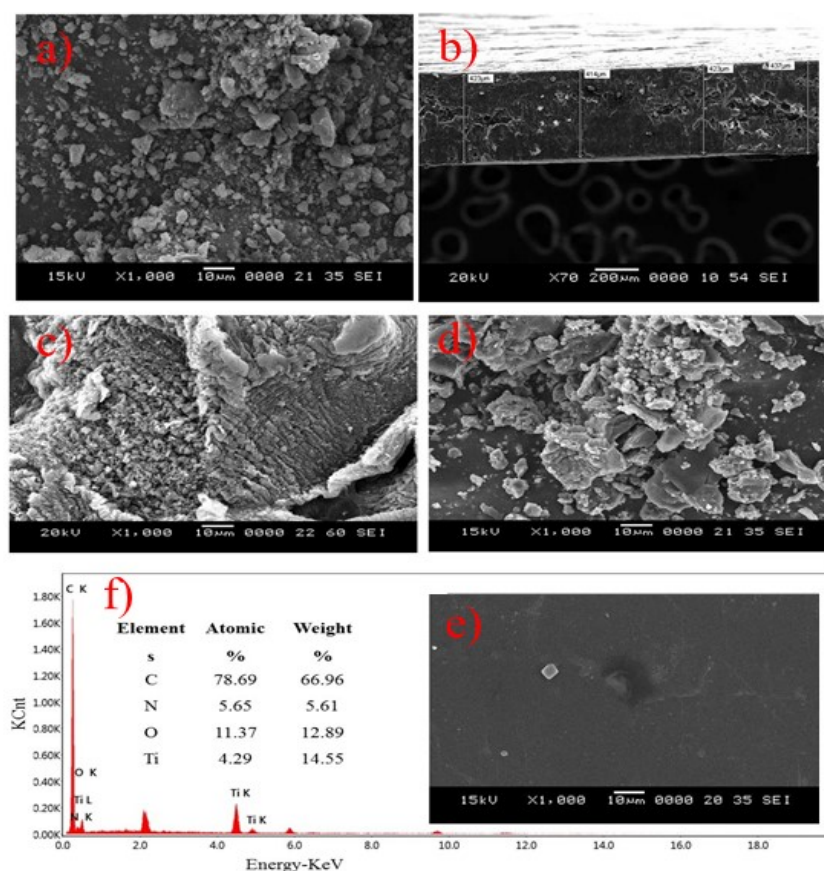


Figure 5.1. SEM images of a) TiO_2 , b) rGO, c) $\text{g-C}_3\text{N}_4$, d) cross-sectional SEM of PPF, e) PPF surface f) EDX analysis of PPF.

5.2.1.2. FTIR analysis

Figure 5.2(a–e) shows the FTIR spectra of The FTIR spectra of the different catalyst powders, plain polystyrene film and polystyrene film loaded with the catalyst admixture. **Figure 5.2(a–c)** shows the spectrum of the powder TiO₂, rGO and g–C₃N₄ respectively. For plain polystyrene film and PPF FTIR plot is presented in **Figure 5.2d** and **e**. All the plots (**Figure 5.2(a–e)**) are analysed in **Table 5.1**. The characteristic peaks for catalysts as well as polystyrene can easily be observed in the PPF film as given in **Table 5.1**.

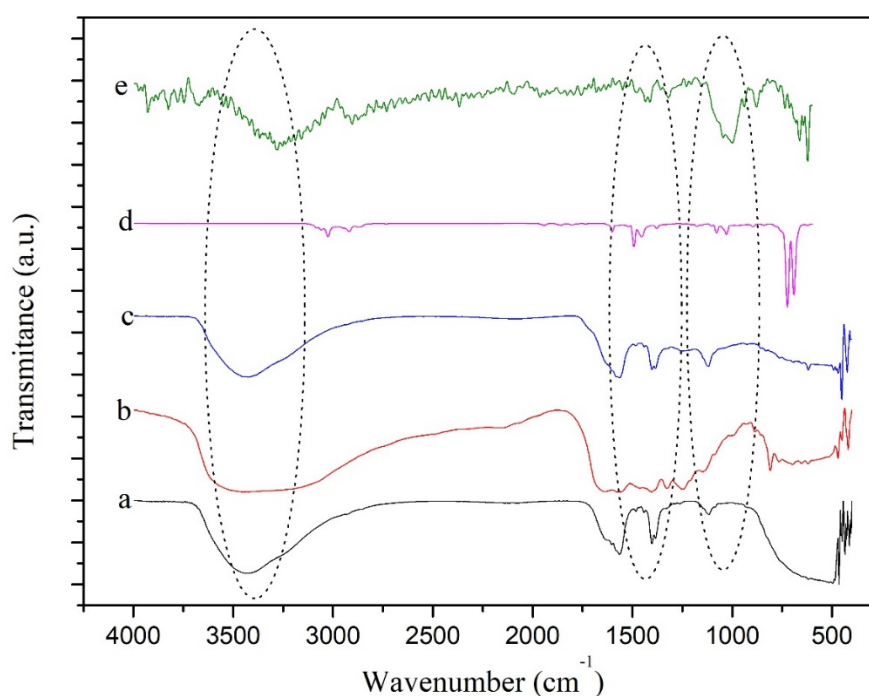


Figure 5.2. FTIR Analysis of catalysts, a) TiO₂, b) rGO, c) g–C₃N₄, d) plain polystyrene film, e) PPF.

Table 5.1. Details of FTIR spectra of catalysts and PPF.

Type of vibration	Wavenumber (cm ⁻¹)				
	a	b	c	d	e
Stretching vibration of					
OH group on TiO ₂	1635–	–	–	–	–
surface (Shavisi et al. 2014; León et al. 2017)	1645				

Type of vibration	Wavenumber (cm ⁻¹)				
	a	b	c	d	e
Adsorbed H ₂ O on the TiO ₂ surface (Shavisi et al. 2014; León et al. 2017)	2750–3750	–	–	–	–
Indication of TiO ₂ was confirmed by the characteristic peaks (Chellappa et al. 2015)	1641 and 1157	–	–	–	–
Aromatic C=C bond stretch in rGO (Fan et al. 2007; Du et al. 2018)	–	1625	–	–	–
Vibration peak for methylene (–CH ₂ –) in rGO (Du et al. 2018)	–	3000–3750	–	–	–
Stretching modes of C–N heterocyclic bond in g–C ₃ N ₄ . (Aleksandrzak et al. 2017)	–	–	1245, 1320, 1420, 1560 and 1640.	–	–
Phenyl ring present in pure polystyrene sample (Shang et al. 2003; Song et al. 2009; Jaleh et al. 2011)	–	–	–	697, 756, 1028, 1450 and 1492	–
C–H bond in benzene ring present in polystyrene (Luo et al. 2008)	–	–	–	3026	–

Type of vibration	Wavenumber (cm ⁻¹)				
	a	b	c	d	e
C–C bond stretching vibration (Jaleh et al. 2011)				1500	
Aromatic C–H bond stretching vibration (Luo et al. 2008)	–	–	–	1600, 1496 and 1455	–
Aromatic C–H deformation vibration(Luo et al. 2008)	–	–	–	1080, 1031, 725 and 693	–
Confirmation of the indication of the catalysts in the PPF	–	–	–	–	3292, 1430, 1419, 1001 and 880

5.2.1.3. XRD analysis

The crystal structure and orientation of p25 TiO₂, rGO and g–C₃N₄ nanoparticles have been investigated by X–ray diffraction (XRD) method. The sharp and intense peaks in **Figure 5.3** indicate that the samples are crystalline. The XRD analysis confirmed the presence of the pure anatase and rutile crystallite structure at $2\theta = 25.12^\circ$ and 27.27° respectively for a P25 TiO₂ sample from **Figure 5.3a**, similar peaks were also reported in literature (Ocwelwang and Tichagwa 2014; Kamrannejad et al. 2014; Lebedev et al. 2016; Sinirtas et al. 2016). **Figure 5.3b** represented the XRD pattern of crystalline reduced graphene oxide with a distinct peak at $2\theta=26.46^\circ$; other peaks show the impurities (Sulphur, Potassium and Manganese) are present in the catalyst (Fan et al. 2011; Alam et al. 2017; Wu et al. 2015). A distinct peak for graphitic carbon nitride at $2\theta=27.38^\circ$ has been observed (**Figure 5.3c**), indicates the presence of g–C₃N₄; confirmed from (Dong et al. 2014; Cheng et al. 2013; Aleksandrzak et al. 2017).

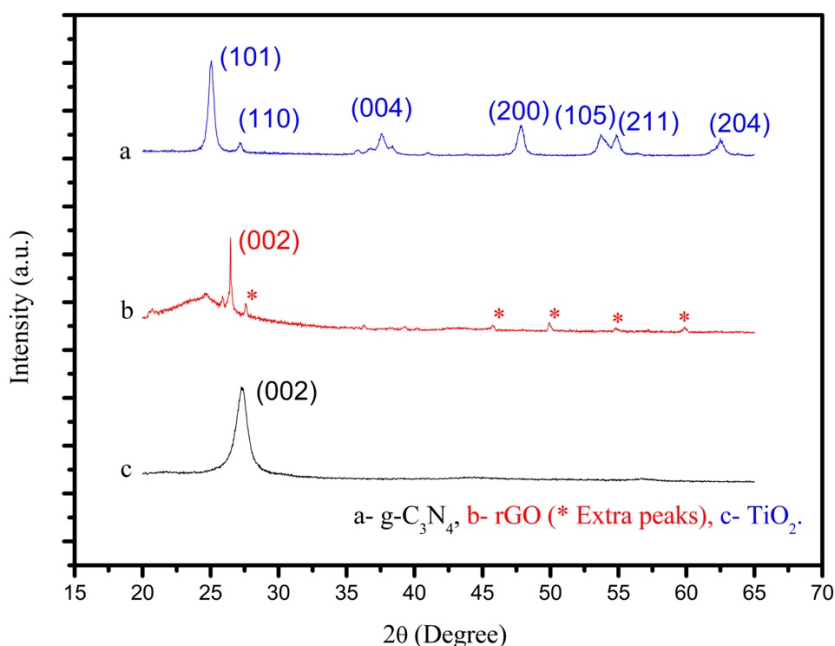


Figure 5.3. XRD analysis of catalysts, a) TiO₂, b) rGO, and c) g-C₃N₄.

5.2.1.4. XPS analysis

The XPS analysis is used to determine the chemical composition as well as the chemical state of the elements present in the film. The reported XPS spectra for the photocatalyst loaded polystyrene film confirms the presence of titanium, oxygen, carbon, and nitrogen in the film with their chemical composition (atomic %) in **Figure 5.4a**. The typical assessment of high-resolution spectra is shown in **Figure 5.4(b–e)**. Two peaks centred at bandgap energy of 283.5 and 290.5 eV in **Figure 5.4b** shows the C – C and C – O bonds respectively for C1s spectra. The C – O – Ti bond is identified at a peak value of 531 eV for O1s spectra (**Figure 5.4c**). The Ti2p spectra at 459 eV is acknowledged for Ti – C bond in **Figure 5.4d**. The N1s spectra show the N – (C)₃ bond at 399 eV in **Figure 5.4e**. The bond formation among different elements present in the film confirms the successful integration between the photocatalysts and polystyrene (Hu et al. 2013).

5.2.1.5. Contact angle analysis and Particle size measurement

For the PPF, a contact angle of approximately 65° was measured, which means that the film is hydrophilic. Even though polystyrene and two out of the three catalysts (TiO₂ –

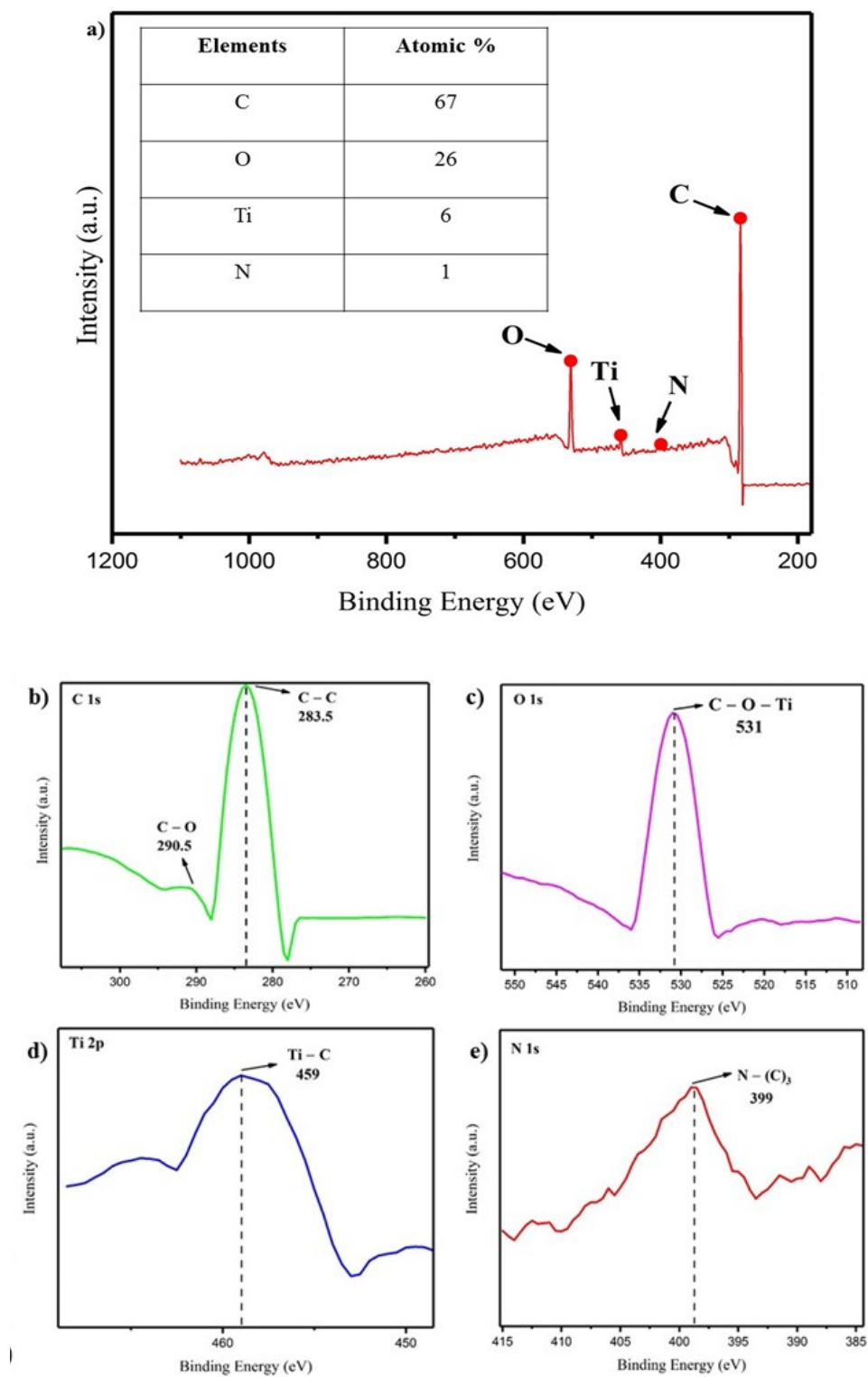


Figure 5.4. XPS analysis of a) photocatalyst loaded polymer film and High resolution scanning of b) C1s, c) O1s, d) Ti2p, and e) N1s.

hydrophilic (Bolis et al. 2012), rGO – hydrophobic (Mhamane et al. 2011), g-C₃N₄ – hydrophobic (Li et al. 2015)) are hydrophobic, but after the catalyst immobilization, it behaves as a hydrophilic film, possibly because the polystyrene seems to lose its expected hydrophobic nature in the presence of the catalyst admixture. From the DLS analysis, the particle sizes of the TiO₂, Reduced graphene Oxide and Graphitic–Carbon Nitride are found to be 25, 77 and 3.7 nm respectively confirming that all the catalysts used in this study are in the nanoparticle size range.

5.2.1.6. ICP–OES analysis

The possible leaching out of the titanium ions from the film was analysed by using inductively coupled plasma optical emission spectrometer (ICP–OES). For this, the film was immersed in 200 mL distilled water for 24 h under UV light. After 24 h, a sample was collected and the amount of Ti³⁺ leached out was found to be 0.06 – 0.08 ppm which is much less than the recommended limit of titanium ions in drinking water (0.1 ppm) (Dong et al. 1993).

5.2.2. Optimization of photocatalytic parameters

5.2.2.1. Effect of catalyst loading

Optimisation of the catalyst concentration is of primary importance to accomplish the efficient degradation of the dye. To find out the optimised ratio of the three catalysts for the photocatalytic degradation of RTB, the total catalyst loading was kept at 10 wt.% of polystyrene. In **Figure 5.5**, the photocatalytic performance of unary, binary and ternary mixture of catalyst are shown; more than 95% decolourization is noticed when the ratio of three catalysts (TiO₂:rGO:g-C₃N₄) are 1:1:1, 2:1:1, 1:1:2 and 1:2:1 in a polystyrene matrix. Among all these different catalyst ratios, the equal amount of catalyst loading (PS – 1:1:1) showed the best result i.e., almost 99% decolourization. In binary mixtures, the synergistic effect of the catalyst is observed. Among PS–TC (TiO₂:g-C₃N₄ :: 1:1), PS–TG (TiO₂:rGO:: 1:1), and PS–GC (rGO:g-C₃N₄ :: 1:1) binary mixtures, PS–TC showed more than 94% decolourization while TiO₂ and g-C₃N₄ individually showed 82% and 89% decolourization respectively. The synergistic effect was noticed in the case of all the binary and ternary mixtures, which is beneficial for

dye decolorization. The main reason behind this synergistic effect could be ascribed to the interfacial charge transfer among the photocatalysts. To find out other optimised conditions, PS – 1:1:1 film was used as it showed the best performance among all other catalyst dosages. The optimised ratio of the photocatalyst admixture showed better degradation of the model pollutant with improved synergistic effect and favoured the efficient charge/energy transfer among the nanoparticles (Xu et al. 2015).

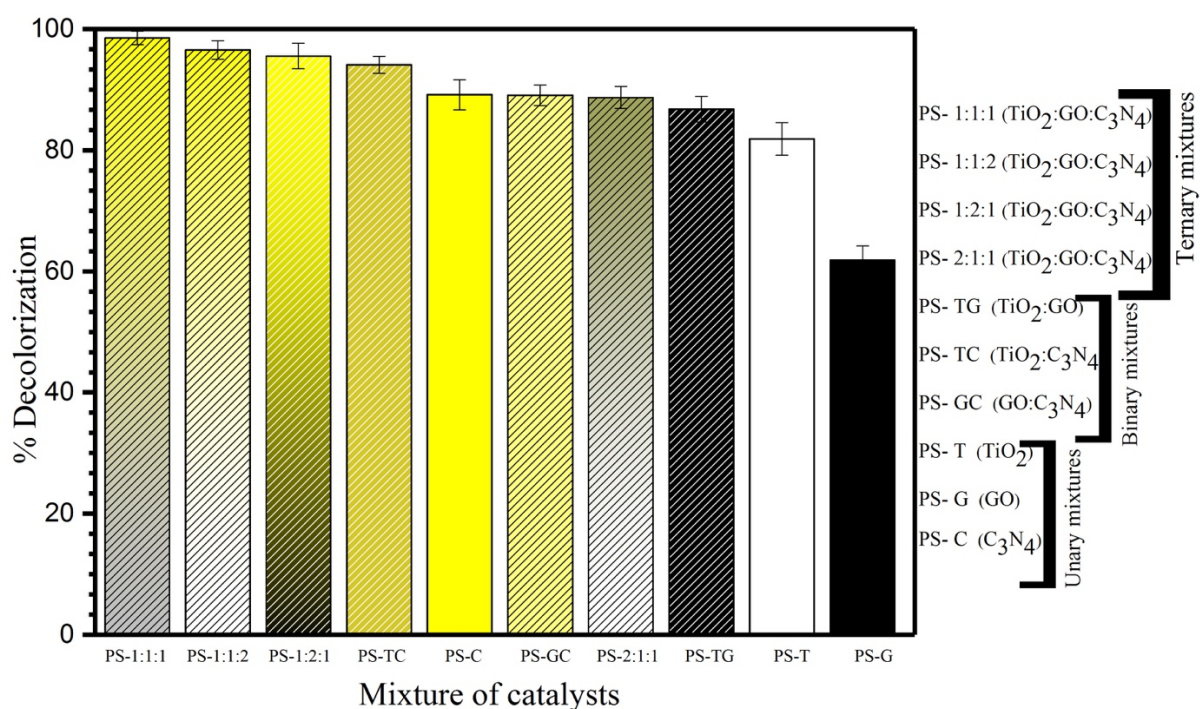


Figure 5.5. Investigation of unary, binary and ternary ad-mixtures in polystyrene film.

5.2.2.2. Effect of pH

To study the effect of pH on the photocatalytic degradation, the solution pH was adjusted using 0.1 N NaOH and 0.1 N H₂SO₄. The data presented in **Figure 5.6**, which represents the adsorption of dye, is much higher at pH 2 and lower at pH 9 (adsorption: pH 2 > pH 4 > pH 11 > pH natural > pH 9). The photocatalytic activity is also highest at pH 9 followed by pH 11 > pH 2 > pH natural > pH 4. At pH 9 the complete decolorization happened within 30 min of irradiation while at natural pH, it was approximately 80%. In acidic medium, the catalyst surface is positively charged, and the dye is in cationic form, which repulses each other during the photocatalytic reaction,

resulting in less productivity compared to that in alkaline medium. At alkaline pH, the negatively charged catalyst surface attracts the positively charged ions resulting in the high decolourization of dye. Further, in the alkaline medium, the more OH radical formation is possible from the abundant hydroxide ions, which also enhances the degradation. From **Figure 5.6**, it is clear that the optimum pH is 9, but since the purpose of this study is to make it feasible for industrial application with minimum possible operating cost, rest of the studies are done at the solution's natural pH.

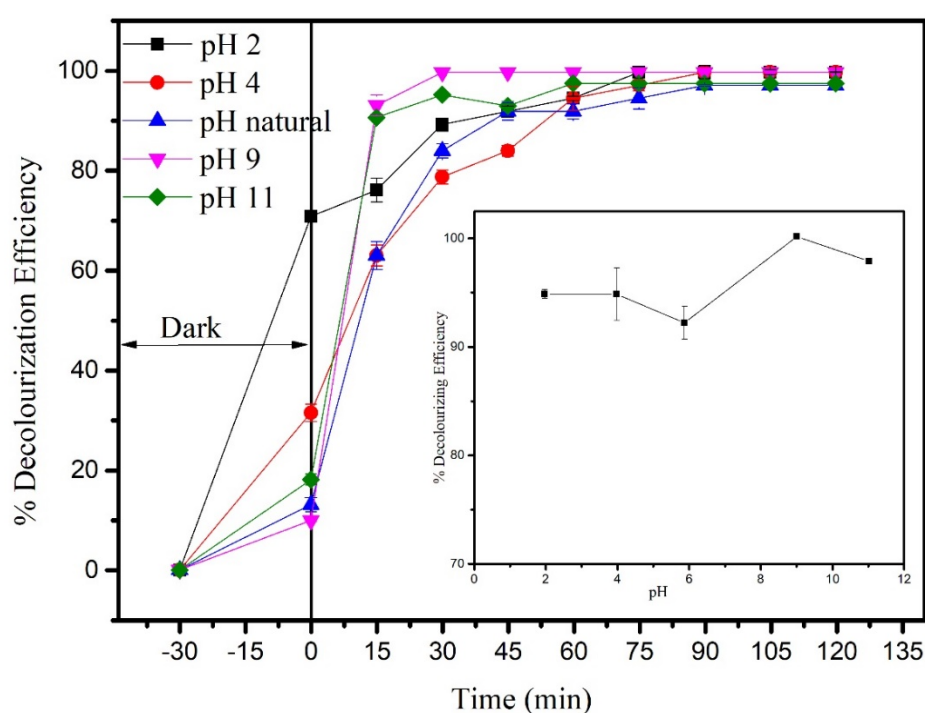


Figure 5.6. pH Optimization (a), comparison of degradation efficiency after 60 min of UV irradiation (b).

5.2.2.3. Effect of initial dye concentration on reaction kinetics

As can be seen in **Figure 5.7a**, the reaction rate is decreasing a bit with increasing the initial dye loading. Even though the initial dye concentration increases, the active catalyst site was constant which decreases the photocatalytic efficiency. **Figure 5.7b** shows the linear plots of $\ln(C)$ as a function of irradiation time for the polystyrene films at different dye concentrations (10, 20 and 30 ppm), which is a typical first-order reaction plot.

Table 5.2. Decolourization reaction kinetics of the RTB dye.

Concentration (ppm)	Rate constant (k) (min^{-1})	R^2 value
10	0.0288	0.909
20	0.0316	0.965
30	0.0234	0.9947

The rate constants were calculated from the slope of the lines (**Table 5.2**). All the experiments satisfactorily follow the first order kinetics as shown in **Table 5.2**, also implying that the higher the concentration of dye, the better it fits the first order kinetics. At 30 ppm RTB concentration, the reaction follows first order kinetics in **Figure 5.7b**, whereas in **Figure 4.7a** it follows zero order reaction, because the catalyst is different.

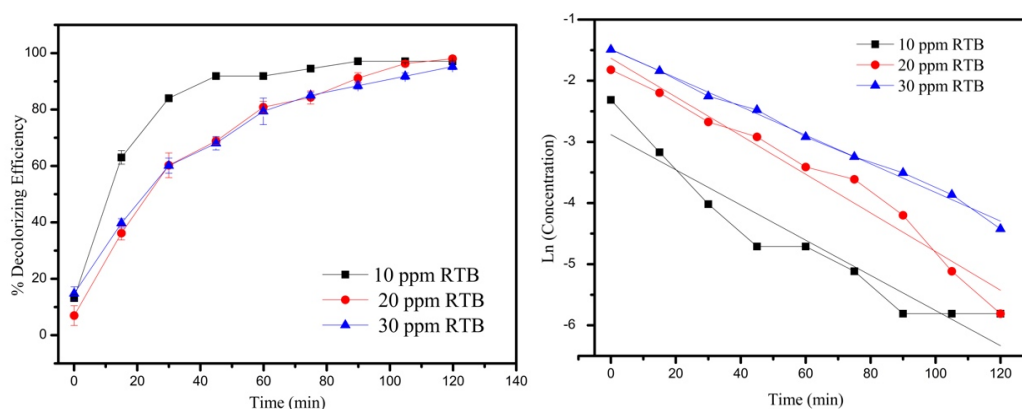


Figure 5.7. Effect of dye concentration (a) on reaction kinetics (b).

5.2.2.4. Effect of light source

The photolysis phenomenon occurs when the chemical substance absorbs light. While studying photocatalysis, it is essential to understand the influence of photolysis since it also affects the degradation of organic pollutants, especially for dyes. An experiment was carried out without a catalyst under visible light, to determine the photolysis effect. As shown in **Figure 5.8**, almost 98% and 45% decolourization occurred under low-intensity UV-C and UV-A light respectively, whereas photolysis showed only 1.1% decolourization. Under UV-C light, the decolourization efficiency is more compared to UV-A because the energy required to excite the electrons from valence band to conduction band is more under UV-C.

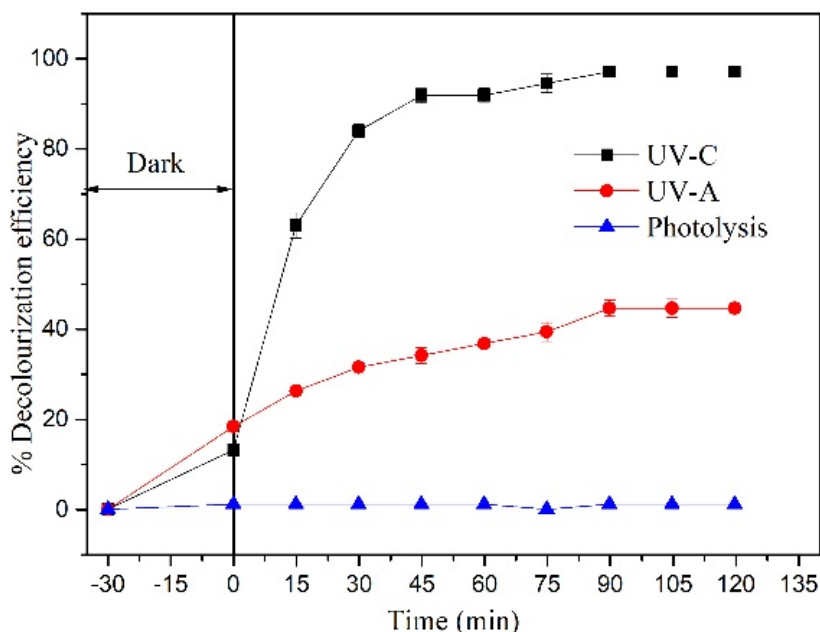


Figure 5.8. Effect of the light source under UV-C, UV-A, and photolysis.

5.2.2.5. Effect of H₂O₂

Different quantities of H₂O₂ were added to the dye solution, to study the effect of H₂O₂ concentration on the decolourization rate (Bali and Karagözoğlu 2007; Silva and Faria 2010; Singh et al. 2011; Wang et al. 2012; Abid 2015;) (**Figure 5.9a and b**). The removal efficiency increases with increasing initial concentration of H₂O₂. However, as the concentration of H₂O₂ reaches a certain level, the decolourization rate starts to decrease as shown in **Figure 5.9a**, the high dosage of H₂O₂ can produce higher amount of electron/hole pair or $\dot{\text{O}}\text{H}$ (Li et al. 1999; Saggiaro et al. 2011) scavenger or react with photocatalysts and form peroxo compounds (Poulios et al. 1999), which were unfavourable to the photocatalytic reaction.

This explains the necessity for an optimal concentration of H₂O₂. The decolourization efficiency was less at a low H₂O₂ concentration (0–0.5 mL/200 mL dye solution), as the formation of hydroxyl radicals was insufficient, but at 1 mL H₂O₂/200 mL dye solution concentration, more $\dot{\text{O}}\text{H}$ radicals were produced leading to a faster oxidation rate. However, after increasing the H₂O₂ dosage to (2–4 mL/200 mL dye solution), an excess amount of $\dot{\text{O}}\text{H}$ radicals has formed, and these excess free radicals preferred to react with the excess amount of H₂O₂ rather than with the dye; leads to a reduction in

dye decolourization efficiency. The most favourable initial H_2O_2 concentration that is observed for the optimum decolourization of RTB was 1 mL H_2O_2 /200 mL dye solution as shown in **Figure 5.9b**.

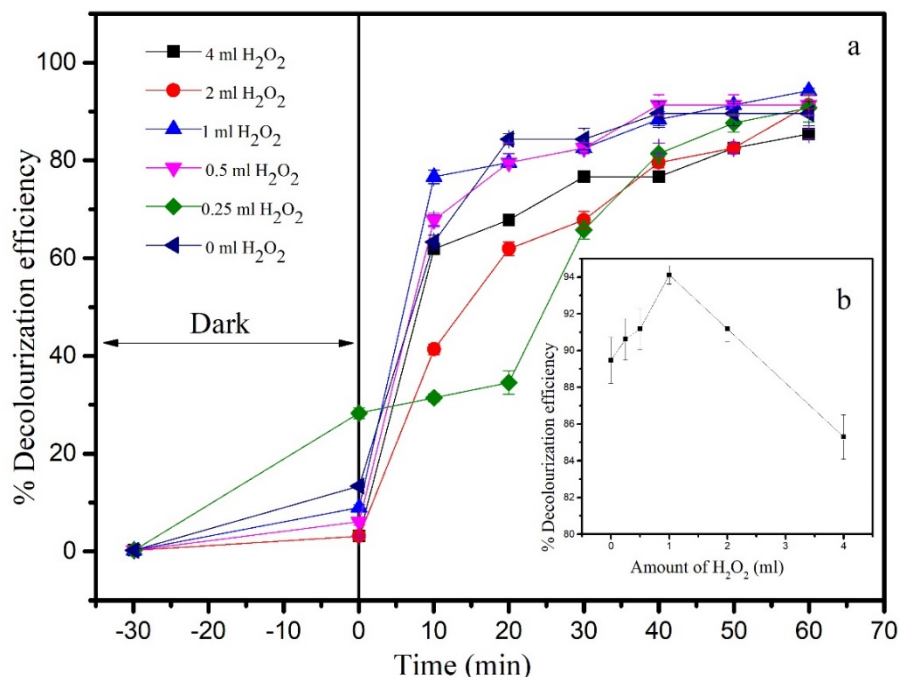


Figure 5.9. Effect of H_2O_2 on decolourization of RTB dye (a) and optimum H_2O_2 loading (b).

5.2.2.6. Slurry and immobilized form comparison

Numerous attempts have been made to immobilize the photocatalysts into the various substrate materials (Dioos et al. 2006; Singh et al. 2013; Srikanth et al. 2017), but even after successful immobilization, the main drawback, i.e., ‘lesser active catalyst surface area’ remains thus hampering the photocatalytic activity. In this work, the primary objective is trying to minimise the gap between immobilized and slurry photocatalytic performance. Although immobilization generally leads to a decrease in the photocatalytic efficiency; however the catalyst can be reused several times (Cámara et al. 2014; Xue et al. 2016; Vaiano et al. 2018;). Using the same amount and optimum ratio of the catalysts, experiments were conducted on slurry and immobilized photocatalysts under UV irradiation. It was noted that the photocatalytic activity of immobilized films was often lower than the corresponding slurry form due to a lower

active surface area to volume ratio and mass transfer limitations (Ray 1997; Srikanth et al. 2017).

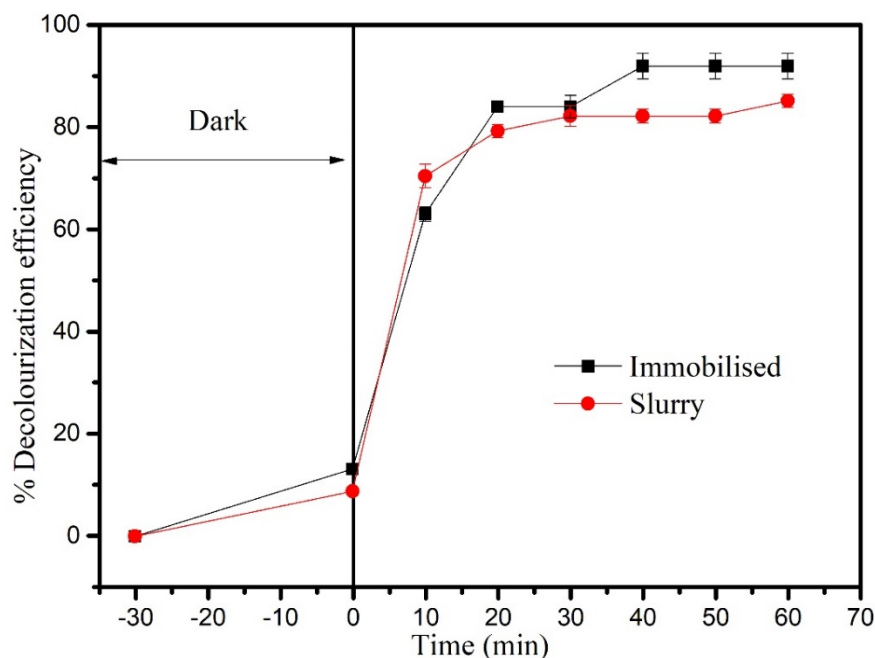


Figure 5.10. Comparison of slurry and immobilized photocatalysts.

As can be seen in **Figure 5.10**, the immobilized photocatalyst admixture matches the performance of the slurry photocatalysts and at times greater than 20 min, in fact, showed surprisingly better results compared to the slurry photocatalyst admixture. This is very intriguing as we know that the surface area is always higher in the case of the slurry photocatalyst and these results confirm very clearly the synergistic interactions of the three photocatalysts in the polymer film. The essential properties of a substrate material such as mechanical strength, high surface area, high stability against oxidising agents and most importantly, no significant reduction in catalyst activity upon immobilization (Srikanth et al. 2017) has been validated in this work. This is a crucial finding paving the way for further research in this area.

5.2.2.7. Recyclability of PST film

The reusability of PS – 1:1:1 film is assessed, as shown in **Figure 5.11**. Reusability is essential for full-scale commercialisation and application of the material to industrial wastewater treatment. The experiment was conducted under optimised conditions

(neutral pH, 10 ppm of RTB, UV light intensity 1.07 Klux) and reusing of the same film 4 times without washing. Consistent degradation kinetics was observed over these cycles, implying the catalyst was firmly attached to the polystyrene film. The first two runs showed almost the same activity of 97%, but in the next two runs, efficiency has decreased by 6% possibly due to the adsorption of dye on the catalyst surface.

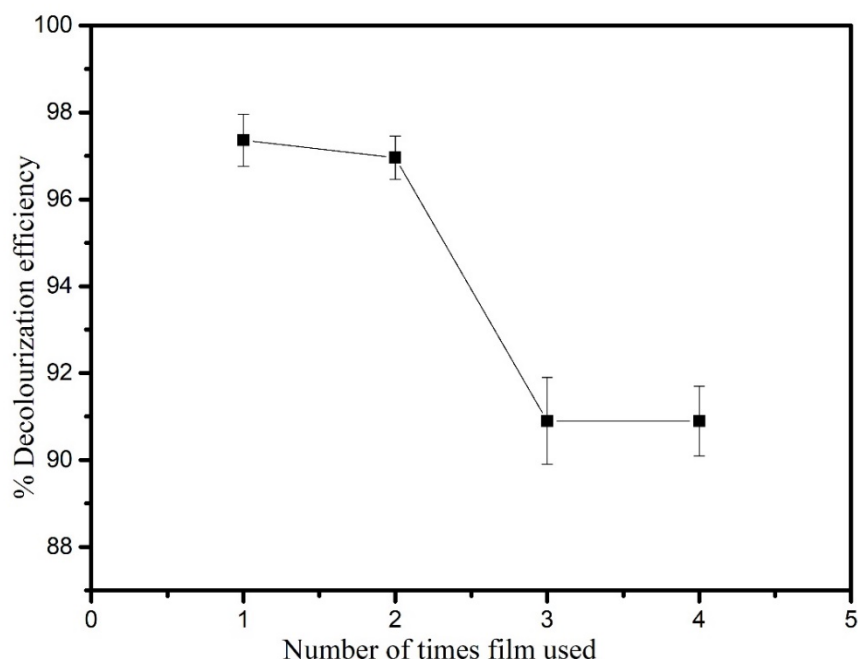


Figure 5.11. Reuse of PPF under optimised conditions (each cycle 2 h).

5.2.3. Photocatalytic degradation analysis of RTB

5.2.3.1. Total organic carbon content (TOC) analysis

The TOC was measured after the degradation of RTB under UV light as shown in **Figure 5.12**. After photodegradation, the %TOC change of RTB was observed to first decrease and then increase over time with a final figure of 40% reported at the end of the experiment indicating that some colourless intermediates may still be present in the solution thus meriting an analysis by LC–MS to find out these degradation by–products. The initial increase in TOC value may be due to the simultaneous degradation of the polymer substrate or due to some carbon from the catalysts leaching out of the polymer film. Similar observations have been reported in other studies (Kimura et al. 2004; Sharma et al. 2012; Das and Mahalingam 2019;).

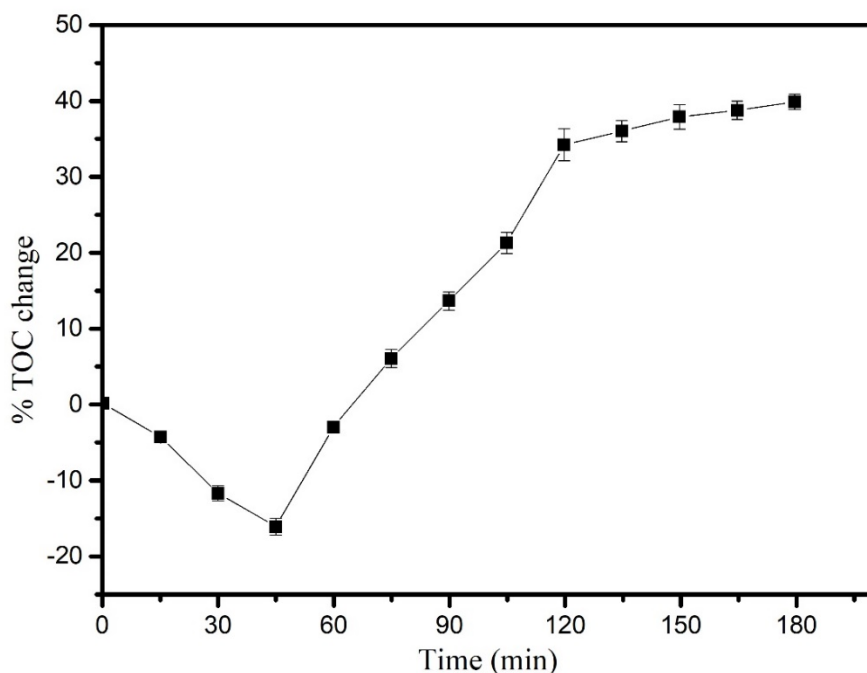


Figure 5.12. TOC Analysis of the degraded dye solution.

5.2.3.2. HPLC–MS analysis

Figure 5.13a shows the HPLC of RTB dye before and after treatment after 120 min of UV irradiation. 97% dye is decolourized, and disappearance of the main peak can be observed at a retention time of 3.2 min. Since only 40% TOC removal has been observed, which means the treated sample still contains carbon compounds, broken down from the parent compound. The copper phthalocyanine ring present in the RTB dye makes it a very strong and difficult to– break–down compound. The breakdown compounds that can be identified from MS analysis are shown in **Figure 5.13b**. The possible degraded compounds from the parent compound (RTB) with signal peaks showing molecular weights at $m/z = 150$ (Hypothetical product (I)) (Conneely et al. 2002), 191, 293 (Hypothetical pro– duct (IV)) (Marchis et al. 2011), 331, 391, 479 (Hypothetical product (III)) and 538 (Hypothetical product (II)) (Silva et al. 2012) are observed. The structure of these possible degraded compounds are shown in **Figure 5.14**.

uV

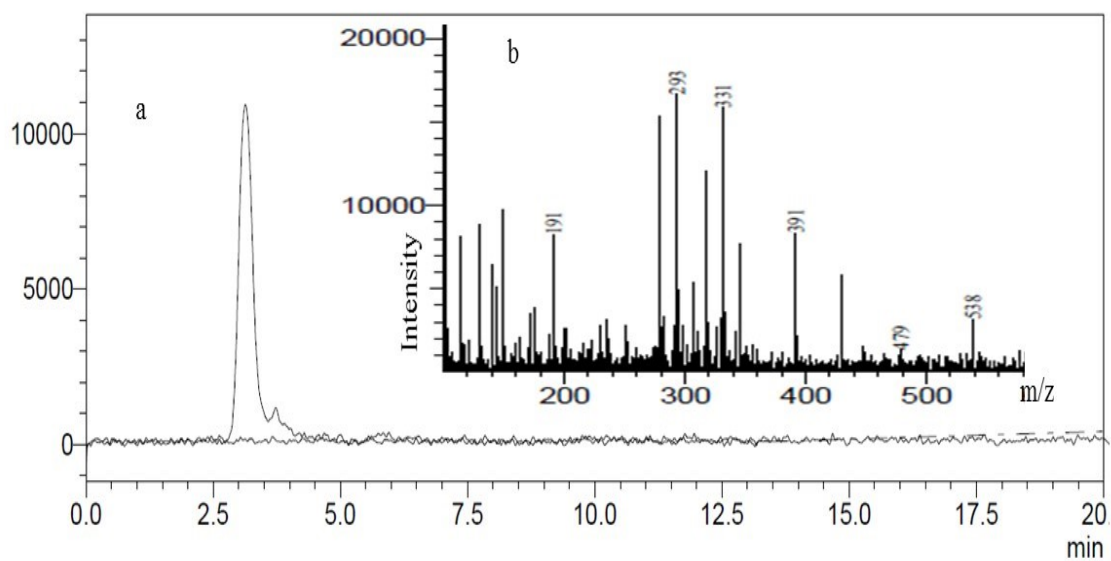


Figure 5.13. HPLC–MS analysis of the dye solution, a) HPLC analysis and b) MS spectra.

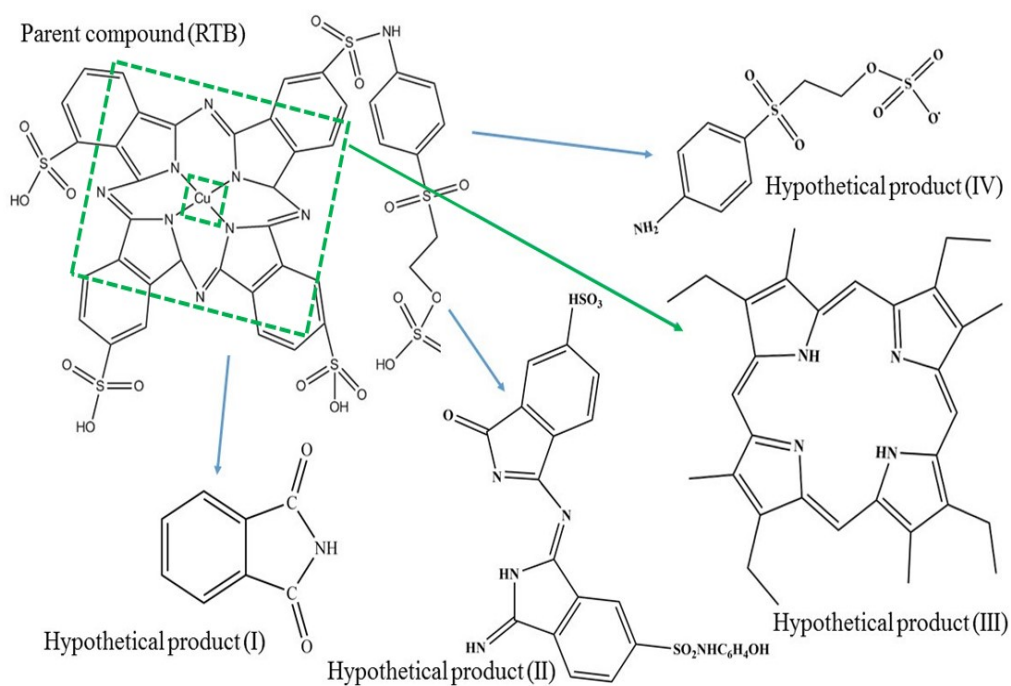


Figure 5.14. The possible degraded compounds after photocatalytic treatment.

5.3. Conclusions

The photocatalytic activity of a catalyst admixture was analysed to check the synergistic effect at optimized conditions and the conclusions that can be mentioned below:

- The synergistic effect of the photocatalyst admixtures was explored with polystyrene immobilized photocatalysts by the solvent casting method.
- In the prepared stable film, crystalline nano-size photocatalysts were evenly distributed, as confirmed from the characterization studies.
- The optimum conditions determined for fastest RTB degradation at an initial concentration of 10 ppm (200 mL) were 10 wt.% catalyst loading (with respect to polymer, catalyst ratio was $\text{TiO}_2:\text{rGO}:\text{g-C}_3\text{N}_4 :: 1:1:1$), under UV-C light intensity of 1.07 Klux and at natural pH of 5.88. Under these conditions, almost complete decolorization of the dye solution was observed within 90 min.
- The comparison of immobilized vs slurry catalysts shows there is very less time difference between these two processes for the same amount of RTB degradation, which implies that the photocatalysts are highly effective even in immobilized form (almost same as the slurry form in the beginning of the reaction and it becomes more efficient over time).
- The reaction kinetics follows first order kinetics at different range of concentration.
- The presence of H_2O_2 seems to encourage the photocatalytic activity but using an excess amount of H_2O_2 reduces the productivity.
- The recyclability of PPF has been tested for four times and the efficiency of the film was more than 90% even after the 4th run.
- The degraded dye solution was characterized in HPLC and TOC to confirm degradation. Both showed a positive result for the degradation of RTB dye. However, only 40% mineralization was observed from the TOC analysis thus presenting an environmental concern possibly due to the negative impact of the intermediate compounds present in the system, however the system is quite promising and further work is needed to optimize the process for the total mineralization of the dye.

CHAPTER 6

RESULTS AND DISCUSSION

**(POLYSTYRENE TiO₂, g-C₃N₄ AND
rGO ADMIXTURE
PHOTOCATALYTIC FILMS:
MULTIPHASE AIRLIFT
PHOTOCATALYTIC REACTOR
STUDIES)**

CHAPTER 6

POLYSTYRENE TiO₂, g-C₃N₄ AND rGO ADMIXTURE PHOTOCATALYTIC FILMS: MULTIPHASE AIRLIFT PHOTOCATALYTIC REACTOR STUDIES

6.1. Introduction

In the previous chapter, a 200 mL crystallizing dish was used as a batch reactor with gentle stirring and optimum conditions were obtained for the degradation of RTB dye using immobilized photocatalyst admixture (TiO₂, g-C₃N₄ and rGO) film under UV irradiation. In this section, the same immobilized photocatalyst admixture (TiO₂, g-C₃N₄ and rGO) film was used for photocatalytic degradation in an internal loop multiphase airlift reactor (ALTR) under UV irradiation. A few modifications have been done in the conventional ALTR reactor before employing it as the photocatalytic reactor (see Section 3.2.7.3.).

The photocatalyst immobilization technique and photocatalytic activity analysis technique are described in section 3.2.6.2. and 3.2.7.3. respectively.

6.2. Results and discussions

6.2.1. Characterization of photocatalyst

Since the same catalyst admixture film was used for the photocatalytic activity analysis, the characterization is as described in section 5.2.1.

6.2.2. Optimization of photocatalytic parameters

6.2.2.1. Effect of catalyst loading

The unary, binary and ternary catalyst mixture in immobilized form is evaluated for the photocatalytic degradation of RTB. The total amount of catalyst loading was 10 wt.% in which the first film has only g-C₃N₄ whereas the second and third film has a catalyst mixture of TiO₂: g-C₃N₄ (1:1 ratio) and TiO₂: rGO: g-C₃N₄ (1:1:1 ratio) respectively. As can be observed in **Figure 6.1**, the synergistic effect of the catalyst mixture is evident as we introduce TiO₂ and then a mixture of TiO₂ and rGO plus g-C₃N₄ into the

polystyrene film. The change in decolourization efficiency is not quite significant, though the catalyst mixture does improve the photocatalytic activity; on the other hand, we can utilise the best properties of each photocatalyst. By adding TiO_2 , the self-cleaning of the film surface can be done whereas addition of rGO leads to better adsorption. Adding two different catalysts into the polymer nanocomposite is shown to increase the productivity as well as save on materials (by reducing the use of expensive photocatalyst). Thus the synergistic effects of these catalysts can improve the overall oxidizing capability as shown in **Figure 6.2**. In the results given below, the ternary (1:1:1) photocatalytic film is used throughout.

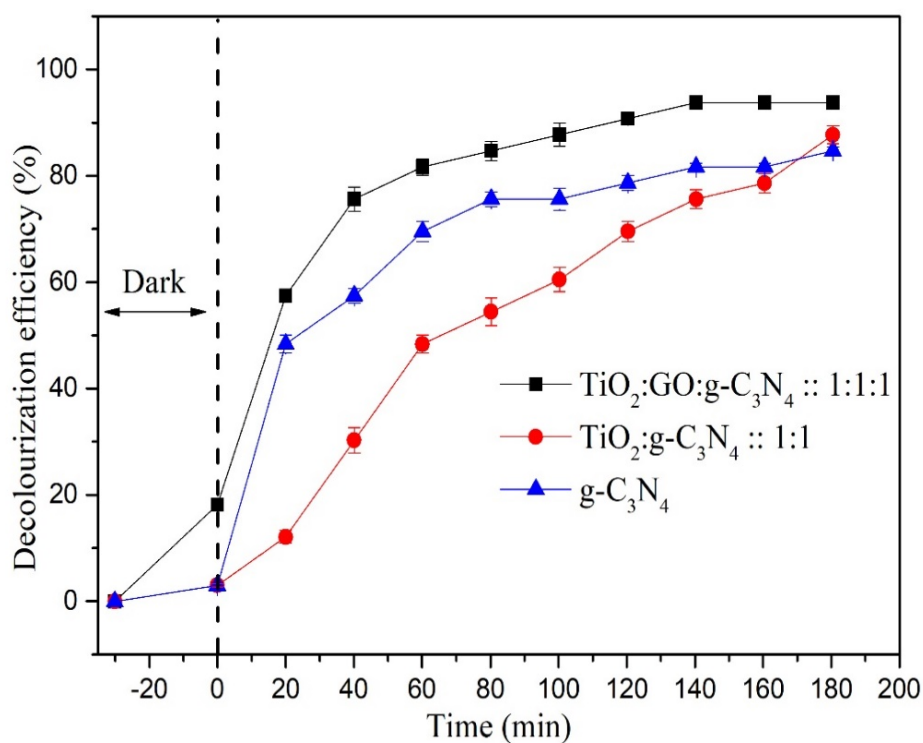


Figure 6.1. Effect of catalyst loading (Draft tube diameter = 6 cm).

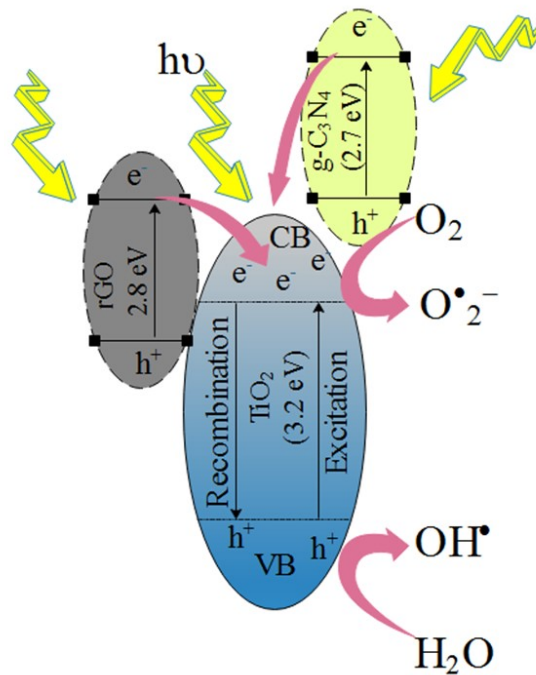


Figure 6.2. Schematic diagram of photocatalytic activity of an admixture.

6.2.2.2. Effect of D_i/D_o ratio

In an internal loop ALTR, the inner draft tube plays a major role especially in the case of photocatalysis. The light has to pass through the quartz glass outer tube and the RTB dye solution to the catalyst surface. As we increase the diameter of the inner draft tube, the distance between the light source and the catalyst surface reduces since the photocatalytic polymer film is attached to the outer surface of the inner draft tube. Also it is noted that as the draft tube diameter increases, the surface area of the film available for irradiation also increases. The outer vessel diameter (8 cm) was kept constant, and the inner draft column diameter (2, 4 and 6 cm in diameter with constant length) was varied to find out the optimum ratio. With increasing values of this ratio, the photocatalytic activity also increases, as the photon energy irradiation on the photocatalyst surface is more. Almost 91% decolourization occurred within 120 min in case of $D_i/D_o = 0.75$, and there was not much change in efficiency even after 3 h of UV irradiation (**Figure 6.3**). From the analysis, the optimum D_i/D_o is found to be 0.75; hence, the rest of the experiments was carried out using this ratio.

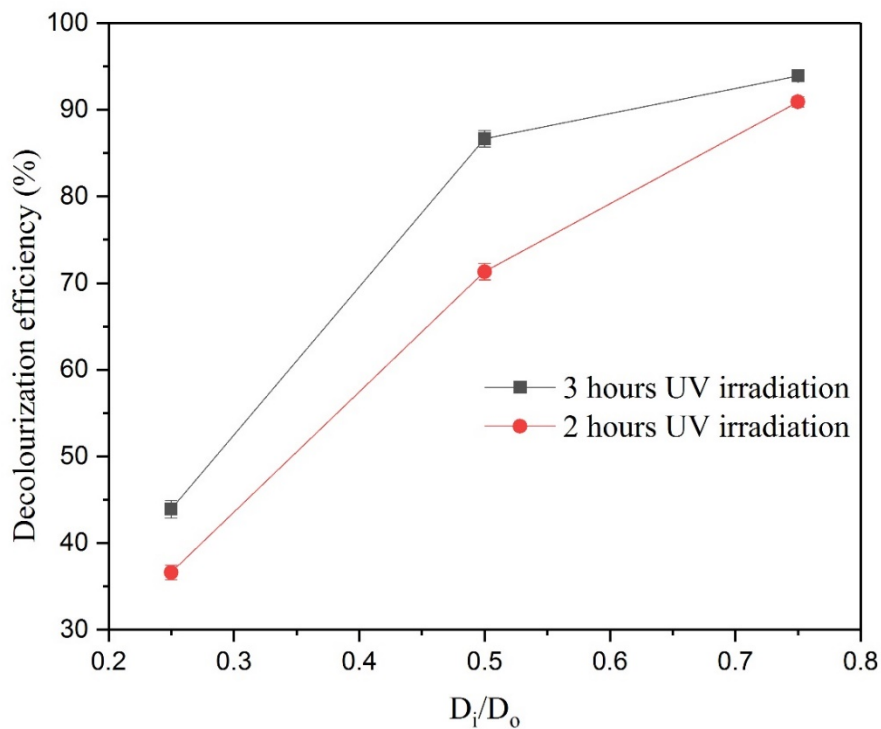


Figure 6.3. Effect of inner draft column diameter.

6.2.2.3. Effect of airflow rate

Figure 6.4. shows the influence of airflow rate on reactor performance at a fixed D_i/D_o ratio of 0.75. It is observed that with increasing airflow rate, the decolourization efficiency decreases. This is on expected lines as the increase in airflow rate leads to higher liquid circulation velocities causing a decrease in the residence time of the fluid. Almost 91% decolourization occurred at an airflow rate of 2 LPM within 120 min of UV irradiation; an additional 1 h of exposure did not show any significant change (only 3% increase) in the decolourization efficiency, and hence the optimum airflow rate was fixed at 2 LPM (superficial air velocity of 0.11724 cm/s). Also, the minimum time required for the reaction to occur, can only be achieved by low airflow rate.

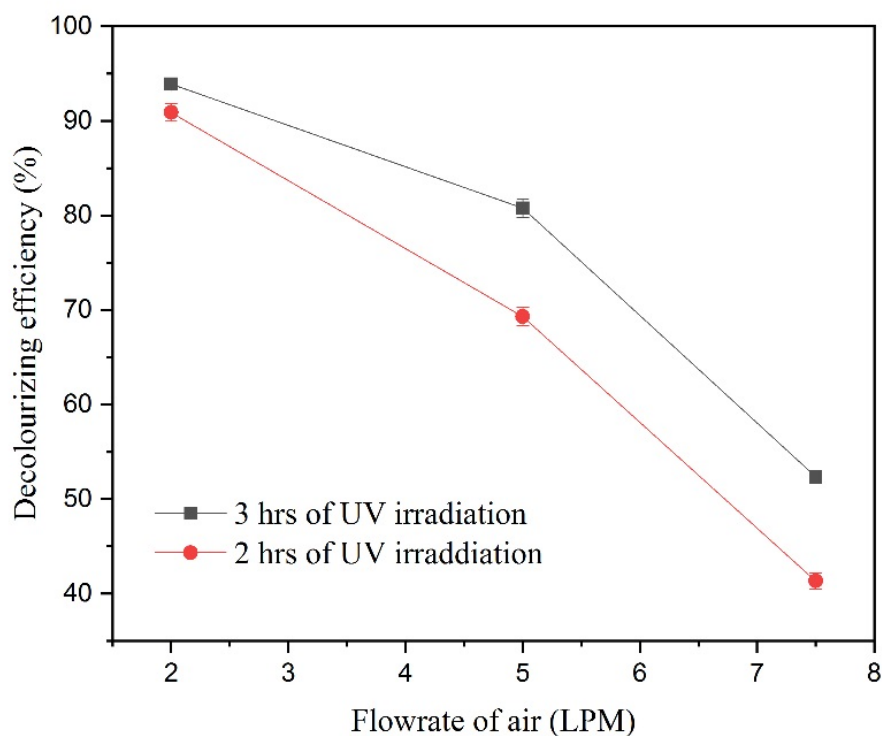


Figure 6.4. Effect of aeration flowrate.

6.2.2.4. Effect of initial dye concentration and reaction kinetics

To analyse the influence of the initial concentration of RTB dye, experiments were carried out at three different concentrations in the range of 10 to 30 ppm using the optimum operating parameters, as shown in **Figure 6.5a**. With increasing initial dye concentration, the decolourization efficiency decreases as it increases the opacity of the dye solution and absorbs the photons which leads to poor UV irradiation on the catalyst surface. The intermediate products which could have formed during the photocatalytic reaction can also interfere with the degradation/decolourization of the parent dye molecule resulting in the reduction of efficiency. Another possible reason for the decreased decolourization percentage may be due to the short life time of $\dot{\text{O}}\text{H}$ radicals (\sim few nanoseconds) and insufficient number of $\dot{\text{O}}\text{H}$ radicals is being generated as the UV light is getting absorbed by the dye molecule rather than the catalyst (El Bouraie and El Din 2016; Calvete et al. 2010). For reactor study and application point of view, it is essential to understand the importance of the reaction rate. As shown in **Figure 6.5b**, the kinetic analysis of the photocatalytic reaction indicates the degradation rates

of the RTB follows first-order kinetics (Table 6.1.), according to the Langmuir–Hinshelwood model. In this case, the reaction rate of photocatalytic degradation of RTB can be fitted by the first order reaction kinetics equation.

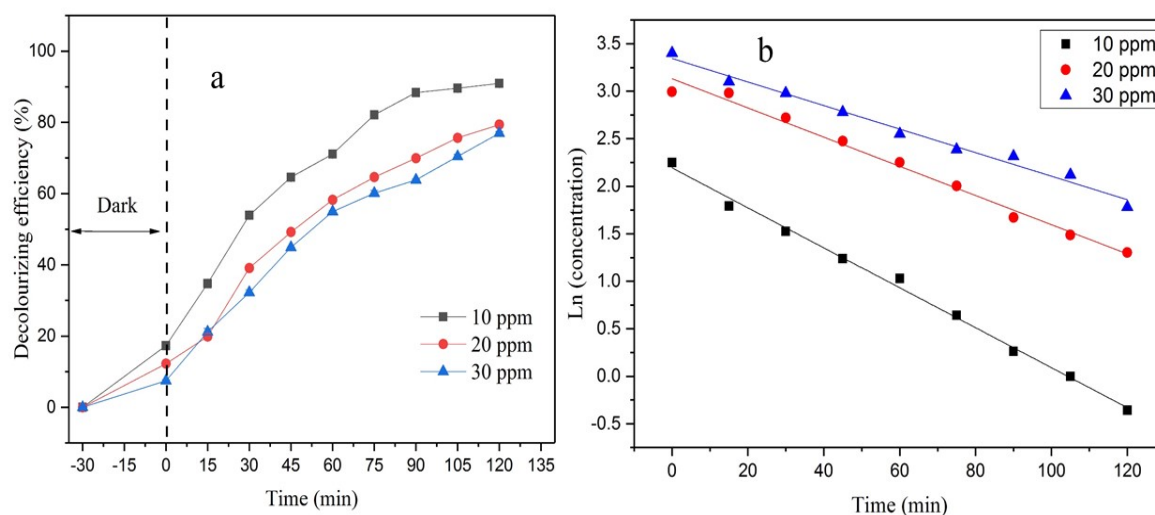


Figure 6.5. (a) Effect of initial dye concentration and (b) reaction kinetics.

Table 6.1. Kinetic study of RTB decolourization for different initial concentrations.

Initial Concentration (ppm)	R ²	k (min ⁻¹)
10	0.9862	0.0124
20	0.9882	0.0154
30	0.9959	0.0210

6.2.2.5. Effect of Different dyes

Three different dyes were used to analyse the effectiveness of the catalyst mixture as shown in Figure 6.6. Among those dyes, RTB showed the best results. The concentration of all the dyes was kept at 10 ppm. Around 18% and 44% decolourization has been noticed for remazol orange 16 (RO16) and remazol black 5 (RB5) respectively, whereas RTB showed 91% decolourization within 120 min of UV irradiation. From the above Figure 6.6, it is visible that the optimised condition is most suitable for RTB dye. From the structures (Osugi et al. 2006; Bostjan et al. 2016) of the RO16 and RB5 (Figure A2 and A3), it is observed that these two dyes are azo dyes

compared to RTB which is a pthalocyanine dye. This could be the reason for the poor photocatalytic performance observed in these two dyes.

6.2.2.6. Reusability of the catalyst film

From the efficiency point of view, the recycle and reuse of the catalyst is very much needed to achieve the highest outcome from the catalyst. The reusability of the photocatalytic film was done for four times without any regeneration (time = 3 h). For the first two runs, there was no significant change in efficiency, but after the third and fourth run, a 20% decrease in efficiency for RTB decolourization is noticed as shown in **Figure 6.7**. The adsorption of RTB dye or intermediate products on the photocatalytic film surface may have blocked the irradiation on the catalyst surface and could be the main reason for the decrease in photocatalytic efficiency. Overall, the results seem quite promising and indicate that the prepared catalytic film is quite stable.

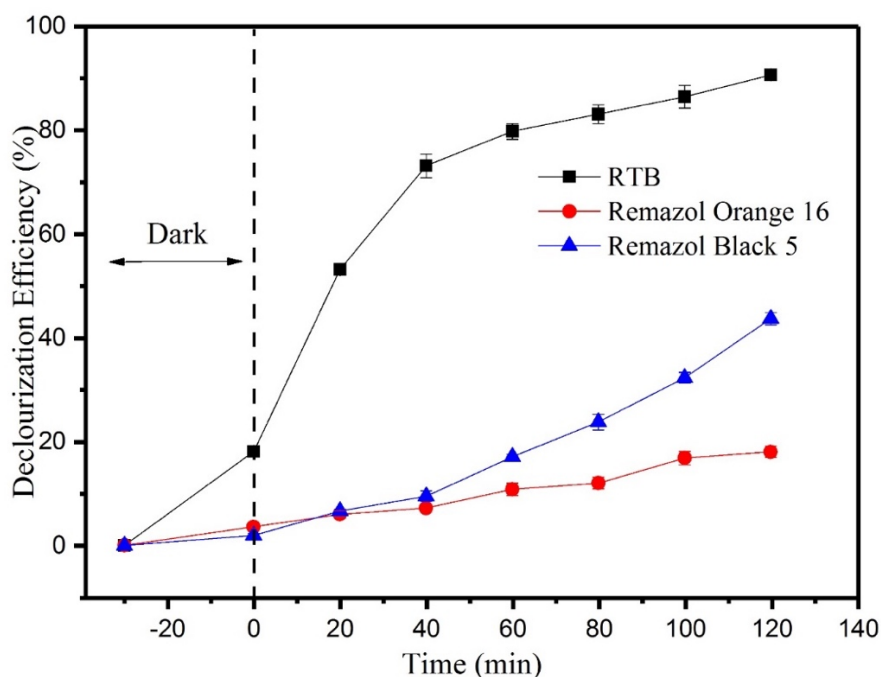


Figure 6.6. Decolourization of RTB and two other dyes.

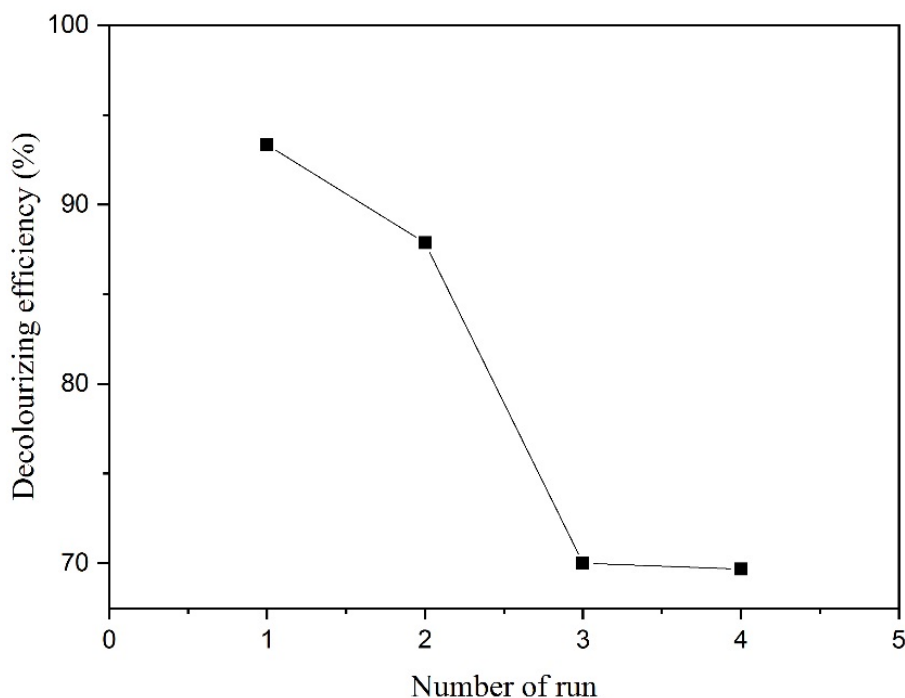


Figure 6.7. Recyclability test of the photocatalytic film.

6.2.2.7. Comparison of slurry and immobilized catalyst performance

It is well known that the photocatalytic activity in slurry form is better than the immobilized form since the catalyst surface area is more. According to **Figure 6.8**, 91% decolourization of the dye occurred within 40 min of the UV irradiation in slurry form whereas it took 120 mins in case of immobilized form. It is also observed that the decolourization efficiency never increased in slurry form after reaching 91% and was constant throughout the reaction time (3 h) whereas in the immobilized form it has increased slightly to 94% after 140 min and then stays constant for rest of the reaction time. It is evident that at longer timeframes, immobilized catalysts are actually better than the slurry form thus promising complete mineralization of the organic pollutants.

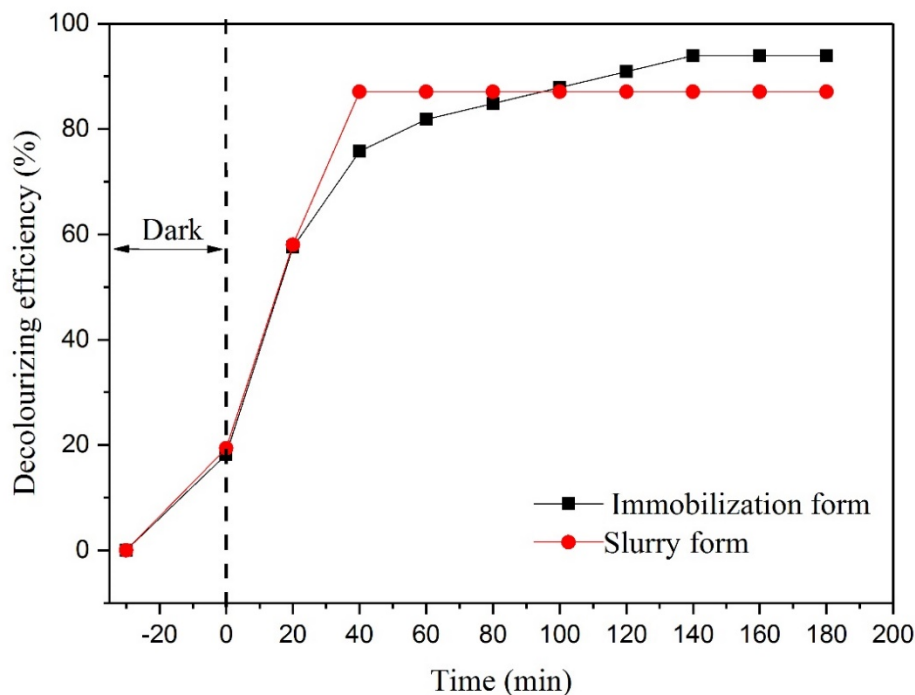


Figure 6.8. Comparison of immobilized and slurry photocatalytic activity.

6.2.2.8. Effect of different oxidizing agents in the presence of immobilized photocatalytic film (IP):

Molecular oxygen or hydroxyl radical ($\cdot\text{OH}$) is commonly used as an electron acceptor to capture electrons. Therefore, quantum effectiveness may partially be increased by inhibiting electron-hole recombination to enhance photocatalytic efficiency. In the present study, liquid H_2O_2 , pure oxygen, and pure ozone were investigated in the photocatalytic reactor to analyse the effect of different oxidising agents in the presence of immobilized photocatalytic film and UV irradiation on the RTB degradation (**Figure 6.9**). The degradation per cent of RTB solution under pure oxygen aeration at the rate of 2 LPM reached 95% within 140 min. This percentage was slightly higher than that under airflow. Under the influence of pure oxygen aeration, the per cent of RTB degradation was not as efficient as H_2O_2 (1 mL/L). More than 97% of decolourization occurred in the presence of H_2O_2 within 40 min, whereas it took only 15 min in the presence of ozone (2 LPM flowrate). The generation of active oxygen and $\cdot\text{OH}$ radicals by different oxidizing agents can vary depending on their oxidizing potential. The

production of active oxygen or hydroxyl radicals follows the order Ozone > H₂O₂ > O₂ > air as can be seen in **Figure 6.9**.

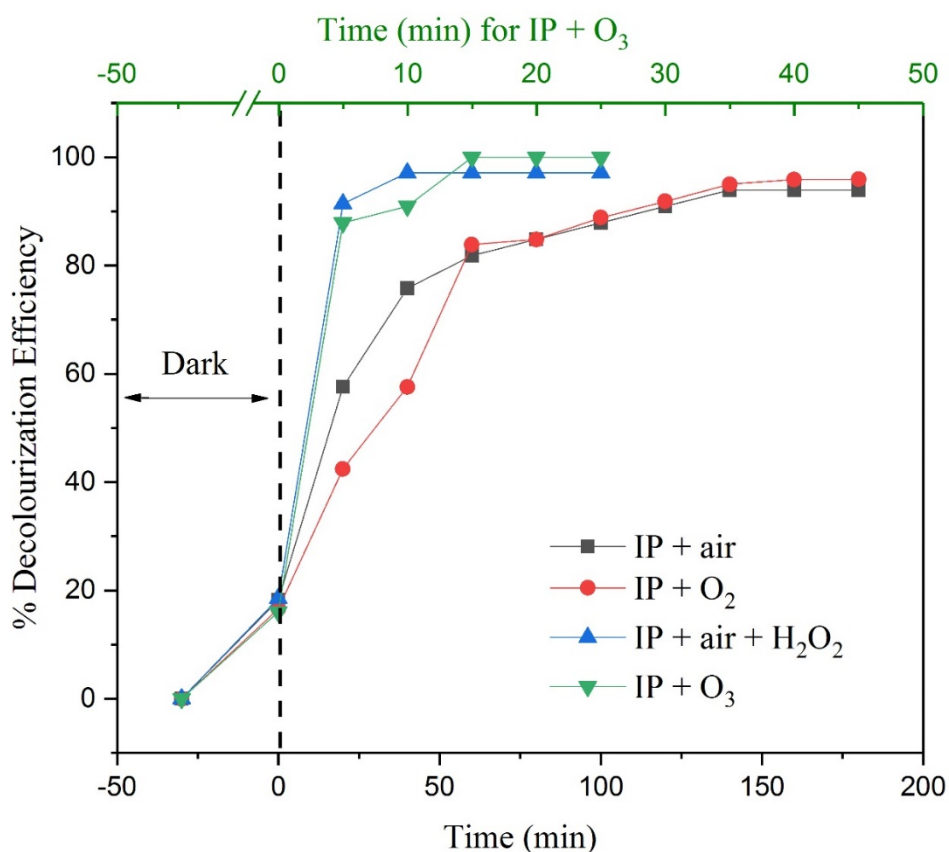


Figure 6.9. Effect of different oxidising agents on photocatalytic activity.

6.2.3. Photocatalytic degradation analysis of RTB

6.2.3.1. TOC analysis

TOC measurements estimated the sample collected from the photocatalytic study. The results obtained from TOC experiments after 140 min of the photocatalytic reaction of 10 ppm of RTB dye solution under normal pH. As can be seen in **Figure 6.10**, 92.25% of mineralisation is reached after 140 min of photocatalysis, which is almost the same as decolourization efficiency (94%). The results suggest that the total mineralisation of the RTB dye solution to CO₂ and H₂O probably did not take place, but the photocatalytic

results are very significant, compared to other processes and very close to the decolourization efficiency (Osugi et al. 2006; Boštjan et al. 2016).

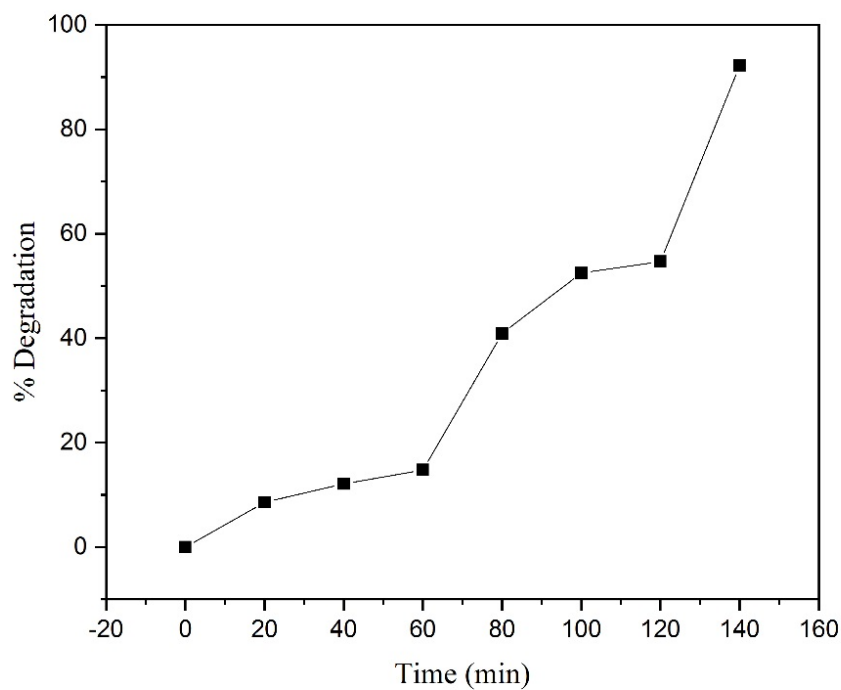


Figure 6.10. TOC analysis of the degraded RTB dye.

6.2.3.2. HPLC/LCMS analysis

To detect the final products after degradation of RTB, HPLC followed by MS analysis were carried out. **Figure 6.11a** shows the HPLC profile of the sample (dye without treatment) showed two peaks with retention times of 3.2 and 3.67 min respectively. After photocatalytic treatment, the chromatogram shows that the respective peaks with retention times of 3.2 and 3.67 min have almost mineralised. These results indicate the possible breakdown of the parent molecule and the formation of the new products.

uV

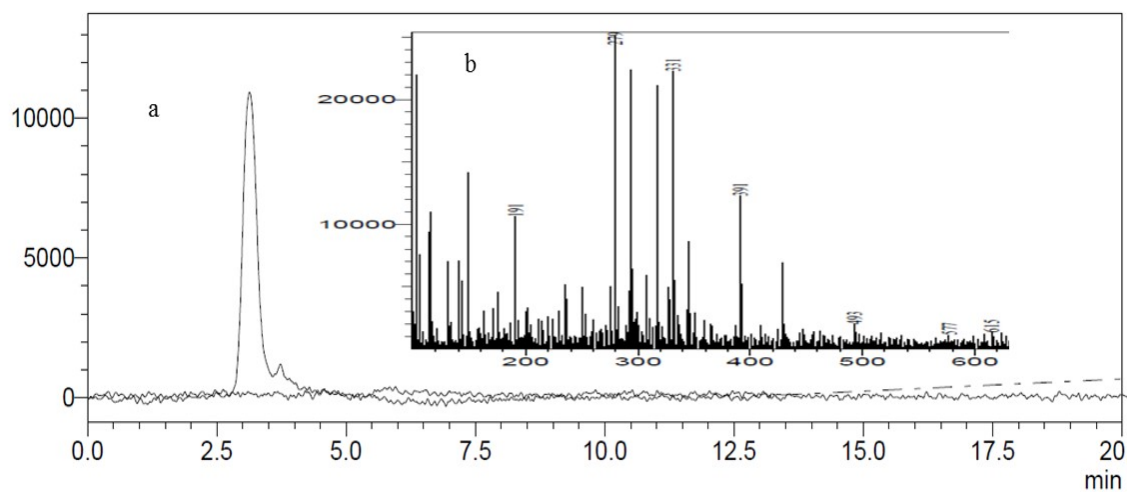


Figure 6.11. HPLC–MS analysis of RTB dye.

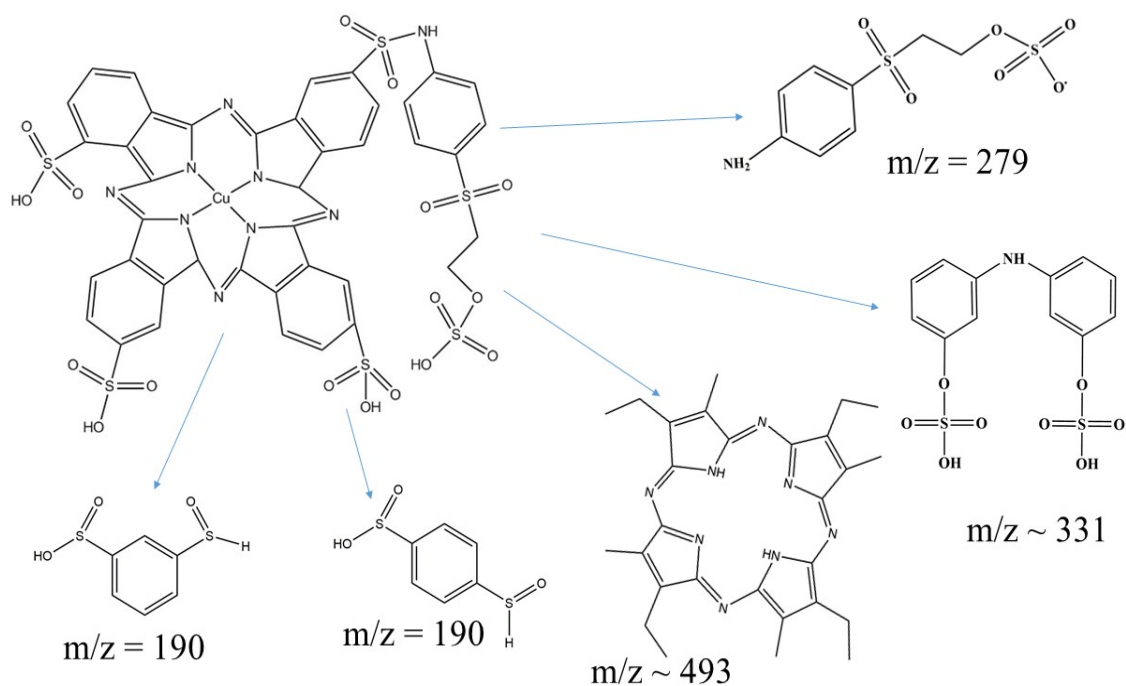


Figure 6.12. Degraded hypothetical by-products.

The MS spectra (**Figure 6.11b.**) of a degraded sample shows the molecular weights of the degraded compounds at $m/z = 191, 279, 331, 391, 493$. Among the acknowledged molecular weights, the identified compound from literature is 2-(4-

Aminophenylsulfonyl hydrogen sulphate) with a molecular weight of 279 (Pardiwala et al. 2017). The degraded hypothetical by-products from the parent compound are shown in **Figure 6.12**.

6.3. Conclusions

The multiphase reactor for the photocatalytic degradation of the RTB dye was used in this part of the work and the various parameters were studied. The conclusions withdrawn from this part of the work are mentioned below:

- The prepared stable photocatalyst admixture (TiO_2 : rGO : g- C_3N_4 :: 1:1:1) immobilized polymer film was used in a novel photocatalytic airlift reactor under UV light for the degradation of RTB dye.
- 94% colour removal and 92.25% TOC removal occurred within 140 min in the reactor respectively at optimum conditions (10 ppm, 1200 mL RTB). Correspondingly, HPLC-MS confirms the degradation of dye, and the possible degradation products were identified and enlisted.
- The crucial parameters of the reactor show that the D_i/D_o ratio and air flowrate has a severe impact on the photocatalytic degradation of the dye.
- Other key findings from this part of the work are that the immobilized catalyst showed better activity than the slurry catalyst over time, the presence of oxidizing agents enhances the photocatalytic activity, the optimum conditions are best suitable for RTB compared to other dyes, and the reusability of the prepared film was also feasible.

CHAPTER 7

RESULTS AND DISCUSSION

**(POLYSTYRENE – TiO₂/g-C₃N₄/rGO
COMPOSITE PHOTOCATALYTIC
FILM: MULTIPHASE AIRLIFT
PHOTOCATALYTIC REACTOR)**

CHAPTER 7

POLYSTYRENE – TiO₂/g-C₃N₄/rGO COMPOSITE PHOTOCATALYTIC FILM: MULTIPHASE AIRLIFT PHOTOCATALYTIC REACTOR

7.1. Introduction

The photocatalytic degradation study of RTB dye using TiO₂ (Chapter 4); admixture of TiO₂, g-C₃N₄, and rGO (Chapters 5 and 6) in batch mode as well as scaled up mode under UV irradiation is examined systematically. The next part of this work comprises the degradation of the same dye using composite material of TiO₂, g-C₃N₄, and rGO in a multiphase airlift reactor under sunlight. The composite material is synthesised by simple calcination method (described in section 3.2a). The immobilization of the catalyst was done using solvent casting method (described in section 3.2c) and the same airlift reactor (at optimised reactor parameters) was used in this work. The characterization of the photocatalyst powder and the prepared immobilised film is evaluated using Particle Size Analyser, BET surface area analysis, SEM-EDX, FTIR, XPS, XRD, ICP-OES and DRS. The parameters effecting the photocatalytic activity are analysed here namely g-C₃N₄ concentration, catalyst loading, initial dye concentration, slurry vs immobilised and reusability. The degradation of the dye was confirmed by TOC and HPLC, whereas LCMS analysis helped to find out the by-products generated during the photocatalytic process. To make this process more suitable for industrial application, waste polystyrene was used as a substrate material instead of pristine polystyrene. The catalyst immobilization technique and the photocatalytic activity analysis procedure are already mentioned in section 3.2.6.3. and 3.2.7.4.

7.2. Results and discussions

7.2.1. Characterization of photocatalyst and the PPCF

7.2.1.1. SEM–EDX, BET surface area and Particle size analysis

The surface morphology of the prepared photocatalyst powder and PPCF was analysed by SEM (**Figure 7.1**). The surface morphology of the synthesized powdered composite material is depicted in **Figure 7.1a**. A mean particle size of 87.4 nm is observed from the particle size analysis and the BET surface area is 22.9 m²/g. The elemental analysis from the SEM–EDX (**Figure 7.1b**) of the composite confirms the presence of the Ti, C, N and O elements. Among these, nitrogen is the dominating element, thereby confirming that the g–C₃N₄ is the base material. The elemental mapping of the Ti, C, N and O in the TiO₂/rGO/g–C₃N₄ composite (**Figure 7.1c**) shows that all the elements are uniformly distributed among the entire composite.

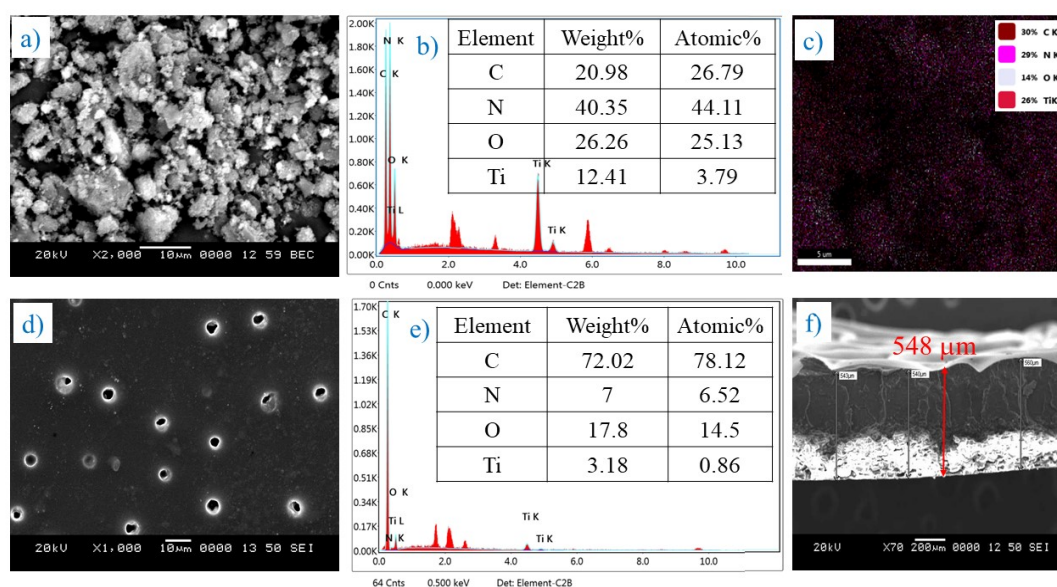


Figure 7.1. SEM image of the a) composite photocatalyst powder, b) EDX analysis of composite powder, c) elemental mapping of composite powder, d) surface morphology of PPCF (10 wt% catalyst loading), e) EDX analysis of PPCF (10 wt% catalyst loading) and f) cross-sectional image of PPCF (10 wt% catalyst loading).

From the SEM image of the PPCF (**Figure 7.1d**), it is observed that there are a number of uniformly sized pores on the PPCF surface (white circular spots) possibly due to the evaporation of solvent, which increases the available surface area of the catalyst and

thus improves the overall efficiency of the film. The SEM–EDX of the PPCF surface confirmed the presence of C, N, O and Ti (**Figure 7.1e**) and the SEM image of the PPCF surface (**Figure 7.1d**) shows the uniform distribution of the photocatalyst. Also, the average thickness of the PPCF as observed from the cross–sectional SEM image of the film is 548 μm (**Figure 7.1f**).

7.2.1.2. XRD analysis

The phase structure of the g–C₃N₄, rGO, TiO₂, composite material and the PPCF is analyzed by XRD, as shown in **Figure 7.2**. The characteristic peak for g–C₃N₄ (Hafeez et al. 2018; Wu et al. 2017; Aleksandrzak et al. 2017; Dong et al. 2014; Cheng et al. 2013) is observed at 27.38° for (002) plane (JCPDS, 87–1526) whereas for rGO (Fan et al. 2011; Alam et al. 2017; Thirumalraj et al. 2017) at 26.46° (002) as shown in **Figure 7.2a and b** respectively.

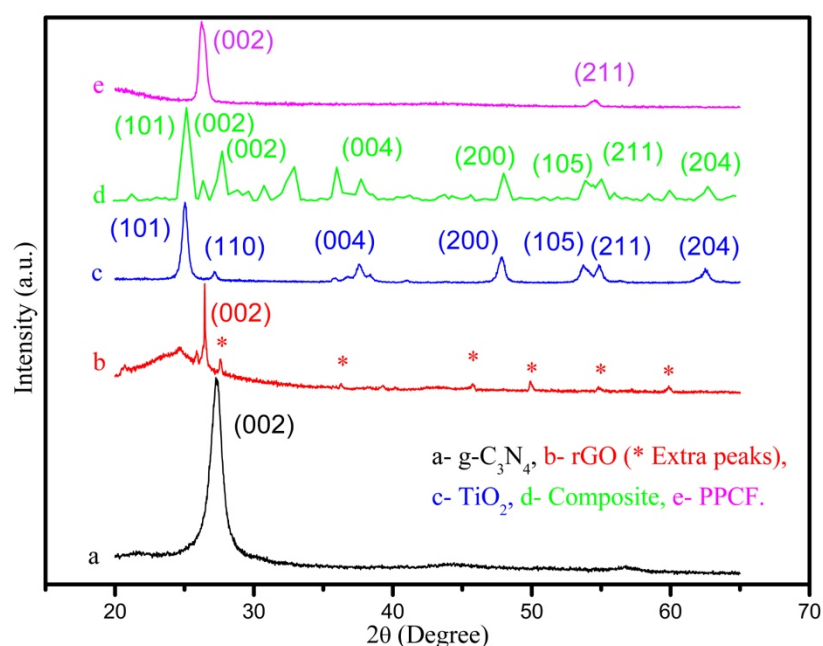


Figure 7.2. XRD spectra of the photocatalyst powders a) g–C₃N₄, b) rGO c) TiO₂, d) TiO₂/rGO/g–C₃N₄ composite and e) PPCF film (10 wt% catalyst loading).

The extra small peaks (*) in XRD plot of rGO may be because of the impurities present in the sample. The XRD plot of TiO₂ in **Figure 7.2c** shows two distinct peaks at 25.12° (101), and 27.27° (110) (Ocwelwang and Tichagwa 2014; Kamrannejad et al. 2014; Sinirtas et al. 2016) corresponding to the anatase and rutile phases respectively (all

other peaks at crystal plane (004), (200), (105), (211), and (204) corresponds to the anatase TiO₂, according to JCPDS Card no. 21–1272 and 1276). Moreover, it can also be observed from the XRD plot of TiO₂ that the anatase phase is predominant. In the XRD pattern of the g-C₃N₄/ rGO/TiO₂ composite (**Figure 7.2d**), the diffraction peaks are shifted a little, but all peaks (g-C₃N₄ (002); TiO₂ (101, 004, 200, 105, 211, and 204)) are in agreement with the characteristic peaks of g-C₃N₄ and TiO₂ photocatalysts. However, there is no distinct peak detected for rGO in the composite material, probably because the rGO diffraction peak at 26.46° (002) with much lower intensity collapses into the anatase TiO₂ strong peak at 25.12° (101). The high temperature during the preparation of the photocatalyst composite can promote the change in phase from anatase to rutile TiO₂ and also leads to the generation of the impurities, which explains the enlargement of the peak intensities and extra peaks present into the XRD plot of the composite material (Yang et al. 2012). The XRD analysis of the PPCF (**Figure 7.2e**) shows that the amorphous nature of polystyrene and sharp peaks at 26.24° (002) and 54.55° (211) corresponding to the presence of composite photocatalyst (dominating spectra of g-C₃N₄ (002) and TiO₂ (211)) in the film.

7.2.1.3. XPS analysis

The quantitative XPS analysis of the PPCF was performed for the detailed depth profile/ elemental analysis (chemical composition) of the film (**Figure 7.3a**). On comparison of the XPS spectra of the PPCF with the XPS spectra of plain polystyrene as given in (Girardeaux and Pireaux 1996), the presence of C (284.72 eV) and O (~533 eV) is not only confirmed but also the existence of Ti and N is established. This is in line with the SEM–EDX results presented earlier. The typical survey of high–resolution spectra is presented in **Figure 7.3b–d**. The C1 s spectra (**Figure 7.3b**) shows the presence of three fitted peaks of carbon matrixes with C – C, C – O, and C – N at the bandgap of 284, 289, and 297.5 eV respectively (Li et al. 2013). The O1 s spectra (**Figure 7.3c**) confirmed the presence of the C – O – Ti and N – C – O bonds at the specific bandgap of 532 and 540 eV respectively (Erdem et al. 2001; Li et al. 2013; Shen et al. 2016). The Ti2p spectra (**Figure 7.3d**) of Ti – C bond is observed at the binding energy of 460 eV (Li et al. 2013). The high–resolution N1s spectra in **Figure 7.3e** shows the contribution of N – (C)₃ at the bandgap energy of 400.5 eV (Xu et al. 2013). The XPS

analysis confirms the different bond formations among the elements present in the composite and the polystyrene and thus, the successful incorporation of the photocatalyst composite in the polystyrene matrix.

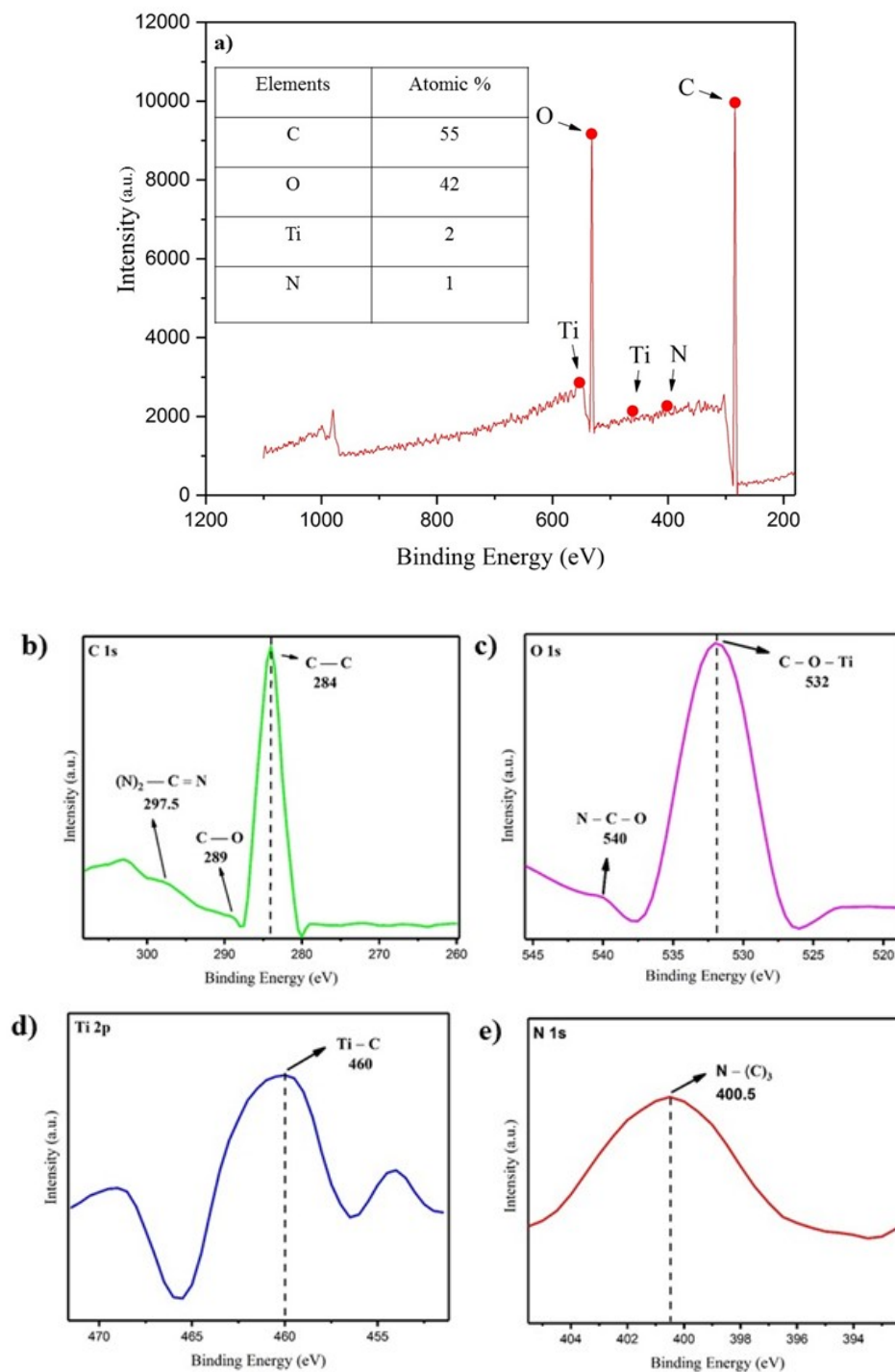


Figure 7.3. XPS spectra of the a) PPCF (10 wt% catalyst loading), b) C 1s, c) O 1s, d) Ti 2p, e) N 1s.

7.2.1.4. FTIR and Bandgap energy analysis

Figure 7.4 shows the FTIR spectra for plain polystyrene and PPCF. The identified bonds present in the films are tabulated in **Table 7.1** (Shang et al. 2003; Song et al. 2009; Jaleh et al. 2011; Luo et al. 2008; Yu et al. 2017; Chen et al. 2019). It can be observed that the characteristic peaks to the corresponding bonds for the polystyrene are present in both the spectra and the extra peaks (1744.17 and 128.13 cm^{-1}) which are observed in PPCF corresponds to the photocatalyst present in the film. The perturbation of the PPCF FTIR plot intensity (at 1028.14 , 1450.4 , 1491.2 , 1599.33 , 2849.8 , 2925.3 , and 3027.3 cm^{-1}) is observed due to the change in the chemical state of the polystyrene in the presence of photocatalyst.

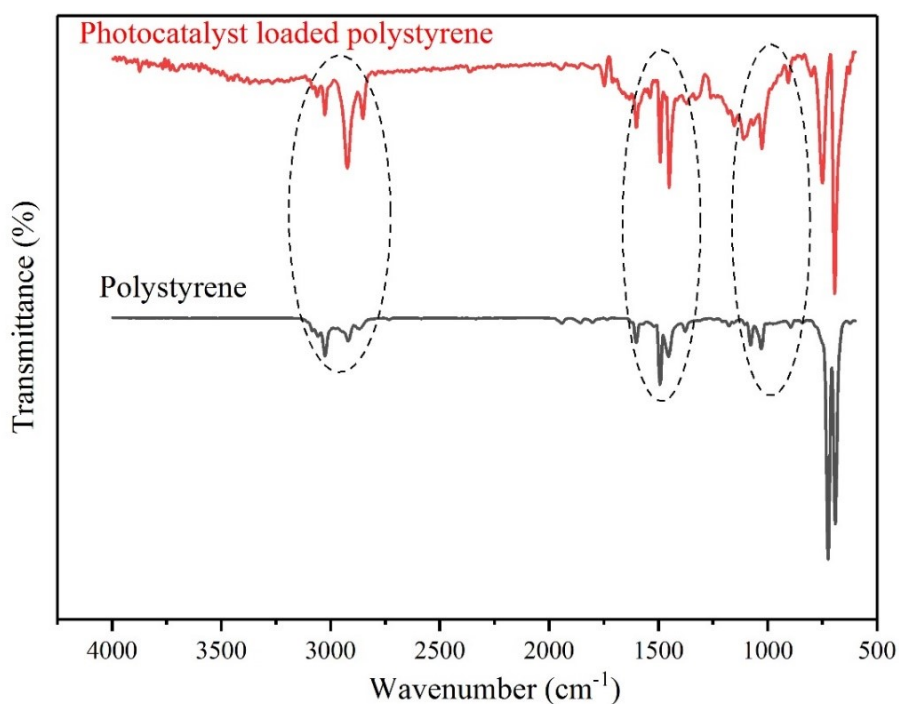


Figure 7.4. FTIR spectra of plain polystyrene film and PPCF (10 wt% catalyst loading).

The confirmation of different bonds present in the PPCF from FTIR analysis is in agreement with the findings from XPS results. The UV-vis diffuse absorbance spectra of the TiO_2 , rGO and $\text{TiO}_2/\text{rGO}/\text{g-C}_3\text{N}_4$ composite powder materials are presented in **Figure 7.5a**. It is observed that the absorption edges of the composite sample are quite distinct in the visible light range, which indicate the higher visible light photocatalytic activity. The energy bandgap was estimated by assuming indirect bandgap in **Figure**

7.5b (Wu et al. 2017; Lin et al. 2018). The calculated bandgap of the TiO₂/rGO/g-C₃N₄ composite powder material is 2.41 eV which is in agreement with the values reported in (Wu et al. 2017). On the other hand, the bandgap of RTB dye (1.86 eV) is narrow enough to absorb sunlight, thus bringing in the possibility of self-sensitization of the dye. A possible schematic mechanism of the self-sensitized photocatalytic reaction under sunlight is depicted in **Figure 7.6** (Molla et al. 2017).

Table 7.1. Details of FTIR spectra for the PPCF film (10 wt% catalyst loading).

Type of vibration	Wavenumber (cm ⁻¹)	
	Polystyrene film	PPCF
Phenyl ring present in pure polystyrene sample (Shang et al. 2003; Song et al. 2009; Jaleh et al. 2011)	697, 756, 1028, 1450, and 1492	1024
C – H bond in benzene ring present in polystyrene (Luo et al. 2008)	3026	3027
C – C bond stretching vibration (Jaleh et al. 2011)	1500	1500, and 1600
Aromatic C – H bond stretching vibration (Luo et al. 2008; Yu et al. 2017)	1600, 1496, 1455, and 2919	1600, 1493, 1450, and 2925
Aromatic C – H deformation vibration (Luo et al. 2008)	1080, 1031, 725, and 693	3025, 3061, and 3082
Confirmation of the indication of the catalysts in the film		903.7, 1109.7, 1369, 1750, 2852, and 3064
Aromatic C – N bond stretching		1283

7.2.1.5. ICP–OES analysis

The stability of the PPCF with respect to the possibility of the titanium ions leaching out was checked by the Inductively Coupled Plasma Atomic Emission Spectroscopy

(ICP–OES). In order to check the stability of the PPCF, the film was submerged in distilled water and kept under vigorous stirring for 24 h. The resulting solution was then analyzed and the amount of Ti^{3+} content was found to be 0.05 ppm on an average. The actual quantities during reactor operation may be much lesser than this value and thus are in compliance with the suggested maximum allowable titanium content in drinking water (Dong et al. 1993).

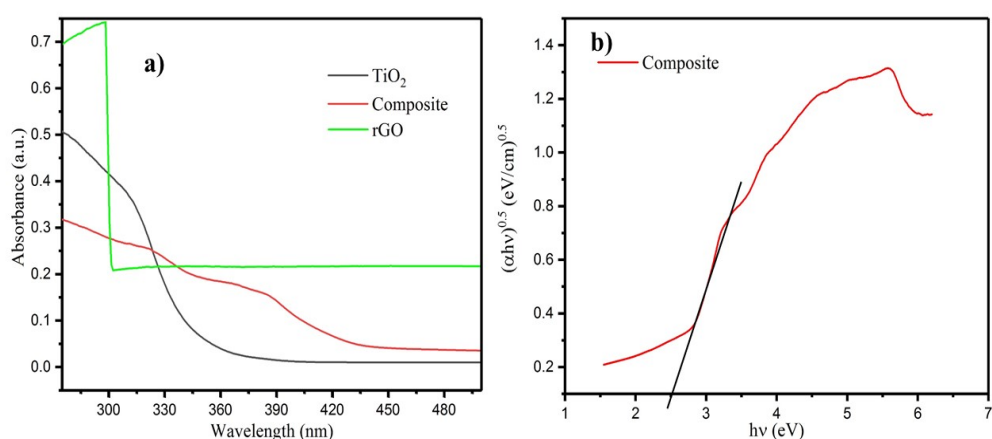


Figure 7.5. a) Absorbance spectra of TiO_2 , rGO and $\text{TiO}_2/\text{rGO}/\text{g-C}_3\text{N}_4$ composite and b) calculated bandgap of the composite material.

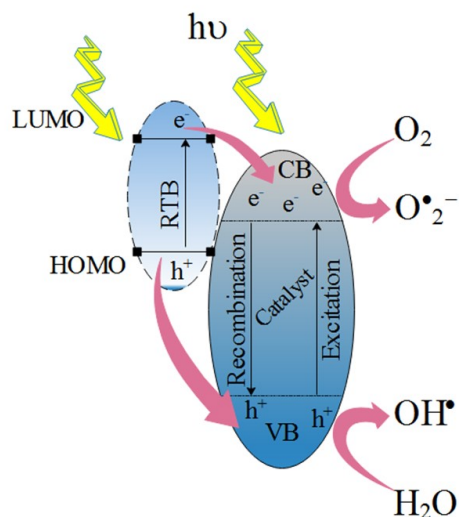


Figure 7.6. Schematic mechanism of self-sensitized composite photocatalyst (LUMO: lowest unoccupied molecular orbital, HOMO: highest occupied molecular orbital).

7.2.2. Optimization of photocatalytic parameters

7.2.2.1. Effect of g-C₃N₄ concentration

As mentioned earlier, during the preparation of the photocatalyst composite, the quantities of the TiO₂ and rGO were kept constant whereas the amount of melamine was varied to find out the optimum loading or the influence of g-C₃N₄. The g-C₃N₄ converted from melamine in the composite photocatalyst clearly indicates a crucial effect on photocatalytic activity of the immobilized film as shown in **Figure 7.7a**.

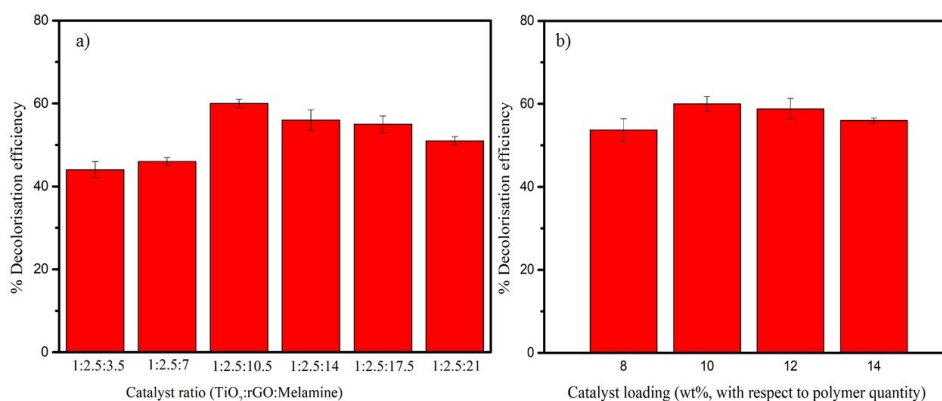


Figure 7.7. Effect of a) g-C₃N₄ loading (10 wt% catalyst loading, 10 ppm RTB) and b) catalyst loading on photocatalytic activity (10 ppm RTB).

The increasing melamine concentration leads to high photocatalytic activity, but after the optimum melamine loading, it started decreasing as the active sites of the catalyst reduces. The inferior photocatalytic efficiency is because a low amount of g-C₃N₄ has insufficient sunlight absorption to excite the catalyst, while an excess g-C₃N₄ in the composite can produce severe recombination of electrons and holes (Lin et al. 2018). Moreover, the surfeit amount of melamine reduces the photocatalytic activity by bringing down the active sites of the catalyst. The optimized melamine loading (1:2.5:10.5) was used further to analyze the influence of other parameters on photodegradation.

7.2.2.2. Effect of catalyst loading

The optimized photocatalyst composite (catalyst ratio, TiO₂: rGO: melamine=1:2.5:10.5) was immobilized in a polystyrene substrate with different

amounts of loading, to find out the optimized catalyst loading (**Figure 7.7b**). The amount of catalyst in the PPCF was varied from 8 to 14 wt.% (with respect to polystyrene). Increase in catalyst concentration from 8 to 10 wt% led to an increase in efficiency from 53.7% to 60% (**Figure 7.7b**). A further increase in catalyst loading to 12 and 14 wt % did not increase in the yield and this may be due to the reduced number of active sites or due to the inability of reactant to react the active sites. Also, an excess amount of catalyst after saturation point can reduce the number of pores or size of the pores, which leads to less catalyst active surface area resulting low yield. A maximum conversion of 60% was observed at 10 wt% catalyst loading after 90 min of irradiation. Based on the above observations, the catalyst loading in subsequent experiments was kept at the optimum value of 10 wt%.

7.2.2.3. Effect of initial RTB concentration and reaction kinetics

The effect of the initial dye concentration on the photocatalytic decolourization is shown in **Figure 7.8a**.

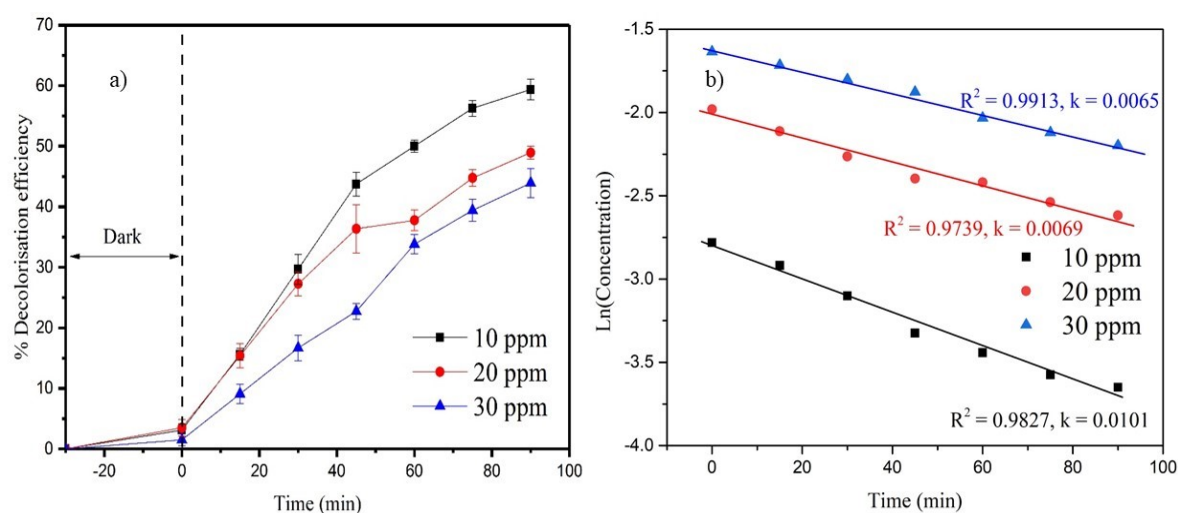


Figure 7.8. (a) Effect of initial concentration of the dye and (b) the kinetics of the reaction.

The RTB initial concentration is varied from 10 to 30 ppm keeping other experimental conditions constant. **Figure 7.8a** shows that the colour removal of the RTB decreases with increasing initial dye concentration. This is due to the observation that with increased dye concentration, the opacity of the solution increases, thus hampering the passage of photons to the catalyst surface; less photon irradiation means low

photocatalytic yield. Thus, high initial dye concentration affects the decolourization efficiency, but in longer time frames, the total mineralization of the dye is possible. The photocatalytic process follows the first order kinetics as can be seen in **Figure 7.8b** and **Table 7.2**.

Table 7.2. Kinetic study of RTB decolourization for different initial concentrations.

Initial Concentration (ppm)	R ²	Rate constant (<i>k</i>) (min ⁻¹)
10	0.9827	0.0101
20	0.9739	0.0069
30	0.9913	0.0065

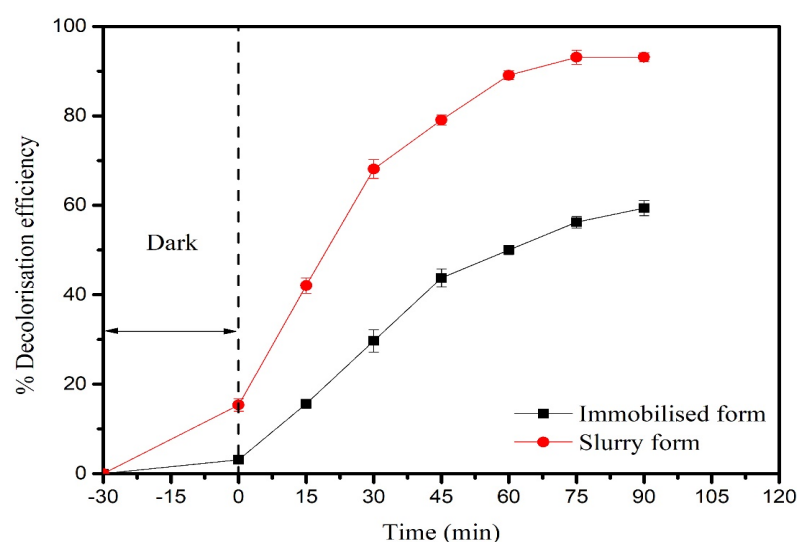


Figure 7.9. Comparison of immobilized and slurry photocatalytic activity (10 wt% catalyst loading, 10 ppm RTB).

7.2.2.4. Effect of slurry and immobilized photocatalyst

The slurry form of the photocatalyst is usually more efficient than the immobilized form (Shi et al. 2012; Iatsunskyi et al. 2015) due to greater available surface area. As observed from **Figure 7.9**, more than 93% decolourization of the RTB dye is obtained within 90 min in the slurry system, whereas 60% decolourization occurred for the same time in the immobilized form. Even though the photocatalytic efficiency is 33% more

in the slurry system compared to the immobilized system for the same time interval, the separation and reuse of the catalysts after the operation is complicated (in terms of post recovery of the catalyst) thus necessitating the need for effective immobilization.

7.2.2.5. Effect of catalyst reuse

Photostability and catalyst life are crucial economic parameters in photocatalysis operation (especially in large-scale / industrial scale operations). Reusability of the PPCF was checked for four times under solar light with optimized catalyst loading (Figure 7.10).

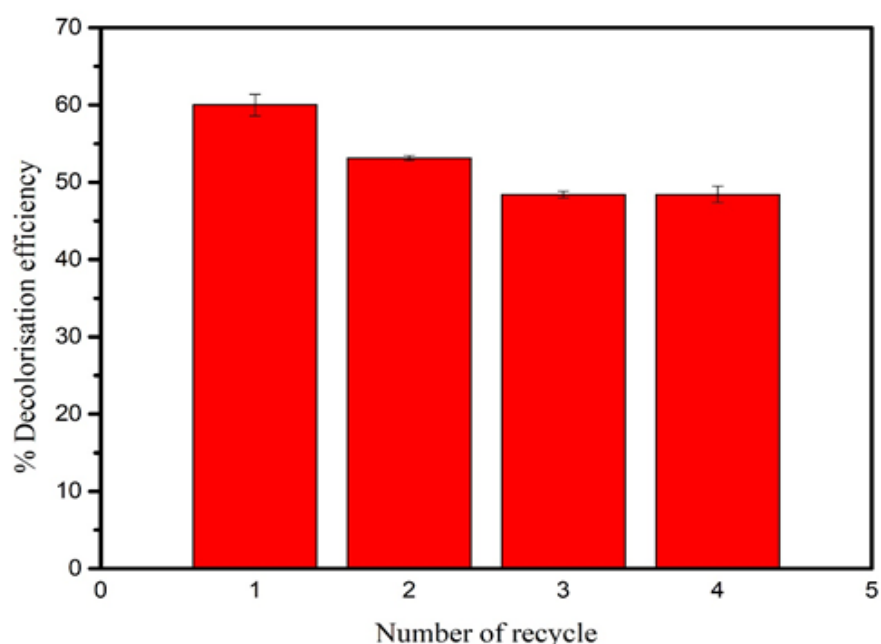


Figure 7.10. Reuse of the PPCF under optimized conditions (10 wt% catalyst loading, 10 ppm RTB).

After each experiment, the PPCF was used without cleaning or washing. It was found that the decolourization of the dye decreased marginally to around 50% from 60% over four reuses indicating that the film is quite stable. The gradual decrease in the efficiency is may be due to increased adsorption of the dye on the catalyst surface.

7.2.2.6. Effect of waste polystyrene as a substrate material

From the environmental point of view, the use of waste polystyrene is more favourable, instead of pristine polystyrene as it helps in reducing the polymer waste materials in the environment.

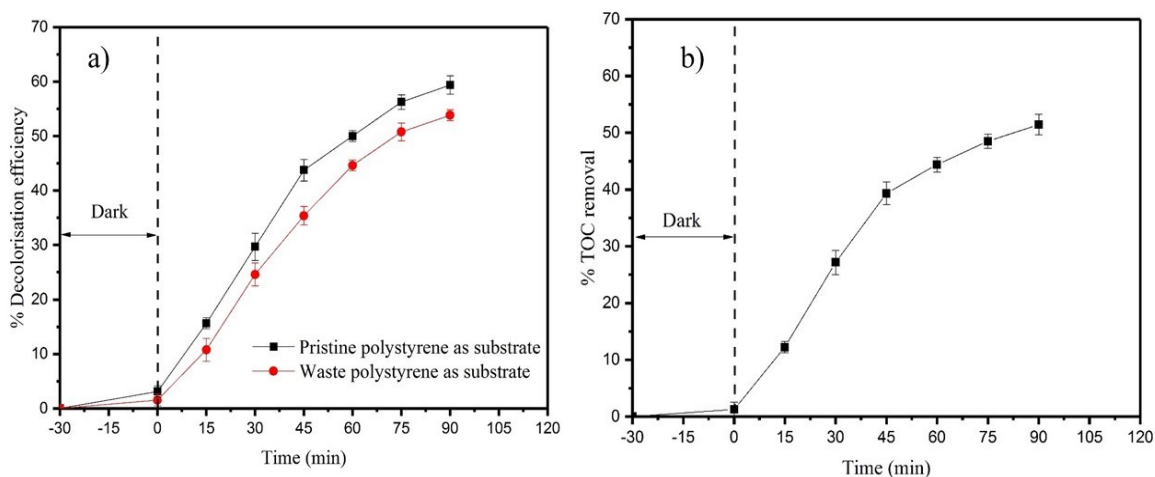


Figure 7.11. a) Comparison of the photocatalytic activity of the film made with waste and pristine polystyrene, b) TOC analysis of the treated solution; (10 wt% catalyst loading, 10 ppm RTB).

The performance of PPCF made with waste polystyrene was compared with that made using pristine polystyrene and it can be seen from **Figure 7.11a** that the performance of the waste polystyrene matches very closely that of the pristine polystyrene indicating that the use of waste polystyrene does not significantly affect the photocatalytic efficiency of the catalyst. This is quite encouraging and further work is needed in this regard to confirm the wider applicability of the waste polystyrene in photocatalytic devices.

7.2.3. Photocatalytic degradation analysis of RTB

7.2.3.1. TOC analysis

In **Figure 7.11b**, the TOC removal after 1.5 h of photocatalytic operation under sunlight was 51.43% compared to the corresponding decolourization of 60%, which indicates that the RTB dye is not completely mineralized to CO_2 and H_2O . The TOC analysis indicates that there may be some intermediate products. The degraded by-products are

identified from the HPLC–MS analysis. However, the encouraging feature of this analysis is that the TOC reduction closely matches the decolorization percentage indicating that there may be very few intermediate compounds present after longer time periods of treatment.

7.2.3.2. HPLC–MS analysis

The HPLC peak at 3.2 min (**Figure 7.12a**) before and after the photocatalytic study shows that the intensity of the parent compound (RTB) peak has reduced after the experiment and the parent compound has broken down into intermediate compounds with low molecular weights.

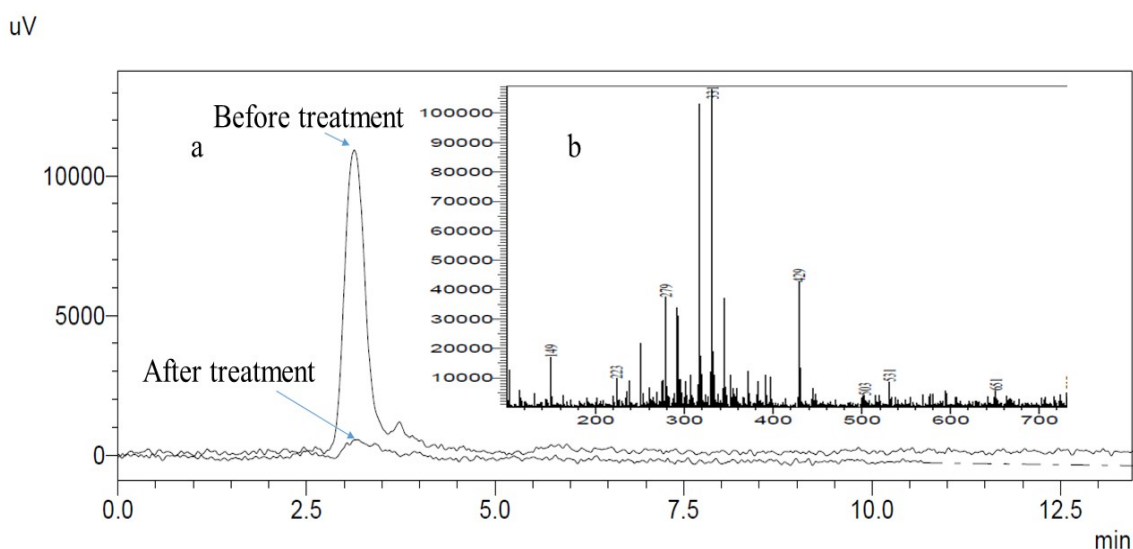


Figure 7.12. HPLC analysis of the solution before and after treatment (a) and MS spectra of degraded solution (b).

To find out the final degradation products, MS analysis (**Figure 7.12b**) is carried out, and the results indicate that the main final degraded compounds are having a molecular weight of 191, 223, 279, 290, 318, 331, 343, and 429. The formation of these products confirms the breakdown of the parent compound (molecular weight of 1250) into smaller molecular weight components and the hypothetical identified compounds are listed in **Figure 7.13**. The degradation of the dye might have taken place not only due to photocatalytic activity but also to self-sensitization. The prepared photocatalyst composite material absorbs photons on visible light irradiation and generates e^- and h^+

pairs. Contrarily, the bandgap energy of the RTB dye is narrow enough to absorb visible light and increases the possibility of self-sensitized photocatalytic degradation of the dye. In such cases, not only the photocatalysts generate e^- and h^+ pairs but also the dye produces e^- and h^+ in the conduction band (LUMO: lowest unoccupied molecular orbital) and valance band (HOMO: highest occupied molecular orbital) respectively.

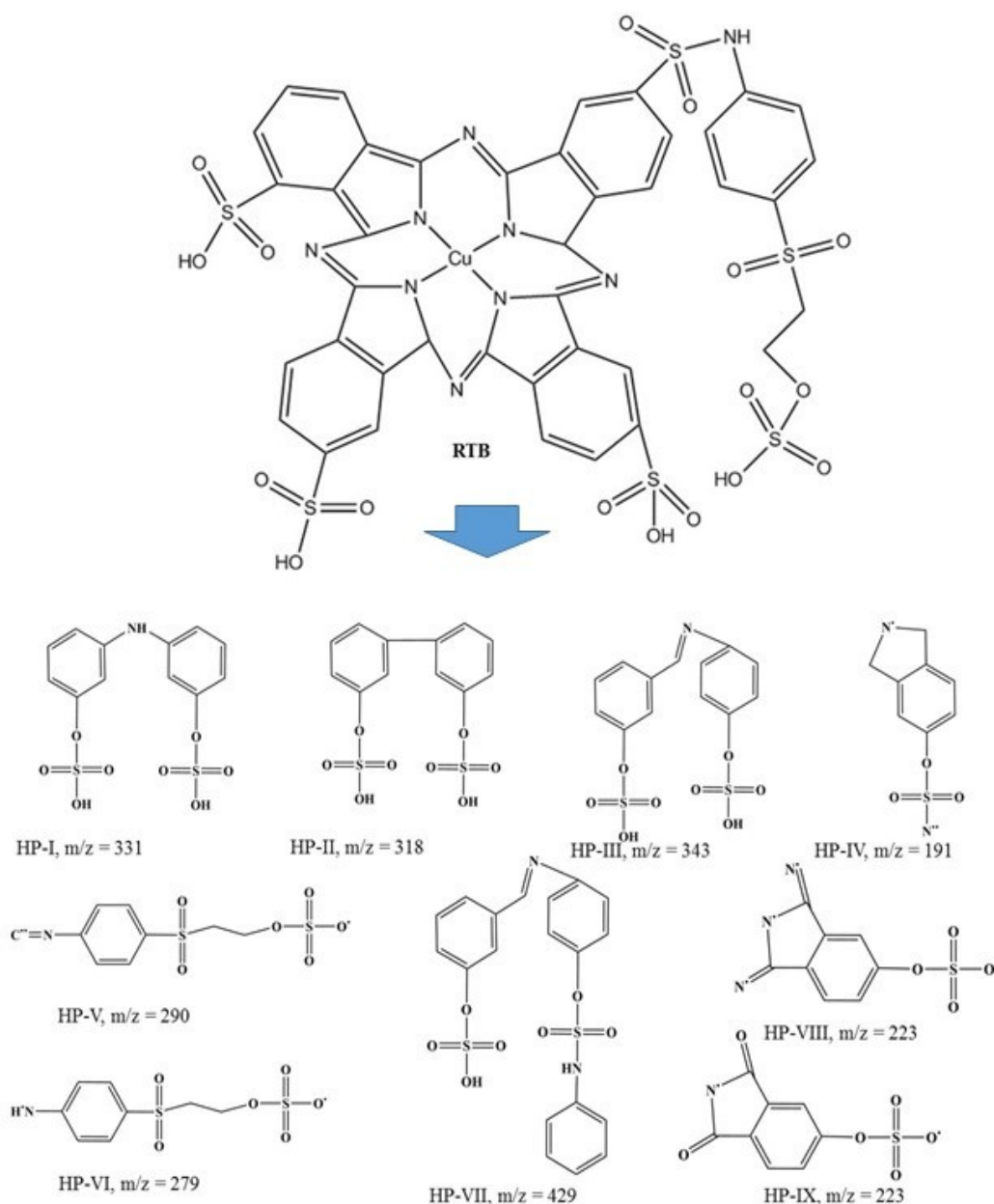


Figure 7.13. Degraded by-products from the parent dye (RTB) molecule, (HP– Hypothetical Product).

The generated electrons in the LUMO then transfer to the conduction band of the photocatalyst, which captures the absorbed molecular oxygen to form $\bullet\text{O}_2^-$. This highly oxidizing agent ($\bullet\text{O}_2^-$) reacts with the RTB to break down into simple molecules. The holes generated in the HOMO react with the OH^- to form $\bullet\text{OH}$ and also attack the dye molecules (**Figure 7.6**) (Molla et al. 2017).

7.3. Conclusions

The photocatalytic activity of the prepared catalyst was analysed in an airlift reactor under sunlight. The optimum parameters were also quantified and described systematically. The conclusions from this work are enlisted below:

- In this part of the work, a modified method was proposed to prepare the photocatalyst nanocomposite of $\text{TiO}_2/\text{rGO}/\text{g-C}_3\text{N}_4$ (2.41 eV bandgap) with high photocatalytic efficiency.
- The evenly distributed photocatalyst nanoparticles were immobilized in the stable polystyrene film by a solvent casting method and used in an airlift reactor under solar light. The characterizations of the nanoparticle was done using different sophisticated analytical tools.
- The results obtained in this work represents the influence of the various parameters ($\text{g-C}_3\text{N}_4$ quantity in catalyst composite, catalyst loading, initial concentration of dye, reuse of the film) on photocatalytic decolourization of RTB in MAPR.
- The possible enhancement of the decolourization efficiency by self-sensitization of the dye was also proposed.
- The maximum decolourization achieved for RTB dye (10 ppm, 1200 mL) was 60% in 90 min under optimized conditions. The degradation of RTB is confirmed by TOC (51.43%) and HPLC analysis under optimized conditions. Moreover, the final degraded hypothetical by-products are also identified by LC-MS analysis.
- The effect of waste polystyrene was also analyzed to make this process economical, and more eco-friendly from environmental point of view for catalyst immobilization.

CHAPTER 8

CONCLUSIONS AND SCOPE FOR FUTURE WORK

CHAPTER 8

CONCLUSIONS AND SCOPE FOR FUTURE WORK

8.1. Summary

In this work, the photocatalytic degradation of RTB dye using TiO₂ – PS film, (TiO₂, rGO, g-C₃N₄)-admixture PS film and TiO₂/rGO/g-C₃N₄ chemical composite – PS film were analysed in different reactor configurations (Batch, Batch scaleup, Recirculation, and a novel airlift reactor). The characterization of the photocatalysts as well as the photocatalytic films were analysed. Experiments were performed as per the methodologies outlined earlier to achieve the objectives of the present research work. A detailed discussion on the results with proper justification and literature support is also presented. A summary of the important results is tabulated below (**Table 8.1**):

Table 8.1. Performance of the photocatalytic films based on decolourization, degradation, reaction rate and reuse.

Photocatalytic performance (10 ppm)	Decolourization (%)	Degradation (%)	Reaction rate <i>k</i> (min⁻¹)	% decolourization after 4 times reuse
Polystyrene – TiO ₂ batch study (200 mL, UV light)	100	24	0.0214	70
Polystyrene – TiO ₂ , g-C ₃ N ₄ and rGO admixture (200 mL, UV light)	~100	40	0.0288	90
Polystyrene – TiO ₂ , g-C ₃ N ₄ and rGO admixture (1200 mL, UV light)	94	92	0.0124	70
Polystyrene – TiO ₂ /g-C ₃ N ₄ /rGO composite (1200 mL, Sunlight)	60	51	0.0101	50

8.2. Conclusions

The important conclusions which can be drawn from this study are listed below:

- I. Photocatalyst nanoparticles (rGO, g-C₃N₄, and TiO₂/rGO/g-C₃N₄ chemical composite) were synthesised by simple and economical methods. The characterization of the nanoparticles (TiO₂, rGO, g-C₃N₄, and TiO₂/rGO/g-C₃N₄-composite) confirms that all the particles are crystalline in nature and their surface morphology studies helped to identify the structure.
- II. An efficient and simple solvent casting method was employed to immobilize the photocatalysts in polystyrene. The characterization of the prepared photocatalytic films was done using different tools and it was confirmed that all the films were stable and the catalyst powder was evenly distributed in the film.
- III. The best performance observed based on decolourization was using polystyrene TiO₂ (200 mL) and admixture of (TiO₂, g-C₃N₄ and rGO) (200 mL) photocatalytic film, whereas based on reaction kinetics and degradation point of view, the best performance was noticed for the admixture of polystyrene – (TiO₂, g-C₃N₄ and rGO) photocatalytic film for 200 mL and 1200 mL reactor respectively. It can be easily concluded that the reactors and catalytic films used in this study are efficient.
- IV. All the photocatalysts used in this work were proven highly efficient for the degradation of RTB dye. The various parameters affecting the RTB degradation were evaluated to find out the optimum conditions in batch reactor, scaled-up batch reactor, recirculation reactor and multiphase airlift reactor. The decolourization efficiency obtained from various reactors using 10 ppm RTB solution were in between 70 – 100%, whereas the corresponding degradation or mineralization was in the range of 24 – 92%.
- V. The effect of waste polystyrene was also evaluated in this work, the efficiencies were almost same; which implies that the waste polystyrene can be a good choice from the environmental point of view.

8.3. Scope for future work

The work done in this area can further be improved or lead to other relevant areas of work. Specific recommendations in this regard are given below:

- Different combinations of photocatalyst admixture can be employed for the photocatalytic study.
- The biodegradable or eco-friendly or reusable substrate material can be a good choice in this regard.
- Multiple applications in single operation can also be a good choice for efficient and low-cost industrial operation. Eg: wastewater treatment as well as electricity generation or gas production.
- The simple composite material preparation method used here can be employed for other photocatalyst preparation especially when $g\text{-C}_3\text{N}_4$ is involved.
- The multiphase reactor used in this work can be a breakthrough for the industrial scale immobilised photocatalyst reactor.
- The same reactor can be tried for the degradation of different organic pollutants.

REFERENCES

Abdel-Maksoud, Y., Imam, E., and Ramadan, A. (2016). "TiO₂ Solar Photocatalytic Reactor Systems: Selection of Reactor Design for Scale-up and Commercialization—Analytical Review." *Catalysts*, 6(9), 138.

Abdel-Maksoud, Y. K., Imam, E., and Ramadan, A. R. (2018). "Sand supported TiO₂ photocatalyst in a tray photo-reactor for the removal of emerging contaminants in wastewater." *Catal. Today*, 313(August), 55–62.

Abdennouri, M., Baâlala, M., Galadi, A., Makhfouk, M. El, Bensitel, M., Nohair, K., Sadiq, M., Boussaoud, A., and Barka, N. (2016). "Photocatalytic degradation of pesticides by titanium dioxide and titanium pillared purified clays." *Arab. J. Chem.*, 9, S313–S318.

Abdennouri, M., Elhalil, A., Farnane, M., Tounsadi, H., Mahjoubi, F. Z., Elmoubarki, R., Sadiq, M., Khamar, L., Galadi, A., Baâlala, M., Bensitel, M., Hafiane, Y. El, Smith, A., and Barka, N. (2015). "Photocatalytic degradation of 2,4-D and 2,4-DP herbicides on Pt/TiO₂ nanoparticles." *J. Saudi Chem. Soc.*, 19(5), 485–493.

Abid, M. F. (2015). "Desulfurization of Gas Oil Using a Solar Photocatalytic Microreactor." *Energy Procedia*, 74, 663–678.

Addepalli, S. (2019). "Industrial applications of X-Ray Photoelectron Spectroscopy (XPS) in India." *J. Electron Spectros. Relat. Phenomena*, 231(May), 11–42.

Affam, A. C., and Chaudhuri, M. (2013). "Degradation of pesticides chlorpyrifos, cypermethrin and chlorothalonil in aqueous solution by TiO₂ photocatalysis." *J. Environ. Manage.*, 130, 160–165.

Ahmad, M., Ahmed, E., Zafar, F., Khalid, N. R., Niaz, N. A., Hafeez, A., Ikram, M., and Khan, M. A. (2015). "Enhanced photocatalytic activity of Ce-doped ZnO nanopowders synthesized by combustion method." *J. Rare Earths*, 33(3), 255–262.

Ahmadi, Z., Afshar, S., Vafaei, L., and Salehi, A. (2008). "Photocatalytic degradation of E . coli bacteria using TiO₂/SiO₂ nanoparticles with photodeposited platinum." *Int. J. Nanosci. Nanotechnol.*, 4(1), 39–48.

Akbari Shorgoli, A., and Shokri, M. (2017). "Photocatalytic degradation of imidacloprid pesticide in aqueous solution by TiO₂ nanoparticles immobilized on the glass plate." *Chem. Eng. Commun.*, 204(9), 1061–1069.

Akhavan, H., Mohebbi, P., Firouzi, A., and Noroozi, M. (2016). "X-ray Diffraction Analysis of ProRoot Mineral Trioxide." *Iran. Endod. J.*, 11(2), 111–113.

AL-Mashhadani, M. K. H., Wilkinson, S. J., and Zimmerman, W. B. (2015). "Airlift bioreactor for biological applications with microbubble mediated transport processes." *Chem. Eng. Sci.*, 137, 243–253.

Alam, S. N., Sharma, N., and Kumar, L. (2017). "Synthesis of Graphene Oxide (GO) by Modified Hummers Method and Its Thermal Reduction to Obtain Reduced Graphene Oxide (rGO)*." *Graphene*, 6, 1–18.

Aleksandrak, M., Kukulka, W., and Mijowska, E. (2017). "Graphitic carbon nitride/graphene oxide/reduced graphene oxide nanocomposites for photoluminescence and photocatalysis." *Appl. Surf. Sci.*, 398, 56–62.

Ali, S. A., Mmuo, C. C., Abdulraheem, R. O., Abdulkareem, S. S., Alemika, E. T., Sani, M. A., and Ilyas, M. (2011). "High performance liquid chromatography (HPLC) method development and validation indicating assay for ciprofloxacin hydrochloride." *J. Appl. Pharm. Sci.*, 1(8), 239–243.

Amano, F., Ishinaga, E., and Yamakata, A. (2013). "Effect of particle size on the photocatalytic activity of WO₃ particles for water oxidation." *J. Phys. Chem. C*, 117(44), 22584–22590.

Ang, L. F., Yam, M. F., Fung, Y. T. T., Kiang, P. K., and Darwin, Y. (2014). “HPLC Method for Simultaneous Quantitative Detection of Quercetin and Curcuminoids in Traditional Chinese Medicines.” *J. Pharmacopuncture*, 17(4), 36–49.

Angel, J., and Loftus, A. (2019). “With-against-and-beyond the human right to water.” *Geoforum*, 98(May 2017), 206–213.

Aoudjit, L., Martins, P. M., Madjene, F., Petrovykh, D. Y., and Lanceros-Mendez, S. (2018). “Photocatalytic reusable membranes for the effective degradation of tartrazine with a solar photoreactor.” *J. Hazard. Mater.*, 344, 408–416.

Ardrey, R. E. (2003). *Encyclopedia of Materials: Science and Technology (Second Edition)*, 4508-4511. ISBN: 0-08-0431526.

Ashok kumar, R., and Ramaswamy, M. (2014). “Phytochemical screening by FTIR spectroscopic analysis of leaf extracts of selected Indian Medicinal plants.” *Int. J. Curr. Microbiol. App. Sci*, 3(1), 395–406.

Ba, O. M., Marmey, P., Anselme, K., Duncan, A. C., and Ponche, A. (2016). “Surface composition XPS analysis of a plasma treated polystyrene: Evolution over long storage periods.” *Colloids Surfaces B Biointerfaces*, 145, 1–7.

Bai, H., Liu, Z., and Sun, D. D. (2012). “Solar-light-driven photodegradation and antibacterial activity of hierarchical TiO₂/ZnO/CuO material.” *Chempluschem*, 77(10), 941–948.

Balaji, V., Vinayagamoorthi, D., Palanisamy, A., and Anbalagan, S. (2012). “Degradation of Reactive Red HE7B and Yellow FN2R dyes by fungal isolates.” *J. Acad. Ind. Res.*, 1(3), 132–136.

Bali, U., and Karagözoğlu, B. (2006). "Performance comparison of Fenton process, ferric coagulation and H₂O₂/pyridine/Cu(II) system for decolorization of Remazol Turquoise Blue G-133." *Dye. Pigment.*, 74(1), 73–80.

Bali, U., and Karagözoğlu, B. (2007). "Decolorization of Remazol-Turquoise Blue G-133 and other dyes by Cu(II)/pyridine/H₂O₂ system." *Dye. Pigment.*, 73(2), 133–140.

Barakat, M. A. (2011). "New trends in removing heavy metals from industrial wastewater." *Arab. J. Chem.*, 4(4), 361–377.

Barros, A. L. De, Domingos, A. A. Q., Fachine, P. B. A., Keukeleire, D. De, and Nascimento, R. F. Do. (2014). "PET as a support material for TiO₂ in advanced oxidation processes." *J. Appl. Polym. Sci.*, 131(9), 1–9.

Barth, G. H., Sun, S.-T., and Nicol, M. R. (1987). "Particle-size analysis." *Proc. Soc. Anal. Chem.*, 59, 142R-162R.

Bhatkhande, D. S., Pangarkar, V. G., and Beenackers, A. A. C. M. (2002). "Photocatalytic degradation for environmental applications - A review." *J. Chem. Technol. Biotechnol.*, 77(1), 102–116.

Bhattacharjee, S., Chakraborty, S., Mandol, K., Liu, L., and Bhattacharjee, C. (2015). "Optimization of process parameters during photocatalytic degradation of phenol in UV annular reactor." *Desalin. Water Treat.*, 54 (February 2016), 2270–2279.

Bian, X., Chen, J., and Ji, R. (2013). "Degradation of 2,4-dichlorophenoxyacetic acid (2,4-D) by novel photocatalytic material of tourmaline-coated TiO₂ nanoparticles: Kinetic study and model." *Materials (Basel)*, 6(4), 1530–1542.

Bickley, R. I. Æ., Slater, M. J., and Wang, W. (2005). "Engineering development of a photocatalytic reactor for waste water treatment." *Process Saf. Environ. Prot.*, 83(B3 May), 205–216.

Bickley, R. I., and Munuera, G. (1973). "Photoadsorption and Photocatalysis at Rutile Surfaces." *J. Catal.*, 31, 398–407.

Boštjan, E., Hudoklin, P., Perc, K., Tiš, T., Sollner, M., and Pintar, A. (2016). "Glass fiber-supported TiO₂ photocatalyst: Efficient mineralization and removal of toxicity / estrogenicity of bisphenol A and its analogs." *Appl. Catal. B Environ.*, 183, 149–158.

Bolis, V., Busco, C., Ciarletta, M., Distasi, C., Erriquez, J., Fenoglio, I., Livraghi, S., and Morel, S. (2012). "Hydrophilic/hydrophobic features of TiO₂ nanoparticles as a function of crystal phase, surface area and coating, in relation to their potential toxicity in peripheral nervous system." *J. Colloid Interface Sci.*, 369(1), 28–39.

Boonen, E., and Beeldens, A. (2014). "Recent Photocatalytic Applications for Air Purification in Belgium." *Coatings*, 4(2005), 553–573.

Bott, R. (2011). "Principles of TiO₂ Photocatalysis." *Applications of Titanium Dioxide Photocatalysis to Construction Materials*, 1–5. ISBN: 978-94-007-1296-6.

Bourai, M. El, and Din, W. S. El. (2016). "Biodegradation of Reactive Black 5 by *Aeromonas hydrophila* strain isolated from dye-contaminated textile wastewater." *Sustain. Environ. Res.*, 26(5), 209–216.

Brooms, T. J., Onyango, M. S., and Ochieng, A. (2014). "Photocatalytic Activity of Polyaniline/TiO₂/ZnO Composite for Degradation of Aromatic Compounds in Abattoir Wastewater." *Integr. Waste Manag. Environ. Eng.*, 1(April 15-16), 124–130.

Bullman, V. (2003). "Automated three-dimensional analysis of particle measurements using an optical profilometer and image analysis software." *J. Microsc.*, 211(1), 95–100.

Byrne, H. E., and Mazyck, D. W. (2009). "Removal of trace level aqueous mercury by adsorption and photocatalysis on silica-titania composites." *J. Hazard. Mater.*, 170(2–3), 915–919.

Calvete, T., Lima, E. C., Cardoso, N. F., Vaggetti, J. C. P., Dias, S. L. P., and Pavan, F. A. (2010). "Application of carbon adsorbents prepared from Brazilian-pine fruit shell for the removal of reactive orange 16 from aqueous solution: Kinetic, equilibrium, and thermodynamic studies." *J. Environ. Manage.*, 91(8), 1695–1706.

Cámara, R. M., Portela, R., Gutiérrez-Martín, F., and Sánchez, B. (2014). "Evaluation of several commercial polymers as support for TiO₂ in photocatalytic applications." *Glob. NEST J.*, 16(3), 525–535.

Carbonaro, S., Sugihara, M. N., and Strathmann, T. J. (2013). "Continuous-flow photocatalytic treatment of pharmaceutical micropollutants: Activity, inhibition, and deactivation of TiO₂ photocatalysts in wastewater effluent." *Appl. Catal. B Environ.*, 129, 1–12.

Chan, A. H. C., Chan, C. K., Barford, J. P., and Porter, J. F. (2003). "Solar photocatalytic thin film cascade reactor for treatment of benzoic acid containing wastewater." *Water Res.*, 37(5), 1125–1135.

Chan, S. H. S., Wu, T. Y., Juan, J. C., and Teh, C. Y. (2011a). "Recent developments of metal oxide semiconductors as photocatalysts in advanced oxidation processes (AOPs) for treatment of dye waste-water." *J. Chem. Technol. Biotechnol.*, 86(9), 1130–1158.

Chan, S. H. S., Wu, T. Y., Juan, J. C., and Teh, C. Y. (2011b). "Recent developments of metal oxide semiconductors as photocatalysts in advanced oxidation processes (AOPs) for treatment of dye waste-water." *J. Chem. Technol. Biotechnol.*, 86(9), 1130–1158.

Chellappa, M., Anjaneyulu, U., Manivasagam, G., and Vijayalakshmi, U. (2015). "Preparation and evaluation of the cytotoxic nature of TiO₂ nanoparticles by direct contact method." *Int. J. Nanomedicine*, 10, 31–41.

Chen, A., Lu, G., Tao, Y., Dai, Z., and Gu, H. (2001). "Novel photocatalyst immobilised on springs and packed photoreactor." *Mater. Phys. Mech.*, 4, 121–124.

Chen, D., Sivakumar, M., and Ray, A. K. (2000). "Heterogeneous Photocatalysis in Environmental Remediation." *Dev. Chem. Eng. Miner. Process.*, 8(5/6), 505–550.

Chen, F., Zou, W., Qu, W., and Zhang, J. (2009a). "Photocatalytic performance of a visible light TiO₂ photocatalyst prepared by a surface chemical modification process." *Catal. Commun.*, 10(11), 1510–1513.

Chen, G., Wang, X., Wang, R., and Liu, G. (2019a). "Ecotoxicology and Environmental Safety Health risk assessment of potentially harmful elements in subsidence water bodies using a Monte Carlo approach : An example from the Huainan coal mining area, China." *Ecotoxicol. Environ. Saf.*, 171(April 2018), 737–745.

Chen, W., Shen, Y., Ling, Y., Peng, Y., Ge, M., and Pan, Z. (2019b). "Synthesis of Positively Charged Polystyrene Microspheres for the Removal of Congo Red, Phosphate, and Chromium(VI)." *ACS Omega*, research-article, 4(4), 6669–6676.

Chen, Y., Fang, J., Lu, S., Xu, W., Liu, Z., Xu, X., and Fang, Z. (2014). "One-step hydrothermal synthesis of BiOI/Bi₂WO₆ hierarchical heterostructure with highly photocatalytic activity." *J. Chem. Technol. Biotechnol.*, (90), 947–954.

Chen, Y. L., Kuo, L., Tseng, M. L., Chen, H. M., Chen, C., Huang, H. J., Liu, R., and Tsai, D. P. (2013). "ZnO nanorod optical disk photocatalytic reactor for photodegradation of methyl orange." *Opt. Express*, 21(6), 7240–7249.

Chen, Y., Wan, H., Han, M., and Guan, G. (2009b). "Photocatalytic degradation of organic pollutants in purified terephthalic acid wastewater with activated carbon supported titanium dioxide." *Int. Conf. Energy Environ. Technol. (ICEET 2009)*, 2, 658–661.

Cheng, N., Tian, J., Liu, Q., Ge, C., Qusti, A. H., Asiri, A. M., Al-youbi, A. O., and Sun, X. (2013). "Au-Nanoparticle-Loaded Graphitic Carbon Nitride Nanosheets: Green Photocatalytic Synthesis and Application toward the Degradation of Organic Pollutants." *Appl. Mater. interfaces*, 4–8.

Cheriyian, A. J., Sarkar, J. P., Sheik, F., and Baawain, M. S. (2013). "Photocatalytic Degradation of Organics in Municipal Treated Wastewater in a Re-Circulation Reactor." *J. Environ. Prot. (Irvine, Calif.)*, 4(December), 1449–1452.

Childs, L. P., and Ollis, D. F. (1980). "Is Photocatalysis Catalytic?" *J. Catal.*, 390(66), 383–390.

Choma, J., and Jaroniec, M. (2001). "Determination of the specific surface areas of non-porous and macroporous carbons." *Adsorpt. Sci. Technol.*, 19(9), 765–776.

Christensen, P. A., Egerton, T. A., Kosa, S. A. M., Tinlin, J. R., and Scott, K. (2005). "The photoelectrocatalytic oxidation of aqueous nitrophenol using a novel reactor." *J. Appl. Electrochem.*, 35(7–8), 683–692.

Conneely, A., Smyth, W. F., and McMullan, G. (2002). "Study of the white-rot fungal degradation of selected phthalocyanine dyes by capillary electrophoresis and liquid chromatography." *Anal. Chim. Acta*, 451(2), 259–270.

Cuesta, E., Álvarez, B. J., García-Diéguez, M., González-Madruga, D., and Rodríguez-Cortés, J. A. (2013). "Conformity analysis in the measurement of machined metal surfaces with optoelectronic profilometer." *Procedia Eng.*, 63, 463–471.

Das, S., and Mahalingam, H. (2019). "Reusable floating polymer nanocomposite photocatalyst for the efficient treatment of dye wastewaters under scaled-up conditions in batch and recirculation modes." *J. Chem. Technol. Biotechnol.*, 94(8), 2597–2608.

Davezza, M., Fabbri, D., Pramauro, E., and Bianco Prevot, A. (2012). "Photocatalytic degradation of bentazone in soil washing wastes containing alkylpolyoxyethylene surfactants." *Chemosphere*, 86(4), 335–340.

Deng, Y., and Zhao, R. (2015). "Advanced Oxidation Processes (AOPs) in Wastewater Treatment." *Curr Pollut. Rep*, 1, 167–176.

- Devipriya, S., and Yesodharan, S. (2005). "Photocatalytic degradation of pesticide contaminants in water." *Sol. Energy Mater. Sol. Cells*, 86(3), 309–348.
- Dhar, N. R. (1937). "Allgemeine Photochemie." *Nature*, 140(3541), 444.
- Dhiman, P., Bato, K. M., Kotnala, R. K., and Singh, M. (2012). "Fe-doped ZnO nanoparticles synthesised by solution combustion method." *Micro Nano Lett.*, 7(12), 1333–1335.
- Dhir, A., Prakash, N. T., and Sud, D. (2011). "Studies on coupled biological and photochemical treatment of soda pulp bleaching effluents from agro residue based pulp and paper mill." *J. Chem. Technol. Biotechnol.*, 86(12), 1508–1513.
- Dillip, G. R., Sreekanth, T. V. M., and Joo, S. W. (2017). "Tailoring the bandgap of N-rich graphitic carbon nitride for enhanced photocatalytic activity." *Ceram. Int.*, 43(8), 6437–6445.
- Ding, H., Sun, H., and Shan, Y. (2005). "Preparation and characterization of mesoporous SBA-15 supported dye-sensitized TiO₂ photocatalyst." *J. Photochem. Photobiol. A Chem.*, 169(1), 101–107.
- Dioos, B. M. L., Vankelecom, I. F. J., and Jacobs, P. A. (2006). "Aspects of immobilisation of catalysts on polymeric supports." *Adv. Synth. Catal.*, 348(12–13), 1413–1446.
- Długosz, M., Waś, J., Szczubiałka, K., and Nowakowska, M. (2014). "TiO₂-coated EP as a floating photocatalyst for water purification." *J. Mater. Chem. A*, 2(19), 6931–6938.
- Dong, G., Zhang, Y., Pan, Q., and Qiu, J. (2014). "A fantastic graphitic carbon nitride (g-C₃N₄) material: Electronic structure, photocatalytic and photoelectronic properties." *J. Photochem. Photobiol. C Photochem. Rev.*, 20(1), 33–50.

Dong, S. Z., Chen, C. Z., Li, D. M., and Sun, Y. S. (1993). "A study of hygienic standard for titanium in the source of drinking water." *Chinese J. Prev. Med.*, 27(1), 26–28.

Dou, B., and Chen, H. (2011). "Removal of toxic mercury (II) from aquatic solutions by synthesized TiO₂ nanoparticles." *Desalination*, 269(1–3), 260–265.

Dudukovic, M. P., Larachi, F., and Mills, P. L. (1999). "Multiphase reactors – revisited." *Chem. Eng. Sci.*, 54(13–14), 1975–1995.

Du, F., Cao, N., Zhang, Y., Fu, P., Wu, Y., and Lin, Z. (2018). "PEDOT : PSS / graphene quantum dots films with enhanced thermoelectric properties via strong interfacial interaction and phase separation." *Sci. Rep.*, 8(April), 1–12.

Erdem, B., Hunsicker, R. A., Simmons, G. W., Sudol, E. D., Dimonie, V. L., and El-Aasser, M. S. (2001). "XPS and FTIR Surface Characterization of TiO₂ Particles Used in Polymer Encapsulation." *Langmuir*, 17(9), 2664–2669.

Fan, M., Li, T., Hu, J., Cao, R., Wei, X., Shi, X., and Ruan, W. (2007). "Artificial Neural Network Modeling and Genetic Algorithm Optimization for Cadmium Removal from Aqueous Solutions by Reduced Graphene." *Materials (Basel)*, 10(544), 1–22.

Fan, W., Lai, Q., Zhang, Q., and Wang, Y. (2011). "Nanocomposites of TiO₂ and reduced graphene oxide as efficient photocatalysts for hydrogen evolution." *J. Phys. Chem. C*, 115(21), 10694–10701.

Farrell, J. B. (2006). "Solar detoxification of fuel-contaminated groundwater using fixed-bed photocatalysts." *Water Environ. Res.*, 69(2), 254–254.

Fatehizadeh, A., Rahimi, S., Ahmadian, M., Barati, R., Yousefi, N., Moussavi, S., Rahimi, K., Reshadat, S., Ghasemi, S., and Gilan, N. (2014). "Photocatalytic removal of cadmium (II) and lead (II) from simulated wastewater at continuous and batch system." *Int. J. Environ. Health Eng.*, 3(1), 31.

Foss, N. J. (2002). "Methods for the determination of total organic carbon (TOC) in soils and sediments." *J. Manage.*, 52(1), 1–5.

Frank, S. N., and Bard, A. J. (1977). "Heterogeneous Photocatalytic Oxidation of Cyanide and Sulfite in Aqueous Solutions at Semiconductor Powders." *J. Phys. Chem.*, 81(15), 1484–1488.

Frontistis, Z., Daskalaki, V. M., Mantzavinos, D., Rizzo, L., and Fulgione, I. (2012). "Solar light-induced photoelectrocatalytic degradation of bisphenol-A on TiO₂/ITO film anode and BDD cathode." *Catal. Today*, 209, 74–78.

Fu, J., Ji, M., and An, D. (2005). "Fulvic acid degradation using nanoparticle TiO₂ in a submerged membrane photocatalysis reactor." *J. Environ. Sci.*, 17(6), 942–945.

Fujishima, A., and Honda, K. (1972). "Electrochemical Photolysis of Water at a Semiconductor Electrode." *Nature*, 238(5358), 37–38.

Fujishima, A., Rao, T. N., and Tryk, D. A. (2000). "Titanium dioxide photocatalysis." *J. Photochem. Photobiol. C Photochem. Rev.*, 1(1), 1–21.

Gallo, J. C., Mariano, B. M., Lucanas, A. D., Ko, M. B., Borja, J. Q., Hinode, H., and Gallardo, S. M. (2015). "Photocatalytic degradation of turquoise blue dye using immobilized AC/TiO₂: optimization of process parameters and pilot." *J. Eng. Sci. Technol.*, 1(6 1/2015), 64–73.

Gardy, J., Hassanpour, A., Lai, X., Ahmed, M. H., and Rehan, M. (2017). "Biodiesel production from used cooking oil using a novel surface functionalised TiO₂ nano-catalyst." *Appl. Catal. B Environ.*, 207, 297–310.

Ghaly, A., Ananthashankar, R., Alhattab, M., and Ramakrishnan, V. (2013). "Production, Characterization and Treatment of Textile Effluents: A Critical Review." *J. Chem. Eng. Process Technol.*, 5(1), 1–19.

- Ghaly, A., Ananthashankar, R., Alhattab, M., and Ramakrishnan, V. (2014). "Production , Characterization and Treatment of Textile Effluents : A Critical Review." *J. Chem. Eng. Process Technol.*, 5(1), 1–18.
- Giahi, M., Ghanbari, F., and Issazadeh, K. (2013). "Photocatalytic degradation of nonionic surfactant using zinc oxide nanoparticles." *Asian J. Chem.*, 25(9), 5047–5050.
- Gilmour, C. R., Ray, A., Zhu, J., and Ray, M. B. (2013). "Photocatalytic Performance of Titanium Dioxide Thin Films from Polymer-Encapsulated Titania." *Ind. Eng. Chem. Res.*, 52, 17800–17811.
- Girardeaux, C., and Pireaux, J.-J. (1996). "Analysis of Polystyrene (PS) by XPS." *Surf. Sci. Spectra*, 4(2), 130–133.
- Giwa, A., Nkeonye, P. O., Bello, K. A., and Kolawole, K. A. (2012). "Photocatalytic Decolourization and Degradation of C . I . Basic Blue 41 Using TiO₂ Nanoparticles." *Sci. Res.*, 2012(September), 1063–1069.
- Gogate, P. R., and Pandit, A. B. (2004). "A review of imperative technologies for wastewater treatment I : oxidation technologies at ambient conditions." *Adv. Environ. Res.*, 8(3), 501–551.
- Gombac, V., Rogatis, L. De, Gasparotto, A., Vicario, G., Montini, T., and Barreca, D. (2007). "TiO₂ nanopowders doped with boron and nitrogen for photocatalytic applications." *Chem. Phys.*, 339, 111–123.
- Gómez, C. M., Angel, G. Del, Ramos-Ramírez, E., Rangel-Vázquez, I., González, F., Arrieta, A., Vázquez-Zavala, A., Bonilla-Sánchez, A., and Sánchez Cantú, M. (2016). "Alumina coating with TiO₂ and its effect on catalytic photodegradation of phenol and *p*-cresol." *J. Chem. Technol. Biotechnol.*, 91(8), 2211–2220.

- Goode, K. R., Asteriadou, K., Robbins, P. T., and Fryer, P. J. (2013). “Fouling and cleaning studies in the food and beverage industry classified by cleaning type.” *Compr. Rev. Food Sci. Food Saf.*, 12(2), 121–143.
- Govindan, K., Chandran, H. T., Raja, M., Maheswari, S. U., and Rangarajan, M. (2017). “Electron scavenger-assisted photocatalytic degradation of amido black 10B dye with Mn₃O₄ nanotubes: A response surface methodology study with central composite design.” *J. Photochem. Photobiol. A Chem.*, 341, 146–156.
- Grieken, R. van, Marugán, J., Sordo, C., Martínez, P., and Pablos, C. (2009). “Photocatalytic inactivation of bacteria in water using suspended and immobilized silver-TiO₂.” *Appl. Catal. B Environ.*, 93(1), 112–118.
- Guimarães, B. D. S., Bernardes, A. A., Salcedo, G. M., Caldas, S. S., Jorge, M. B., Bianchini, A., Wolke, S. I., and Primel, E. G. (2016). “Photocatalytic degradation for treating multipesticide residues using [Ru(bipy)₃]Cl₂-doped TiO₂/SiO₂ based on surface response methodology.” *J. Braz. Chem. Soc.*, 27(12), 2256–2263.
- Haarstrick, A., Kut, O. M., and Heinzle, E. (1996). “TiO₂ Assisted Degradation of Environmentally Relevant Organic Compounds in Wastewater Using a Novel Fluidized Bed Photoreactor.” *Environ. Sci. Technol.*, 30(3), 817–824.
- Hafeez, H. Y., Lakhera, S. K., Bellamkonda, S., Rao, G. R., Shankar, M. V., Bahnemann, D. W., and Neppolian, B. (2018). “Construction of ternary hybrid layered reduced graphene oxide supported g-C₃N₄-TiO₂ nanocomposite and its photocatalytic hydrogen production activity.” *Int. J. Hydrogen Energy*, 43(8), 3892–3904.
- Hameed, B. S., Bhatt, C. S., Nagaraj, B., and Suresh, A. K. (2018). “Chromatography as an Efficient Technique for the Separation of Diversified Nanoparticles.” *Nanomater. Chromatogr.*, Elsevier Inc.

Han, F., Kambala, V. S. R., Srinivasan, M., Rajarathnam, D., and Naidu, R. (2009). "Tailored titanium dioxide photocatalysts for the degradation of organic dyes in wastewater treatment: A review." *Appl. Catal. A Gen.*, 359(1–2), 25–40.

Han, H., and Bai, R. (2009). "Buoyant photocatalyst with greatly enhanced visible-light activity prepared through a low temperature hydrothermal method." *Ind. Eng. Chem. Res.*, 48(6), 2891–2898.

Hashimoto, K., Irie, H., and Fujishima, A. (2006). "TiO₂ Photocatalysis : A Historical Overview and Future Prospects." *Jpn. J. Appl. Phys.*, 44(12), 8269–8285.

He, Y., Sutton, N. B., Rijnaarts, H. H. H., and Langenhoff, A. A. M. (2016). "Degradation of pharmaceuticals in wastewater using immobilized TiO₂ photocatalysis under simulated solar irradiation." *Appl. Catal. B Environ.*, 182, 132–141.

Hennig, H., and Billing, R. (1993). "Advantages and disadvantages of photocatalysis induced by light-sensitive coordination compounds." *Coord. Chem. Rev.*, 125(1–2), 89–100.

Herrmann, J. M., and Guillard, C. (2000). "Photocatalytic degradation of pesticides in agricultural used waters." *Comptes Rendus l'Academie des Sci.-Ser. IIC Chem.*, 3(6), 417–422.

Hisaindee, S., Meetani, M. A., and Rauf, M. A. (2013). "Application of LC-MS to the analysis of advanced oxidation process (AOP) degradation of dye products and reaction mechanisms." *TrAC - Trends Anal. Chem.*, 49(December 2017), 31–44.

Hong, C., Zainon, Z., Sabrina, N., Mutamim, A., and Kim, C. (2016). "Green technology in wastewater treatment technologies : Integration of membrane bioreactor with various wastewater treatment systems." *Chem. Eng. J.*, 283, 582–594.

- Hsiao, C. Y., Lee, C. L., and Ollis, D. F. (1983). "Heterogeneous photocatalysis: Degradation of dilute solutions of dichloromethane (CH_2Cl_2), chloroform (CHCl_3), and carbon tetrachloride (CCl_4) with illuminated TiO_2 photocatalyst." *J. Catal.*, 82(2), 418–423.
- Hu, C., Guo, J., Qu, J., and Hu, X. (2007). "Photocatalytic Degradation of Pathogenic Bacteria with AgI/TiO_2 under Visible Light Irradiation." *Langmuir*, 23(9), 4982–4987.
- Hu, M., Fang, M., Tang, C., Yang, T., Huang, Z., Liu, Y., Wu, X., and Min, X. (2013). "The effects of atmosphere and calcined temperature on photocatalytic activity of TiO_2 nanofibers prepared by electrospinning." *Nanoscale Res. Lett.*, 8(1), 548.
- Huang, C. P., and Huang, Y. H. (2009). "Application of an active immobilized iron oxide with catalytic H_2O_2 for the mineralization of phenol in a batch photo-fluidized bed reactor." *Appl. Catal. A Gen.*, 357(2), 135–141.
- Huang, F., Yan, A., and Zhao, H. (2018). "Influences of Doping on Photocatalytic Properties of TiO_2 Photocatalyst." *Intech Open*, 31–80.
- Huang, M., Yu, J., Hu, Q., Su, W., Fan, M., Li, B., and Dong, L. (2016). "Preparation and enhanced photocatalytic activity of carbon nitride/titania (001 vs 101 facets)/reduced graphene oxide ($\text{g-C}_3\text{N}_4/\text{TiO}_2/\text{rGO}$) hybrids under visible light." *Appl. Surf. Sci.*, 389, 1084–1093.
- Hurtado, L., Solís-Casados, D., Escobar-Alarcón, L., Romero, R., and Natividad, R. (2016). "Multiphase photo-capillary reactors coated with TiO_2 films: preparation, characterization and photocatalytic performance." *Chem. Eng. J.*, 304, 39-47.
- Iatsunskyi, I., Kempniński, M., Nowaczyk, G., Jancelewicz, M., Pavlenko, M., Załeski, K., and Jurga, S. (2015). "Structural and XPS studies of PSi/TiO_2 nanocomposites prepared by ALD and Ag-assisted chemical etching." *Appl. Surf. Sci.*, 347, 777–783.

Idris, A., Hassan, N., Rashid, R., and Ngomsik, A. F. (2011). “Kinetic and regeneration studies of photocatalytic magnetic separable beads for chromium (VI) reduction under sunlight.” *J. Hazard. Mater.*, 186(1), 629–635.

Islam, M. A., Uddin, M. R., Amin, M. S. A., Haque, M. I., and Molla, M. S. R. (2013). “Design and Operation of a Photocatalytic Reactor: A Study of Dye (Methylene Blue) Removal Process.” *J. Chem. Eng.*, 28(1), 41–44.

Jackson, N., and Wang, C. (1991). “Attachment of TiO₂ Powders to Hollow Glass Microbeads: Activity of the TiO₂-Coated Beads in the Photoassisted Oxidation of Ethanol to Acetaldehyde.” *J. Electrochem. Soc.*, 138(12), 3660–3664.

Jaiswal, R., Patel, N., Dashora, A., Fernandes, R., Yadav, M., Edla, R., Varma, R. S., Kothari, D. C., Ahuja, B. L., and Miotello, A. (2016). “Efficient Co-B-codoped TiO₂ photocatalyst for degradation of organic water pollutant under visible light.” *Appl. Catal. B Environ.*, 183, 242–253.

Jaleh, B., Madad, M. S., Tabrizi, M. F., Habibi, S., Golbedaghi, R., and Keymanesh, M. R. (2011). “UV-Degradation Effect on Optical and Surface Properties of Polystyrene-TiO₂ Nanocomposite Film.” *J. Iran. Chem. Soc.*, 8(February), 161–168.

Jang, I., Sung, J., Choi, H., and Chin, I. (2005). “Synthesis and characterization of TiO₂/polystyrene hybrid nanoparticles via admicellar polymerization.” *J. Mater. Sci.*, 40, 3021–3024.

Jarandehi, A., Golpayegani, M. K., and Visscher, A. De. (2008). “Kinetic modeling of photocatalytic degradation reactions: Effect of charge trapping.” *Appl. Catal. B Environ.*, 84(1–2), 65–74.

Jitta, R. R., Gundeboina, R., Veldurthi, N. K., Guje, R., and Muga, V. (2015). “Defect pyrochlore oxides: as photocatalyst materials for environmental and energy applications - a review.” *J. Chem. Technol. Biotechnol.*, 90(May), 1937–1948.

Kalikeri, S., Kamath, N., Gadgil, D. J., and Shetty Kodialbail, V. (2017). "Visible light-induced photocatalytic degradation of Reactive Blue-19 over highly efficient polyaniline-TiO₂ nanocomposite: a comparative study with solar and UV photocatalysis." *Environ. Sci. Pollut. Res. Int.*, 25, 3731–3744.

Kalsoom, U., Ashraf, S. S., Meetani, M. A., Rauf, M. A., and Bhatti, H. N. (2012). "Degradation and kinetics of H₂O₂ assisted photochemical oxidation of Remazol Turquoise Blue." *Chem. Eng. J.*, 200–202, 373–379.

Kamble, S. P., Sawant, S. B., and Pangarkar, V. G. (2004). "Novel solar-based photocatalytic reactor for degradation of refractory pollutants." *AIChE J.*, 50(7), 1647–1650.

Kamrannejad, M. M., Hasanzadeh, A., Nosoudi, N., Mai, L., and Babaluo, A. A. (2014). "Photocatalytic degradation of polypropylene/TiO₂ nano-composites." *Mater. Res.*, 17(4), 1039–1046.

Kanmani, S., Than, K., and Beck, D. (2003). "Performance studies on novel solar photocatalytic reactors for decolourisation of textile dyeing wastewaters." *Indian J. Chem. Technol.*, 10, 638–643.

Kant, R. (2012). "Textile dyeing and printing industry: An environmental hazard." *Nat. Sci.*, 4(1), 22–26.

Kato, T., Tohma, H., Miki, O., Shibata, T., and Tamura, M. (2005). "Degradation of norovirus in sewage treatment water by photocatalytic ultraviolet disinfection." *Nippon Steel Tech. Rep.*, (92), 41–44.

Kete, M., Pliexhova, O., Matoh, L., and Štangar, U. L. (2018). "Design and evaluation of a compact photocatalytic reactor for water treatment." *Environ. Sci. Pollut. Res.*, 25(21), 20453–20465.

Khan, R., Woo, S., Kim, T., and Nam, C. (2008). “Comparative study of the photocatalytic performance of boron – iron Co-doped and boron-doped TiO₂ nanoparticles.” *Mater. Chem. Phys. J.*, 112, 167–172.

Kim, S., Cho, H., Joo, H., Her, N., Han, J., Yi, K., Kim, J. O., and Yoon, J. (2017). “Evaluation of performance with small and scale-up rotating and flat reactors; photocatalytic degradation of bisphenol A, 17B–estradiol, and 17A–ethynyl estradiol under solar irradiation.” *J. Hazard. Mater.*, 336, 21–32.

Kimura, T., Yoshikawa, N., Matsumura, N., and Kawase, Y. (2004). “Photocatalytic degradation of nonionic surfactants with immobilized TiO₂ in an airlift reactor.” *J. Environ. Sci. Heal. - Part A Toxic/Hazardous Subst. Environ. Eng.*, 39(11–12), 2867–2881.

Klausner, J. F., Li, P., and Pond, S. (1994). “Performance of Nonconcentrating Solar Photocatalytic Oxidation Reactors, Part II: Shallow Pond Configuration.” *J. Sol. Energy Eng.*, 116(February), 8–13.

Koř, K., Matě, K., Hospodková, A., and Solcová, O. (2010). “Applied Catalysis B : Environmental Effect of silver doping on the TiO₂ for photocatalytic reduction of CO₂.” *Appl. Catal. B Environ.*, 96, 239–244.

Konstantinou, I. K., and Albanis, T. A. (2004). “TiO₂-assisted photocatalytic degradation of azo dyes in aqueous solution: Kinetic and mechanistic investigations: A review.” *Appl. Catal. B Environ.*, 49(1), 1–14.

Konstantinou, I. K., Sakellarides, T. M., Sakkas, V. A., and Albanis, T. A. (2001). “Photocatalytic degradation of selected s-triazine herbicides and organophosphorus insecticides over aqueous TiO₂ suspensions.” *Environ. Sci. Technol.*, 35(2), 398–405.

Kosa, G., Shapaval, V., Kohler, A., and Zimmermann, B. (2017). “FTIR spectroscopy as a unified method for simultaneous analysis of intra- and extracellular metabolites in high-throughput screening of microbial bioprocesses.” *Microb. Cell Fact.*, 16(1), 1–11.

Kositzi, M., Poullos, I., Malato, S., Caceres, J., and Campos, A. (2004). "Solar photocatalytic treatment of synthetic municipal wastewater." *Water Res.*, 38(5), 1147–1154.

Kraeutler, B., and Bard, A. J. (1978). "Heterogeneous photocatalytic preparation of supported catalysts. Photodeposition of platinum on titanium dioxide powder and other substrates." *J. Am. Chem. Soc.*, 100(13), 4317–4318.

Kudlek, E., Dudziak, M., and Bohdziewicz, J. (2016). "Influence of Inorganic Ions and Organic Substances on the Degradation of Pharmaceutical Compound in Water Matrix." *Water (Switzerland)*, 8(11), 1–18.

Kuen, W., and Tayade, R. J. (2014). "Recent developments in photocatalytic dye degradation upon irradiation with energy - efficient light emitting diodes." *Chinese J. Catal.*, 35(11), 1781–1792.

Kumar, M. S., Sonawane, S. H., and Pandit, A. B. (2017). "Degradation of methylene blue dye in aqueous solution using hydrodynamic cavitation based hybrid advanced oxidation processes." *Chem. Eng. Process. Process Intensif.*, 122(September), 288–295.

Kwok, D. Y., Gietzelt, T., Grundke, K., Jacobasch, H.-J., and Neumann, A. W. (1997). "Contact Angle Measurements and Contact Angle Interpretation. 1. Contact Angle Measurements by Axisymmetric Drop Shape Analysis and a Goniometer Sessile Drop Technique." *Langmuir*, 13(10), 2880–2894.

Lai, R. S., Hsu, H. K., Lu, J. Y., Ger, L. P., and Lai, N. S. (1996). "*Photocatalytic Semiconductors: Synthesis, Characterization and Environmental Applications.*" Springer Cham Heidelberg, New York, 1-289.

Lai, T. Y., and Lee, W. C. (2009). "Killing of cancer cell line by photoexcitation of folic acid-modified titanium dioxide nanoparticles." *J. Photochem. Photobiol. A Chem.*, 204(2–3), 148–153.

Laidler, K. J. (1950). *Chemical Kinetics*, Third Edition. Pearson, 1-530. ISBN: 978-81-317-0972-6.

Laskin, A., and Cowin, J. P. (2001). “Automated single-particle SEM/EDX analysis of submicrometer particles down to 0.1 μm .” *Anal. Chem.*, 73(5), 1023–1029.

Lathe, S., Liu, S., Terashima, C., Nakata, K., and Fujishima, A. (2014). “Transparent, Adherent, and Photocatalytic $\text{SiO}_2\text{-TiO}_2$ Coatings on Polycarbonate for Self-Cleaning Applications.” *Coatings*, 4(3), 497–507.

Lavand, A. B., and Malghe, Y. S. (2016). “Visible-light photocatalytic degradation of ethidium bromide using carbon- and iron-modified TiO_2 photocatalyst.” *J. Therm. Anal. Calorim.*, 123(2), 1163–1172.

Lazar, M. A., Varghese, S., and Nair, S. S. (2012). “Photocatalytic Water Treatment by Titanium Dioxide: Recent Updates.” *Catalysts*, 2, 572–601.

Lea, J., and Adesina, A. A. (1999). “Continuous flow bubble column reactor for the photocatalytic causticisation of sodium oxalate.” *Chem. Eng. Sci.*, 54, 2209–2216.

Lebedev, V. A., Kozlov, D. A., Kolesnik, I. V., Poluboyarinov, A. S., Becerikli, A. E., Grünert, W., and Garshev, A. V. (2016). “The amorphous phase in titania and its influence on photocatalytic properties.” *Appl. Catal. B Environ.*, 195, 39–47.

Lee, D. K., Kim, S. C., Cho, I. C., Kim, S. J., and Kim, S. W. (2004). “Photocatalytic oxidation of microcystin-LR in a fluidized bed reactor having TiO_2 -coated activated carbon.” *Sep. Purif. Technol.*, 34(1–3), 59–66.

Lei, P., Wang, F., Gao, X., Ding, Y., Zhang, S., Zhao, J., Liu, S., and Yang, M. (2012). “Immobilization of TiO_2 nanoparticles in polymeric substrates by chemical bonding for multi-cycle photodegradation of organic pollutants.” *J. Hazard. Mater.*, 227–228, 185–194.

Lenzi, G. G., Fávero, C. V. B., Colpini, L. M. S., Bernabe, H., Baesso, M. L., Specchia, S., and Santos, O. A. A. (2011). "Photocatalytic reduction of Hg(II) on TiO₂ and Ag/TiO₂ prepared by the sol-gel and impregnation methods." *Desalination*, 270(1–3), 241–247.

León, A., Reuquen, P., Garín, C., Segura, R., Vargas, P., Zapata, P., and Orihuela, P. (2017). "FTIR and Raman Characterization of TiO₂ Nanoparticles Coated with Polyethylene Glycol as Carrier for 2-Methoxyestradiol." *Appl. Sci.*, 7(1), 49.

Leshuk, T., Krishnakumar, H., Livera, D. de O., and Gu, F. (2018a). "Floating photocatalysts for passive solar degradation of naphthenic acids in oil sands process-affected water." *Water (Switzerland)*, 10(2), 1–8.

Leshuk, T., Krishnakumar, H., Livera, D. de O., and Gu, F. (2018b). "Floating photocatalysts for passive solar degradation of naphthenic acids in oil sands process-affected water." *Water*, 10(2), 1–8.

Li, D., Xiong, K., Li, W., Yang, Z., Liu, C., Feng, X., and Lu, X. (2010). "Comparative Study in Liquid-Phase Heterogeneous Photocatalysis : Model for Photoreactor Scale-Up." *Ind. Eng. Chem. Res.*, 49, 8397–8405.

Li, H., Zhou, J., and Zhang, X. (2015a). "Constructing stable NiO / N-doped TiO₂ nanotubes photocatalyst with enhanced visible-light photocatalytic activity." *J Mater Sci Mater Electron*, 26, 2571–2578.

Li, K., Gao, S., Wang, Q., Xu, H., Wang, Z., Huang, B., Dai, Y., and Lu, J. (2015b). "In Situ Reduced Synthesis of Ti³⁺ Self-Doped TiO₂/g-C₃N₄ Heterojunctions with High Photocatalytic Performance under LED Light Irradiation." *Appl. Mater. Interfaces*, 7(17), 9023–9030.

Li, L., Li, Y., Xu, H., and Zhang, W. (2015c). "Novel Floating TiO₂ Photocatalysts for Polluted Water Decontamination Based on Polyurethane Composite Foam." *Sep. Sci. Technol.*, 50(2), 164–173.

- Li, W., Guo, C., Su, B., and Xu, J. (2012). "Photodegradation of four fluoroquinolone compounds by titanium dioxide under simulated solar light irradiation." *J. Chem. Technol. Biotechnol.*, 87(5), 643–650.
- Li, Y. S., You, Y. H., and Lien, E. T. (1999). "Oxidation of 2,4-dinitrophenol by hydrogen peroxide in the presence of basic oxygen furnace slag." *Arch. Environ. Contam. Toxicol.*, 37(4), 427–433.
- Li, Y., Zhang, H., Liu, P., Wang, D., Li, Y., and Zhao, H. (2013). "Cross-linked g-C₃N₄/rGO nanocomposites with tunable band structure and enhanced visible light photocatalytic activity." *Small*, 9(19), 3336–3344.
- Lin, L., Wang, H., Luo, H., and Xu, P. (2016). "Photocatalytic Treatment of Desalination Concentrate Using Optical Fibers Coated with Nanostructured Thin Films: Impact of Water Chemistry and Seasonal Climate Variations." *Photochem. Photobiol.*, 92(3), 379–387.
- Lin, L., Wang, H., and Xu, P. (2017). "Immobilized TiO₂-reduced graphene oxide nanocomposites on optical fibers as high performance photocatalysts for degradation of pharmaceuticals." *Chem. Eng. J.*, 310, 389–398.
- Lin, P., Hu, H., Lv, H., Ding, Z., Xu, L., Qian, D., Wang, P., Pan, J., Li, C., and Cui, C. (2018). "Hybrid reduced graphene oxide/TiO₂/graphitic carbon nitride composites with improved photocatalytic activity for organic pollutant degradation." *Appl. Phys. A Mater. Sci. Process.*, 124(7), 510.
- Linley, S., Leshuk, T., and Gu, F. X. (2013). "Magnetically separable water treatment technologies and their role in future advanced water treatment: A patent review." *Clean - Soil, Air, Water*, 41(12), 1152–1156.
- Liu, L., Qi, Y., Lu, J., Lin, S., An, W., Liang, Y., and Cui, W. (2016). "A stable Ag₃PO₄@g-C₃N₄ hybrid core@shell composite with enhanced visible light photocatalytic degradation." *Appl. Catal. B Environ.*, 183, 133–141.

- López-Muñoz, M. J., Aguado, J., Arencibia, A., and Pascual, R. (2011). “Mercury removal from aqueous solutions of HgCl₂ by heterogeneous photocatalysis with TiO₂.” *Appl. Catal. B Environ.*, 104(3–4), 220–228.
- Luan, J., Shen, Y., Wang, S., and Guo, N. (2017). “Synthesis, Property Characterization and Photocatalytic Activity of the Polyaniline/BiYT₂O₇ Polymer Composite.” *Polymers (Basel)*, 9(69), 1–21.
- Luo, H. L., Sheng, J., and Wan, Y. Z. (2008). “Preparation and characterization of TiO₂/polystyrene core-shell nanospheres via microwave-assisted emulsion polymerization.” *Mater. Lett.*, 62(1), 37–40.
- Magalhães, F., and Lago, R. M. (2009). “Floating photocatalysts based on TiO₂ grafted on expanded polystyrene beads for the solar degradation of dyes.” *Sol. Energy*, 83(9), 1521–1526.
- Magalhães, F., Moura, F. C. C., and Lago, R. M. (2011). “TiO₂/LDPE composites: A new floating photocatalyst for solar degradation of organic contaminants.” *Desalination*, 276(1–3), 266–271.
- Malato, S., Blanco, J., Vidal, A., Fernández, P., Cáceres, J., Trincado, P., Oliveira, J. C., and Vincent, M. (2002). “New large solar photocatalytic plant: Set-up and preliminary results.” *Chemosphere*, 47(3), 235–240.
- Mansilla, H. D., Mora, A., Pincheira, C., Mondaca, M. A., Marcato, P. D., Durán, N., and Freer, J. (2007). “New photocatalytic reactor with TiO₂ coating on sintered glass cylinders.” *Appl. Catal. B Environ.*, 76(1–2), 57–63.
- Marandi, R., Mahanpoor, K., Abdollah, A., Sharif, M., Olya, M. E., and Moradi, R. (2013). “Photocatalytic Degradation of Azo Dye Acid Yellow 23 in Water Using NiFe₂O₄ Nanoparticles Supported on Clinoptilolite as a Catalyst in a Circulating Fluidized Bed Reactor.” *J. Basic Appl. Sci. Res.*, 3(5), 347–357.

- Marchis, T., Avetta, P., Bianco-Prevot, A., Fabbri, D., Viscardi, G., and Laurenti, E. (2011). "Oxidative degradation of Remazol Turquoise Blue G 133 by soybean peroxidase." *J. Inorg. Biochem.*, 105(2), 321–327.
- Markham, M. C., and Upreti, M. C. (1965). "Photoelectric effects at semiconductor electrodes." *J. Catal.*, 4(2), 229–238.
- Martínez, S., Morales-Mejía, J. C., Hernández, P. P., Santiago, L., and Almanza, R. (2014). "Solar photocatalytic oxidation of Triclosan with TiO₂ immobilized on volcanic porous stones on a CPC pilot scale reactor." *Energy Procedia*, 57(55), 3014–3020.
- Matsunaga, T., Tomoda, R., Nakajima, T., and Wake, H. (1985a). "Photoelectrochemical sterilization of microbial cells by semiconductor powders." *FEMS Microbiol. Lett.*, 29, 211–214.
- Matsunaga, T., Tomoda, R., Nakajima, T., and Wake, H. (1985b). "Photoelectrochemical sterilization of microbial cells by semiconductor powders." *FEMS Microbiol. Lett.*, 29(1), 211–214.
- Mccullagh, C., Skillen, N., Adams, M., and Robertson, P. K. J. (2011). "Photocatalytic reactors for environmental remediation: a review." *J. Chem. Technol. Biotechnol.*, 86(May), 1002–1017.
- McIntock, B. Y. I. S. (1965). "Reactions on Titanium Dioxide; Photo-adsorption and Oxidation of Ethylene and Propylene." *Trans. Faraday Soc.*, 61, 1007–1016.
- Mehrjouei, M., Müller, S., and Möller, D. (2013). "Design and characterization of a multi-phase annular falling-film reactor for water treatment using advanced oxidation processes." *J. Environ. Manage.*, 120, 68–74.

Mekprasart, W., and Pecharapa, W. (2011). "Synthesis and characterization of nitrogen-doped TiO₂ and its photocatalytic activity enhancement under visible light." *Energy Procedia*, 9, 509–514.

Mhamane, D., Ramadan, W., Fawzy, M., Rana, A., Dubey, M., Rode, C., Lefez, B., Hannoyer, B., and Ogale, S. (2011). "From graphite oxide to highly water dispersible functionalized graphene by single step plant extract-induced deoxygenation." *Green Chem.*, 13(8), 1990–1996.

Miguel, N., Ormad, M. P., Mosteo, R., Ovelleiro, J. L., Miguel, N., Ormad, M. P., Mosteo, R., and Ovelleiro, J. L. (2012). "Photocatalytic Degradation of Pesticides in Natural Water: Effect of Hydrogen Peroxide." *Int. J. Photoenergy*, 2012, 1–11.

Miranda-García, N., Suárez, S., Sánchez, B., Coronado, J. M., Malato, S., and Maldonado, M. I. (2011). "Photocatalytic degradation of emerging contaminants in municipal wastewater treatment plant effluents using immobilized TiO₂ in a solar pilot plant." *Appl. Catal. B Environ.*, 103(3–4), 294–301.

Mirhoseini, F., and Salabat, A. (2015). "Antibacterial activity based poly(methyl methacrylate) supported TiO₂ photocatalyst film nanocomposite." *Tech. J. Eng. Appl. Sci.*, 25, 115–118.

Mohd Adnan, M. A., Muhd Julkapli, N., Amir, M. N. I., and Maamor, A. (2018). "Effect on different TiO₂ photocatalyst supports on photodecolorization of synthetic dyes: a review." *Int. J. Environ. Sci. Technol.*

Molinari, R., Lavorato, C., and Argurio, P. (2017). "Recent progress of photocatalytic membrane reactors in water treatment and in synthesis of organic compounds. A review." *Catal. Today*, 281, 144–164.

Molla, M. A. I., Tateishi, I., Furukawa, M., Katsumata, H., Suzuki, T., and Kaneco, S. (2017). "Evaluation of Reaction Mechanism for Photocatalytic Degradation of Dye with

Self-Sensitized TiO₂ under Visible Light Irradiation.” *Open J. Inorg. Non-metallic Mater.*, 07(01), 1–7.

Monteserín, C., Blanco, M., Aranzabe, E., Aranzabe, A., Laza, J. M., Larrañaga-Varga, A., and Vilas, J. L. (2017). “Effects of graphene oxide and chemically-reduced graphene oxide on the dynamic mechanical properties of epoxy amine composites.” *Polymers (Basel)*., 9(9), 1–16.

Moo, G. S. J., Khezri, B., Webster, R. D., and Pumera, M. (2014). “Graphene Oxides Prepared by Hummers’, Hofmann’s, and Staudenmaier’s Methods: Dramatic Influences on Heavy-Metal-Ion Adsorption.” *Chem. Phys. Chem.*, 15(14), 2922–2929.

Motegh, M., Ommen, J. R. Van, Appel, P. W., and Kreutzer, M. T. (2014). “Scale-up study of a multiphase photocatalytic reactor - Degradation of cyanide in water over TiO₂.” *Environ. Sci. Technol.*, 48(3), 1574–1581.

Mudunkotuwa, I. A., Minshid, A. Al, and Grassian, V. H. (2014). “ATR-FTIR spectroscopy as a tool to probe surface adsorption on nanoparticles at the liquid-solid interface in environmentally and biologically relevant media.” *Analyst*, 139(5), 870–881.

Muhamad, S. G. (2010). “Kinetic studies of catalytic photodegradation of chlorpyrifos insecticide in various natural waters.” *Arab. J. Chem.*, 3(2), 127–133.

Mukherjee, D., Barghi, S., and Ray, A. K. (2014). “Preparation and Characterization of the TiO₂ Immobilized Polymeric Photocatalyst for Degradation of Aspirin under UV and Solar Light.” *Processes*, 2, 12–23.

Mukherjee, P. S., and Ray, A. K. (1999a). “Major challenges in the design of a large-scale photocatalytic reactor for water treatment.” *Chem. Eng. Technol.*, 22(3), 253–260.

Mukherjee, P. S., and Ray, A. K. (1999b). “Major Challenges in the Design of a Large-Scale Photocatalytic Reactor for Water Treatment.” *Chem. Eng. Technol.*, 22(3), 253–260.

- Mukhlis, M. Z. Bin, Najnin, F., Rahman, M. M., and Uddin, M. J. (2013). "Photocatalytic Degradation of Different Dyes Using TiO₂ with High Surface Area: A Kinetic Study." *J. Sci. Res.*, 5(2), 301–314.
- Munari, S., Bottino, A., Roda, G. C., and Capannelli, G. (1990). "Preparation of ultrafiltration membranes. State of the art." *Desalination*, 77(C), 85–100.
- Mustafa, Y. A., Alward, A. I., and Ebrahim, M. (2014). "Heterogeneous Photocatalytic Degradation for Treatment of Oil from Wastewater." *Al-Khwarizmi Eng. J.*, 10(3), 53–61.
- Mwangi, I. W., Ngila, J. C., Ndungu, P., Msagati, T. A. M., and Kamau, J. N. (2013). "Immobilized Fe (III)-doped titanium dioxide for photodegradation of dissolved organic compounds in water." *Environ. Sci. Pollut. Res.*, 20(9), 6028–6038.
- Na, Y. S., Kim, D. H., Lee, C. H., Lee, S. W., Park, Y. S., Oh, Y. K., Park, S. H., and Song, S. K. (2004). "Photocatalytic decolorization of Rhodamine B by fluidized bed reactor with hollow ceramic ball photocatalyst." *Korean J. Chem. Eng.*, 21(2), 430–435.
- Na, Y., Song, S., and Park, Y. (2005). "Photocatalytic Decolorization of Rhodamine B by Immobilized TiO₂/UV in a Fluidized-bed Reactor." *Korean J. Chem. Eng.*, 22(2), 196–200.
- Nainani, R., Thakur, P., and Chaskar, M. (2012). "Synthesis of Silver Doped TiO₂ Nanoparticles for the Improved Photocatalytic Degradation of Methyl Orange." *J. Mater. Sci. Eng. B*, 2(1), 52–58.
- Nam, W., Kim, J., and Han, G. (2002). "Photocatalytic oxidation of methyl orange in a three-phase fluidized bed reactor." *Chemosphere*, 47(9), 1019–1024.
- Namatame, Y., and Sato, H. (2013). "Evaluation of polymorphic forms by powder X-ray diffraction and thermal analysis methods." *Rigaku J.*, 29(3), 8–15.

- Nan, M., and Jin, B. (2012). "Photocatalytic treatment of high concentration carbamazepine in synthetic hospital wastewater." *J. Hazard. Mater.*, 199–200, 135–142.
- Nan, M., Jin, B., Chow, C. W. K., and Saint, C. (2010). "Recent developments in photocatalytic water treatment technology: A review." *Water Res.*, 44(10), 2997–3027.
- Neti, N., Chaturvedi, V., and Li, G. (2012). "Novel pebble bed photocatalytic reactor for solar treatment of textile wastewater." *Chem. Eng. J.*, 184, 90–97.
- Nidheesh, P. V., Zhou, M., and Oturan, M. A. (2018). "An overview on the removal of synthetic dyes from water by electrochemical advanced oxidation processes." *Chemosphere*, 197, 210–227.
- Nirmala, M., Nair, M. G., Rekha, K., Anukaliani, A., Samdarshi, S. K., and Nair, R. G. (2010). "Photocatalytic Activity of ZnO Nanopowders Synthesized by DC Thermal Plasma." *African J. Basic Appl. Sci.*, 2(5–6), 161–166.
- Ocwelwang, A. R., and Tichagwa, L. (2014). "Synthesis and Characterisation of Ag and Nitrogen Doped TiO₂ Nanoparticles Supported on A Chitosan-Pvae Nanofibre Support." *Int. J. Adv. Res. Chem. Sci.*, 1(2), 28–37.
- Ohno, T., Sarukawa, K., Tokieda, K., and Matsumura, M. (2001). "Morphology of a TiO₂ photocatalyst (Degussa, P-25) consisting of anatase and rutile crystalline phases." *J. Catal.*, 203(1), 82–86.
- Olesik, J. W. (2012). "Elemental Analysis Using ICP-OES and ICP/MS." *Anal. Chem.*, 63(1), 12A-21A.
- Ollis, D. F. (1984). "Complete Heterogeneously Photocatalyzed Transformation of 1,1- and 1,2-Dibromoethane to COP and HBr T." *J. Phys. Chem.*, 88(9), 3386–3388.

Ong, S.-T., Keng, P.-S., Lee, W.-N., Ha, S.-T., and Hung, Y.-T. (2011). "Dye Waste Treatment." *Water*, 3(4), 157–176.

Ong, W., Tan, L., Ng, Y. H., Yong, S., and Chai, S. (2016). "Graphitic Carbon Nitride (g-C₃N₄) - Based Photocatalysts for Artificial Photosynthesis and Environmental Remediation: Are We a Step Closer To Achieving Sustainability?" *Chem. Rev.*, 116, 7159–7329.

Osugi, M. E., Umbuzeiro, G. A., Castro, F. J. V. De, and Zanoni, M. V. B. (2006). "Photoelectrocatalytic oxidation of remazol turquoise blue and toxicological assessment of its oxidation products." *J. Hazard. Mater.*, 137(2), 871–877.

Huang, Y., Sai, S., Ho, H., Lu, Y., Niu, R., Xu, L., and Cao, J. (2016). "Removal of Indoor Volatile Organic Compounds via Photocatalytic Oxidation: A Short Review and Prospect." *Molecules*, 21(56), 1–20.

Pachauri, T., Singla, V., Satsangi, A., Lakhani, A., and Maharaj Kumari, K. (2013). "SEM-EDX characterization of individual coarse particles in Agra, India." *Aerosol Air Qual. Res.*, 13(2), 523–536.

Pang, Y. L., and Abdullah, A. Z. (2013). "Current status of textile industry wastewater management and research progress in malaysia: A review." *Clean - Soil, Air, Water*, 41(8), 751–764.

Pangarkar, V. G. (2015). "Design of Multiphase Reactors." John Wiley & Sons, Inc., Hoboken, New Jersey, Multiphase Reactors: types and criteria for selection for a given application, 47–86.

Gupta, V.K., Khamparia, S., Tyagi, I., Jaspal, D., and Malviya, A. (2015). "Decolorization of mixture of dyes : A critical review." *Glob. J. Environ. Sci. Manag.*, 1(1), 71–94.

Pardiwala, J. M., Patel, F. J., and Patel, S. S. (2017). "Photocatalytic degradation of RB21 dye by TiO₂ and ZnO under natural sunlight, Microwave irradiation and UV-reactor." *Int. J. Adv. Reseach Eng. Technol.*, 8(1), 8–16.

Pareek, V., Chong, S., Tadé, M., and Adesina, A. A. (2008). "Light intensity distribution in heterogenous photocatalytic reactors." *Asia-Pacific J. Chem. Eng.*, 3, 171–201.

Peerakiathajorn, P., Chawengkijwanich, C., Onreabroy, W., and Chiarakorn, S. (2012). "Novel Photocatalytic Ag/TiO₂ Thin Film on Polyvinyl Chloride for gaseous BTEX Treatment." *Mater. Sci. Forum*, 712, 133–145.

Perkowski, J., Bzdon, S., Bulska, A., and Józwiak, W. K. (2006). "Decomposition of detergents present in car-wash sewage by titania photo-assisted oxidation." *Polish J. Environ. Stud.*, 15(3), 457–465.

Pirilä, M., Saouabe, M., Ojala, S., Rathnayake, B., Drault, F., Valtanen, A., Huuhtanen, M., Brahmi, R., and Keiski, R. L. (2015). "Photocatalytic degradation of organic pollutants in wastewater." *Top. Catal.*, 58(14–17), 1085–1099.

Pitt, J. (2009). "Principles and Applications of Liquid Chromatography." *Clin. Biochem. Rev.*, 30(February), 19–34.

Plantard, G., Janin, T., Goetz, V., and Brosillon, S. (2012). "Solar photocatalysis treatment of phytosanitary refuses: Efficiency of industrial photocatalysts." *Appl. Catal. B Environ.*, 115–116, 38–44.

Pongyeela, P., Chungsiriporn, J., Kaewpradit, P., and Sikong, L. (2013). "Process modeling of NH₃ contaminated waste air treatment in photocatalytic reactor using TiO₂ coated glass tubes." *Songklanakarinn J. Sci. Technol.*, 35(3), 361–368.

Poulios, I., Makri, D., and Prohaska, X. (1999). "Photocatalytic treatment of olive milling waste water: oxidation of protocatechuic acid." *Glob. Nest Int. J.*, 1(1), 55–62.

Priya, R., and Kanmani, S. (2013). "Design of pilot-scale solar photocatalytic reactor for the generation of hydrogen from alkaline sulfide wastewater of sewage treatment plant." *Environ. Technol.*, 34(20), 2817–2823.

Pujara, K., Kamble, S. P., and Pangarkar, V. G. (2007). "Photocatalytic degradation of phenol-4-sulfonic acid using an artificial UV/TiO₂ system in a slurry bubble column reactor." *Ind. Eng. Chem. Res.*, 46(12), 4257–4264.

Puma, G. L., and Yue, P. L. (2001). "A Novel Fountain Photocatalytic Reactor for Water Treatment and Purification : Modeling and Design." *Ind. Eng. Chem. Res.*, 40(23), 5162–5169.

Qiu, J., Sun, X., Xing, J., and Liu, X. (2014). "Preparation and Photocatalytic Activity of B, Ce Co doped TiO₂ Hollow Fibers Photocatalyst." *Russ. J. Phys. Chem. A*, 88(7), 1236–1240.

Rachel, A., Subrahmanyam, M., and Boule, P. (2002). "Comparison of photocatalytic efficiencies of TiO₂ in suspended and immobilised form for the photocatalytic degradation of nitrobenzenesulfonic acids." *Appl. Catal. B Environ.*, 37(4), 301–308.

Raj, K. J. A., and Viswanathan, B. (2009). "Effect of surface area , pore volume and particle size of P25 titania on the phase transformation of anatase to rutile." *Indian J. Chem.*, 48(October), 1378–1382.

Rajeshwar, K. (2011). "Solar energy conversion and environmental remediation using inorganic semiconductor-liquid interfaces: The road traveled and the way forward." *J. Phys. Chem. Lett.*, 2(11), 1301–1309.

Ray, A. K. (1997). "New Photocatalytic Reactors for Destruction of Toxic Water Pollutants." *Dev. Chem. Eng. Miner. Process.*, 5(1/2), 115–128.

Ray, A. K., and Beenackers, A. A. C. M. (1998). "Development of a new photocatalytic reactor for water purification." *Catal. Today*, 40(1), 73–83.

Regmi, C., Joshi, B., Ray, S. K., Gyawali, G., and Pandey, R. P. (2018). "Understanding Mechanism of Photocatalytic Microbial Decontamination of Environmental Wastewater." *Front. Chem.*, 6(February), 1–6.

Ren, Y., Chen, Y., Zeng, T., Feng, J., Ma, J., and Mitch, W. A. (2016). "Influence of Bi-doping on $Mn_{1-x}Bi_xFe_2O_4$ catalytic ozonation of di-n-butyl phthalate." *Chem. Eng. J. J.*, 283, 622–630.

Renu, M. A., Singh, K., Upadhyaya, S., and Dohare, R. K. (2017). "Removal of heavy metals from wastewater using modified agricultural adsorbents." *Mater. Today Proc.*, 4(9), 10534–10538.

Reyes, C., Fernandez, J., Freer, J., Mondaca, M. A., Zaror, C., Malato, S., and Mansilla, H. D. (2006). "Degradation and inactivation of tetracycline by TiO_2 photocatalysis." *J. Photochem. Photobiol. A Chem.*, 184(1–2), 141–146.

Reza, M., Fazli, M., and Hossein, M. (2016). "Decomposition of organic chemicals by zeolite- TiO_2 nanocomposite supported onto low density polyethylene film under UV-LED powered by solar radiation." *Appl. Catal. B Environ.*, 183, 407–416.

Robertson, P. K. J., Adams, M., and Campbell, I. (2008). "Novel photocatalytic reactor development for removal of hydrocarbons from water." *Int. J. Photoenergy*, 2008, 1–7.

Rocha, O. R. S., Duarte, M. M. M. B., Dantas, R. F., Duarte, M. M. L., and Silva, V. L. (2014). "Oil sludge treatment by solar TiO_2 -Photocatalysis to remove Polycyclic Aromatic Hydrocarbons (PAH)." *Brazilian J. Pet. Gas*, 8(3), 89–96.

Rodríguez Couto, S., Domínguez, A., and Sanromán, A. (2002). “Photocatalytic degradation of dyes in aqueous solution operating in a fluidised bed reactor.” *Chemosphere*, 46(1), 83–86.

S, S., and B, L. G. (2009). “Removal of Dyes from Wastewater using Adsorption - A Review.” *Int. J. Biosci. Technol.*, 2(4), 47–51.

Sacco, O., Sannino, D., and Vaiano, V. (2019). “Packed Bed Photoreactor for the removal of water pollutants using Visible Light Emitting Diodes.” *Appl. Sci.*, 9(3), 472.

Sadi, S. Al, Feroz, S., and Rao, L. N. (2015a). “Treatment of Industrial Wastewater by Solar Nano Photocatalysis.” Proceedings of International Conference on Recent Trends in Mechanical Engineering 2K15(NECICRTME-2K15), 8(7), 177–182.

Sadi, S. Al, M, G. D., Syed, M. A., Feroz, S., and Varghese, M. J. (2015b). “Treatment of textile Industry Waste water using Solar photo Catalysis.” *Res. J. Recent Sci.*, 5(10), 20–27.

Saggiaro, E. M., Oliveira, A. S., Pavesi, T., Maia, C. G., Ferreira, L. F. V., and Moreira, J. C. (2011). “Use of titanium dioxide photocatalysis on the remediation of model textile wastewaters containing azo dyes.” *Molecules*, 16(12), 10370–10386.

Saien, J., and Shahrezaei, F. (2012). “Organic pollutants removal from petroleum refinery wastewater with nanotitania photocatalyst and UV light emission.” *Int. J. Photoenergy*, 2012, 1-5.

Salgot, M., and Folch, M. (2018). “Wastewater treatment and water reuse.” *Curr. Opin. Environ. Sci. Heal.*, 2, 64–74.

Sangchay, W., Sikong, L., and Kooptarnond, K. (2012). “Comparison of photocatalytic reaction of commercial P25 and synthetic TiO₂-AgCl nanoparticles.” *Procedia Eng.*, 32, 590–596.

Saran, S., Kamalraj, G., Arunkumar, P., and Devipriya, S. P. (2016). "Pilot scale thin film plate reactors for the photocatalytic treatment of sugar refinery wastewater." *Environ. Sci. Pollut. Res.*, 23(17), 17730–17741.

Saravanan, R., Gracia, F., and Stephen, A. (2017). "Nanocomposites for Visible Light-induced Photocatalysis." *Nanocomposites visible Light. Photocatal.*, 19–41.

Satuf, M., Brandi, R., Alfano, O., and Cassano, A. (2007). "Modeling of a Flat Plate, Slurry Reactor for the Photocatalytic Degradation of 4-Chlorophenol." *Int. J. Chem. React. Eng.*, 5(A59), 1–12.

Sboui, M., Nsib, M. F., Rayes, A., Swaminathan, M., and Houas, A. (2017). "TiO₂–PANI/Cork composite: A new floating photocatalyst for the treatment of organic pollutants under sunlight irradiation." *J. Environ. Sci.*, 1–11.

Serra, M., Baldovi, H. G., Albarracin, F., and Garcia, H. (2016). "Visible light photocatalytic activity for hydrogen production from water – methanol mixtures of open-framework V-doped mixed-valence titanium phosphate." *Appl. Catal. B Environ.*, 183, 159–167.

Shallenberger, J. (2014). "Surface and Interface Characterization of Polymer Films Surface and Interface Characterization of Polymer Films." *Evans Anal. Gr.*, 3–6.

Shang, J., Chai, M., and Zhu, Y. (2003a). "Photocatalytic degradation of polystyrene plastic under fluorescent light." *Environ. Sci. Technol.*, 37(19), 4494–4499.

Shang, J., Chai, M., and Zhu, Y. (2003b). "Solid-phase photocatalytic degradation of polystyrene plastic with TiO₂ as photocatalyst." *J. Solid State Chem.*, 174(1), 104–110.

Shao, L., Xing, G., Lv, W., Yu, H., Qiu, M., Zhang, X. M., and Qi, C. (2013). "Photodegradation of azo-dyes in aqueous solution by polyacrylonitrile nanofiber mat-supported metalloporphyrins." *Polym. Int.*, 62(2), 289–294.

Sharma, A. K., Tiwari, R. K., and Gaur, M. S. (2016). "Nanophotocatalytic UV degradation system for organophosphorus pesticides in water samples and analysis by Kubista model." *Arab. J. Chem.*, 9, S1755–S1764.

Sharma, R., and Singhal, S. (2014). "Photodegradation of textile dye using magnetically recyclable heterogeneous spinel ferrites." *J. Chem. Technol. Biotechnol.*, 90(5), 955–962.

Sharma, S. K., Bhunia, H., and Bajpai, P. K. (2012). "Photocatalytic Decolorization Kinetics and Mineralization of Reactive Black 5 Aqueous Solution by UV/TiO₂ Nanoparticles." *Clean - Soil, Air, Water*, 40(11), 1290–1296.

Shavisi, Y., Sharifnia, S., Hosseini, S. N., and Khadivi, M. A. (2014). "Application of TiO₂/perlite photocatalysis for degradation of ammonia in wastewater." *J. Ind. Eng. Chem.*, 20(1), 278–283.

Shen, L., Xing, Z., Zou, J., Li, Z., Wu, X., Zhang, Y., Zhu, Q., Yang, S., and Zhou, W. (2017a). "Black TiO₂ nanobelts/g-C₃N₄ nanosheets Laminated Heterojunctions with Efficient Visible-Light-Driven Photocatalytic Performance." *Sci. Rep.*, 7(December 2016), 1–11.

Shen, Y., Li, L., and Zhang, Z. (2016). "Scalable and environmentally friendly synthesis of hierarchical magnetic carbon nanosheet assemblies and their application in water treatment." *J. Phys. Chem. C*, 120(12), 6659–6668.

Shen, Y., Zhou, Y., Zhang, Z., and Xiao, K. (2017b). "Cobalt–copper oxalate nanofibers mediated Fenton degradation of Congo red in aqueous solutions." *J. Ind. Eng. Chem.*, 52, 153–161.

Shetty, R., Chavan, V. B., Kulkarni, P. S., Kulkarni, B. D., and Kamble, S. P. (2017). "Photocatalytic Degradation of Pharmaceuticals Pollutants Using N-Doped TiO₂ Photocatalyst: Identification of CFX Degradation Intermediates." *Indian Chem. Eng.*, 59(3), 177–199.

Shi-Hong, X., Dong-Dong, T., De-Fu, B., Peng-Hui, S., Wei, L., Wen-Feng, S., and Chun-Yan, M. (2013). "Effect of Magnetic Carrier NiFe₂O₄ Nanoparticles on Physicochemical and Catalytic Properties of Magnetically Separable Photocatalyst TiO₂/NiFe₂O₄." *Chem. Res. Chin. Univ.*, 29(1), 121–125.

Shi, M., Shen, J., Ma, H., Li, Z., Lu, X., Li, N., and Ye, M. (2012). "Preparation of graphene-TiO₂ composite by hydrothermal method from peroxotitanium acid and its photocatalytic properties." *Colloids Surfaces A Physicochem. Eng. Asp.*, 405, 30–37.

Shivaraju, H. P. (2011). "Removal of Organic Pollutants in the Municipal Sewage Water by TiO₂ based Heterogeneous Photocatalysis." *Int. J. Environ. Sci.*, 1(5), 911–923.

Shivaraju, H. P., Muzakkira, N., and Shahmoradi, B. (2016). "Photocatalytic treatment of oil and grease spills in wastewater using coated N-doped TiO₂ polyscales under sunlight as an alternative driving energy." *Int. J. Environ. Sci. Technol.*, 13(9), 2293–2302.

Shvadchina, Y., Vakulenko, V., Alekseenko, E., and Sova, A. (2013). "Evaluation of efficacy of anionic surfactant degradation in the presence of concomitant impurities of natural waters." *J. Chem.*, 2013, 1-8.

Si, C., Zhou, J., Gao, H., Liu, G., and Wu, J. (2015). "Typical application of sound field in wastewater treatment with fluidized bed photocatalytic reactor." *Water Environ. Res.*, 87(4), 378–383.

Silva, C. G., and Faria, J. L. (2010). "Photocatalytic oxidation of phenolic compounds by using a carbon nanotube-titanium dioxide composite catalyst." *Chem. Sus. Chem.*, 3(5), 609–618.

Silva, F. V. (2012). "A comparison of slurry and immobilized TiO₂ in the photocatalytic degradation of phenol." *Lat. Am. Appl. Res.*, 280, 275–280.

Silva, M. C., Corrêa, A. D., Amorim, M. T. S. P., Parpot, P., Torres, J. A., and Chagas, P. M. B. (2012). “Decolorization of the phthalocyanine dye reactive blue 21 by turnip peroxidase and assessment of its oxidation products.” *J. Mol. Catal. B Enzym.*, 77, 9–14.

Singh, C., Chaudhury, R., and Thakur, S. R. (2011). “Performance of advanced photocatalytic detoxification of municipal wastewater under solar radiation - A mini review.” *Int. J. Energy Environ.*, 2(2), 337–350.

Singh, S., Chaki, A., Chand, D. P., Raghuwanshi, A., and Singh, P. K. (2013a). “A novel polystyrene-supported titanium dioxide photocatalyst for degradation of methyl orange and methylene blue dyes under UV irradiation.” *J. Chem. Eng.*, 28(1), 9–13.

Singh, S., Mahalingam, H., and Singh, P. K. (2013b). “Polymer-supported titanium dioxide photocatalysts for environmental remediation : A review.” *Appl. Catal. A Gen.*, 462–463, 178–195.

Singh, S., Singh, P. K., and Mahalingam, H. (2015a). “A novel and effective strewn polymer-supported titanium dioxide photocatalyst for environmental remediation.” *J. Mater. Environ. Sci.*, 6(2), 349–358.

Singh, S., Singh, P. K., and Mahalingam, H. (2015b). “An Effective and Low-Cost TiO₂ / Polystyrene Floating Photocatalyst for Environmental Remediation.” *Int. J. Environ. Res.*, 9(2), 535–544.

Sinha, S., Orozco, N. G. T., Ramírez, D. S. A., and Rodríguez-Vázquez, R. (2009). “Effect of surfactant on TiO₂/UV mediated heterogeneous photocatalytic degradation of DDT in contaminated water.” *Tech. Proc. 2009 NSTI Nanotechnol. Conf. Expo, NSTI-Nanotech 2009*, 2, 411–414.

Sinirtas, E., Isleyen, M., and Soyulu, G. S. P. (2016). “Photocatalytic degradation of 2,4-dichlorophenol with V₂O₅-TiO₂ catalysts: Effect of catalyst support and surfactant additives.” *Cuihua Xuebao/Chinese J. Catal.*, 37(4), 607–615.

Sivakumar, S., Selvaraj, A., and Ramasamy, A. K. (2013). "Photocatalytic degradation of organic reactive dyes over MnTiO₃/TiO₂ heterojunction composites under UV-visible irradiation." *Photochem. Photobiol.*, 89(5), 1047–1056.

Sivlim, T., Akkan, Ş., Altın, İ., Koç, M., and Sökmen, M. (2012). "TiO₂ Immobilized Biodegradable Polymer for Photocatalytic Removal of Chlorophenol." *Water Air Soil Pollut*, 223, 3955–3964.

Soares, E., Lausarin, M., and Moro, C. (2007). "A study of process variables for the photocatalytic degradation of Rhodamine B." *Brazilian J. Chem. Eng.*, 24(1), 29–36.

Sobana, N., Selvam, K., and Swaminathan, M. (2008). "Optimization of photocatalytic degradation conditions of Direct Red 23 using nano-Ag doped TiO₂." *Sep. Purif. Technol.*, 62(3), 648–653.

Song, X., Zhao, Y., Wang, H., and Du, Q. (2009). "Fabrication of Polymer Microspheres Using Titania as a Photocatalyst and Pickering Stabilizer." *Am. Chem. Soc.*, 25(21), 4443–4449.

Soroush, F., Ganjidoust, H., and Ayati, B. (2017). "Removal of petroleum hydrocarbons from contaminated waters using a solar photocatalytic process." *J. Ferdowsi Civ. Eng.*, 29(1), 2–3.

Sridevi, N., Tan, L. T., and Sudesh, K. (2011). "Solar Photocatalytic Decolorization and Detoxification of Industrial Batik Dye Wastewater Using P(3HB)-TiO₂ Nanocomposite Films." *Clean - Soil, Air, Water*, 39(3), 265–273.

Srikanth, B., Goutham, R., Badri Narayan, R., Ramprasath, A., Gopinath, K. P., and Sankaranarayanan, A. R. (2017). "Recent advancements in supporting materials for immobilised photocatalytic applications in waste water treatment." *J. Environ. Manage.*, 200, 60–78.

- Srivastava, A., Jain, V. K., and Srivastava, A. (2009). "SEM-EDX analysis of various sizes aerosols in Delhi India." *Environ. Monit. Assess.*, 150(1–4), 405–416.
- Stasinakis, A. S. (2008). "Use of selected advanced oxidation processes (AOPS) for wastewater treatment – a mini review." *Glob. NEST J.*, 10(3), 376–385.
- Stengl, V., Popelkova, D., and P. Vlacil. (2016). "TiO₂-Graphene Nanocomposite as High Performace Photocatalysts." *J. Phys. Chem. C*, 115(April), 25209–25218.
- Stropa, J. M., Herrero, A. S., Oliveira, S. C., Cavalheiro, A. A., Dantas, F., Oliveira, S. L., and Oliveira, L. C. S. (2015). "Use of Natural Rubber Membranes as Support for Powder TiO₂ and Ag/TiO₂ Photocatalysts." *J. Braz. Chem. Soc.*, 00(00), 1–9.
- Suárez, L., Pulgarin, C., Roussel, C., and Kiwi, J. (2016). "Preparation, kinetics, mechanism and properties of semi-transparent photocatalytic stable films active in dye degradation." *Appl. Catal. A Gen.*, 516, 70–80.
- Sun, B., Shi, T., Peng, Z., Sheng, W., Jiang, T., and Liao, G. (2013). "Controlled fabrication of Sn/TiO₂ nanorods for photoelectrochemical water splitting." *Nanoscale Res. Lett.*, 8(1), 462.
- Sutisna, Rokhmat, M., Wibowo, E., Murniati, R., Khairurrijal, and Abdullah, M. (2017). "Novel Solar Photocatalytic Reactor for Wastewater Treatment." *IOP Conf. Ser. Mater. Sci. Eng.*, 214(1).
- T. LI, J. T. G. (2010). "Colour Removal from Aqueous Solutions of the Reactive Azo Dye Remazol Black B Using the Immobilised Cells (Shewanella Strain J18 143) –Cellulose-g.co-Monomer System." *J. Water Resour. Prot.*, 2(1), 77–84.
- Sudeep, K. T., and Sunil, K. (2018). "Fabrication and Analysis of Thermocol Sandwiched Between Bamboo Fiber-Reinforced Phenol Formaldehyde Composite Laminates." *Int. J. Res. Adv. Dev.*, 01(06), 130–134.

Takizawa, T., Watanabe, T., and Honda, K. (1978). "Photocatalysis through Excitation of Adsorbates. 2. A Comparative Study of Rhodamine B and Methylene Blue on Cadmium Sulfide." *J. Phys. Chem.*, 82(12), 1391–1396.

Tan, L., Ong, W., Chai, S., and Mohamed, A. R. (2013). "Reduced graphene oxide-TiO₂ nanocomposite as a promising visible-light-active photocatalyst for the conversion of carbon dioxide." *Nanoscale Res. Lett.*, 8(1), 1.

Tanaka, K., Capule, M. F. V, and Hisanaga, T. (1991). "Effect of crystallinity of TiO₂ on its photocatalytic action." *Chemical Phy. Letters*, 187(1), 2–5.

Aniszewski, T. (2015). "Alkaloid Chemistry." *Alkaloids*, Elsevier B. V, 1-496.

Tang, B., Chen, H., Peng, H., Wang, Z., and Huang, W. (2018). "Graphene Modified TiO₂ Composite Photocatalysts: Mechanism, Progress and Perspective." *Nanomaterials*, 8(2), 105.

Taoda, H. (2009). "Development and application of photocatalytic technology." *Synthesiology*, 1(4), 287–295.

Teixeira, S., Gurke, R., Eckert, H., Kühn, K., Fauler, J., and Cuniberti, G. (2016). "Photocatalytic degradation of pharmaceuticals present in conventional treated wastewater by nanoparticle suspensions." *J. Environ. Chem. Eng.*, 4(1), 287–292.

Thakare, S. R., and Bhave, N. S. (2005). "Photocatalytic degradation of Thiram (Fungicides) under visible light irradiation." *E-Journal Chem.*, 2(1), 62–69.

Thirumalraj, B., Rajkumar, C., Chen, S. M., and Palanisamy, S. (2017). "One-Pot Green Synthesis of Graphene Nanosheets Encapsulated Gold Nanoparticles for Sensitive and Selective Detection of Dopamine." *Sci. Rep.*, 7(January), 1–11.

Turchi, C. (1990). "Photocatalytic degradation of organic water contaminants: Mechanisms involving hydroxyl radical attack." *J. Catal.*, 122(1), 178–192.

Ulson de Souza, S. M. A. G., Forgiarini, E., and Ulson de Souza, A. A. (2007). "Toxicity of textile dyes and their degradation by the enzyme horseradish peroxidase (HRP)." *J. Hazard. Mater.*, 147(3), 1073–1078.

Vaiano, V., and Iervolino, G. (2018). "Facile method to immobilize ZnO particles on glass spheres for the photocatalytic treatment of tannery wastewater." *J. Colloid Interface Sci.*, 518, 192–199.

Vaiano, V., Matarangolo, M., and Sacco, O. (2018). "UV-LEDs floating-bed photoreactor for the removal of caffeine and paracetamol using ZnO supported on polystyrene pellets." *Chem. Eng. J.*, 350(May), 703–713.

Vaiano, V., Sacco, O., Pisano, D., Sannino, D., and Ciambelli, P. (2015). "From the design to the development of a continuous fixed bed photoreactor for photocatalytic degradation of organic pollutants in wastewater." *Chem. Eng. Sci.*, 137, 152–160.

Vaiano, V., Sacco, O., Sannino, D., Ciambelli, P., Longo, S., Venditto, V., and Guerra, G. (2014). "N-doped TiO₂/s-PS aerogels for photocatalytic degradation of organic dyes in wastewater under visible light irradiation." *J. Chem. Technol. Biotechnol.*, 89(8), 1175–1181.

Valadés-pelayo, P. J., Sosa, F. G., Serrano, B., and Lasa, H. De. (2015). "Eight-lamp externally irradiated bench-scale photocatalytic reactor: Scale-up and performance prediction." *Chem. Eng. J.*, 282, 142–151.

Velasco-Soto, M. A., Pérez-García, S. A., Alvarez-Quintana, J., Cao, Y., Nyborg, L., and Licea-Jiménez, L. (2015). "Selective band gap manipulation of graphene oxide by its reduction with mild reagents." *Carbon N. Y.*, 93, 967–973.

Veldurthi, N. K., Velchuri, R., Pola, S., Prasad, G., Muniratnam, N. R., and Vithal, M. (2015). "Synthesis, characterization and silver/copper-nitrogen substitutional effect on

visible light driven photocatalytic performance of sodium hexatitanate nanostructures.” *J. Chem. Technol. Biotechnol.*, 90(8), 1507–1514.

Verfahrenstechnik, T. (1996). “Photocatalytic detoxification with the thin-film fixed-bed reactor (TFFBR): Clean-up of highly polluted landfill effluents using a novel TiO₂-photocatalyst.” *Solar energy*, 56(5), 455-469.

Verma, A., Prakash, N. T., and Pal, A. (2014). “Photocatalytic Degradation of Herbicide Isoproturon in TiO₂ Aqueous Suspensions: Study of Reaction Intermediates and Degradation Pathways.” *Environ. Prog. Sustain. Energy*, 33(2), 402–409.

Vijayageetha, V. A., Rajan, A. P., Arockiaraj, S. P., Annamalai, V., Janakarajan, V. N., Balaji, M. D. S., Dheenadhayalan, M. S. (2014). “Treatment Study of Dyeing Industry Effluents using Reverse Osmosis Technology.” *Res. J. Recent Sci.*, 3, 58–61.

Wahyuningsih, S., Ramelan, A. H., Pramono, E., Argawan, P., Djatisulistya, A., Firdiyono, F., Sulistiyono, E., and Sari, P. P. (2018). “The Effects of Leaching Process to the TiO₂ Synthesis from Bangka Ilmenite.” *IOP Conf. Ser. Mater. Sci. Eng.*, 333(1), 1–6.

Wang, G. (2016). “Photocatalytic Degradation of Polyacrylamide in Oilfield Sewage by Nano-sized TiO₂ Doped with W Ion.” *MATEC Web Conf.*, 39, 3–5.

Wang, J., Du, J., Yao, H., and Wilkie, C. A. (2001). “XPS characterization of Friedel-Crafts cross-linked polystyrene.” *Polym. Degrad. Stab.*, 74(2), 321–326.

Wang, J., Li, C., Zhuang, H., and Zhang, J. (2013). “Photocatalytic degradation of methylene blue and inactivation of Gram-negative bacteria by TiO₂ nanoparticles in aqueous suspension.” *Food Control*, 34(2), 372–377.

Wang, J., Liu, G., Lu, H., Jin, R., and Zhou, J. (2012a). “Degradation of 1-amino-4-bromoanthraquinone-2-sulfonic acid using combined airlift bioreactor and TiO₂-photocatalytic ozonation.” *J. Chem. Technol. Biotechnol.*, 88(5), 970–974.

- Wang, J., Liu, G., Lu, H., Jin, R., and Zhou, J. (2012b). "Degradation of 1-amino-4-bromoanthraquinone-2-sulfonic acid using combined airlift bioreactor and TiO₂-photocatalytic ozonation." *J. Chem. Technol. Biotechnol.*, 88(5), 970–974.
- Wang, X., Wang, W., Wang, X., Zhao, J., Zhang, J., and Song, J. (2016). "Insight into visible light-driven photocatalytic degradation of diesel oil by doped TiO₂-PS floating composites." *Environ. Sci. Pollut. Res.*, 23(18), 18145–18153.
- Wang, X., Wang, X., Wang, W., Zhang, J., Gu, Z., Zhou, L., and Zhao, J. (2015). "Enhanced visible light photocatalytic activity of a floating photocatalyst based on B–N-codoped TiO₂ grafted on expanded perlite." *RSC Adv.*, 5(52), 41385–41392.
- Wegewitz, L., Prowald, A., Meuthen, J., Dahle, S., Hofft, O., Endres, F., and Maus-Friedrichs, W. (2014). "Plasma chemical and chemical functionalization of polystyrene colloidal crystals." *Phys. Chem. Chem. Phys.*, 16(34), 18261–18267.
- Williamson, B. J., Mikhailova, I., Purvis, O. W., and Udachin, V. (2004). "SEM-EDX analysis in the source apportionment of particulate matter on Hypogymnia physodes lichen transplants around the Cu smelter and former mining town of Karabash, South Urals, Russia." *Sci. Total Environ.*, 322(1–3), 139–154.
- Wu, F., Li, X., Liu, W., and Zhang, S. (2017). "Highly enhanced photocatalytic degradation of methylene blue over the indirect all-solid-state Z-scheme g-C₃N₄-RGO-TiO₂ nanohetero-junctions." *Appl. Surf. Sci.*, 405, 60–70.
- Wu, Y., Luo, H., and Zhang, L. (2015). "Pd nanoparticles supported on MIL-101 / reduced graphene oxide photocatalyst: an efficient and recyclable photocatalyst for triphenylmethane dye degradation." *Env. Sci Pollut Res*, 22, 17238–17243.
- Xing, Z., Li, J., Wang, Q., Zhou, W., Tian, G., Pan, K., Tian, C., Zou, J., and Fu, H. (2013). "A floating porous crystalline TiO₂ ceramic with enhanced photocatalytic performance for wastewater decontamination." *Eur. J. Inorg. Chem.*, (13), 2411–2417.

Xing, Z., Zhang, J., Cui, J., Yin, J., Zhao, T., Kuang, J., Xiu, Z., Wan, N., and Zhou, W. (2018). “Recent advances in floating TiO₂-based photocatalysts for environmental application.” *Appl. Catal. B Environ.*, 225(December 2017), 452–467.

Xu, B., Zhang, Q., Yuan, S., Zhang, M., and Ohno, T. (2016a). “Synthesis and photocatalytic performance of yttrium-doped CeO₂ with a porous broom-like hierarchical structure.” *Appl. Catal. B Environ.*, 183, 361–370.

Xu, H., Li, M., and Jun, Z. (2013a). “Preparation, characterization, and photocatalytic studies on anatase nano-TiO₂ at internal air lift circulating photocatalytic reactor.” *Mater. Res. Bull.*, 48(9), 3144–3148.

Xu, H., Li, M., and Wang, J. K. (2012). “Photocatalytic Degradation of Methylene Blue Using Nano-ZnO at Air Lift Circulating Reactor.” *Adv. Mater. Res.*, 476–478, 1910–1914.

Xu, H., Yan, J., Xu, Y., Song, Y., Li, H., Xia, J., Huang, C., and Wan, H. (2013b). “Novel visible-light-driven AgX/graphite-like C₃N₄(X=Br, I) hybrid materials with synergistic photocatalytic activity.” *Appl. Catal. B Environ.*, 129, 182–193.

Xu, J., Wang, L., and Cao, X. (2016b). “Polymer supported graphene – CdS composite catalyst with enhanced photocatalytic hydrogen production from water splitting under visible light.” *Chem. Eng. J.*, 283, 816–825.

Xu, T., Zheng, H., Zhang, P., and Lin, W. (2016c). “Photocatalytic degradation of a low concentration pharmaceutical pollutant by nanoporous TiO₂ film with exposed {001} facets.” *RSC Adv.*, 6(98), 95818–95824.

Xu, Z., Quintanilla, M., Vetrone, F., Govorov, A. O., Chaker, M., and Ma, D. (2015). “Harvesting lost photons: Plasmon and upconversion enhanced broadband photocatalytic activity in core@shell microspheres based on lanthanide-doped NaYF₄, TiO₂, and Au.” *Adv. Funct. Mater.*, 25(20), 2950–2960.

Xue, H., Jiang, Y., Yuan, K., Yang, T., Hou, J., Cao, C., Feng, K., and Wang, X. (2016a). “Floating photocatalyst of B-N-TiO₂/expanded perlite: a sol-gel synthesis with optimized mesoporous and high photocatalytic activity.” *Sci. Rep.*, 6(June), 2–10.

Xue, H., Jiang, Y., Yuan, K., Yang, T., Hou, J., Cao, C., Feng, K., and Wang, X. (2016b). “Floating photocatalyst of B-N-TiO₂/expanded perlite: a sol-gel synthesis with optimized mesoporous and high photocatalytic activity.” *Sci. Rep.*, 6(June), 1–9.

Xue, Q., Liu, Y., Zhou, Q., Utsumi, M., Zhang, Z., and Sugiura, N. (2016c). “Photocatalytic degradation of geosmin by Pd nanoparticle modified WO₃ catalyst under simulated solar light.” *Chem. Eng. J.*, 283, 614–621.

Yang, G., Yan, Z., and Xiao, T. (2012). “Preparation and characterization of SnO₂/ZnO/TiO₂ composite semiconductor with enhanced photocatalytic activity.” *Appl. Surf. Sci.*, 258(22), 8704–8712.

Yang, N., Li, G., Wang, W., Yang, X., and Zhang, W. F. (2011). “Photophysical and enhanced daylight photocatalytic properties of N-doped TiO₂/g-C₃N₄ composites.” *J. Phys. Chem. Solids*, 72(11), 1319–1324.

Yang, Y., Javed, H., Zhang, D., Li, D., Kamath, R., McVey, K., Sra, K., and Alvarez, P. J. J. (2017). “Merits and limitations of TiO₂-based photocatalytic pretreatment of soils impacted by crude oil for expediting bioremediation.” *Front. Chem. Sci. Eng.*, 11(3), 387–394.

Yang, Y., and Luan, J. (2012). “Synthesis, Property Characterization and Photocatalytic Activity of the Novel Composite Polymer Polyaniline/Bi₂SnTiO₇.” *Molecules*, (3), 2752–2772.

Yoshikawa, N., Kimura, T., and Kawase, Y. (2003). “Oxidative degradation of nonionic surfactants with TiO₂ photocatalyst in a bubble column reactor.” *Can. J. Chem. Eng.*, 81(3–4), 719–724.

- Yousif, E., Abdalla, M., Ahmed, A., Salimon, J., and Salih, N. (2016). "Photochemical stability and photostabilizing efficiency of poly(methyl methacrylate) based on 2-thioacetic acid-5-phenyl-1,3,4-oxadiazole complexes." *Arab. J. Chem.*, 9, S595–S601.
- Yu, H., Song, L., Hao, Y., Lu, N., Quan, X., Chen, S., Zhang, Y., and Feng, Y. (2016). "Fabrication of pilot-scale photocatalytic disinfection device by installing TiO₂ coated helical support into UV annular reactor for strengthening sterilization." *Chem. Eng. J. J.*, 283, 1506–1513.
- Yu, J., Li, Q., Liu, S., and Jaroniec, M. (2013). "Ionic-liquid-assisted synthesis of uniform fluorinated B/C-codoped TiO₂ nanocrystals and their enhanced visible-light photocatalytic activity." *Chem. - A Eur. J.*, 19(7), 2433–2441.
- Yu, M. J. and Kim, B. W. (2004). "Photocatalytic Cell Disruption of *Giardia lamblia* in a UV/TiO₂ Immobilized Optical-Fiber Reactor." *J Microbiology Biotechnol.*, 14(6), 1105–1113.
- Yu, Q. B., Fang, S. H., and Wang, X. Z. (2017). "The g-C₃N₄ Nanosheets Separated by PS for Photocatalytic Degradation of Dye." *J. Nano Res.*, 49, 215–224.
- Yuan, C., Hung, C.-H., Yuan, C.-S., and Li, H.-W. (2017). "Preparation and Application of Immobilized Surfactant-Modified PANi-CNT/TiO₂ under Visible-Light Irradiation." *Materials (Basel)*, 10(8), 877.
- Yuan, S. J., Li, X. W., and Dai, X. H. (2014). "Efficient degradation of organic pollutants with a sewage sludge support and in situ doped TiO₂ under visible light irradiation conditions." *RSC Adv.*, 4(105), 61036–61044.
- Zagórski, Z. P. (2003). "Diffuse reflection spectrophotometry (DRS) for recognition of products of radiolysis in polymers." *Int. J. Polym. Mater. Polym. Biomater.*, 52(4), 323–333.

Zan, L., Tian, L., Liu, Z., and Peng, Z. (2004). "A new polystyrene-TiO₂ nanocomposite film and its photocatalytic degradation." *Appl. Catal. A Gen.*, 264(2), 237–242.

Zhai, H. S., Cao, L., and Xia, X. H. (2013). "Synthesis of graphitic carbon nitride through pyrolysis of melamine and its electrocatalysis for oxygen reduction reaction." *Chinese Chem. Lett.*, 24(2), 103–106.

Zhang, X., Wu, Y., Xiao, G., Tang, Z., Wang, M., Liu, F., and Zhu, X. (2017). "Simultaneous photocatalytic and microbial degradation of dye-containing wastewater by a novel g-C₃N₄-P25/photosynthetic bacteria composite." *PLoS One*, 12(3), 1–16.

Zhang, Y. (2014). "Heterogeneous Photocatalytic Degradation of Triton X-100 in Aqueous TiO₂ Suspensions." *Am. J. Environ. Prot.*, 3(1), 28–35.

Zhang, Z., and Gamage, J. (2010). "Applications of photocatalytic disinfection." *Int. J. Photoenergy*, 2010, 1–11.

Zhang, Z., Jiang, D., Li, D., He, M., and Chen, M. (2016). "Construction of SnNb₂O₆ nanosheet/g-C₃N₄ nanosheet two-dimensional heterostructures with improved photocatalytic activity: Synergistic effect and mechanism insight." *Appl. Catal. B Environ.*, 183, 113–123.

Zhao, H., Qu, S., Guo, S., Zhao, H., Liang, S., and Xu, M. (2019). "Virtual Water Scarcity Risk under Climate Change." *J. Clean. Prod.* DOI: 10.1016/j.jclepro.2019.05.114

Zhao, J., Hidaka, H., Takamura, A., Pelizzetti, E., and Serpone, N. (1993). "Photodegradation of Surfactants. 11. ζ -Potential Measurements in the Photocatalytic Oxidation of Surfactants in Aqueous TiO₂ Dispersions." *Langmuir*, 9(7), 1646–1650.

Zheng, X., Shen, Z.-P., Shi, L., Cheng, R., and Yuan, D.-H. (2017). "Photocatalytic Membrane Reactors (PMRs) in Water Treatment: Configurations and Influencing Factors." *Catalysts*, 7(8), 224.

Zhiyong, Y., Keppner, H., Laub, D., Mielczarski, E., Mielczarski, J., Kiwi-Minsker, L., Renken, A., and Kiwi, J. (2008). “Photocatalytic discoloration of Methyl Orange on innovative parylene-TiO₂ flexible thin films under simulated sunlight.” *Appl. Catal. B Environ.*, 79(1), 63–71.

Zhu, H., Jiang, R., Fu, Y., Guan, Y., Yao, J., Xiao, L., and Zeng, G. (2012a). “Effective photocatalytic decolorization of methyl orange utilizing TiO₂/ZnO/chitosan nanocomposite films under simulated solar irradiation.” *Desalination*, 286, 41–48.

Zhu, S., and Wang, D. (2017). “Photocatalysis: Basic Principles, Diverse Forms of Implementations and Emerging Scientific Opportunities.” *Adv. Energy Mater.*, 1700841, 1700841.

Zhu, S., Yang, X., Yang, W., Zhang, L., Wang, J., and Huo, M. (2012b). “Application of Porous Nickel-Coated TiO₂ for the Photocatalytic Degradation of Aqueous Quinoline in an Internal Airlift Loop Reactor.” *Int. J. Environ. Res. Public Health*, 2, 548–563.

Zhu, Y., Murali, S., Cai, W., Li, X., Suk, J. W., Potts, J. R., and Ruoff, R. S. (2010). “Graphene and graphene oxide: Synthesis, properties, and applications.” *Adv. Mater.*, 22(35), 3906–3924.

Zolgharnein, J., Shahmoradi, A., and Ghasemi, J. (2011). “Pesticides Removal Using Conventional and Low-Cost Adsorbents: A Review.” *Clean - Soil, Air, Water*, 39(12), 1105–1119.

APPENDIX A

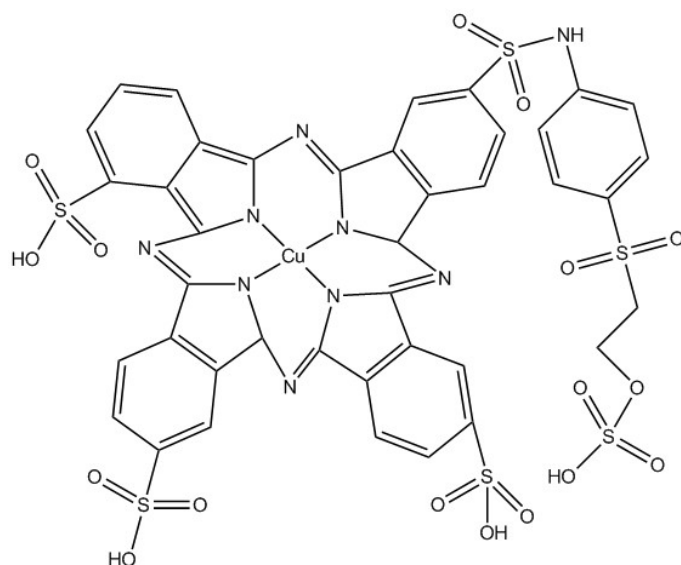


Figure A1. Structure of Remazol turquoise blue G-133 dye.

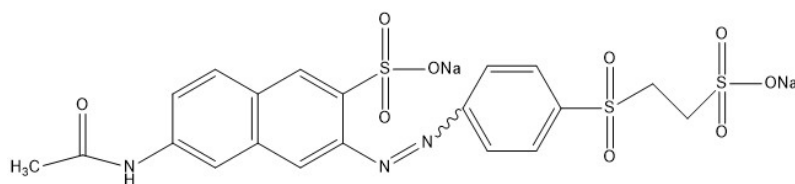


Figure A2. Structure of Remazol Orange 16 dye.

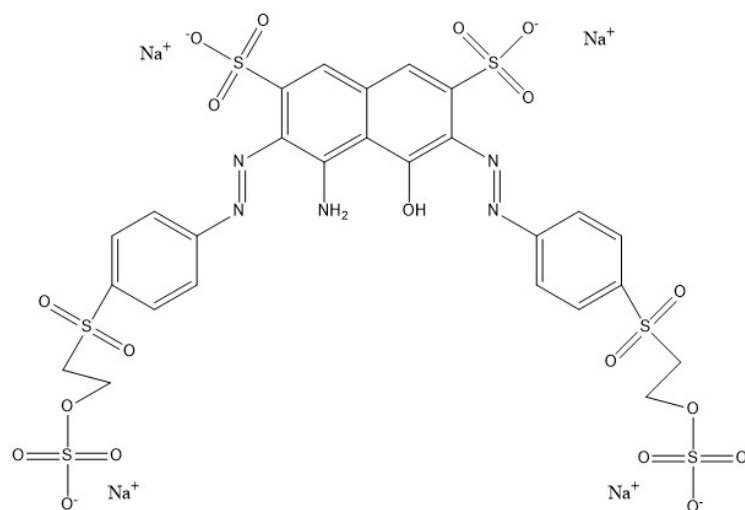


Figure A3. Structure of Remazol Black 5 dye.

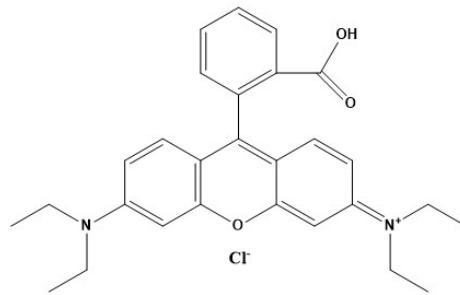


Figure A4. Rhodamine B dye.

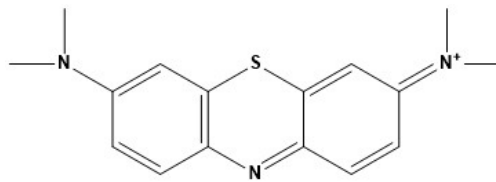


Figure A5. Methylene blue dye.

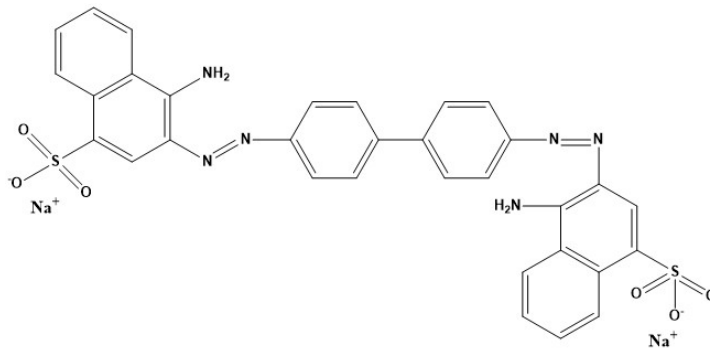


Figure A6. Congo Red dye.

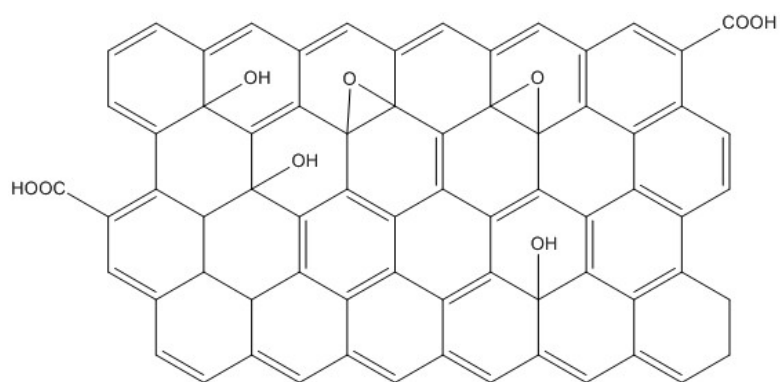


Figure A7. Structure of GO.

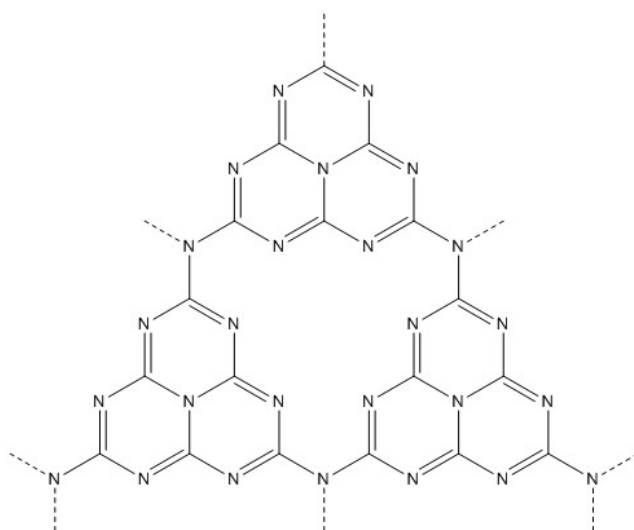


Figure A8. Structure of g-C₃N₄.

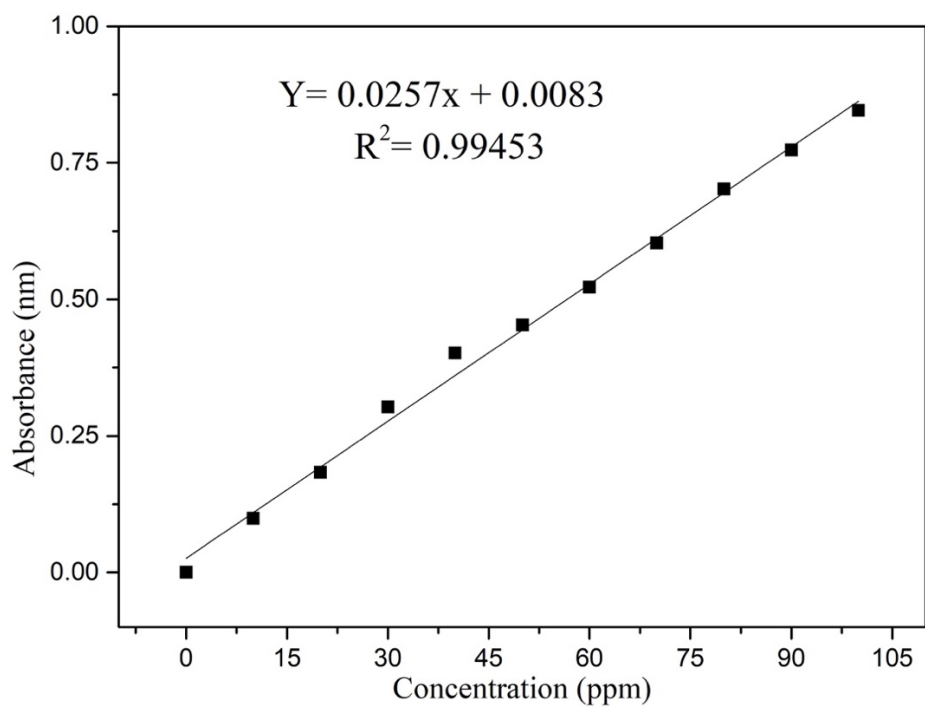


Figure A9. Calibration curve for RTB.

Table A1. Characteristics of dyes used in this work.

Parameter	Remazol turquoise blue	Remazol Orange 16	Remazol Black 5	Congo red	Methylene blue	Rhodamine B
Class	Copper phthalocyanine	Azo	Azo	Diazo dye	Synthetic basic dye	Xanthene dye
Mol. Form.	$CuC_{40}H_{24}N_9O_{17}S_6Na_4$	$C_{20}H_{17}N_3O_{10}S_3Na_2$	$C_{26}H_{21}N_5Na_4O_{19}S_6$	$C_{32}H_{22}N_6Na_2O_6S_2$	$C_{16}H_{18}ClN_3S$	$C_{28}H_{31}ClN_2O_3$
Reactive group	Sulphatoethylsulphone	-	-	-	-	-
Color index name	Reactive Blue 21/ Remazol turquoise blue G-133	Reactive Orange 16/ Brilliant orange 3R	Reactive Black 5/ Remazol black B/ Remazol Black GF	Congo red/ Direct red 28	Methylthioninium chloride/ Basic blue 9	Basic Violet 10/ Brilliant Pink B/ Tetraethylrhodamine
pH (10 ppm solution)	5.88	-	-	-	-	-
Molecular wt. (g/mol)	1250	601	991	697	320	479
λ_{max} (nm, visible UV)	666	493	420	497	663	544

**RESEARCH
PUBLICATIONS**

RESEARCH PUBLICATIONS

(A) Research Papers in International Journals

1. **Suman Das**, Hari Mahalingam (2019). “Reusable floating polymer nanocomposite photocatalyst for the efficient treatment of dye wastewaters under scaled-up conditions in batch and recirculation modes”. *Journal of Chemical Technology and Biotechnology*, 94 (8) 2597-2608. DOI: 10.1002/jctb.6069.
2. **Suman Das**, Hari Mahalingam (2019). “Exploring the synergistic interactions of TiO₂, rGO, and g-C₃N₄ catalyst admixtures in a polystyrene nanocomposite photocatalytic film for wastewater treatment: Unary, binary and ternary systems”. *Journal of Environmental Chemical Engineering*, 7(4), 103246.
DOI: 10.1016/j.jece.2019.103246.
3. **Suman Das**, Hari Mahalingam (2019). “Novel immobilized ternary photocatalytic polymer film based airlift reactor for efficient degradation of complex phthalocyanine dye wastewater”. *Journal of Hazardous Materials*, 383, 121219. DOI: 10.1016/j.jhazmat.2019.121219.
4. **Suman Das**, Hari Mahalingam (2019). “Dye degradation studies using immobilized pristine and waste polystyrene-TiO₂/rGO/g-C₃N₄ nanocomposite photocatalytic film in a novel airlift reactor under solar light”. *Journal of Environmental Chemical Engineering*, 7(5), 103289.
DOI: 10.1016/j.jece.2019.103289.

(B) Oral Presentation /Poster Presented in International Conference

1. Anna Maria, **Suman Das**, and Hari Mahalingam (2019). “Investigation of Unary, Binary and Ternary Mixtures of Photocatalysts in Immobilized Form for Treatment of Dye Wastewaters.” IWA-RMTC (Department of Applied Chemistry, The Maharaja Sayajirao University of Baroda, India), 10-12th Dec 2018.
2. **Suman Das**, and Hari Mahalingam (2018). “Development of polystyrene-TiO₂ nanocomposite photocatalyst for treatment of dye wastewaters”. ASP-17 (Chemical Engineering Dept, IIT Guwahati, India), 8-11th January 2018.

BIO-DATA

Suman Das

Email ID: sumands133@gmail.com

Contact no: +91-9008900553/8073619773

Personal Details:

Name : Suman Das
Father's name : Harekrishna Das
Date of birth : 30th November, 1991
Gender : Male
Nationality : Indian
Permanent address : Suman Das,
S/O, Harekrishna Das, Morgangpara,
Kamalnagar, Moharchera, Teliamura-
799203, Tripura, India.

Organization:

Research Associate, Jawaharlal Nehru Centre for Advanced Scientific Research (JNCASR), Rachanahalli Lake Road, Jakkur, Bengaluru-560064.

Educational qualification:

- Ph.D. in Chemical Engineering (CGPA – 6), 2015-2020
Department of Chemical Engineering,
National Institute of Technology Karnataka,
Surathkal, Mangalore, Karnataka-575025.
- M.Tech in Chemical Engineering (CGPA – 8.05), 2013-2015
NIT Agartala, Department of Chemical Engineering,
National Institute of Technology Agartala,
Barjala, Jirania, Agartala, Tripura-799046.
- B.Tech in Chemical Engineering (67.51%), 2009-2013
P.I.E.T. Nagpur, (R.T.M.N.U.), Department of Chemical Engineering,
Mouza Shivangaon, Behind CRPF Campus,
Hingna Road, Nagpur, Maharastra-440019.

Declaration:

I hereby declare that the above written particulars are true to the best of my knowledge.

Place: Surathkal, India

Suman Das

Date: 27/02/2020